eman ta zabal zazu

Universidad del País Vasco
Euskal Herriko Unibertsitatea

Chemistry Faculty
Department of Polymer Science and Technology

Computational study of the effect of Aluminum cation on aromatic amino acids

DOCTORAL THESIS

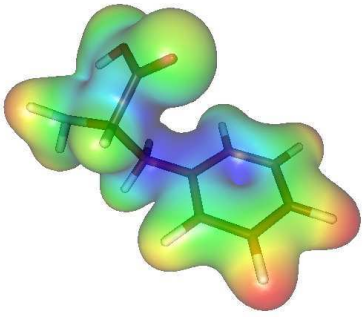

Julen Larrucea Corchero
Donostia, September 2009

Computational study of the effect of Aluminum cation on aromatic amino acids

Doctoral Dissertation
Julen Larrucea Corchero
Director: Jesus M. Ugalde profesorea

June 14, 2009

"Shut up and calculate"

David Mermin

" - *calcular y*
\+ *artículos con los cálculos ya hechos"*

Mario Piris

"I think I can safely say that nobody understands quantum mechanics"

Richard P. Feynmann

Acknowledgements

When giving the acknowledgements, it is difficult to mention all the persons who have been around me and my work in these last four years.

First of all, I would like to thankfully acknowledge my thesis supervisor Prof. Jesus M. Ugalde, because he brought me back home from Finland and gave me the chance of developing my main research field.

It has not been easy to carry out this thesis, but thanks to Jesus I always had the chance for getting whatever I needed, and with whatever, I mean all the thrust I have needed for carrying out whichever initiative I had. Moreover, working in his group, gave me the chance for having my own computing cluster or calculating in the awesome world's third most powerful supercomputer.

It is difficult for me to imagine some other place where it feels the freedom and confidence I have felt in here.

Apart from Jesus, I want to mention my "constant" coworkers, Xabi for cheering the office, Txema for listening me in the critical moments, Txoni "handia", my quantum mechanics and life professor Mario Piris and the valuable Elena, because after these four years they have became somehow part of my life.

In addition to the "constants", there are also the coworkers who have left the "nest" Joni, Iñaki, Eli and Eider with whom I shared many nice moments too, and the ones who got into the nest after me Oier, Elisa and Jon Mikel.

...and although they have not been in the PhD nest, I want to mention my coworkers Andreas and Ivan and also to Prof. Eduardo Ludeña who visits us from time to time.

And talking about constants..., the lunch time has been quite constant last years, one o'clock, and almost as constant as the lunch time the people that shared lunches and talks about science, news or whatever. Must mention (once again) Iñaki, Eneko, Aizpea, Fernando, Ana, the bunch of DIPC including Andres, Daniel, Elton, Thomas,

Vito and the rest of the people, and also the guy from outside the atomistic field who opened us a new science point of view Mikel 'Kinti".

Since there are not any more rehearsals of the "Larru & Kinti" albokari panderujole couple in the yard of Berio the neighbours can relax and sleep.

I must mention many other persons who had their little contributions on this thesis. Starting from my master's thesis supervisor Prof. Kari Laasonen, because he was the one who got me into the CPMD field and has been ready to help also in these last four years. Also the friends/coworkers I met first at the university of Oulu Giorgio Lanzani and Jaime Zaratiegui who taught me all the tricks about quantum chemistry and computers, and who in the same way as Mauricio, Anne, Yrjö and Johanna have been far but also close to me in these years.

Many other people made their little contributions to this thesis, and I must mention too Ari Seitsonen, Axel Kohlmeyer and Pradip Biswas for the quantum/computational support, Hannele Ylilehtö and Markku Pulkkinen (and their daughters Marika, Riikka and Johanna) for their generosity and for helping me to link my computational research with the medicine field, and also Nico, which I met physically just in the PhD courses of Tarragona and in the Euro Master of Perugia, but with whom I have shared friendship and code fragments through the network.

Although they did not have any direct influence in this work, I want to acknowledge also to the people who helped me to disconnect a little bit from the computers and work, the members of my music bands: Joseba, Gontxas, Aizpea and Unai from *Xau* and Arantza, Amaia and Ruth from *Sabur*. Also to the people in the *Suomitar* Basque Country-Finland cultural association, for all the nice moments we spent together.

I want to thank also to Itsaso, who has been worried about my thesis in the last years, and also to the Swedish connection Itxaso and Björn.

Finally, I want to thank to my family, and specially to my parents Encarni and Gabi who have been always next to me, ... and of course, to my grand mother Teresa and also, although unfortunately she will not see the end of this thesis, to my grand mother Agustina, who will be always in my heart, for all the prays they did and the candles they switched for helping me to achieve my goals. This thesis is dedicated to you.

Abbreviations & Conversions

Abbreviations

MD	Molecular Dynamics
CPMD	Car-Parrinello Molecular Dynamics
AIMD	Ab-Initio Molecular Dynamics
DFT	Density Functional Theory
RDF	Radial Distribution Function
PBC	Periodic Boundary Conditions
Al	Aluminum
COO^-	Carboxylate anion
AAA	Aromatic Amino Acid
phe	Phenylalanine
tyr	Tyrosine
trp	Tryptophan
C_α / C_1	Alpha Carbon. The one in the ring where the side chain is attached to.
a.u.	Atomic Units
a.m.u.	Atomic Mass Unit
Ry	Rydberg
ps	pico-second
MO	Molecular Orbital
Fig.	Figure
Eq.	Equation

Conversion Factors

time step	1 a.u.= 0.0241888428 10^{-15}s
distance	1 Bohr = 1 a_0 = 0.529177249 Å
energy	1 Ha = 27.21161 eV = 627.5095 kcal/mol = 2625.5 kJ/mol
plane wave cutoff	1 Ry = 1/2 Ha = 13.6058 eV

Contents

Chapter 1

The importance of the biochemistry of aluminum

Aluminum (Al) is the third most abundant metal and the third most abundant chemical element in the Earth crust. Most of Al is incorporated into aluminosilicate soil minerals, but only an small part of them are in soluble forms that can influence living organisms.

On other hand, in spite of its abundance, Al is not an essential bioelement [1], and there is no known biological reaction that requires it, but on other hand the modern society foments the presence of aluminum in our water, food and air [2] for example, by being leached from the soil by polluted acidic rainwater, reaching the plants and so on.

As a result of modern life, Al is introduced in our organisms in many different ways, from cans or aluminum paper to underarm antiperspirants.

Aluminum has been found to be toxic but nowadays the chemistry of this toxicity is not yet completely understood. Many metals have crucial functions in biology and usually bind to the biomolecules trough specific binding sites [3]. For the case of Al, in general words, one could say that the chemistry of aluminum has elements in common with two other groups of elements: divalent magnesium and calcium, and trivalent chromium and iron [4].

Due to their biological similarities, different researches have studied the competition between aluminum and magnesium when complexing with amino acids [5][6].

In the case of humans, the toxicity process of the Al starts by binding transferrins. Transferrins are a family of proteins that serve the crucial role of Fe(III) sequestration and transport in vertebrates and insects. Although Al is found not to be able to displace Fe(III), it has many unloaded sites for binding transferring, and in fact, it is now accepted that 90 % or more of aluminum in serum is bound to the transferrin [7] [8] in the same binding site where Fe^{+3} should be [9].

On other hand, due to the stability of the complex [10], Al stays permanently in the binding site once it gets there, in the place where some other metal cations could go, changing this way the properties of he whole protein [11].

Aluminum has been also related with various neurodegenerative diseases [12]. In

fact, an increased level of Al and decreased levels of Ca and Mg are suspected to underlie the pathogenesis of Amyotrophic Lateral Sclerosis (ALS) and Parkinsonism Dementia (PD). In particular, a relationship between Al and the pathogenesis of Alzheimer's disease (AD) was suggested by Klatzo et al. in 1965 [13], when they obtained a degeneration of the neuorofibrils and the appearance of tangle-like structures, similar to neurofibrilary tangles in the brains of the AD patients induced by intracerebral administration of Al to experimental animals [14] [15].

As Al is transported in blood, the brain has lower aluminum levels than many other tissues due to the blood-brain barrier, but on other hand, it has been found that the complexation amyloid β protein with Al yields to an enhancement of penetration in brain [16].

Many other researches have been carried out around the effect of Al in Alzheimer's disease, and nowadays the link between both is already well established [17] [18].

On other hand, Al is found to bind many other different biomolecules like osteopontin, osteocalcin and phosphophoryn (in bone ant teeth) [19], Ca^{+2} transporting calmodulin protein [20], citrate acid [21] [22] (derived from root exudates, decomposing organic matter and other sources), and many others [23].

The key on understanding all these protein-Al interactions relies on their chemistry, thus in being able to understand why and how Al binds in some specific sites instead of others getting an idea of what is really going on at molecular level.

In this case, the necessary tools for studying the molecular level are going to be given by quantum chemistry, and due to it's limitations on handling systems with too many atoms, the problem will have to be simplified to the minimum (accurate) number of atoms.

So, as Al binds the protein, and the protein is made up by amino acids, first approach would be to study the interactions between Al and amino acids, but due to some researches [24] [25] we know that the cation-π interactions are going to have special importance, and as the only amino acids with the ability to have cation-π interactions (the ones with aromatic ring) are Phenylalanine (Phe), Tyrosine (Tyr) and Tryptophan (Trp), the hole problem can be first approached to be just these amino acids and Al.

The study method used in this work has been based on theoretical models, by performing different static and dynamic calculations. Static calculations were used to obtain accurate data from the most interesting structures and the dynamic calculations were used for studying the time evolution of the systems. The theory models used for these calculations are *ab-initio* or first principles without any empirical data, in order to achieve the maximum accuracy. The use of ab-initio techniques is necessary in order to be able to model the electronic structure around the atoms and being able to describe chemical bonds and interatomic interactions.

The obtained results will be shown in three different parts, first one will be aimed to understand the general behavior of Al in solution, second one will study the effect of aluminum on isolated amino acids in microsolvation conditions (just a couple of water molecules around) and third and last part will be focused on the effect of Al on the amino acids in full solvation environment.

Chapter 2

Computational Tools

2.1 Introduction

As a difference with the most of the people researching this field, the procedure used for this project was purely based in theoretical methods. This chapter tries to introduce some of the basic concepts of theoretical chemistry in order to put the results in context. The main method used in this research is called Molecular Dynamics (MD) and it is particularly helpful in order to understand the behavior of a molecular system.

Since Sir Isaac Newton published his "PhilosophiæNaturalis Principia Mathematica" in 1687, the human being has been able to understand and even predict the natural phenomena by using the equations given by classical mechanics.

In fact, following the laws of classical mechanics, one can easily understand the motion of some bouncing balls in a pool table and even predict where will they be in future. If that could be possible, if we are able to understand which behavior of some particles and even predict them, why not to try same thing at molecular level?

Most of the chemists feel sometimes the impotence of not knowing what is going on in their colorful glasses, but in fact these colorful glasses and their content are actually full of atoms, and we could simulate them in an inaccurate way, by using similar equations to the ones used on the pool table. So, why not to try to use these equations for describe the motion of the atoms? ...and if atoms could be understood by equations and we assume that everything in the world is made up with atoms, does it mean that we could understand and even predict the whole world?!

The answer to this question is **NO**, because the complexity of the nature and the size of the systems would make the calculations extremely expensive. On other hand, systems can be simplified, and really interesting information can be obtained by simulating the key-regions of the phenomena.

2.1.1 A simple model for understanding the Molecular Dynamics concept

Molecular dynamics (MD) is a tool from theoretical chemistry for studying the time evolution of molecular systems by applying different kind of physical laws and propagating the particles in the time-space.

The particles in the system can be studied just by the interaction that they have with each other one by one. If the forces between particles are known, the velocities too, so that the system can be propagated in the time and space. A draft code for an algorithm that would do this could be easily written.

1. Load parameters needed for the simulation (number of steps, time step, temperature, simulation box size ...)

2. Load coordinates and velocities ($\mathbf{r}_1, \mathbf{v}_1, \mathbf{r}_2, \mathbf{v}_2, \mathbf{r}_3, \mathbf{v}_3, ...$)

3. Calculate the Temperature of the system based on the velocities

$$\overline{E_K} = \overline{\left[\frac{1}{2} m \dot{\mathbf{r}}^2\right]} = \frac{3}{2} NkT,$$

   where $\overline{E_K}$ is the averaged kinetic energy, m the mass of the particle, $\dot{\mathbf{r}}$ the velocity of the particle, k Boltzmann's constant ($1.38 \times 10^{-23} JK^{-1}$) and T the temperature of the system

4. Scale the velocity of the particles for fitting into the given temperature interval or thermostat

5. Re-fold the particles into the simulation cell (Periodic Boundary Conditions) by dividing the position vectors of the particles by the cell size until they fit into the box

6. Calculate the forces between the particles. This can be done simply (and inaccurately) by applying a Lennard-Jones 12-6 kind pair potential [26]

$$V_{LJ} = 4\epsilon \left[\left(\frac{\sigma}{\mathbf{r}}\right)^{12} - \left(\frac{\sigma}{\mathbf{r}}\right)^{6} \right],$$

   and calculating the force or acceleration on each particle one by one

$$\mathbf{F}_i = -\nabla V_i = m\ddot{\mathbf{r}}_i.$$

7. Propagate the particles to new positions by

$$\mathbf{r}_i(t+\delta t) = \mathbf{r}_i(t) + \dot{\mathbf{r}}_i\delta t + \frac{1}{2}\ddot{\mathbf{r}}_i\delta t^2 + \dots$$

8. Move time to $t = t + \delta t$

9. If this process is made as many times as required simulation steps, then STOP and print statistics, otherwise, return to second step and reload the new coordinates.

So that we can get the trajectories and rest of interesting parameters from the system each step.

The "quality" of the simulation is given by the theory behind the equations that describe the interactions between the particles.

The choice of the method should be done by thinking mostly in three different factors: the available computational resources, the size of our system and the kind of interactions we want to study.

The accuracy of the description of the physical phenomena behind the interactions are usually proportional to the computational cost of the calculations, so that Ab-initio molecular dynamics methods describing electronic structure, scale in the over the fourth power of the number of atoms in the system, while in a classical molecular dynamics simulation based in force fields and neglecting the electronic structure, time is just proportional to the square of the number of atoms.

Classical molecular dynamics methods are specially interesting for studying big systems but do not describe the electronic structure. On other hand Ab-initio calculations restrain us to choosing smaller systems.

Our research has been focused in the interaction of aluminum atoms with the water and the amino acids, and as the phenomena we want to study is almost purely electronic (i.e. covalent and H-bonds, cation-π interactions,...) Ab-Initio simulation techniques will be used.

2.2 Ab-Initio description of a system

In previous section a simple example for molecular dynamics was shown. The proposed algorithm uses a very simple Lennard-Jones potential, but a better physical description is needed in order to be able to simulate properly the behavior of a molecular system, so that, physical description must be given by using the concepts from quantum mechanics.

Following, some basic concepts from ab-initio techniques will be introduced.

2.2.1 Density Functional Theory

Classical Mechanics is based in Newton's laws and Quantum Mechanics is based in Schrödinger's equation, but due to the exponential grow of the complexity of the equations with the number of particles, unfortunately this equation can not be solved for cases with more than two electrons. Here is where the approaches start.

Popular approaches like Hartre-Fock, are based on complicated many-electron wave functions, but Density Functional Theory (DFT) is an alternative to the heavy task of solving these many-electron wave functions. DFT states that the whole system and its ground state can be described based on the electronic density of the system. In the practice, for an N-electronic system where the wave function of every electron is dependent on 3 variables (3N in total), DFT allows us to express the whole system as a function of just three spatial coordinates.

Although the idea of describing the properties of the system by the electronic density was first proposed by the Thomas-Fermi model, DFT as we know it today was the result of the work of Hohenberg and Kohn [27] on 1964 trough their two theorems.

The first of these theorems demonstrates the existence of a one-to-one mapping between the ground-state electron density ρ_0 and the ground-state wave function Ψ_0 of a many-particle system

$$\rho(r) = \sum_{i=1}^{N} |\Psi_i(\mathbf{r}|^2. \tag{2.1}$$

This way the energy of a system $E[\rho]$ and the external potential $\nu_{ext}(\mathbf{r})$ are uniquely determined by the ground state density ρ_0 as

$$E_0 = E_0[\rho_0] \tag{2.2}$$

$$E_0 = T_0[\rho] + \int \rho(\mathbf{r})\nu_{ext}(\mathbf{r})d\mathbf{r} + \mathbf{V}_{ee}[\rho_0] \tag{2.3}$$

where $T[\rho_0]$ is the kinetic energy and $\mathbf{V_{ee}}[\rho_0]$ is the electron-electron interaction energy.

The second theorem introduces the energy variational principle. It states that there exists a universal functional $(\tilde{\rho})$ that yields the lowest energy if and only if input density is the true ground stated density ρ_0,

$$E[\tilde{\rho}] \geq E[\rho_0]. \tag{2.4}$$

However the Hohenberg and Kohn theorems are not constructive, they do not tell us the value of true total energy density functional, only that it exists.

The next year Kohn and Sham proposed to express the kinetic energy as the kinetic energy of a fictitious reference system s of N non-interacting electrons [28]

$$T_s[\rho_s] = \sum_i^N \langle \phi_i^{KS} | -\frac{1}{2}\nabla^2 | \phi_i^{KS} \rangle. \tag{2.5}$$

The connection of this artificial system to the one we are really interested in is established by choosing the effective potential $\nu_{ext,s}$ such that the density resulting from the summation of the moduli of the squared orbitals exactly equals the ground state density of our real target system of interacting electrons

$$\rho(\mathbf{r}) = \rho_0(\mathbf{r}) = \sum_i^n |\phi_i^{KS}(\mathbf{r})|^2 \tag{2.6}$$

where $\phi_i^{KS}(\mathbf{r})$ are the orthonormal Kohn-Sham orbitals. The expression of the electron density and the kinetic energy is exact for a one determinant wave function of a system of non-interacting electrons. The difference in kinetic energy and in electronic interaction energy between the reference system and the real system is

$$\Delta T[\rho] \equiv T[\rho] - T_s[\rho] \tag{2.7}$$

$$\Delta V_{ee}[\rho] \equiv V_{ee}[\rho] - \frac{1}{2}\int\int \frac{\rho(\mathbf{r}_1)\rho(\mathbf{r}_2)}{|\mathbf{r}_1 - \mathbf{r}_2|} d\mathbf{r}_1 d\mathbf{r}_2. \tag{2.8}$$

Insertion in the Hohenberg-Kohn Eq. 2.3 yields

$$E^{KS}[\rho] = \int \rho(\mathbf{r})\nu_{ext}(\mathbf{r})d\mathbf{r} + T_s[\rho] + \frac{1}{2}\int\int \frac{\rho(\mathbf{r}_1)\rho(\mathbf{r}_2)}{|\mathbf{r}_1 - \mathbf{r}_2|} d\mathbf{r}_1 d\mathbf{r}_2 + E_{xc}[\rho] \tag{2.9}$$

with

$$E_{xc}[\rho] \equiv \Delta T[\rho] + \Delta V_{ee}[\rho]. \tag{2.10}$$

The exchange-correlation functional $E_{xc}[\rho]$ represents the non-classical part of the electronic interaction energy and the difference in kinetic energy between the reference system and the real system. The Kohn-Sham orbitals are found by minimization of Eq. 2.9 under constraint that $\langle \phi_i | \phi_j \rangle = \delta_{ij}$. This results into the Kohn-Sham equations

$$\left\{ -\frac{1}{2}\nabla^2 + \nu_{xc} + \int \frac{\rho(\mathbf{r}')}{|\mathbf{r} - \mathbf{r}'|} d\mathbf{r}' + \nu_{xc} \right\} \psi_i(\mathbf{r}) = \epsilon_i \psi_i(\mathbf{r}), \tag{2.11}$$

which has to be solved self-consistently.

If the only correct expression for the exchange-correlation potential,

$$\nu_{xc}(\mathbf{r}) \equiv \frac{\delta E_{xc}[\rho(\mathbf{r})]}{\delta \rho(\mathbf{r})}, \tag{2.12}$$

was known, solving Eq. 2.11 would be equivalent to solving the exact electronic Schrödinger equation. Unfortunately, the exact exchange-correlation potential is unknown and much effort has been and is being devoted to find good approximation to ν_{exc}. Therefore, the quality of the electronic structure calculation depends on the quality of the approximation used for E_{xc}.

The most straight forward approximation for this potential is the one called Local Density Approximation (LDA) which assumes a locally uniform electron density ρ so that the energy can be given by

$$E_{xc}^{LDA}[\rho] = \int \rho(\mathbf{r}) \epsilon_{xc}^{LDA}(\rho) d\mathbf{r} \tag{2.13}$$

where $\epsilon_{xc}(\rho)$ is the sum of the exchange and correlation energy of the electron gas.

The next approximation could be to include, not just the electronic density, but the gradient $\nabla\rho(\mathbf{r})$ as well, and that is the one called Generalized gradient approximation (GGA) [29]. Many functionals have been developed in the framework of the GGA.

The exchange-correlation functional chosen for this work was the so called PBE by Perdew, Burke and Ernzerhof [29].

The exchange correlation energy for the PBE functional can be writer in a similar way as in equation 2.13

$$E_{xc}^{PBE}[\rho] = \int \rho(\mathbf{r}) \epsilon_{xc}^{PBE}(r_s(\mathbf{r}, s(\mathbf{r}, \xi(\mathbf{r})))(\rho) d\mathbf{r}, \tag{2.14}$$

where s is the reduced density gradient

$$s = \frac{|\nabla\rho|}{2k_F\rho}, \tag{2.15}$$

ξ is the spin polarization

$$\xi = \frac{\rho_\uparrow - \rho_\downarrow}{\rho}, \tag{2.16}$$

k_F the Fermi radius

$$k_F = (3\pi^2\rho)^{\frac{1}{3}}, \tag{2.17}$$

and r_s the Wigner-Seitz radius

$$r_s = \left(\frac{4\pi\rho}{3}\right)^{-\frac{1}{3}}. \tag{2.18}$$

2.2.2 Basis Sets

There are two different ways for constructing Molecular Orbitals (MOs): numerically or algebraically by linear expansion in a set of basis functions. Numerical approaches offer a great accuracy and flexibility but they became quite difficult to handle computationally due to their huge amount of grid points. Therefore, for polyatomic systems an algebraic approach is needed, where MOs (ψ_{MO}) are expanded by Linear Combination of Atomic Orbitals (LCAO) in a set of simple analytical one-electron functions [30]

$$\psi_{MO}(\mathbf{r}) = \sum_{i}^{n} c_i \chi_i(\mathbf{r}), \tag{2.19}$$

and depending on the shape of χ_i basis sets can be of different kinds.

Usually these functions are atomic orbitals, centered on atoms, but also possible on bonds, lone pairs and so on. The simplest ones are the Slater Type Orbitals (STO) which look like

$$\chi_i^{STO}(\mathbf{r}) = N r^{n-1} e^{\zeta \mathbf{r}} Y_{lm}(\theta, \varphi) \tag{2.20}$$

where n is the principal quantum number (n= 1, 2, 3, ...), N is the normalization constant, $r = |\mathbf{r}|$ is the distance of the electron from the atomic nucleus, ζ is a constant related to effective charge of the nucleus after being partly shielded by electrons and $Y_{lm}(\theta, \phi)$ the spherical harmonics.

Another type of atomic orbitals are the Gaussian Type Orbitals (GTO) which look like

$$\chi_i^{GTO}(\mathbf{x}) = N x^l e^{\alpha \mathbf{r}^2} \chi_i^{GTO}(\mathbf{y}) = N y^m e^{\alpha \mathbf{r}^2} \chi_i^{GTO}(\mathbf{z}) = N z^n e^{\alpha \mathbf{r}^2} \tag{2.21}$$

where l is the quantum number of the orbital.

Atom centered basis sets are computationally efficient for gas phase calculations and localised orbitals. However, their use for complexes and hydrogen bonded systems introduces one error: the Basis Set Superposition Error (BSSE). The BSSE derives from the fact that in practice incomplete basis sets are used to express the wave function.

There are different ways for avoiding BSSE, but for non gas phase systems, the best way is to switch to some other basis set type.

The basis set used for the CPMD [31] calculations in this project, were the Plane

Wave (PW) basis sets, which are also specially convenient for expressing the wave function in periodic systems like Periodic Boundary Conditions (PBC). PW basis set look like

$$\chi_i^{PW}(\mathbf{r}) = \Omega^{-\frac{1}{2}} e^{i\mathbf{G}_\nu \cdot \mathbf{r}} \tag{2.22}$$

where Ω is the volume of the simulation cell and $\mathbf{G}_\nu$ are the reciprocal lattice vectors of the simulation cell.

In practice, PW basis sets are often used in combination with an "effective core potential" or pseudo potential, so that the plane waves are only used to describe the valence charge density.

2.2.3 Pseudo potentials

The pseudo potential concept was first introduced by Hans Hellmann in the 1930s. The idea is to replace the atomic all-electron core states potential by an effective core potential, keeping inner electrons "frozen" while the only electrons that actually have to be explicitly calculated are the valence ones.

The pseudo potentials show an acceptable fitting with the all-electron potential after certain distance from the center, this distance is called "cutoff radius" ($\mathbf{r}_c$) which can be larger or smaller depending on the hardness or softness of the pseudo potential.

Most common pseudo potentials are Norm-Conserving and Ultra-Soft pseudo potentials. The Norm-Conserving pseudo potentials are derived from an atomic reference state, requiring that the pseudo- and all-electron valence eigenstates have the same energies and amplitude (and thus density) outside a chosen core cutoff radius r_c.

The mathematical representation of a norm-conserving pseudo potential looks like

$$V^{PP}(\mathbf{r}, \mathbf{r\prime}) = \left[V_{core}(\mathbf{r}) + \Delta V_{local}(\mathbf{r}) \delta_{\mathbf{r},\mathbf{r\prime}} + \sum_{k,l} P_k^\star(\mathbf{r}) h_{kl} P_l(\mathbf{r\prime}) \right], \tag{2.23}$$

where ΔV_{local} and the projectors P_k are atom centered functions of the form

$$\varphi(\mathbf{r}) = \varphi(|r - \mathbf{R}_I|) Y_{lm}(\theta, \phi), \tag{2.24}$$

been $Y_{lm}(\theta, \phi)$ the spherical harmonics and $\mathbf{R}_I$ atomic positions.
Eq.2.24 expanded in plane waves:

$$\varphi(\mathbf{r}) = \sum_{\mathbf{G}} \varphi(G) e^{i\mathbf{G}\cdot\hat{\mathbf{r}}} S_I(\mathbf{G}) Y_{lm}(\tilde{\theta}, \tilde{\phi}), \tag{2.25}$$

where S_I are the so called structure factors defined as

$$S_I(\mathbf{G}) = e^{-i\mathbf{G}\cdot\mathbf{R}_I}. \tag{2.26}$$

Apart from the norm-conserving pseudo potentials, there are some other kind of pseudo potentials with shorter cutoff radius which are told to be softer, that is more rapidly convergent, but at the same time less transferable, that is less accurate to reproduce realistic features in different environments.

In this project, not soft, but ultra-soft pseudo potentials where used, strictly speaking the Vanderbilt's ultra soft pseudo potentials [32] [33] . This pseudo potentials are told to be tricky to use, but after their accuracy for the analyzed system is proof they offer much shorter cutoffs and thus, much better computational performance.

The cutoff is measured in Rydbergs (Ry) for historical reasons, and it's typical values are over 70 Ry for Norm-Conserving and around 35 for Ultra soft pseudo potentials.

The needed cutoff value can be calculated by representing wave functions (or potentials) for the pseudo potential and it's analogous all-electron system. This can be seen in Fig. 2.2.3, where at certain $\mathbf{r}$'s value ($\mathbf{r}_c$), the wave functions and potentials are overlapped for all electron and pseudo potential.

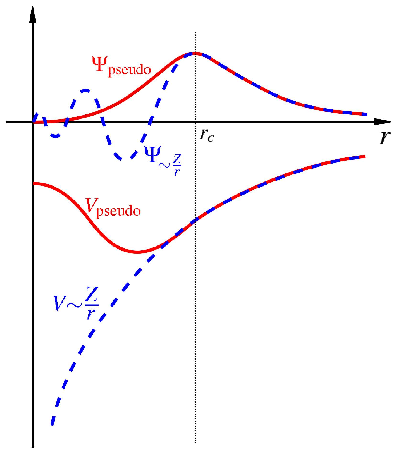

Figure 2.1: *Comparison of a wave function in the Coulomb potential of the nucleus (blue) to the one in the pseudo potential (red). The real and the pseudo wave function and potentials match above a certain cutoff radius* $\mathbf{r}_c$.

Another criteria for searching the cutoff radius, actually the one I used for testing this pseudo potentials, was the convergence of the energy. If we assume our pseudo

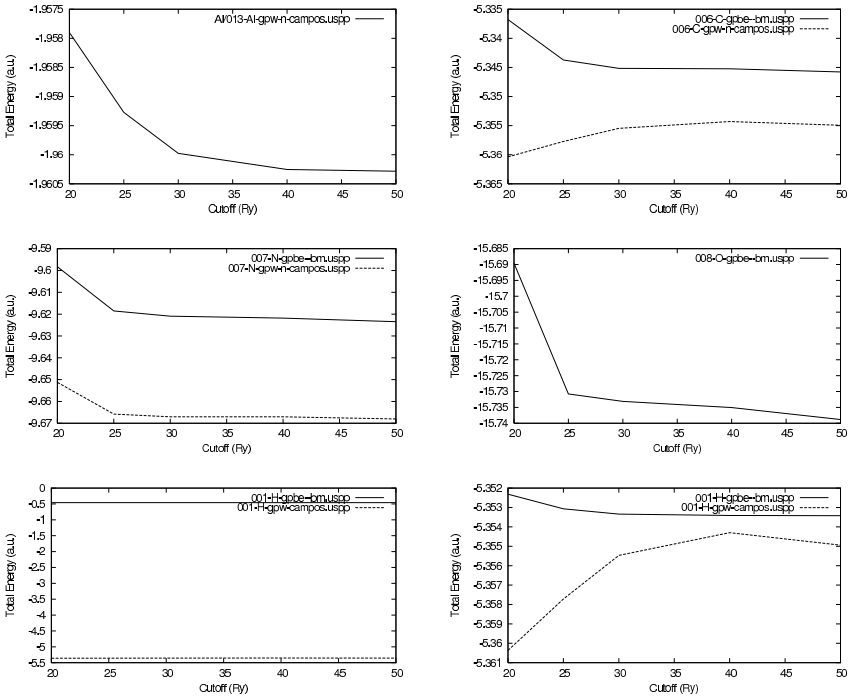

Figure 2.2: *Graphical representation of the total energy vs plane wave cutoff for some Vanderbilt pseudo potentials. Last figure is scaled for appreciate the convergence curve.*

potentials to be "acceptable", they should have a perfect overlap with the all-electron curve at enough large radii. On other hand, the bigger the cutoff is, the bigger computational effort we need, so it is interesting to use as small cutoff as possible, that is, to find the $\mathbf{r}_c$.

This means that it is possible to calculate the total energy of an atom at enough large cutoff, and then recalculate again progressively decreasing the cutoff, and there will be some point where the energy difference with the first point starts to be meaningful (see Fig. 2.2[1]). This will be the cutoff radius.

[1]All this kind of graphics in this thesis were created by using gnuplot [34].

2.2.4 Propagation algorithms

If the forces in a system are known, the accelerations ($\ddot{\mathbf{r}}$) can be calculated and consequently velocities ($\dot{\mathbf{r}}$) and positions $\mathbf{r}$

$$\mathbf{r} = \int \left[\frac{d\mathbf{r}}{dt}\right] dt = \iint \left[\frac{d^2\mathbf{r}}{dt^2}\right] d^2t. \tag{2.27}$$

However, the point in molecular dynamics is to propagate the positions of the atoms and for this task "propagation algorithms", "finite difference methods" or "Integrators" are used. All these algorithms assume the force to be constant during the time step and the positions and the dynamic properties to be approximated by Taylor series expansions [35]:

$$\begin{aligned}
\mathbf{r}(t+\delta t) &= \mathbf{r}(t) + \delta t\dot{\mathbf{r}}(t) + \frac{1}{2}\delta t^2\ddot{\mathbf{r}}(t) + \ldots \\
\dot{\mathbf{r}}(t+\delta t) &= \dot{\mathbf{r}}(t) + \delta t\ddot{\mathbf{r}}(t) + \ldots \\
\ddot{\mathbf{r}}(t+\delta t) &= \ddot{\mathbf{r}}(t) + \ldots
\end{aligned}$$

The simplest way to propagate the system is the Euler's integrator, which is just to apply the previous equations directly. The Verlet algorithm uses the positions and accelerations at time t, and the positions from the previous step ($\mathbf{r}(t-\delta t)$

$$\begin{aligned}
\mathbf{r}(t+\delta t) &= \mathbf{r}(t) + \delta t\dot{\mathbf{r}}(t) + \frac{1}{2}\delta t^2\ddot{\mathbf{r}}(t) + \ldots \\
\mathbf{r}(t-\delta t) &= \mathbf{r}(t) - \delta t\dot{\mathbf{r}}(t) + \frac{1}{2}\delta t^2\ddot{\mathbf{r}}(t) - \ldots
\end{aligned}$$

The Verlet algorithm does not have the velocities explicitly and this can be a problem in some cases. Many variations of Verlet's algorithm have been done, for example the "leap-frog" algorithm:

$$\begin{aligned}
\mathbf{r}(t+\delta t) &= \mathbf{r}(t) + \delta t\dot{\mathbf{r}}(t+\frac{1}{2}\delta t) \\
\dot{\mathbf{r}}(t+\frac{1}{2}\delta t) &= \dot{\mathbf{r}}(t-\frac{1}{2}\delta t) + \delta t\ddot{\mathbf{r}}(t)
\end{aligned} \tag{2.28}$$

The velocity Verlet algorithm method, gives positions, velocities and accelerations at the same time

$$\mathbf{r}(t+\delta t) = \mathbf{r}(t) + \delta t\dot{\mathbf{r}}(t) + \frac{1}{2}\delta t^2\ddot{\mathbf{r}}(t)\dot{\mathbf{r}}(t+\delta t) = \dot{\mathbf{r}}(t+\delta t) + \frac{1}{2}\delta t[\ddot{\mathbf{r}}(t) + \ddot{\mathbf{r}}(t+\delta t).] \tag{2.29}$$

CPMD code uses velocity Verlet algorithm.

2.2.5 Temperature control

In a molecular dynamics simulation, the total kinetic energy of the system tends to fluctuate, and these fluctuations can sometimes bring the particles to some energetic states that might be non desired. When performing molecular dynamics simulations of certain systems, one wants to keep the particles behaving as they would do at some certain temperature. For example, when simulating a biological system, molecules should have a kinetic energy according to the environment, so (as long as we are not specially interested) it does not make sense to perform a protein simulation at 1000K, since it is not possible to find proteins in the nature at this temperature in the nature.

The temperature of the system is directly calculated from

$$\overline{E_k} = \frac{1}{2}\frac{1}{N}\sum_{i=1}^{N} m_i \dot{\mathbf{r}}_i{}^2 = \frac{3}{2}k_B T \rightarrow T = \frac{1}{3Nk_B}\sum_{i=1}^{N} m_i \dot{\mathbf{r}}_i{}^2 \tag{2.30}$$

where $k_B = \frac{R}{N_A}$ being R the ideal gas constant ($8.3144\frac{J}{K.mol}$) and N_A the Avogadro number ($6.022.10^{23}\frac{particles}{mol}$).

There is a way for controlling the fluctuations of the total kinetic energy of the system, and it is called "thermostat".

The simplest way to control the temperature of a simulation is just to fix a temperature (for example 300K) and applying a cutoff interval of $\pm\Delta T$ (for example $\pm 20K$), so that every simulation step, kinetic energy of the nuclei is recalculated and then a simple logical operation is performed:

```
if (T > (300+20)) (T<(300-20))
 then
   {
     RESFACTOR = T(t) / 300
     do i=N
        v(i)= v(i) * sqrt(RESFACTOR) / N
     enddo
   }
endif
```

This way, every time the total kinetic energy of the system yields to a temperature out of the cutoff, the kinetic energy of each particle will be rescaled by the square root of the difference. This method is called "temperature control by rescaling" [36].

There are many other thermostat types which perform a better simulation on the temperature fluctuations by smoothing the rescaling process, for instance, the Nose[37]-Hoover[38] thermostat [39], which will be used in the full solvated simulations.

2.3 Ab-Initio Molecular Dynamics

In section 2.1.1 a first introduction to molecular dynamics trough Newtonian mechanics was made, but from now on, quantum mechanics will rule the behavior of the particles, and there will be also a different kind of mathematical formulation, Lagrangian formulation.

In Lagrangian mechanics, first concept to introduce is the "Lagrangian" itself. The Lagrangian of a system is given by the kinetic energy minus the potential energy

$$\mathcal{L} = \mathcal{T} - \mathcal{V}, \tag{2.31}$$

and under Lagrangian mechanics conditions, if the Lagrangian of the system is known, the equations of motion can be obtained directly by substituting the expression of the Lagrangian into the Euler-Lagrange equation

$$\frac{d}{dt}\left(\frac{\partial \mathcal{L}}{\partial \dot{\mathbf{x}}_i}\right) - \frac{\partial \mathcal{L}}{\partial \mathbf{x}_i} = 0 \quad , \quad i = 1, \ldots, N. \tag{2.32}$$

so that we get an expression as function of the acceleration ($\ddot{\mathbf{R}}$) from where atoms motion can be described via propagation algorithms (see section 2.2.4).

Ab-Initio Quantum Mechanics description of the dynamics, as a difference with the previous one governed by classical (Newtonian) equations, the equations of motion are going to be determined by the time-dependent Schrodinger equation [40]

$$i\hbar\frac{\partial}{\partial t}\Phi(\{\mathbf{r}_i\},\{\mathbf{R}_i\};t) = \mathcal{H}\Phi(\{\mathbf{r}_i\},\{\mathbf{R}_i\};t). \tag{2.33}$$

In this equation one must define a Hamiltonian operator ($\mathcal{H}$) that acts on the particle's wave function (Φ) the same way as the Lagrangian operator acts on the position in the previous section. An standard Hamiltonian operator for a molecular system can be built as the sum of the kinetic and potential energy for nuclei and electrons and a correlation term between nuclei and electrons [41]

$$\begin{aligned}\mathcal{H} &= -\sum_I \frac{\hbar^2}{2M_i}\nabla^2{}_I - \sum_i \frac{\hbar^2}{2m_e}\nabla^2{}_i + \sum_{i<j}\frac{e^2}{|\mathbf{r_i}-\mathbf{r_j}|} + -\sum_{I,i}\frac{e^2 Z_I}{|\mathbf{R_I}-\mathbf{r_i}|} + \sum_{I<J}\frac{e^2 Z_I Z_I}{|\mathbf{R_I}-\mathbf{R_J}|} \\ &= -\sum_I \frac{\hbar^2}{2M_i}\nabla^2{}_I - \sum_i \frac{\hbar^2}{2m_i}\nabla^2{}_i + V_{n-e}(\{\mathbf{r_i}\},\{\mathbf{R_I}\}) \\ &= -\sum_I \frac{\hbar^2}{2M_i}\nabla^2{}_I + \mathcal{H}_e(\{\mathbf{r_i}\},\{\mathbf{R_I}\}). \end{aligned} \tag{2.34}$$

where $\{\mathbf{r_i}\}$ are the electronic and $\{\mathbf{R_I}\}$ the nuclear degrees of freedom respectively.

The wave function Φ, needs to have both nuclear and electronic coordinates separated, and this can be approached in a simple way, just by writing them separately and adding a phase factor, as

$$\Phi(\{\mathbf{r_i}\},\{\mathbf{R_I}\};t) \approx \Psi(\{\mathbf{r_i}\};t)\chi(\{\mathbf{R_I}\};t) exp\left[\frac{i}{\hbar}\int_{t_0}^{t} dt' \tilde{E}_e(t')\right], \tag{2.35}$$

where the nuclear and electronic wave function are separately normalized to unity at every instant of time, i.e. $\langle\chi;t|\chi;t\rangle = 1$ and $\langle\Psi;t|\Psi;t\rangle = 1$, respectively. In addition, a convenient phase factor was introduced as well such that the final equation looks more compact, so that

$$\tilde{E}_e = \int d\mathbf{r} d\mathbf{R} \Psi^*(\{\mathbf{r_i}\};t)\chi^*(\{\mathbf{R_I}\};t)\mathcal{H}_e\Psi(\{\mathbf{r_i}\};t)\chi(\{\mathbf{R_I}\};t),$$

what is known as one determinant or single-configuration ansatz for the total wave function.

This ansatz differs from the Born-Oppenheimer one (excepting the phase factor) in the fact that it separates the fast and slow variables. Born-Oppenheimer ansatz is written as

$$\Phi_{BO}(\{\mathbf{r_i}\},\{\mathbf{R_I}\};t) = \sum_{k=0}^{\infty} \tilde{\Psi}_k(\{\mathbf{r_i}\},\{\mathbf{R_I}\};t)\tilde{\chi}_k(\{\mathbf{R_I}\};\mathbf{t}). \tag{2.36}$$

After introducing the expression 2.34 and 2.35 in the equation 2.33, multiply the left part by $\langle\Psi|$ and $\langle\chi|$ respectively and imposing energy conservation $d\langle\mathcal{H}\rangle/dt \equiv 0$ the result is:

$$i\hbar\frac{\partial\Psi}{\partial t} = -\sum_i \frac{\hbar^2}{2m_e}\nabla^2{}_i\Psi + \left\{\int d\mathbf{R}\chi^*(\{\mathbf{R_I}\};t)V_{n-e}(\{\mathbf{r_i}\},\{\mathbf{R_I}\})\chi(\{i\mathbf{R_I}\,t)\right\}\Psi$$

$$i\hbar\frac{\partial\chi}{\partial t} = -\sum_i \frac{\hbar^2}{2M_I}\nabla^2{}_i\chi\left\{\int d\mathbf{r}\Psi^*(\{\mathbf{r_i}\};t)\mathcal{H}_e(\{\mathbf{r_i}\},\{\mathbf{R_I}\})\Psi(\{\mathbf{r_i}\};t)\right\}\chi$$

what defines the basis of the time-dependent self-consistent field (TDSCF), because both electrons and nuclei move quantum-mechanically in time-dependent effective potentials (or self-consistently obtained average fields).

At this point, an approximation is needed in order to describe nuclei as classical particles. This is achieved by rewriting the nuclear wave function

$$\chi(\{\mathbf{R_i}\};t) = A(\{\mathbf{R_I}\};t)e^{\left[\frac{iS(\{\mathbf{R_I}\};t)}{\hbar}\right]} \tag{2.37}$$

in terms of amplitude factor A and phase S. So introducing this new ansatz for the nuclear wave function in TDSCF equation 2.37

$$\frac{\partial S}{\partial t} + \sum_I \frac{1}{2M_I}(\nabla_I S)^2 + \int d\mathbf{r}\Psi^*\mathcal{H}_e\Psi = \hbar^2\sum_I \frac{1}{2M_I}\frac{\nabla_I^2 A}{A} \tag{2.38}$$

$$\frac{\partial A}{\partial t} + \sum_I \frac{1}{M_I}(\nabla_I S) + \sum_I \frac{1}{2M_I}A(\nabla_I^2 S) = 0 \tag{2.39}$$

we get what is known as "quantum fluid dynamical representation" from where time-dependent Schrödinger equation can be solved. If the classical limit is taken as $\hbar \to 0$ the term on the right of the eq. 2.38 disappears, hence

$$\frac{\partial S}{\partial t} + \sum_I \frac{1}{2M_I}(\nabla_I S)^2 + \int d\mathbf{r}\Psi^*\mathcal{H}_e\Psi = 0$$

which it looks like the Hamilton-Jacobi formulation

$$\Psi = \frac{\partial S}{\partial t} + \mathcal{H}(\{\mathbf{R}\}_\mathbf{I},\{\nabla_\mathbf{I}\mathbf{S}\}) = \mathbf{0}$$

of classical dynamics with classical Hamilton function

$$\mathcal{H}(\{\mathbf{R}\}_I,\{\mathbf{P}\}_I) = T(\{\mathbf{P}\}_I) + V(\{\mathbf{P}\}_I)$$

where $\mathbf{P} \equiv \nabla_I S$ and the Newtonian equation of motion corresponding to eq. 2.38

$$\frac{d\mathbf{P_I}}{dt} = -\nabla_I \int dt\Psi^*\mathcal{H}_e\Psi$$

or written in another way

$$\begin{aligned} M_I\ddot{\mathbf{R}}_\mathbf{I}(t) &= -\nabla_I \int d\mathbf{r}\Psi^*\mathcal{H}_e\Psi \\ &\quad -\nabla_I V_e^E(\{\mathbf{R_I}\}(t)), \end{aligned} \tag{2.40}$$

so, nuclei move according to classical mechanics in an effective potential V_e^E due to the electrons. This effective potential can be developed starting from eq. 2.37 so that

$$V_e^E = \int d\mathbf{r}\Psi_0^*\mathcal{H}_e\Psi_0 \equiv E_0(\{\mathbf{R_I}\}) \tag{2.41}$$

and the nuclei will move under it. The potential in eq. 2.41 can be computed from the time-independent Schrödinger equation, which is usually approached in terms of truncated expansion of many-body contributions

$$V_e^E \approx V_e^{approx}(\{\mathbf{R_i}\}) = \sum_{I=1}^{N} v_1(\mathbf{R_I}) + \sum_{I<J}^{N} v_2(\mathbf{R_I},\mathbf{R_J}) + \sum_{I<J<K}^{N} v_3(\mathbf{R_I},\mathbf{R_J},\mathbf{R_K}) + \ldots$$

2.3.1 Born-Oppenheimer Molecular Dynamics

Born-Oppenheimer approach uses classical equations to describe the nuclei and adds the electronic structure by solving statically (time-independent) Schrödinger equation for each time step [42]. The resulting molecular dynamics method is defined by

$$M_I\ddot{\mathbf{R}}_I(t) = -\nabla_I min_{\{\Psi_0\}}\{\langle\Psi_0|\mathcal{H}_e|\Psi_0\rangle\} \tag{2.42}$$

$$E_0\Psi_0 = \mathcal{H}_e\Psi_0. \tag{2.43}$$

So the electronic ground state has to be reached every step. After applying Hartree-Fock approximation

$$\begin{aligned} M_I\ddot{\mathbf{R}}_I(t) &= -\nabla_I min_{\{\psi_i\}}\langle\Psi_0|\mathcal{H}_e^{HF}|\Psi_0\rangle \\ 0 &= -\mathcal{H}_e^{HF}\psi_i + \textstyle\sum_i \Lambda_{i,j}\psi_j. \end{aligned} \tag{2.44}$$

This can be also written according to Lagrange's formalism

$$\mathcal{L} = -\langle\Psi_0|\mathcal{H}_e|\Psi_0\rangle + \sum_{i,j}\Lambda_{i,j}(\langle\psi_i|\psi_j\rangle - \delta_{i,j}), \tag{2.45}$$

where Λ_ij are the associated Lagrangian multipliers. And deriving this Lagrangian with respect to the orbitals

$$\frac{\delta \mathcal{L}}{\delta \psi_i^*} = 0$$

leads to Hartree-Fock equations

$$\mathcal{H}_e^{HF} \psi_i = \sum_j \Lambda_{ij} \psi_j.$$

2.3.2 Car-Parrinello molecular dynamics

Car-Parrinello method proposes a special Lagrangian for the motion of the nuclei, which in addition to the terms of potential energy and constraints in eq. 2.45 contains also two terms for the kinetic energy of nuclei and electrons [43]. This last one is described in a pseudo-classical way by using a "fictitious" mass μ term for the electrons and a time derivative of the electronic wave functions for describe some kind of "velocity"

$$\mathcal{L}_{CP} = \sum_i \frac{1}{2} \mu_i \left\langle \dot{\psi}_i | \dot{\psi}_i \right\rangle + \sum_i \frac{1}{2} M_i \dot{\mathbf{R}}_\mathbf{i}^2 - \langle \Psi_0 | \mathcal{H}_e | \Psi_0 \rangle + \sum_{i,j} \Lambda_{i,j} \left(\langle \psi_i | \psi_i \rangle - \delta_{i,j} \right). \quad (2.46)$$

In the same way as in the classical model, the Newtonian equations of motion can be obtained by Euler-Lagrange equation (Eq. 2.32)

$$\begin{array}{c} \frac{d}{dt} \left(\frac{\partial \mathcal{L}_{CP}}{\partial \dot{\mathbf{R}}_i} \right) - \frac{\partial \mathcal{L}_{CP}}{\partial \mathbf{R}_i} = 0 \\ \frac{d}{dt} \left(\frac{\partial \mathcal{L}_{CP}}{\partial \dot{\psi}_i^*} \right) - \frac{\partial \mathcal{L}_{CP}}{\partial \psi_i^*} = 0 \end{array} \quad (2.47)$$

and after solving and applying Hartree-Fock approximation, the Car-Parrinello equations of motion are

$$\begin{array}{c} M_I \ddot{\mathbf{R}}_I(t) = -\frac{\delta E}{\delta \mathbf{R_I}} \\ \mu_i \ddot{\psi}_i(t) = -\frac{\delta E}{\delta \psi_i^*} + \sum_i \Lambda_{i,j} \psi_j \end{array} \quad (2.48)$$

which at variance with eq. 2.45 does not need to reach the ground state every step.

In order to solve the 2^{nd} and 3^{rd} terms in eq. 2.46 it is necessary to solve the electronic Schrödinger equation [40] but this becomes too expensive so it is necessary to make approximations and one of the main ones is given by the Density Functional Theory.

2.4 Analysis tools

In the following section there will be a little introduction to some of the concepts that are going to be discussed when presenting the results, as well as some of the tools for getting them.

2.4.1 Wannier Functions

The Wannier functions are an alternative to the plane wave basis set for periodic calculations with the advantage that can be exponentially localized under certain circumstances [44] [42]. These functions are normally obtained by unitary transformation of the Bloch orbitals

$$\Psi(\mathbf{r}) = \Psi_i(\mathbf{r}, \mathbf{k}) = e^{i\mathbf{k}\cdot\mathbf{r}} u_i(\mathbf{r}, \mathbf{k}) \tag{2.49}$$

where $\mathbf{k}$ is a vector in the first Brillouin zone and the $u_i(\mathbf{r}, \mathbf{k})$

$$u_i(\mathbf{r}, \mathbf{k}) = u_i(\mathbf{r} + \mathbf{L}, \mathbf{k}) \tag{2.50}$$

where L are the direct lattice vectors.

The so called maximally localized generalized Wannier functions are the periodic analogues of Boys localized orbitals defined for isolated systems.

In the practice, Wannier functions are just something that will allow us to know where the bond centers are located. They can be directly calculated with the CPMD package.

2.4.2 Energies and temperature

The total energy is calculated in CPMD as the sum of kinetic, external (local and non-local pseudo potential), exchange and correlation and electrostatic energy

$$E_{total} = E_{kin} + E^{PP}_{local} + E^{PP}_{nonlocal} + E_{XC} + E_{ES}, \tag{2.51}$$

where

$$E_{kin} = \sum_{\mathbf{k}} w_{\mathbf{k}} \sum_{i} \sum_{\mathbf{G}} \frac{1}{2} f_i(\mathbf{k}|\mathbf{G}+\mathbf{k}|^2 |c_i(\mathbf{G},\mathbf{k})|^2 \tag{2.52}$$

$$E^{PP}_{local} = \sum_{I} \sum_{\mathbf{G}} \Delta V^{I}_{local}(\mathbf{G}) S_I(\mathbf{G}) \rho^{\star}(\mathbf{G}) \tag{2.53}$$

$$E^{PP}_{nonlocal} = \sum_{\mathbf{k}} w_{\mathbf{k}} \sum_{i} f_i(\mathbf{k}) \sum_{I} \sum_{\alpha,\beta \in I} (F^{\alpha}_{I,i}(\mathbf{k}))^{\star} h^{I}_{\alpha\beta} F^{\beta}_{I,i}(\mathbf{k}) \tag{2.54}$$

$$E_{XC} = \omega \sum_{\mathbf{G}} \varphi_{XC}(\mathbf{G}) \rho^{\star}(\mathbf{G}) \tag{2.55}$$

$$E_{ES} = 2\pi\omega \sum_{\mathbf{G}\neq 0} \frac{|n_{tot}(\mathbf{G})|^2}{G^2} + E_{ovrl} + E_{self}. \tag{2.56}$$

The temperature of the system is straightforwardly calculated from

$$\overline{E_k} = \frac{1}{2}\frac{1}{N}\sum_{i=1}^{N} m_i \dot{\mathbf{r}}_i^{\,2} = \frac{3}{2}kT \rightarrow T = \frac{1}{3Nk}\sum_{i=1}^{N} m_i \dot{\mathbf{r}}_i^{\,2} \tag{2.57}$$

where $k = \frac{R}{N_A}$ being R the ideal gas constant ($8.3144 \frac{J}{K.mol}$) and N_A the Avogadro number ($6.022.10^{23} \frac{particles}{mol}$).

2.4.3 Free energies

Usually the free energies in ab-initio molecular dynamics world are calculated by complex methods such as meta-dynamics, but in this project, the calculation of free energy was done by an approximation based on statistical mechanics [45].

Since our systems use canonical ensemble (NVT), the free energy "type" easiest to calculate is the Helmholtz free energy (A), which can be defined as

$$A = \langle E \rangle - TS = -k_B T \ln Z, \tag{2.58}$$

where $\langle E \rangle = U$ is the total energy, S entropy, k_B Boltzmann's constant and Z the partition function, which in our canonical ensemble is defined as

$$Z = \sum_{j} e^{-\beta E_j}, \tag{2.59}$$

and the so called "inverse temperature" $\beta = \frac{1}{k_B T}$.

Now our approach for calculating the Helmholtz energy from a molecular dynamics simulation.

We could approach Z as the total number of states in "j".

Let the distance between to atoms r be our mono-dimensional reaction coordinate partitioned at each Δr steps. Let the "j" be the number of states (or total number or times we find distance r) inside Δr.

Then we can plot an histogram counting how many times our only variable (the distance between the two atoms) is found on each interval (see Fig. 2.4.3).

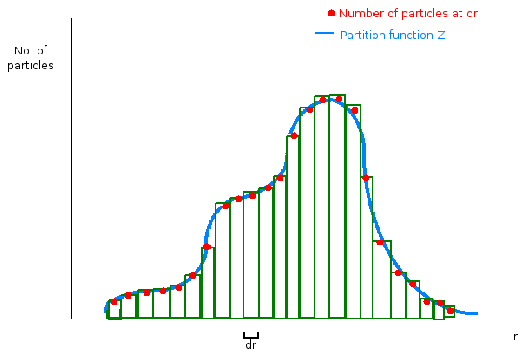

Figure 2.3: *Histogram counting how many times we find distance r at Δr.*

So that we can introduce this partition function into Helmhotz energy equation 2.58 and we can plot another graphic, this time Helmholtz energy (A) versus r.

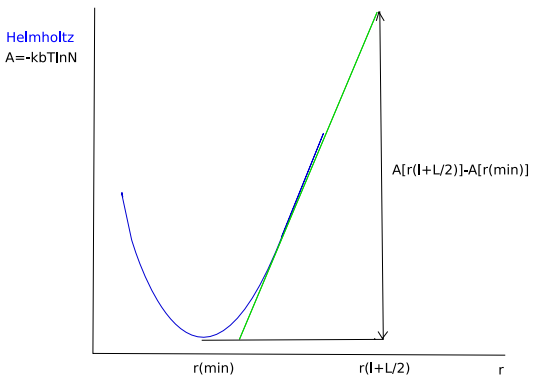

Figure 2.4: *Helmhotz free energy profile around coordinate r. The graphic shows a minimum for the free energy at r_{min}.*

By using the graphic 2.4.3 we are able to calculate i.e. the solvation or binding energies, by measuring the energy difference between the total minimum and the

energy at target distance (infinite for binding). Since we are using PBC, the infinite distance can be approached to be half of the distance of the simulation cell $r = \frac{L}{2}$ further away and the energy we need to separate these two particles will be given by the energy difference at these two points (on other hand pushing the integration beyond the half of the lattice distance would cause the atom to interact with it's own periodic replica).

On other hand, in nature, aromatic amino acid-aluminum interactions occur in a non isolated environment so that the binding energies will depend not only on the closer atoms, but also on the long-range interactions with the solvent. This could be compared to the Madelung constant in crystal. There are many practical methods for calculating Madelung's constant, CPMD [31] uses does it by integral transforms, through the Ewald method [46].

Therefore the Helmholtz free energies for our biological systems are going to be calculated just for the cases of full solvation environments.

In this project, the calculation of Helmholtz free energies was performed by using a self made code, freely available at writer's site.

2.4.4 Radial Distribution Functions

Radial Distribution Function (RDF) is the term called for naming the density of inter-atomic distances in a material.

This distribution can be calculated experimentally from physical measurements like light scattering or x-ray powder diffraction.

Computationally an RDF can be obtained by using statistical mechanics from

$$g_{AB} = \frac{V}{N_B}\frac{1}{N_A}\left\langle \sum_{i}^{N_A}\sum_{ij}^{N_B} \frac{\delta(\mathbf{r}-\mathbf{r}_{ij})}{4\pi\mathbf{r}^2} \right\rangle, \tag{2.60}$$

where N are the number of atoms of type A and B and δ is the Dirac delta function.

In the practise, a RDF can be graphically represented (RDF vs $|\mathbf{r}|$) and it will show some peaks or bands at the bond distances between the two atoms (or atom types). Said in a simpler way, taking a vertical line, the higher the line is, the more atoms there are just at this $\mathbf{r}$ distance.

According to eq. 2.60 the area under the "g vs r" curve gives the total number of particles A and B, and partitioning this curve in intervals, it is possible to get the averaged total number of particles at this distance or said in another words, the coordination numbers.

The coordination number or number of neighbors to certain volume ΔV, is given by the integration of the pair correlation function $G_{ij}(\mathbf{r}$ over the three spatial coor-

dinates in spherical coordinates r, φ and θ

$$n_{ij}(\Delta V) = \rho_j \int_{r_i}^{r_f} \int_{\varphi_i}^{\varphi_f} \int_{\theta_i}^{\theta_f} G_{ij}(\mathbf{r}) r^2 \sin\theta d\theta d\varphi dr. \tag{2.61}$$

where, ρ_j is the number density of j.

Figure 2.4.4 shows an example of RDF and it's integral. First peak of RDF at around 3 Åtells us that from the aluminum atom, the closest oxygen atoms are located to 3 $\AA$, which corresponds to the first solvation layer, second peak at around 3.4 Åcorresponds to the second water in the carbonyl group and the band around 4 $\AA$ describes the second solvation shell. Dashed line in Fig. 2.4.4 shows the integral of the RDF and grows up to first step at the distance corresponding to the first solvation layer. Second solvation layer is not very clear but a second step can be appreciated.

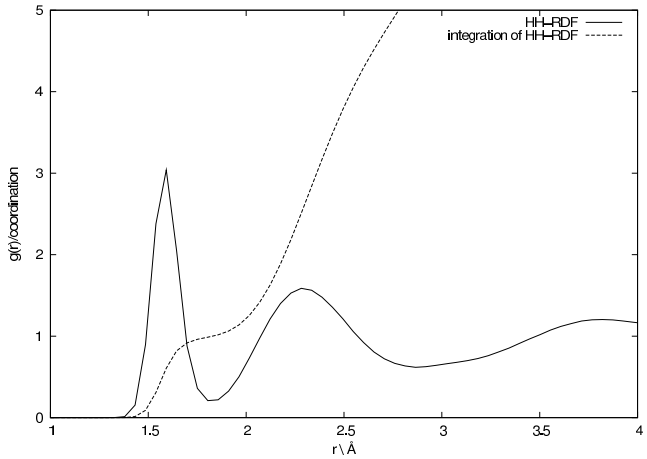

Figure 2.5: *HH-RDF, from a simulation with tyrosine, 50 water molecules and an aluminum atom. Solid line describes the RDF and dashed line the integral. RDF says there are H atoms at the distances of 1.6 and 2.3 Å and the integration says that there are one atom at 1.6 (the other H bonded to the same O) and between 2 and 3 atoms around 2.3 Å distance (behind the H bond).*

The RDFs on this project were calculated by using a self modified code initially written by Prof. Kari Laasonen's group in Oulu.

2.4.5 Diffusion

During a molecular dynamics simulation, atoms move, and the positions at the beginning of the simulation are not the same as the ones in the last point. This phenomena is called diffusion. The diffusion can be measured by the Mean Square Displacement

(MSD) or the diffusion coefficient.

The MSD can be directly calculated from it's definition

$$MSD = \left\langle |\mathbf{R}(t) + \mathbf{R}(0)|^2 \right\rangle, \tag{2.62}$$

and the diffusion constant

$$D = \lim_{t\to\infty} \frac{\left\langle |\mathbf{R}(t) + \mathbf{R}(0)|^2 \right\rangle}{6t}. \tag{2.63}$$

Our simulations are performed in vacuum, so the translation of the whole system does not affect at all, and on other hand, the energies are calculated in internal coordinates so that the rotational and vibrational degrees of freedom depend only on the internal parameters.

For the simulations on this theses, the diffusion can show how the mass center of the system is behaving.

Chapter 3

Background research on AAAs and Al^{+3}

Cation-π interactions were found to be specially interesting in chemistry and biology due to their surprisingly strong nature and their role in protein structure stabilization [25].

This project is aimed to understand the effect of Al in amino acids, but before introducing any results it is convenient to introduce a few previously performed researches around the topic.

3.1 Solvation of Al^{+3} in water

Since in this project cation-π interactions are going to be studied between aromatic amino acids and aluminum, it is interesting to know about the behavior of Al^{+3} in a biological environment. So first approximation is to understand the behavior of Al^{+3} in bulk water, but this work has been already done, by Thomas W. Swaddle et al.[47] or Takashi Ikeda et al.[48], trough detailed CPMD studies showing all possible conformations.

According to these studies, the coordination of the Al^{+3} in bulk water changes depending on the pH of the solution. In solutions with pH under 3.0, Al^{+3} is six-coordinated, so the first solvation layer is octahedral. Solutions with pH over 7 are clearly four-coordinated, with tetrahedral conformation and there is also the evidence of five-coordinated aluminum at pH around 5 [47] [49] which will be well described in this work. The heptacoordination is impossible in any case due to geometrical restrains [50].

At microscopic scale, a connection between coordination number and pH can be done trough the presence of -OH groups on first solvation layer [51], so that $[Al(H_2O)_6]^{+3}$ is hexacoordinated and $[Al(OH)_4]^{-}$ is tetracoordinated.

There is also a two-way connection between Al^{+3}'s charge neutralization trough -OH ligands and the coordination number.

In fact, for the very similar case of the Mg^{+2} cation, Kluge et al. [52] found out that the substitution of a -OH instead of-OH_2 can trigger a coordination number reduction from 6 to 5 on Mg^{+2} and from 5 to 4 for the case of two -OH ligands.

About the structure of the water Al^{+3} complexes, just say that from a simple model many distances and angles could be measured, then same for different acidity states, temperatures, theory levels... [53]. In this work just a few of them will be taken into account, just the ones that will help us understanding the phenomena we are studying. Two of these distances are the Al-O distances to the first and second solvation layers, which have been found to be 1.9 and 3.9 Å in average [54], agreeing with our calculations.

Figure 3.1 shows an estimation of the solvation layers parameters after a geometry optimization[1]. First solvation layer is shown as octahedral coordination, with the maximum coordination (6 waters), and the second coordination is shown with just some of the possible waters (remember that it is liquid state, not crystal).

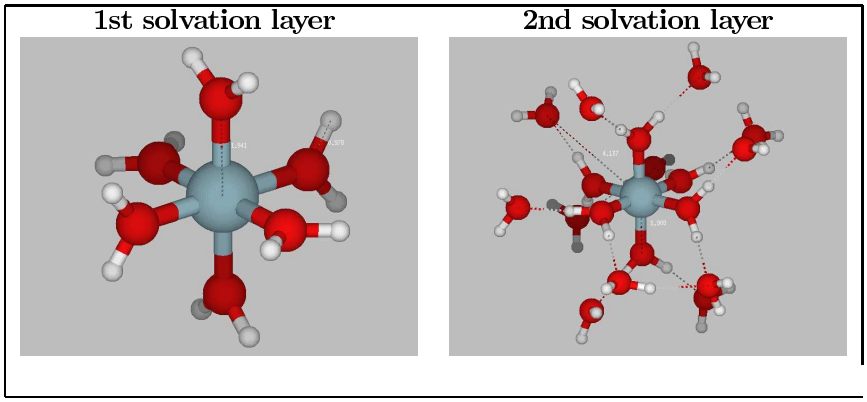

Figure 3.1: *First and first two solvation layers around Al^{+3} from a B3LYP/6-31++G(d,p) geometry optimization with Gaussian 03 [55].*

3.2 Al^{+3} with AAA

The systems that are going to be studied in this project consist of aromatic amino acids with aluminum, so at least one of the ligands in the first coordination shell of Al^{+3} is going to be part of the amino acid.

[1]Geometry optimization with "Gaussian 03" [55] at B3LYP/6-31++G(d,p). Figures generated with molden [56].

Before starting the simulation, proper initial structures must be chosen, and it is specially interesting to find the place where Al^{+3} gets better stabilized, since it will be the most probable binding site for the Al^{+3} in the reality. Before starting to create our initial structures, one must get an idea of how the charge is distributed at isolated amino acids.

There is an issue to take into account when modelling these amino acids: naked amino acids in gas phase and pure water solution have been found to have charge solvated conformation [57] [58] [59], while our simulations show three different charge distributions:

- Charge Solvated (**CS**): nominal or un-ionized form, uniform charge distribution. Usually this means that there is an -NH_2 and a -COOH group.
- Zwitterionic (**ZW**): although the total charge remains neutral, there are formal positive and negative charges on different atoms. Zwitterionic amino acids, usually have -COO^- and -NH_3^+.
- Inverse Zwitterionic (**IZW**): strictly speaking this case could be a particular case of Zwitterionic charge distribution, but keeping the charged atoms and switching their sing. This means that the nitrogen has negative charge and the -COO group positive (check Fig. 3.2). This case occurs due to high polarization on the nitrogen produced by the cation (Al^{+3}).

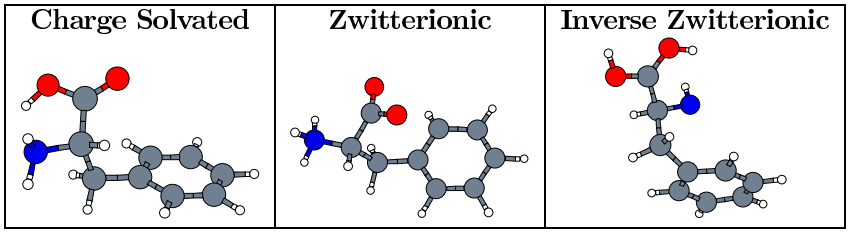

Figure 3.2: *Different charge distributions on amino acids (Figures by xmakemol [60]).*

An initial guess for the location of the Al^{+3} in the amino acid could be found by checking how the electrostatic charge is distributed trough isodensity maps, so that Al^{+3} could be first assumed to bind to the site with higher negative charge density. Figure 3.3 gives an idea of howthe electrostatic potential is distributed.

According to these maps, most probable binding sites would be around the amino (-NH_2) and the carbonyl (-COOH) groups.

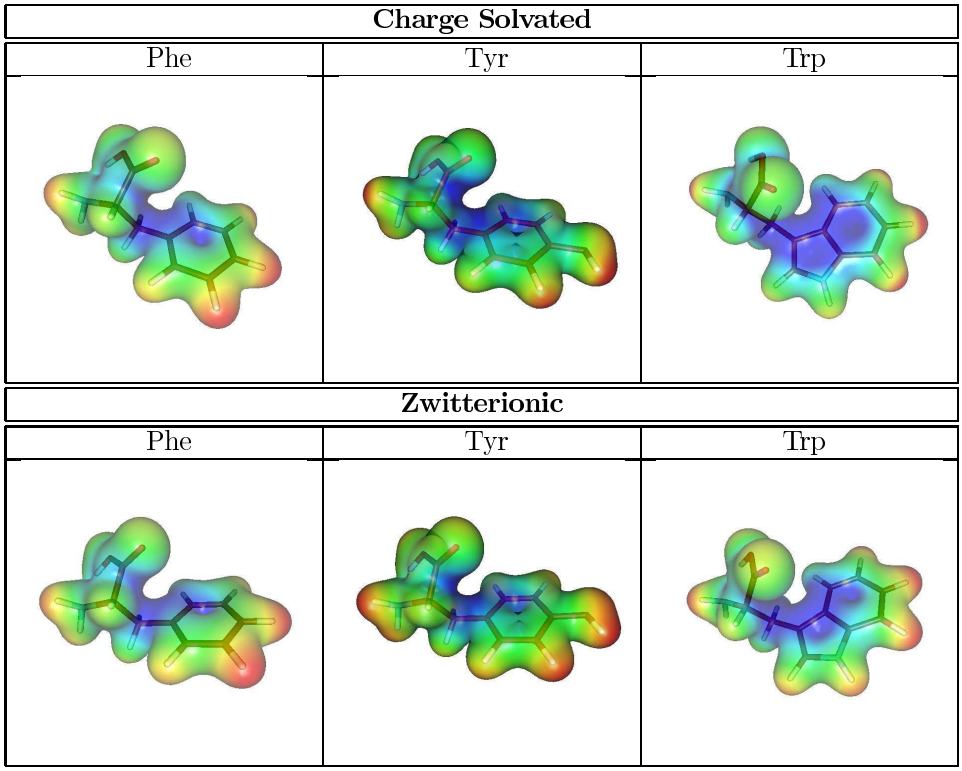

Figure 3.3: *Colorcoded electrostatic potential obtained from the isodensity surfaces for the naked aromatic amino acids in charge solvated and Zwitterionic conformations. Blue is negative, green neutral and red positive.*

On other hand, the importance of cation-π interactions must be taken into account due to their strong nature [25], and the study of possible interactions of the Al^{+3} cation will be focused not only to the amino and carbonyl groups, but also to the aromatic ring.

These ideas were merged to the ones found in the literature of computational [61] [62] and experimental [63] researches in order to find optimum starting geometries.

In addition, in most of the MD simulations, the number of -OH_2 ligands around Al^{+3} remains constant [64] and there is not any water exchange between first and second solvation layers.

The lifetime of the Al-O bond is much longer than the few tens of ps we can afford in our CPMD simulations with the current computational infrastructure, and

therefore, there will not be any water exchange between first and second solvation shells around Al^{+3}.

Chapter 4

Al^{+3} in solution: a detailed description of the solvation layers

Aluminum is one of the most ubiquitous elements in the earth. Since its isolation in 1825, aluminum has found many technological uses, and therefore its presence in our environments has became quite common.

Understanding the structure and dynamics of the water molecule in the hydration shells of ions is essential in order to make an interpretation of many chemical processes in aqueous solutions.

This chapter is aimed to research the behavior in the different solvation shells around Al^{+3} in order to understand it's effect on the amino acids.

The environment around Al^{+3} was studied by performing different static and dynamic calculations.

First of all, the first solvation shell was pictured by static calculations, in order to get reference structural data and then CPMD [31] molecular dynamics simulations were performed on different systems with an Al^{+3} cation and a relatively high number of solvating water molecules for a proper simulation of a real system.

Most of the researches in aluminum's solvation layers have been performed statically and/or using the isolated gas phase idea and assuming the aluminum to have the $Al(H_2O)_m(OH)_n^{3-n}$ form, as one could initially guess from a chemical point of view [65][66][67].

In the calculations of this chapter surrounding waters were kept as H_2O and molecular dynamics simulations will show that the gas phase approach does not necessarily have to occur in water solution.

4.1 1^{st} and 2^{nd} Solvation layers around Al^{+3}

4.1.1 Static calculations

Since attraction force of the Al^{+3} cation towards surrounding lingads is fixed, the distance of the first and second solvation shells is going to be dependent mostly on the number of neighbors at each shell.

In order to compare the results of the RDF data, some static calculations were performed. The figures and data in table 4.1.1 were obtained by geometry optimization with Gaussian 03 [55] at B3LYP/6-311++G(d,p). Initial configurations were created for Al^{+3} with one to seven waters. The case of seven waters is not considered here since the geometry optimization yields one of the waters directly to the second solvation layer, as could be expected [50], keeping the structure as the case of hexacoodination with a water molecule in the second solvation layer.

Taking a first look to the data, as one could guess, the Al-O bond length increases while adding water molecules to the solvation shell, but on other hand, as while sharing the Al^{+3}'s charge each oxygen feels an smaller attraction to the aluminum, the more waters around aluminum the more each oxygen will attract it's hydrogens (these phenomena can be seen in Fig. 4.1).

The rest of the data does not have any clear tendency, except the O-Al-O angle that will decrease for obvious geometric reasons.

	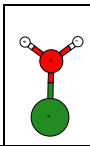	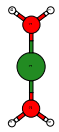	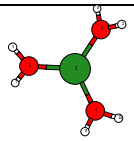	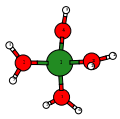	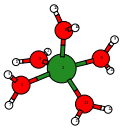	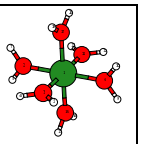
n	1	2	3	4	5	6
r_{AlO}	1.76	1.76	1.79	1.83	1.87-1.93	1.91-1.96
r_{OH}	1.02	1.00	0.99	0.98	0.79-0.81	0.97
r_{AlH}	2.50	2.50	2.52	2.54-2.55	2.58-2.65	2.63-2.64
α_{HOH}	107.5	106.3	106.3	106.3-106.4	106-107	106-107
α_{OAlO}		179.9	119.8	107.8-110.0	94,110,139,170	89-90

Table 4.1: *Different parameters for Al^{+3} + nH_2O complexes: r_{AlO} increases with the ammount of surounding waters while r_{OH} decreases.*

4.1.2 Radial Distribution Functions

After an initial guess trough static calculations a better conformational space sampling will be done trough molecular dynamics.

Molecular Dynamics simulations were performed by following the Car-Parrinello molecular dynamics method [43] trough the CPMD [31] package. Total temperature of the system was set to 300 K by using Nose[37]-Hoover[38] thermostat [39].

Atoms were described trough DFT by using PBE density functional [29] and Vanderbilt ultrasoft pseudopotentials [32] implemented [33] for CPMD [68], with 30 Ry. plane wave cutoff. Electronic fictitious mass (μ) was set at 900 a.m.u. with a time step of 7 a.u.

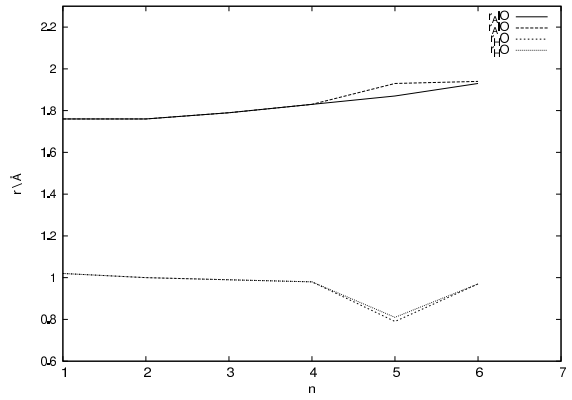

Figure 4.1: *$r_{Al^{+3}O}$ and r_{OH} for different coordination numbers (n) from 1 to 6. $r_{Al^{+3}O}$ decreases the higher the coordination is while r_{OH} decreases.*

Hydrogens (protiums) were substituted by deuteriums in order to be able to increase the usable time step lenght, as the experimental properties of heavy water are well-known and the chemistry will nevertheless be the same. The behavior of the deuterium was compared to the one in experimental results trough their RDFs showing very similar values [69].

Total charge of the system (+3 due to Al^{+3}'s charge) was neutralized by using jellium [70][71]. Simulations were ran for over 100 ps for increase the quality of the statistics, and the main values for the ion displacement were 22.62 (n=4), 28.84 (n=5) and 35.61 (n=6) showing acceptable stability of the system during the simulations.

The size of the simulation cell was calculated so that the density is equals to the density of water, so 1 gr per cubic centimeter. For dealing with atomic units, an equation can be easily developed:

$$density = 1 \frac{\cancel{gr}}{\cancel{cm^3}} \times \frac{6.022.10^{23}\ a.m.u.}{1\ \cancel{gr}} \times \frac{1\ \cancel{cm^3}}{10^{-24}\ \mathring{A}^3} = 6.022.10^{-1}\ \frac{a.m.u.}{\mathring{A}^3} \tag{4.1}$$

$$L = \sqrt[3]{\frac{total\ mass}{density}} = \sqrt[3]{\frac{\sum n_{atoms} \times M_{molar\ weigh}}{0.06022}}$$

In our cases, the lattice parameter for a cubic simulation box was set to 12.62 Å.

The simulated systems had the same number of atoms and size but different initial structures. Three different initial structures were created were the Al^{+3} cation was tetra, pentra and hexa-coordinated. Radial distribution functions were calculated from around 100 ps trajectories and in the case of the pentacoordinated, the final

trajectory part when Al^{+3} got hexacoordinated was neglected. An attempt was made in order to simulate tri- and heptacoordinated Al^{+3} but systems fell down to tetra- and hexacoordinated inmediately, during initial geometry optimization.

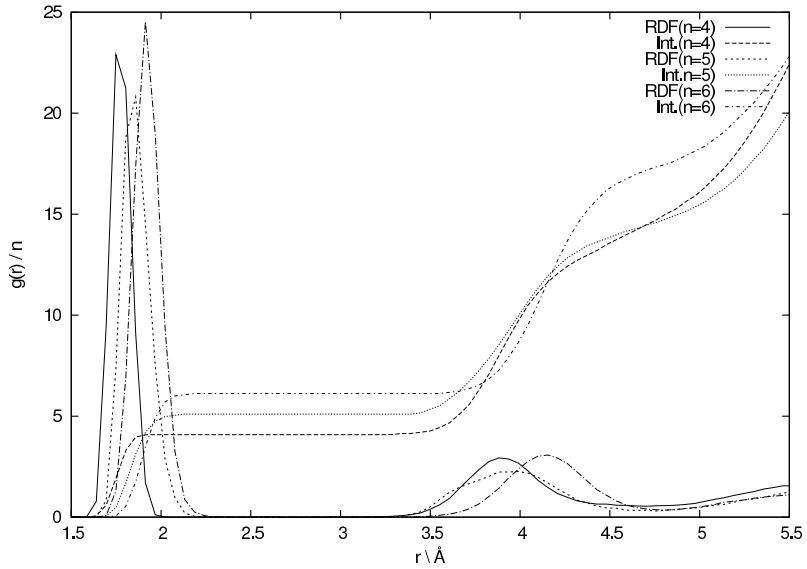

Figure 4.2: *g_{AlO} and corresponding integrals of full solvated (50 H_2O) simulations on Al^{+3} with different coordination numbers (4 to 6).*

If we take a look to the shapes of the RDFs in Fig. 4.3, the influence of the coordination on the bond distance is clear due to three shifted lines.

A more detailed view of the first peak (Fig. 4.3 **a)**) shows the Al-O distances for the first coordination shell. In the case of tetracoordination, the first peak show some kind of chamfer due to the different kind of oxygens, so the edge located to the left describe some -OH oxygen and the edge located more to the right (slightly larger bond distance) describe the oxygens from water molecules. This effect was mostly observed just on tetra- and pentacoordination, therefore the presence of -OH was observed just in the tetra- and penta-coordinated systems.

As shown in the RDF, tetracoordinated structure shows the -**O**H edge at 1.74 Å and -**O**H_2 at 1.80 Å.

The first solvation layer for pentacoordinated system shows an edge for -**O**H at 1.80 Å and the one for -**O**H_2 at 1.86 Å. A difference in the height of the first and second edges between tetra- and pentacoordinated systems can be observed, and as the height of the RDF is proportional to the population, tetracoordinated has more -OH gruops than -OH_2s and just the opposite for the pentacoordinated, which has

more waters instead of -OHs.

The reason for the existence of -OH ligands at tetra- and pentacoordination is because the charge of Al^{+3} is much higher than the sum of the contributions of all suronding neutral/polarized waters together, so it needs to ionize one/some of them.

For hexacoordination, there is no clear evidence of the presence of stable -OH ligands and the oxygens in the $-OH_2$ ligands appear to be at 1.93 Å.

These results happen to be slightly lower than the distances in table 4.1.1 (1.83, 1.87-1.93, 1.91-1.97 Å) due to the deprotonation of the waters during the simulations.

Previous calculations have shown that an -OH instead of$-OH_2$ can trigger a coordination number reduction from 6 to 5 on Mg^{+2} and from 5 to 4 for the case of two -OH ligands [52].

In comparison with data from other structural studies for hexacoordination with Gaussian 03 [55] at B3LYP/6-31+G** [54], the first solvation layer would be located to 1.92 Å and the second to 3.98 Å, slightly higher than the obtained ones.

Solvation layer	1^{st}	2^{nd}
G03	1.93-1.94	3.96
RDF	1.91-1-96	4.14
Ref.[54]	1.92	3.97-3.99
Ref.[72]	1.94	4.08-4.12
Ref.[73]	1.85-2.0	4.01
Ref.[74] (Exp)	1.87-1.90	
Ref.[74][75][76](Exp)		4.01-4.15

Table 4.2: *Comparison of Al-O distances in hexa-coordinated systems obtained with different methods.*

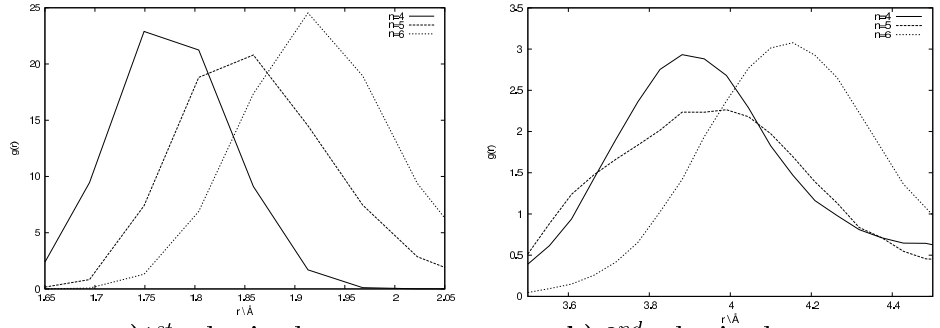

a)1^{st} solvation layer **b)** 2^{nd} solvation layer

Figure 4.3: *Detailed view of g_{OAl} peaks concerning to 1^{st} and 2^{nd} solvation layers of full solvated Al^{+3} with different coordination numbers.*

	r_{AlO} (Å)	
Layer	1^{st}	2^{nd}
n=4	1.75-1.80	3.87
n=5	1.85	3.99
n=6	1.91	4.15

Table 4.3: *Description of the first and second solvation layers around Al^{+3} trough Al-O distances for three different coordination numbers obtained from RDFs.*

A clear influence of the coordination was found also in the case of the aluminum-hydrogen distance (Fig. 4.4 **a)**), showing a similar behavior to the one observed for the aluminum-oxygen distance. Peaks are located at 2.51 (n=4), 2.57 (n=5) and 2.62 Å(n=6) for the hydrogens in first solvation shell and compared with the data in table 4.1.1 (2.54-2.55, 2.58-2.65 and 2.63-2.64) values are a little bit lower, probably due to the use of deuteriums instead of hydrogens.

In contrast with penta- and hexa-coordinated simulations, the simulation in the tetracoordinated system shows a side peak at 3 Å, which is meaningful difference with the other two analogous simulations. This is due to the effect of the aluminum's charge on the waters, so the more waters around the cation, the more shared the charge is, and therefore the higher charge concentration on the tetracoordinated triggers the presence of -OH instead of $-OH_2$ around the aluminum, and these hydrogens at the -OH are the ones located to 3 Å.

The hydrogens at the second solvation layer are specially shifted outwards in the case of hexacoordination. The RDFs show a cleaner band compared to the tetra- and penta- coordinated simulations, which accurs due to the strong stability of the octahedrical coordination in the hexacoordinated system, which does not fluctuate so much and does not allow second layer waters to come closer.

In the case of g_{OH} (Fig. 4.4 **b)**), the statistics belong to the whole system and as a difference with the data in table 4.1.1 the average values are sharply identical, located at 0.98 Å showing a reasonable agreement with some other studies [53]. In comparison with high acidity acid solutions [77], the acidity Al^{+3} cation is not strong enough to trigger the presence of the hydronimum molecule in water solution, so first peak on g_{OH} does not show any small side peak around 1.5 Å.

4.2 Dehydration Helmhotz free energies

Dehydration energies can be calculated trough the method mentioned on Sec. 2.4.3.

The histogram built from r_{AlO} distances and it's transformation into Helmholtz free energy (trough $F(r)=-K_B T \ln P(r)$) are displayed in Fig. 4.5 **a)**.

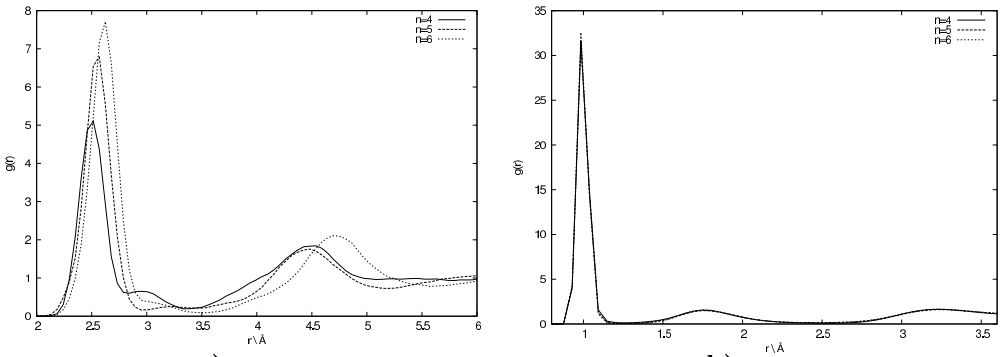

a) g_{AlH} **b)** g_{OH}

Figure 4.4: **a)***g_{AlH} shows that Al-H distance increases with the coordination. First peak shows a side peak in the n=4 simulation due to the H of -OH, and second layer is specially shifted outwards in the case of n=6 due to the stability of the octahedric conformation.* **b)***g_{OH} shows an equivalent behavior independently of the coordination. There is no evidence of the presence of hydronium molecules.*

As in the case of the radial distribution functions in 4.2 first solvation layer is represented trough a narrower peak around 2 Å and second solvation layer with a band around 4 Å. The difference of the histogram/helmholtz and a RDF is that the histogram is made by measuring only one concrete distance.

Fig. 4.5 **b)** shows Helmholtz free energy profiles for the four oxygens around the Al^{+3}, and in order to get the minimum dehydration energy value, the one that was most shifted outwards was selected for the solvation energy calculation (the outer it is the less energy it needs for taking it out), and finally extrapolation of the curve was up to the second solvation layer distance (Fig. 4.5 **c)**) allowing the possibility of measuring the free energy differences at first and second solvation layer distances and therefore solvation energy.

The pentacoordinated Al^{+3} simulation is specially interesting, due to the fact that one of the waters in second solvation layer gets into the first coordination shell. Fig. 4.6 shows distances between Al^{+3} and O so we can appreciate how one of the waters in second layer gets to the first one.

This phenomena allows us to doubly calculate the free energy profile, by using the previously used interpolate and extrapolate technique, not only the waters in first solvation shell, but also get the second shell by using just one atom pair. This can be seen in Fig. 4.7 **a)**

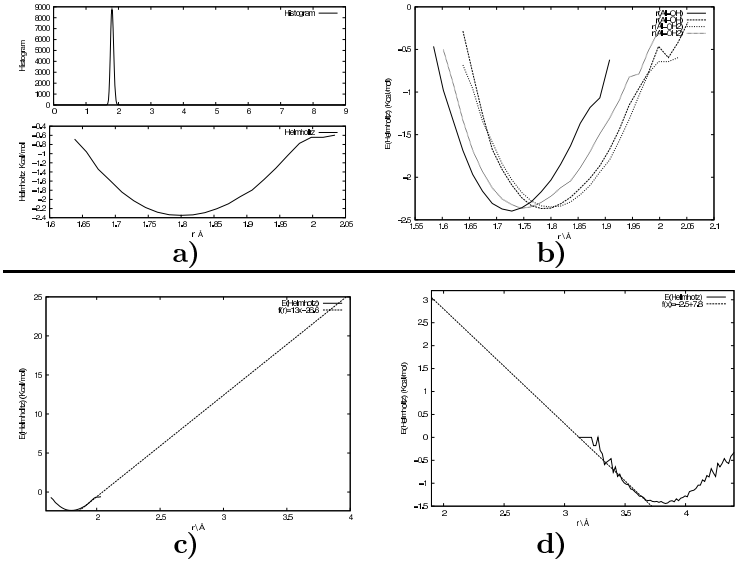

Figure 4.5: *n=4:* **a)** *Bond distance (r_{AlO}) vs number of cases per frame histogram and it's transformation into Helmholtz free energy for one of the waters* **b)***Helmholtz free energy profile for the four waters in first solvation layer of the tetracoordinated system. The oxygens with just one hydrogen are closer to the aluminum.* **c)** *Extrapolation of the tangent of the curve in first solvation layer up to the distance concerning to second solvation layer (around 4 Å).* **d)** *Same as c) but using a second solvation layer water and extrapolating backwards.*

In the case of pentacoordinated structure,the different solvation layers are well described in Fig. 4.7 **a).**

From the graphic in Fig. 4.7 **b)** binding energy and the energy for taking a water molecule from first solvation layer to the second one can be estimated. The first solvation layer in the pentacoordinated structure is at 1.85 Å (from table 4.2), and pushing one of these waters out, would produce a tetracoordinated structure, where Al-O distance concerning to the second layer is at 3.87 Å.

The difference between the energy at the equilibrium point of the first sovation layer, and the energy concerning to the second solvation layer (obtained from the extrapolation of the energy curve), gives a value of $\Delta E = 5.6$ Kcal/mol, which would be the estimation of the energy needed to take one water molecule from first solvation layer to the second one.

From this extrapolation (Fig. 4.7 **b)**) , binding energy for the sixth solvating water can be estimated. If first and second solvation layers for the hexa-coordinated

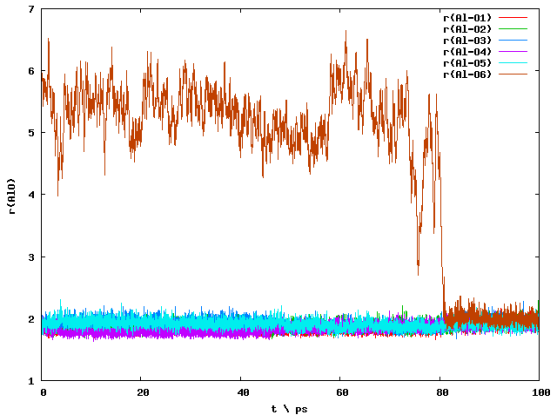

Figure 4.6: *n=5: r_{AlO} of pentacoordinated full solvated (50 H_2O) Al^{+3} simulations. Sixth oxygen gets from second solvation layer to the first one.*

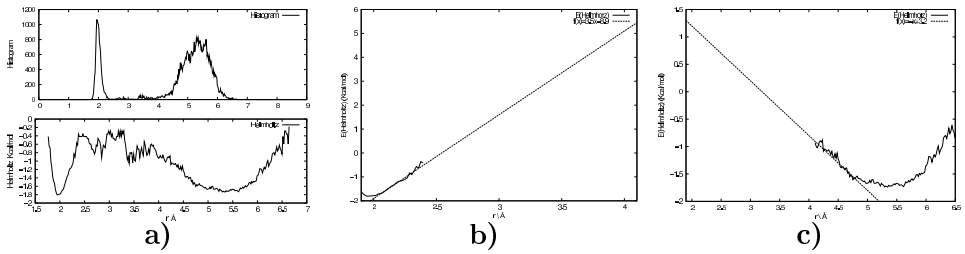

Figure 4.7: *n=5:* **a)** *Population histogram and conversion to Helmholtz free energy graph for the pentacoordinated system.* **b)** *shows the extrapolation of the tangent of the curve in first solvation layer up to the distance concerning to second solvation layer (around 4 Å).* **c)** *shows a reverse extrapolation from n6 to n5 (equivalent to dehydration of n6 or hydration of n5).*

are at the distances shown in 4.2 (1.91 and 4.14 Å) substitution in the interpolated function gives us ΔE= 5.371 Kcal/mol.

In the case of tetracoordination, interpolation of the curve can be approached to f(x)=13x-26.6, and extrapolation to the point where second solvation layer would be 3.85 Å (according to Fig. 4.3 **b)**), which gives an estimation of energy difference of ΔE= 25.8 Kcal/mol. The energy for completely removing the same water molecule (up to the infinite) can be estimated in the same way getting a value of 81 Kcal/mol, which makes sense, since aluminum does not like so low coordination numbers in water solution.

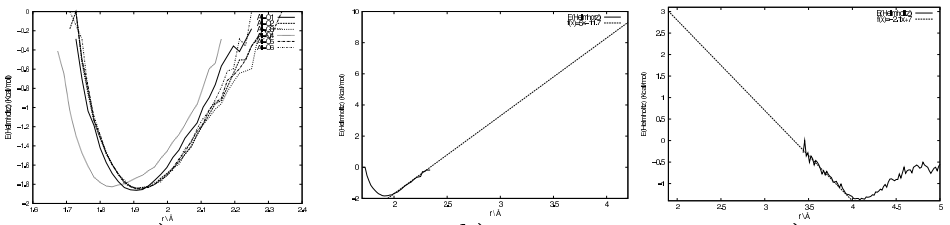

Figure 4.8: *n=6:* **a)** *Helmholtz free energy profile for the six waters in first solvation layer of the hexacoordinated system. The oxygen with just one hydrogen is closer to the aluminum.* **b)** *Extrapolation of the tangent of the curve in first solvation layer up to the distance concerning to second solvation layer (around 4 Å).* **c)** *Same as b) but backwards extrapolation.*

The energy needed for pushing a water molecule from first solvation layer up to the second one and up to the infinity (dehydration) for the n=4, 5 and 6 is displayed table 4.4.

Reaction	$\Delta E_{1\rightarrow 2}$	$\Delta E_{1\rightarrow \infty}$
$Al(H_2O)_4$ - H_2O $\rightarrow$ $Al(H_2O)_3$	25.9	81.0
$Al(H_2O)_5$ - H_2O $\rightarrow$ $Al(H_2O)_4$	5.6	19.0
$Al(H_2O)_6$ - H_2O $\rightarrow$ $Al(H_2O)_5$	10.0	31.1

Table 4.4: *Energy needed for pushing a water molecule from first solvation layer up to the second one and up to the infinty (dehydration) for the n=4, 5 and 6.*

4.3 Conclusions

- As previous researches [47][48] told, the performed simulations proof the stability of the tetra-, penta- and hexacoordinated structures, although pentakoodinated structure tends to jump into tetra- or hexacoordinated one.
- Al-O distance for the waters in the first solvation layer of Al^{+3} increases with the coordination number, while O-H distance decreases.
- Al^{+3} deprotonates the waters from first solvation layer, in the cases of tetra- and pentacoordination, therefore it gets surrounded by -OH_2 and -OH ligands.
- For the hexacoordinated structure, the charge of Al^{+3} is neutralized by the six surrounding waters, so there is no deprotonation.

- The case of tetracoordination is the one who needs higher energy for both ejecting a water to the second solvation layer and for completely removing it. This shows the need of Al^{+3} for ligands.
- Pentacoordinated structure needs less energy for ejecting waters, because although it is stable, tetra- and hexakoodinated ones are even more stable.

Chapter 5

AAAs with Microhydrated Al^{+3}

5.1 Introduction

The interaction between a cation and an aromatic ring, known as cation-π interaction [25], is now recognized as one of the strongest non-covalent binding forces in the gas phase [24]. Cation-π interactions are claim to occur also in aqueous environment [24], where cations are well solvated and a substantial desolvation penalty must be paid to actually bind a cation.

Cation-π interactions ought to occur in proteins. In fact, three of the 20 natural amino acids commonly found as building blocks of the proteins, namely Phe, Tyr, and Trp, have full aromatic characters and can thus participate in cation-π interactions.

Since cations in water are well solvated, a putative binding site must overcome a substantial desolvation penalty to actually pull a cation out of water, but unfortunately, the energetic of the binding in aqueous solution is not well understood, since quantitative measurements are sparse and refer mainly to the interactions between amino acids.

In this chapter a detailed description of cation-π interactions on $Al[^{+3}$ cation and aromatic amino acids will be made, as a continuation to previous works from this group [78][79].

5.2 Minimum energy complexes

Since the energy of a system is inversely proportional to it's lifetime, and since the lifetime is proportional to the probability of finding this system i the reality, it is clear that the energy of the systems is something to take into account.

In this project, the conformational space of the three aromatic amino acids was studied by finding the geometry minima of different possible conformations.

A total of 60 structures were analyzed, 4 for each single amino acid (2 CS (Charge Solvated) + 2 ZW (Zwitterionic)), 12 for possible binding sites for Al^{+3}, and 36 for each hydration state (from one to four water molecules).

The analysis of the structures was done by performing a geometry optimization for each one by two different codes in order to ensure the reliability of the results.

First geometry optimization was performed by Gaussian 03 package [55]. The theory level was set to standard all electron 6-31+G (d,p) basis with the B3LYP (Becke3 Lee-Yang-Parr) density functional. After geometry optimization, a frequency calculation was performed, in order to ensure that there are not normal modes which could make the structure unstable.

A second geometry optimization was performed by using the CPMD package [31], with PBE density functional [29], Vanderbilt ultrasoft pseudopotentials [32] implemented [33] for CPMD [68], with 30 Ry plane wave cutoff.

In the following sections, different tables will be presented, showing optimized structures, and comparison of the energy difference with the lowest energy structure (ΔE) in kcal mol^{-1} units, and some reference distances for both kind of calculations.

5.2.1 Cation-π interactions on phenolic ring

Cation-π interactions are one of the strongest non-covalent forces found in the aromatic amino acid-Al^{+3} clusters. This short section tries to describe the effect of the cation-π interactions on the aromatic ring.

An idea of the interaction force can be done through the binding energies of the Al^{+3} cation with benzene and phenol rings. This comparison also intended to serve as a reference, since after all the aromatic rings of Phe and Tyr are somehow a benzene and a phenol with a side chain.

The binding energy of Al^{+3} with benzene can be calculated from the reactions shown in Fig. 5.2.1 and 5.2.1. Calculations were done with Gaussian 03 [55] at B3LYP/6-311++G(d,p) functional/basis level.

As can be seen in the structures from Fig. 5.2.1, the Al^{+3}-ring energy is around 20 kcal/mol higher in the case of phenol, since the presence of -OH increases the electronic density on the ring, increasing the attraction to the Al^{+3}.

Reference data from benzene can be compared with the data in benzene-Al^{+3} complex, showing a meaningful size increasing in the ring, and same effect can be appreciated on the case of phenol, where Al^{+3} is displaced from the center of the ring towards the -OH ligand.

5.2.2 Single amino acids

Geometry optimization calculations show clearly that single amino acids clearly prefer charge solvated conformations which agrees with many other researches in the literature [61] [58]. On other hand, comparison between **a-b** and **c-d** figures for Phe

Al^{+3}	+	benzene	→	benzene-Al^{+3} complex
		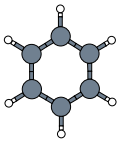		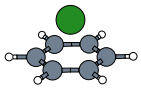
		d_{CC}=1.395 d_{CH}=1.084		d_{CC}=1.442 d_{CH}=1.094 d_{CAl}=2.197
-240.4048	-	-232.3113	→	-473.2970
ΔE = -0.5809 a.u. x 627.51 $\frac{kcal}{a.u.}$ = -364.52 kcal/mol				

Figure 5.1: *Binding energy for Al^{+3} in benzene's ring, and some distances in Å.*

Al^{+3}	+	phenol	→	phenol-Al^{+3} complex
		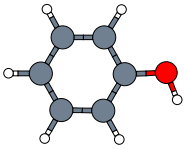		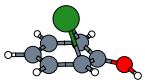
-240.4048	-	-307.5587	→	-548.5794
ΔE = 0.6159 a.u. x 627.51 $\frac{kcal}{a.u.}$ = -386.48 kcal/mol				

Figure 5.2: *Binding energy for Al^{+3} in phenol's ring.*

and Tyr show us that as in the case of some other amino acids [80] the change of the orientation of the aromatic side chain has just a minor effect on the total energy.

Zwitterionic conformations were calculated by constrained geometry optimization, otherwise the structures would fall into the CS ones. In the three cases the **c** structure has one negative frequency, therefore they are marked with an "∗", which shows the difficulty of the naked amino acids to adopt the ZW conformation. These structures were added to the table for being able to compare the energy effect of the aromatic side chain.

In the data shown in the following tables, "Struct. no." stands for the structure number, so that same number should be comparable between different amino acids. "G03" is for the data obtained by Gaussian 03 and "CPMD" for the data obtained by CPMD codes.

Table 5.2.2 shows some reference distances that will be used to compare the structural modification triggered by the presence Al^{+3}.

ΔE (kcal mol^{-1})	**a** (CS)	**b** (CS)	**c** (ZW)	**d** (ZW)
		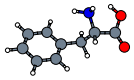	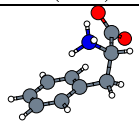	
Struct. no.	2	1	4	3 $*$
G03	0.00	0.01	15.76	16.47
CPMD	0.01	0.00	133.1	12.83

Figure 5.3: *Minimum energy conformations for Phe. Energy differences obtained from G03 and CPMD with respect to the lowest found minimum are displayed below. Energies show a clear preference for CS conformation.*

ΔE (kcal mol^{-1})	**a** (CS)	**b** (CS)	**c** (ZW)	**d** (ZW)
	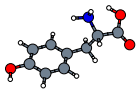	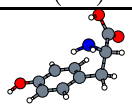	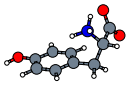	
Struct. no.	1	2	3 $*$	4
G03	0.00	0.06	15.81	16.48
CPMD	0.00	0.04	12.90	13.55

Figure 5.4: *Minimum energy conformations for Tyr. Energy differences obtained from G03 and CPMD with respect to the lowest found minimum are displayed below. Energies show a clear preference for CS conformation.*

ΔE (kcal mol^{-1})	**a** (CS)	**b** (CS)	**c** (ZW)	**d** (ZW)
				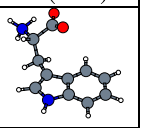
Struct. no.	1	2	3 $*$	4
G03	0.00	6.41	14.88	23.79
CPMD	0.00	7.62	12.00	20.69

Figure 5.5: *Minimum energy conformations for Trp. Energy differences obtained from G03 and CPMD with respect to the lowest found minimum are displayed below. Energies show a clear preference for CS conformation.*

Since this work is focused on the effects of Al^{+3} on the amino acids, these single amino acids will serve just as a reference.

Dist. (Å)	Phe	Tyr	Trp
r_{CC}	1.40	1.40	1.40
r_{CH}	1.08	1.08	1.08
r_{CN}	1.47	1.47	1.47
r_{NH}	1.01	1.01	1.01
r_{CO}	1.21	1.21	1.21
$r_{CO(H)}$	1.33	1.34	1.34

Table 5.1: *Reference distances (in Å) from the lowest energy conformers of naked amino acids (Structure* **a**) *in Fig. 5.2.2, 5.2.2 and 5.2.2). r_{CC} and r_{CH} are the CC and CH distances concerning to the carbons and hydrogens in the aromatic ring.*

Coordinated to Al^{+3}		Conformation
-COO^-	-NH_2	
$\surd$	$\surd$	CS
$\otimes$	$\otimes$	CS
$\surd$	$\otimes$	ZW
$\otimes$	$\surd$	IZW

Table 5.2: *Charge distribution of amino acids depending on the elements in first coordination shell of Al^{+3}. $\surd$ means that there is one of these elements in the first solvation shell and $\otimes$ means there is not.*

5.2.3 Amino acid complexation with Al^{+3}

The presence of Al^{+3} cation induces a charge redistribution on the amino acid due to its positive charge.

All possible binding sites for Al^{+3} are reduced to the carboxylate (in -COOH or -COO^- forms), nitrogen in -NH_2 form and π electrons above aromatic ring. Fig. 3.3 shows the electrostatic charge distribution obtained from the isodensity maps.

Results show that the most favored binding sites for Al^{+3} are the cation-π followed by -COO^- and finally -NH_2.

Charge distribution depends on the position of the Al^{+3} so that the complex will adopt zwitterionic conformation as long as the Al^{+3} is not bonded to the -NH_2, if it is, conformation will be charge solvated, when -COOH is also bonded to Al^{+3}. A new charge distribution model appears when -NH_2 is bonded to the Al^{+3} but -COOH does not, we call it Inverse Zwitterionic (IZW) conformation.

The IZW case can be seen on the **e** structure on table 5.2.3.

When comparing Mulliken charges for the carbon of COO^- at **d** (ZW),**e** (IZW) and **f** (CS) structures in table 5.2.3, a much higher charge can be appreciated for **f** (0.39) compared to the **e** (0.11) and **d** (-0.16).

ΔE	**a** (ZW)	**b** (CS)	**c** (ZW)	**d** (ZW)	**e** (IZW)	**f** (CS)
	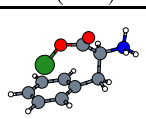	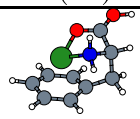	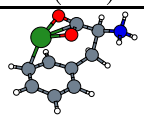	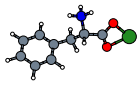		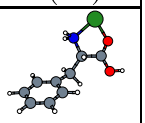
	4.2	2.1	4.1	3.1	1.2	1.1
G03	0.00	0.28	1.16	16.36	18.70	22.91
CPMD	1.58	0.00	2.54	17.70	20.51	25.80

Figure 5.6: *Phe-Al^{+3} complex:* **e** *has IZW conformation. Weak cation-π interaction.*

ΔE	**a** (ZW)	**b** (CS)	**c** (ZW)	**d** (ZW)	**e** (ZW)	**f** (CS)	**g** (CS)
	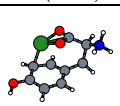	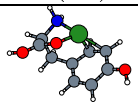	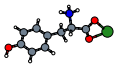	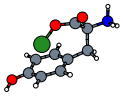	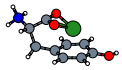	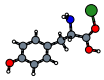	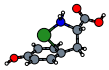
	4.1	2.1	3.1	4.3	4.2	1.1	1.2
G03	0.00	0.60	2.69	2.84	5.00	7.51	36.44
CPMD	0.03	0.00	2.15	2.53	1.25	8.87	21.09

Figure 5.7: *Tyr-Al^{+3} complex: strong cation-π interaction.*

ΔE	**a** (ZW)	**b** (CS)	**c** (ZW)	**d** (ZW)	**e** (CS)
		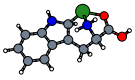	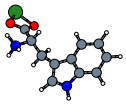		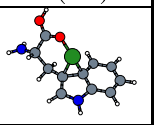
	4.1	1.1	3.1	4.2	2.1
G03	0.00	8.42	11.40	14.84	50.31
CPMD	0.00	9.91	17.81	11.21	45.05

Figure 5.8: *Trp-Al^{+3} complex: strong cation-π interaction.*

Minimum energy structures are not equivalent for the three amino acids. In the three cases the minima have ZW charge distribution and in Tyr and Trp the Al^{+3} seeks the filling of the coordination layer by keeping the bindentate (chelate) binding in the carboxilate, but surprisingly in the case of Phe, the monodentate conformation has lower energy than the bidentate, with just two coordinating ligands.

A possible answer to this effect can be through the interpretation of the data in section 5.2.1. In fact, due to the negative charge of the oxygen, the phenolic ring binds the Al^{+3} more strongly leaving less non-neutralized Al^{+3}'s charge and reducing

the need for electrostaticaly attract the second oxygen in the carboxylate. Same for Trp, but with nitrogen instead of oxygen.

These results differ form previous studies on cation-π interactions with Na^+ [81] where the cation was found to stabilize CS conformations. Although the **b)** structures in Fig. 5.2.3, 5.2.3 and 5.2.3 get stabilized by the "glue" effect on the cation with the nitrogen and oxygen, **a)** structures have still lower energy and they are ZW.

5.2.4 Microhydratation of amino acid complexes with Al^{+3}

Monohydratation

The presence of a water molecule attached to the Al^{+3} helps scattering the charge of Al^{+3} so that the attraction to the neighbours will be weaker.

The coordination number of Al^{+3} is supposed to be around 4, so if one of the coordinating elements is the water, we would need just three elements more for filling the first solvation layer.

In table 5.2.4,"Figure" is the graphic representation of the atomic coordinates, "Let." is the letter for recalling the structure, "n" is the coordination number for Al^{+3}, "CD" is the Charge Distribution (CS, ZW, IZW) "ΔE" is the difference of total energy compared to the lowest energy structure in kcal mol^{-1} units, r_{AlO}, r_{AlN} and r_{AlC_α} are the distances between the aluminum with respect to the oxygen (carboxylate), nitrogen (amino) and alpha carbon atoms respectively,

The performed calculations show an equivalent behavior for the minimum energy structures. In the three cases the global minima are found to be the CS and tetracoordinated with monodentated -COO^-, -NH_2, aromatic ring and microsolvating water. In the case of Trp, the minimum energy structure "a" found with G03 shows to be in competition with the bidentated one "b", which appears to be the minimum energy structure on CPMD.

These monohydrated structures have an unexpected behavior, since they the only Al^{+3}-AAA complex with CS charge distribution on the global minima. In the rest of the cases (Al^{+3}-AAA complex, di-, tri- and tetrahydrated) the charge distribution in the global minima has found to be ZW.

As the Al^{+3} is seeking for coordinating elements, higher coordination numbers will be more stable. On other hand, although the oxygens in the carboxylate can easily form chelate with the Al^{+3} in general terms, it is stericaly favored to bond the nitrogen, since it is easier to bend a four atom chain than the three atom one.

The energy barrier between monodentate and bidentate conformations appears to be quite small, as could have been spected [82].

Phe + Al^{+3} + 1 H_2O								
Figure	Let.	n	CD	Code	ΔE	r_{AlO}	r_{AlN}	r_{AlC_α}
	a	4	CS	G03	0.00	1.82	1.99	2.03
				CPMD	0.00	1.81	1.98	2.03
	b	4	ZW	G03	4.85	1.88	4.52	2.99
				CPMD	2.35	1.87	4.49	2.91
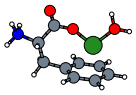	c	3	ZW	G03	6.94	1.70	5.01	2.50
				CPMD	5.53	1.69	4.97	2.46
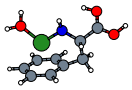	d	3	IZW	G03	33.37	4.43	1.81	2.26
				CPMD	29.93	4.43	1.80	2.24
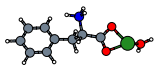	e	3	ZW	G03	38.99	1.89	4.55	6.08
				CPMD	33.53	1.88	4.53	6.06
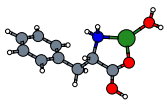	f	3	CS	G03	48.61	1.80	2.02	4.69
				CPMD	44.82	1.79	2.01	4.69

Table 5.3: *Monohydrated Phe-Al^{+3} complex: Minimum energy structure with CS charge distribution.*

Structures without cation-π interactions are clearly unfavored. The IZW charge distribution on Fig. 5.2.4 **d** is something that has not been shown in any other similar research.

Analyzing the results obtained with the different codes, in general terms, energy difference is lower in CPMD calculations compared to the G03 ones, except for the **a** and **c** cases on the Trp.

Structural data is very similar. The value of r_{AlO} are the same or 0.01 Å lower on CPMD calculations compared to the G03 ones. The case of r_{AlN} is complex, since due to the degrees of freedom, the distance can fluctuate meaningfully in the cases when the are not directly bonded, producing large distance differences. The

Tyr + Al^{+3} + 1 H_2O								
Figure	Let.	n	CD	Code	ΔE	r_{AlO}	r_{AlN}	r_{AlC_α}
	a	4	CS	G03	0.00	1.85	1.98	2.03
				CPMD	0.00	1.84	1.97	2.03
	b	4	ZW	G03	5.35	1.82	1.99	2.04
				CPMD	3.07	1.81	1.98	2.03
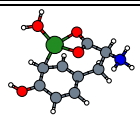	c	4	ZW	G03	7.48	1.89	4.52	3.00
				CPMD	4.76	1.88	4.49	2.91
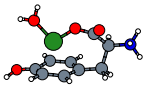	d	3	ZW	G03	8.99	1.71	4.49	2.42
				CPMD	5.55	1.70	4.91	2.36
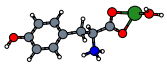	e	3	ZW	G03	30.85	1.93	4.57	6.11
				CPMD	33.96	1.92	4.54	6.08
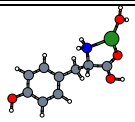	f	3	CS	G03	37.09	1.87	2.11	5.45
				CPMD	31.47	1.84	2.08	5.41

Table 5.4: *Monohydrated Tyr-Al^{+3} complex.*

structures where Al and N are directly bonded are going to be the ones CS and IZW conformations, and once again, the difference between both codes is less than 0.01 Å lower with CPMD. Finally, r_{AlC_α} distance has a similar problem to the r_{AlN}, since in cases with no cation-π interactions the distance can change quite a lot. If we compare the values of the structures with cation-π interactions, the value is again similar or 0.01 Å lower on CPMD. In the case of open structures can have a distance difference up to 0.14 Å.

Trp + Al^{+3} + 1 H_2O								
Figure	Let.	n	CD	Code	ΔE	r_{AlO}	r_{AlN}	r_{AlC_α}
	a	4	CS	G03	0.00	1.84	1.99	3.27
				CPMD	1.33	1.83	1.98	3.24
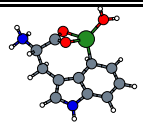	b	4	ZW	G03	0.43	1.88	4.55	3.48
				CPMD	0.00	1.86	4.54	3.46
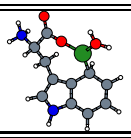	c	4	ZW	G03	11.95	1.68	5.12	3.34
				CPMD	13.43	1.67	5.08	3.26
	d	3	ZW	G03	44.52	1.95	4.53	5.01
				CPMD	43.36	1.95	4.52	5.15
	f	3	CS	G03	44.69	1.76	4.62	2.14
				CPMD	42.04	1.75	4.60	2.14

Table 5.5: *Monohydrated Trp-Al^{+3} complex.*

Dihydratation

A second water around Al^{+3} makes it's coordination number to over four in all the cases.

In the case of two microsolvating waters, energy minima are ZW, as in the case of Al^{+3}-AAA. The energy difference towards CS structures is of many kcal mol^{-1} in all the cases, which show a clear preference for ZW structures. The high energy of the IZW structure in Phe makes it almost negligible.

Once again, as in Sec. 5.2.3, the minimum energy complexes are monodentated for Phe and Tyr with an small barrier towards bidentate ($\sim$ 5-7 kcal/mol), but this behavior became just opposite on Trp, which shows to be more stable in bidentated, and also have a meaningful barrier towards monodentate.

Coordination number is four at the minimum energy structures for Phe and Tyr

and five at Trp, which might be surprising for Phe and Tyr due to their low barrier towards bidentate, and therefore achieving pentacoordination.

The importance of cation-π interactions can be appreciated by the general increasing of the energy difference on open structures.

Comparison of the energies obtained by the different codes show, as in the case of monohydration, very similar values or slightly lower in the case of CPMD compared to the G03. Exceptions are **b** and **c** structure on Tyr and **b**, **c**, **d** eta **f** on Trp where energy values from CPMD are a little higher than the ones obtained by G03.

For the case of **e** structure in Tyr, the CPMD calculation has shown a meaningfully higher energy difference + 5.89 kcal mol^{-1} on CPMD compared to G03.

About the r_{AlO} distances, values are similar or 0.01 Å lower on CPMD calculations. Same for r_{AlN} distances, although structures appear to be ZW. Distance difference on r_{AlC_α} is also small and up to 0.02 Å lower on CPMD, and exceptionally **a** structure on Phe shows a 0.05 Å shorter distance on CPMD. Due to the above mentioned degrees of freedom, distance on **b** structure of Phe appears to be slightly larger on CPMD.

Trihydratation

The third water around Al^{+3} becomes a meaningful change from mono- and dihydration. Aluminums seeks at least tetracoordination and a third water molecule gives the Al^{+3} the chance of having an stericaly easier coordination with the amino acid. On other hand, double bonds with amino acid (bidentate or N+O) gives the change achieving penta or hexacoordination.

In any case, except for "b" structure on Tyr, hexacoordination and cation-π interactions do not appear to be stericaly compatible. Therefore cation-π interactions start to get unfavored for more than three microsolvating waters and the only way to have them is by ejecting a water to the second solvation layer.

Charge distribution on minimum energy structures, appears to be once again ZW and the energy difference with CS configurations becomes larger than in dyhydrated systems. This means that on all of the studied structures ZW structures are going to have lower relative energy than CS ones. On other hand, as CS configurations has a two-way relation with the presence of Al-N bond, the coordination of aluminum with nitrogen is going to be unfavored too. IZW structure in Phe has also higher energy compared to the rest.

Phe + Al^{+3} + 2 H_2O								
Figure	Let.	n	CD	Code	ΔE	r_{AlO}	r_{AlN}	r_{AlC_α}
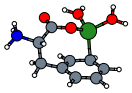	a	4	ZW	G03	0.00	1.76	5.10	3.13
				CPMD	0.00	1.76	5.09	3.08
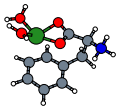	b	5	ZW	G03	5.40	1.91	4.59	3.08
				CPMD	4.36	1.90	4.57	3.11
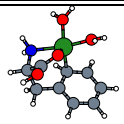	c	5	CS	G03	6.25	1.86	2.08	2.10
				CPMD	7.38	1.85	2.07	2.11
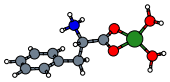	d	4	ZW	G03	15.30	1.82	4.52	5.88
				CPMD	12.65	1.81	4.49	5.85
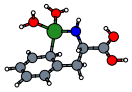	e	4	IZW	G03	27.19	4.45	1.81	2.60
				CPMD	26.82	4.44	1.80	2.57
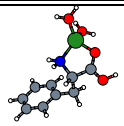	f	4	CS	G03	28.14	1.88	2.15	5.52
				CPMD	27.49	1.76	1.91	4.42

Table 5.6: *Dihydrated Phe-Al^{+3} complex.*

For the case of tryhydration, the tendency of the energy difference between G03 and CPMD changes. In this case, except for two structures on Phe and Trp, energies appear to be the same or higher on CPMD calculations compared to G03.

The values of r_{AlO} and r_{AlN} distances are once again very similar or up to 0.02 Å shorter on CPMD. **f** structure in Phe shows large values for both G03 and CPMD due to the long distance between Al and -COO^- (it is not directly bonded to the Al). r_{AlC_α} are in general terms very similar too, or up to 0.02 Å lower on CPMD. Exceptionally, **e** structure on Tyr a difference of 0.05 Å was found, and on **a**, **c** and **d** structures on Trp, values are 0.01 Å larger on CPMD.

Tyr + Al^{+3} + 2 H_2O								
Figure	Let.	n	CD	Code	ΔE	r_{AlO}	r_{AlN}	r_{AlC_α}
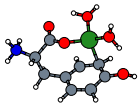	a	4	ZW	G03	0.00	1.76	5.11	3.19
				CPMD	0.00	1.75	5.10	3.13
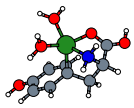	b	5	CS	G03	6.49	1.93	2.02	2.10
				CPMD	7.18	1.92	2.02	2.10
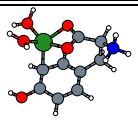	c	5	ZW	G03	7.10	1.91	4.61	3.19
				CPMD	5.53	1.91	4.59	3.12
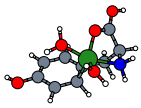	d	5	CS	G03	9.02	1.86	2.08	2.61
				CPMD	7.75	1.85	2.07	2.55
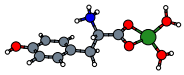	e	4	ZW	G03	9.02	1.82	4.50	5.86
				CPMD	7.75	1.79	4.48	5.83
	f	4	CS	G03	29.86	1.77	1.93	4.44
				CPMD	25.59	1.75	1.92	4.42

Table 5.7: *Dihydrated Tyr-Al^{+3} complex.*

Tetrahydratation

The presence of a fourth water, induces the Al^{+3} to get penta or hexa coordination.

Minimum energy structures are clearly ZW and energy difference between ZW and CS structures becomes larger than in trihydration systems. In this case, IZW structure of Phe, in addition to the high energy difference with the minimum energy structure, shows imaginary frequencies, so that this structure does not appear to be stable.

An estimation of the energy difference between ZW and CS would be difficult to make, since configurations are quite different when aluminum binds the nitrogen that

Trp + Al^{+3} + 2 H_2O								
Figure	Let.	n	CD	Code	ΔE	r_{AlO}	r_{AlN}	r_{AlC_α}
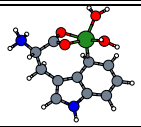	a	5	ZW	G03	0.00	1.88	4.66	3.57
				CPMD	0.00	1.88	4.65	3.56
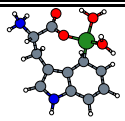	b	4	ZW	G03	0.09	1.76	5.06	3.55
				CPMD	0.36	1.76	5.05	3.55
	c	5	CS	G03	13.12	1.94	2.02	2.07
				CPMD	13.83	1.93	2.01	2.08
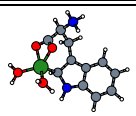	d	5	ZW	G03	15.08	1.93	4.41	2.97
				CPMD	15.95	1.92	4.40	2.96
	f	4	CS	G03	39.15	1.79	4.56	2.01
				CPMD	39.66	1.77	4.54	2.01

Table 5.8: *Dihydrated Trp-Al^{+3} complex.*

makes possible the CS configuration, and also because the position of H changes.

As in the case of tricoordination, the cation-π interactions are possible just by ejecting at least one water molecule to the second solvation layer.

On the case of Phe and Tyr, minimum energy complexes are bidentate and on the case of Tyr monodentate, but the energy differences mono and bidentate are not meaningfully large.

Comparison of the data obtained by both codes show, as in the case of tricoordination, many cases where energy values by CPMD are larger than in G03 and some of the differences can be up to some kcal/mol, which becomes a meaningful difference with the previous calculations.

For the case of r_{AlO}, r_{AlN} and r_{AlC_α}, there is also a difference with previous cases. In fact, in these cases, although Phe keeps the tendency of 0.02 Å shorter distance on

Phe + Al^{+3} + 3 H_2O								
Figure	Let.	n	CD	Code	ΔE	r_{AlO}	r_{AlN}	r_{AlC_α}
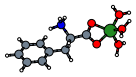	a	5	ZW	G03	0.00	1.87	4.56	5.98
				CPMD	0.00	1.86	4.55	5.95
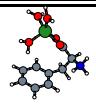	b	5	ZW	G03	0.19	1.87	4.56	4.17
				CPMD	0.42	1.86	4.55	4.12
	c	4	ZW	G03	4.04	1.83	5.27	3.39
				CPMD	4.97	1.84	5.27	3.38
	d	5	CS	G03	10.77	1.88	2.11	2.73
				CPMD	10.10	1.87	2.10	2.72
	e	5	CS	G03	12.77	1.86	2.01	3.79
				CPMD	13.54	1.86	2.00	3.75
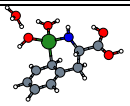	f	4	IZW	G03	31.88	4.43	1.83	2.62
				CPMD	30.38	4.41	1.82	2.60

Table 5.9: *Trihydrated Phe-Al^{+3} complex.*

CPMD, Tyr and Trp show many cases with larger distances obtained from CPMD calculations compared to G03.

5.2.5 Stability of the minimum energy complexes

CPMD molecular dynamics simulations were performed on the minimum energy structures in order to check the stability of the complexes at room temperature.

In total, 12 different clusters were simulated during 20 ps, and 11 of them kept their initial configuration for the whole simulation, which profs their stability. For the case of tetrahydrated Trp, starting structure **a** became **c** by breaking one of the bonds with the carboxylate.

In the case of tetrahydration of Trp, initial structure **a** jumps to structure **c** by breaking the Al-O chelate bond. This jump occurs due to the low energy barrier between both structures and the fluctuations in the total energy of the system.

Tyr + Al^{+3} + 3 H_2O								
Figure	Let.	n	CD	Code	ΔE	r_{AlO}	r_{AlN}	r_{AlC_α}
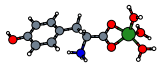	a	5	ZW	G03	0.00	1.87	4.55	5.95
				CPMD	0.00	1.85	4.53	5.93
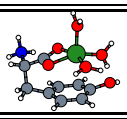	b	6	ZW	G03	1.69	1.92	4.57	3.94
				CPMD	4.97	1.92	4.57	3.91
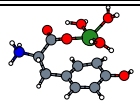	c	5	ZW	G03	7.15	1.80	5.22	3.29
				CPMD	10.69	1.80	5.20	3.26
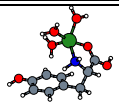	d	5	CS	G03	12.68	1.86	2.01	3.77
				CPMD	14.77	1.86	2.00	3.73
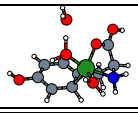	e	5	CS	G03	14.62	1.87	2.11	2.64
				CPMD	14.76	1.87	2.10	2.59
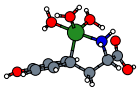	f	5	CS	G03	25.99	3.38	2.06	2.14
				CPMD	27.85	3.87	2.07	2.17

Table 5.10: *Trihydrated Tyr-Al^{+3} complex.*

5.3 Structural analysis

5.3.1 Bond distances

Mean values for all different distances can be obtained by calculating the RDFs from the simulations performed on the minimum energy structures for the section 5.2.5.

The data introduced in tables 5.3.1, 5.3.1 and 5.3.1, d_{OAl} distance was meassured from Al^{+3} to the closest oxygen in the carboxylate, which usually is the shortest one.

d_{AlC} distance shows different values which belong the different carbons in the ring, but in general the distance between the Al and the aromatic ring will be around 2 Å in cases with cation-π interactions and between 5.9-8.7 Å in the cases without them. The distance to the C in the carboxylate is around 2.6 Å in monodentate structures and 2.3 Å in bidentate. Distance to the rest of carbons in the aromatic side chain have very different values, since they change easily when moving the chain.

Trp + Al^{+3} + 3 H_2O								
Figure	Let.	n	CD	Code	ΔE	r_{AlO}	r_{AlN}	r_{AlC_α}
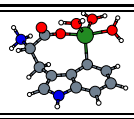	a	5	ZW	G03	0.00	1.85	4.95	3.69
				CPMD	0.00	1.86	4.97	3.70
	b	5	ZW	G03	7.37	1.86	4.53	5.94
				CPMD	3.39	1.84	4.52	5.92
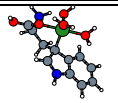	c	5	ZW	G03	8.93	2.00	3.55	2.09
				CPMD	9.73	1.98	3.53	2.10
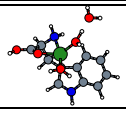	d	5	CS	G03	9.63	1.90	2.07	2.08
				CPMD	9.74	1.90	2.06	2.09

Table 5.11: *Trihydrated Trp-Al^{+3} complex.*

The distance from Al^{+3} to C_1 or C_α shows the presence or not of cation-π interactions. In general terms, the cases with d_{AlC_1} distance lower than 3.5 Å will show cation-π interactions, and on open structures, this distance will be around 4-8 Å.

d_{CC} shows the shortest C-C distance, and it's value has been sharply identical in all calculations, 1.4 Å. Same for d_{CH} and d_{NH} with values of 1.09 and 1.01 Å respectively.

C-N distance shows different values, where in the cases of Phe and Tyr, the first value belongs to the distance from N to the C where it is attached in the aromatic side chain, and the rest of values belong to the distances to the rest of the carbons in the chain or ring. In the case of Trp, the shortest C-N value belongs to the distance from the N in the ring to the carbons in the ring next to it, and the measured distances appear to be between 1.48 and 1.56 Å.

RDFs also show different C-O distances. The one at 1.25 Å belongs to the shortest C-O distance in the monodentate case. The C-O distance at 1.33 Å belongs to the mean distance in the chelate case.

On other hand, the distance of 2.40 Å belongs to the C-O distance of with the oxygen that is not bonded to Al^{+3} in case of monodentate.

Phe + Al^{+3} + 4 H_2O								
Figure	Let.	n	CD	Code	ΔE	r_{AlO}	r_{AlN}	r_{AlC_α}
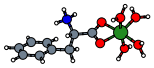	a	6	ZW	G03	0.00	1.90	4.61	6.03
				CPMD	0.00	1.89	4.60	6.00
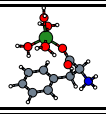	b	5	ZW	G03	3.19	1.79	5.28	4.13
				CPMD	2.55	1.79	5.28	4.11
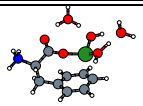	c	4	ZW	G03	8.99	1.78	5.35	3.40
				CPMD	4.43	1.77	5.33	3.38
	d	6	CS	G03	16.67	1.89	2.07	2.99
				CPMD	17.79	1.89	2.07	2.99
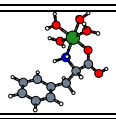	e	6	CS	G03	19.96	1.87	2.02	4.64
				CPMD	20.78	1.86	2.02	4.62
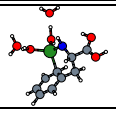	f ∗	4	IZW	G03	37.21	4.32	1.83	2.66
				CPMD	32.45	4.28	1.83	2.65

Table 5.12: *Tetrahydrated Phe-Al^{+3} complex.*

5.3.2 Wannier functions

The concept of Wannier Functions which was introduced in section **??**, has been used by following the criteria of other studies [62].

By representing the maximally localized Wannier Function Centers (WFC) we can get an idea of the electronic structure in the chemical bonds.

As CPMD code is based on electronic structure, detailed information on the electrostatic charge distribution can be directly obtained from CPMD, for example, WFC.

In Fig. 5.3.2 maximally localized WFCs are displayed. As can be seen in the pictures, in the places where each chemical (covalent) bond is located a black dot is displayed and also on the top of every atom with lone pairs.

Tyr + Al^{+3} + 4 H_2O								
Figure	Let.	n	CD	Code	ΔE	r_{AlO}	r_{AlN}	r_{AlC_α}
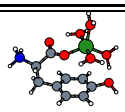	a	5	ZW	G03	0.00	1.81	5.32	4.20
				CPMD	0.00	1.82	5.32	4.20
	b	6	ZW	G03	3.57	1.89	4.60	6.00
				CPMD	0.97	1.88	4.59	5.98
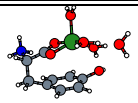	c	5	ZW	G03	8.22	1.90	4.56	4.18
				CPMD	6.08	1.90	4.55	4.16
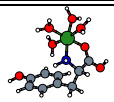	d	6	CS	G03	15.46	1.88	2.03	4.09
				CPMD	14.01	1.88	2.03	4.06
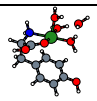	e	5	CS	G03	22.75	1.90	2.07	2.97
				CPMD	19.93	1.90	2.06	2.96
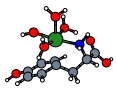	f	6	CS	G03	38.53	3.50	2.05	2.27
				CPMD	36.35	3.52	2.05	2.31

Table 5.13: *Tetrahydrated Tyr-Al^{+3} complex.*

These figures try to describe the nature of the cation-π interactions, or on other words, find out if the interaction between Al^{+3} and the ring has covalent nature, and as can be seen in the figure, there is a black dot between the aluminum and the ring which shows the covalent nature of the interaction.

In theory, these interaction should be purely electrostatic, but due to the charger redistribution induced by Al^{+3}, a high density electronic cloud is placed, which produces a bond that could be taken as covalent when interacting with Al^{+3}.

A general behavior can be appreciated in all simulations. As mentioned before, the WFC between the Al^{+3} and the ring shows the covalent nature of the nature. But on other hand, water molecules have a WFC on each O-H bond and the oxygens have two in the top of each other due to their lone pairs. There are also WFCs in the cases of C-C, C-H, C-N and C-O.

Trp + Al^{+3} + 4 H_2O								
Figure	Let.	n	CD	Code	ΔE	r_{AlO}	r_{AlN}	r_{AlC_α}
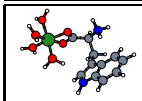	a	6	ZW	G03	0.00	1.92	4.53	4.48
				CPMD	0.00	1.92	4.53	4.42
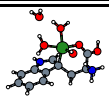	b	5	ZW	G03	0.85	2.02	3.53	2.12
				CPMD	2.09	1.99	3.52	2.13
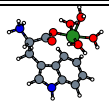	c	5	ZW	G03	1.33	1.86	4.89	3.90
				CPMD	2.41	1.87	4.91	3.93
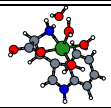	d	6	CS	G03	12.54	1.94	2.04	2.22
				CPMD	14.02	1.93	2.03	2.26

Table 5.14: *Tetrahydrated Trp-Al^{+3} complex.*

ur 1	2 ur	3 ur	4 ur
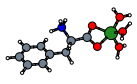	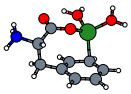	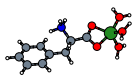	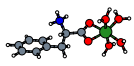

Hidr.	d_{OAl}	d_{AlC}	d_{AlC_1}	d_{CC}	d_{CN}	d_{CH}	d_{CO}	d_{NH}
1× H_2O	1.79-1.87	2.03 2.57-2.65 3.05	2.60	1.40	1.47-1.57 2.40-2.50 3.04-3.12	1.09	1.25-1.32	1.01
2× H_2O	1,87	2.10-2.17 2.73 3.50-3.80	2.97	1.40	1.48 3.66 5.30-6.50	1.09	1.25-1.32	1.01
3× H_2O	1.87	2.26 3.74 4.52	5.93	1.40	1.48-1.56 2.49-2.57 2.80	1.09	1.32	1.01
4× H_2O	1.95	2.26-2.35 3.74-3.82 4.60-4.70	6.01	1.40	1.48-1.56 2.49-2.57 2.80	1.09	1.32	1.01

Table 5.15: *Reference distances in Ås from the simulations on the minimum energy structures for Phe.*

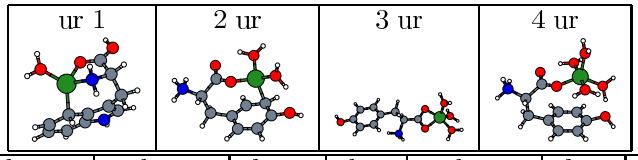

Hidr.	d_{OAl}	d_{AlC}	d_{AlC_1}	d_{CC}	d_{CN}	d_{CH}	d_{CO}	d_{NH}
1× H_2O	1.79-1.87	2.03 2.47-2.57 3.74	2.05	1.40	1.48-1.57 2.40-2.50 2.87-2.96	1.09	1.25-1.32	1.01
2× H_2O	1,87-1.87	2.10-2.17 2.73 3.83	3.06	1.40	1.48-1.57 2.49-2.57 3.83-3.89	1.09	1.25-1.32	1.01
3× H_2O	1.87	2.26 3.74	5.94	1.40	1.48-1.56 2.49-2.57 2.80.2.90	1.09	1.32	1.01
4× H_2O	1.95	2.26-2.34 3.74-3.82	5.97	1.40	1.48-1.56 2.49-2.57 2.80-2.90	1.09	1.32	1.01

Table 5.16: *Reference distances in Å from the simulations on the minimum energy structures for Tyr.*

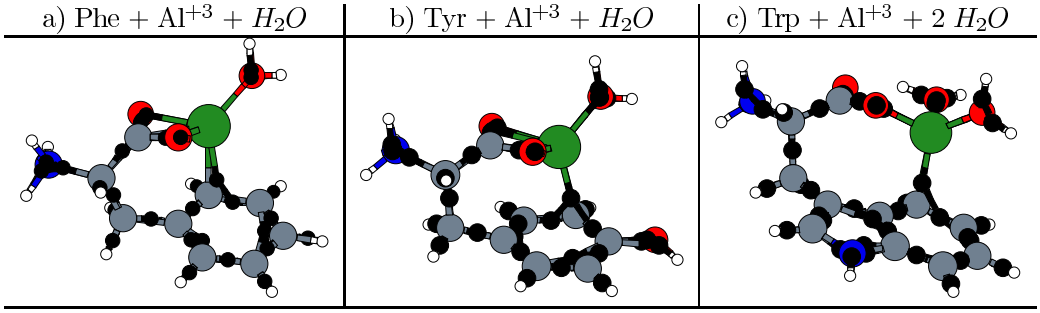

Figure 5.9: *Maximally localized Wannier function centers (black spheres) for different samples.*

5.4 Conclusions

- Single aromatic amino acids have clearly CS conformation, and the orientation of the aromatic side chain does not produce any meaningfull energy changes.
- Charge distribution is clearly ZW for non microsolvated clusters, and Al^{+3} gets coordinated by the aromatic ring, one or two oxygens from the carboxylate (one for Phe and two for Tyr and Trp)

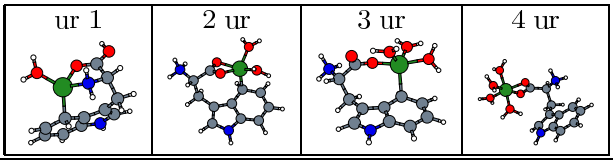

Hidr.	d_{OAl}	d_{AlC}	d_{AlC_1}	d_{CC}	d_{CN}	d_{CH}	d_{CO}	d_{NH}
1× H_2O	1.86	2.03 2.47-2.57 3.74	5.97	1.40	1.32-1.41 2.26-2.50 3.23 3.66-3.75	1.09	1.25-1.33	1.01
× H_2O	1.86-1.95	2.10-2.17 2.73 3.83	3.59	1.40	1.32-1.41 2.49-2.50 3.66-3.75	1.09	1.25-1.33	1.01
3× H_2O	1.86-195	2.26 3.74	3.71	1.40	1.32-1.41 2.49-2.50 3.66.2.75	1.09	1.25-1.33	1.01
4× H_2O	1.72-1.95	2.26-2.34 3.74-3.82	5.47	1.40	1.32-1.48 2.35-2.50 3.66-2.75	1.09	1.25-1.33	1.01

Table 5.17: *Reference distances in Å's from the simulations on the minimum energy structures of Trp.*

- Minimum energy structures of monohydrated clusters show CS charge distribution and Al^{+3} is coordinated by the aromatic ring, O (from carboxylate) and N.

- Dihydrated clusters have ZW charge distribution and Al^{+3} is coordinated by the aromatic ring and one (Trp) or two (Phe/Tyr) oxygens from the carboxylate.

- Cation-π interactions are important for less than three microsolating waters for Phe and Tyr and four microsolvating waters for Trp. For higher hydration states, competition between cation-π interactions and electrostatic interaction with water molecules yields the Al^{+3} to choose waters instead of the aromatic ring.

- IZW charge distribution was found just in the case of Phe. From the energy point of view these structures have high energy ((≈ 20-30 kcal/mol).

- The coordination of Al^{+3} could be expected to be as high as possible in the non microsolvated AAA-Al^{+3} clusters, so 3, but in the minimum energy structure for Phe (structure **a**) is just two-coordinated, having slightly lower energy to

the similar structure **b** on G03 calculations. In contrast, the tri-coordinated structure appears to be more stable.

- Al^{+3} seeks higher coordination number on the case of one microsolvating water, so that tetracoordination is favored. On dihydrated clusters, although Phe and Tyr have the possibility to achieve pentacoordination as Trp, there is just monodentated bond to the carboxylate. Trihydrated structures avoid the aromatic ring and pentacoordinion dominates. In the case tetrahydrated clusters there is a competition between 5 and 6 coordination, for the cases of mono and bidentate bond with the carboxylate.
- Bond distances appear to be about 0.01 Å shorter on CPMD calculations compared to the ones with Gaussian 03.

Chapter 6

Full solvation environment

Previous simulations with microsolvated system are an attempt to understand the structures more accurately and be able to compare results between isomers.

In the next chapter an attempt for full solvated system was made. Since the calculations are studied by CPMD the equilibrium between reasonable statistics and computational cost was set to 50 microsolvating waters by following the example of similar researches [62] over more than 100 ps for each simulation.

Molecular Dynamics simulations were performed by following the Car-Parrinello molecular dynamics method [43] trough the CPMD [31] package, producing over 100 ps trajectories for each system.

Total temperature of the system was set to 300 K by using Nose[37]-Hoover[38] thermostat [39].

Atoms were described by DFT by using PBE density functional [29] and Vanderbilt ultrasoft pseudopotentials [32] implemented [33] for CPMD [68], with 30 Ry. plane wave cutoff. Electronic fictitious mass (μ) was set at 900 a.m.u. with a time step of 7 a.u.

The size of the simulation cell was calculated so that the density is equals to the density of water, so 1 gr per cubic centimeter, and in our cases, the lattice parameter for a cubic simulation box is around 12.18 Å (takin in account the different amino acids have different amount of atoms).

Due to the relatively high amount of atoms (≈ 175) in these solution simulations, and the fact of simulating them for over 100 ps, makes these simulations really expensive, and due to the computational scientists omnipresent problem of having too little amount of CPUs, different structures and coordinations for each amino acid could not be studied, as in the case of Al^{+3} solution.

For making an idea of the cost, each of these simulations cost over 800 CPU hours, and in EHU's "Arina" computational infrastructure [83], the average time consumed per job is of 60-100 CPU hours. Such a expensive cost made us choose just the minimum amount of optimum structures.

Although most of the calculations were performed in Arina, some of the results shown in this thesis were calculated in the resources of i2Basque [84] and BSC's Mare Nostrum [85].

6.1 Radial Distribution Functions and bond distances

In the following simulations, the ligands around Al^{+3} are going to be the oxygen(s) from the carboxylate and the water molecules from the solvent, and therefore there will not be Al-N interactions.

The simulation on Phe starts from tetracoordination, dihydrated, monodentated conformation (two waters, aromatic ring, and the oxygen form carboxylate), and the simulations yields to tricoordination so that interactions with the aromatic ring are lost. The reason for Phe to have so low coordination could be in the effect of the solvent, so that the water molecules in the solvent help in scattering the charge from Al^{+3}, and although the tricoordinated structure would be theoretically unfavored, it gets somehow stabilized. This does not mean that the most stable structure for the Phe complex is tricoordinated, only proofs it's existence and stability for a quite long amount of time ($\approx$ 100 ps). On other hand, the coordination of Al^{+3} could be predicted to increase [47][48], by taking water molecules from second solvation layer, producing an even more stable structure.

Although in the case of Phe, Al^{+3} has just three ligands, due to the -OHs and the carboxylate it is neutralized from a charge point of view.

As a consequence, the charge from the cation is spread more easily thanks to the waters in the solvent, and therefore cation-π interactions loose importance when comparing them with Al-water interactions.

In the case of Tyr and Trp, simulations were started from pentacoordinated, monodentated tetrahydrated structure, and the same structures kept stable for over 100 ps.

RDFs in Fig. 6.2 show the peak concerning to the g_{OAl} for the three amino acids. The first peak for the tetracoordinated Phe appears at 1.79-19 Å, while the equivalent Al-O peak for pentacoordinated Tyr and Trp appears at 1.9-2.0 Å. Second solvation layer for Phe appears at 4.0-4.1 Å, and at 4.0 Å for Tyr and Trp.

The integrals show the averaged coordination of Phe to be 3 at first solvation layer and 8-10 at second one. For the case of Tyr and Trp, coordination at first solvation layer was found of identical pentacoordination, but their solvation layers differ on second solvation layers with around twelve waters for Tyr and eight for Trp.

g_{H-Al} show a similar behavior compared to the g_{OAl}. This time integrals show eight hydrogens on first solvation layer for Tyr and Trp and 6-4 for Phe. Once again, first peak of Phe appears located to shorter distances due to the lower coordination, then the peaks of Tyr and Trp with Tyr located to an slightly higher distance. The peak on Trp show a chamfer end, which points to the presence of -OH groups.

Comparison of this data with the RDFs in chapter 4 show an slightly different

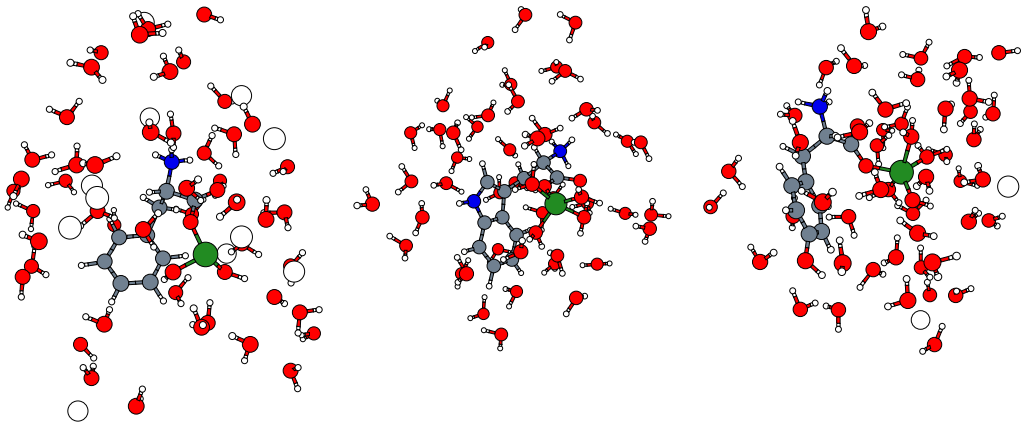

Figure 6.1: *Some illustrative figures of the simulation on full solvated (50 H_2O) simulations on Phe, Tyr and Trp.*

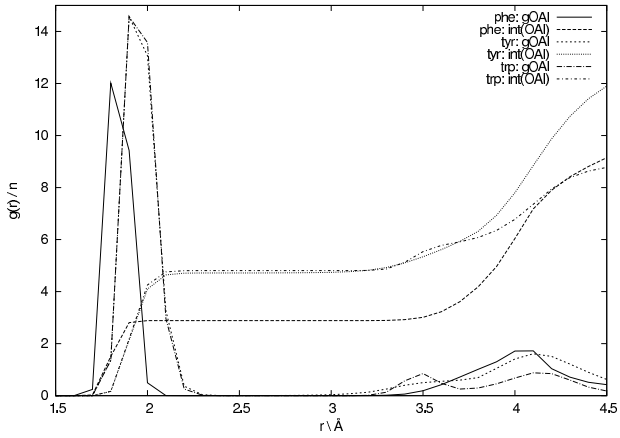

Figure 6.2: g_{OAl} *of full solvated (50 H_2O) simulations on Phe, Tyr and Trp.*

behavior on the solvation shells of Al^{+3} for the full solvated amino acids and Al solution.

As Fig. 6.4 **a)** shows, the O-Al distance at same coordination level is shorter for system with amino acids and same behavior for H-Al distance (Fig. 6.4 **b)**).

One of the reasons for Al^{+3} to have longer distances to the solvation layers is the steric repulsion of the amino acids themselves.

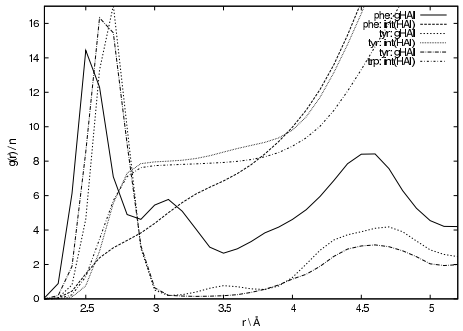

Figure 6.3: *g_{HAl} of full solvated (50 H_2O) simulations on Phe, Tyr and Trp.*

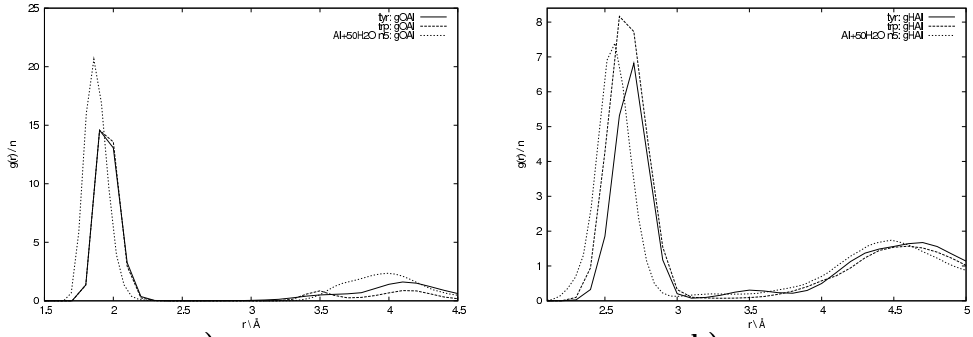

Figure 6.4: *Comparison of g_{OAl} and g_{HAl} of full solvated simulations on Tyr and Trp with the simulation of pentacoordinated aluminium solution.*

The g_{HO} and g_{OO} show the behavior that could be expected for a simulation in solution. The g_{HO} are sharply identical for the three simulations with a peak describing the H-O distance at around 1.02 Å. There is just one clear peak, without any side peak, which dismisses the possibility of finding any hydroniums in water solution. Therefore, no water dissociation is expected in the bulk solution.

In the g_{OO} the three functions are overlapped. First peak appears to be at 2.8 Å, which belongs to the O-O distances from the waters in solution.

On other hand, g_{OO} of the three systems also show an small side peak to the left at 2.3 (for Phe) and 2.4 Å(for Tyr and Trp), which belongs to the oxygens in the carboxylate.

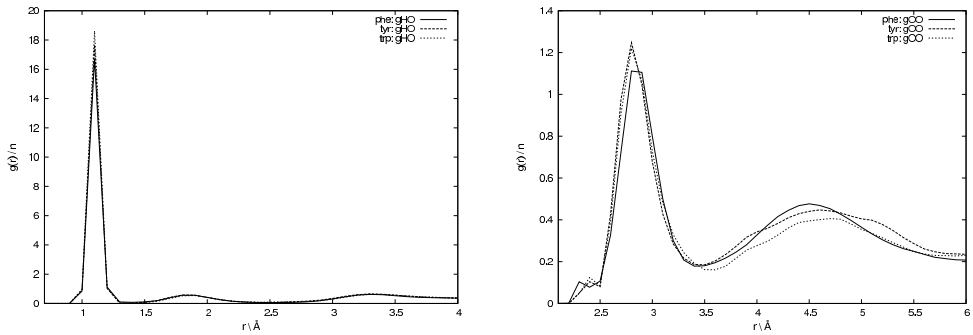

a)g_{HO} b) g_{OO}

Figure 6.5: *g_{HO} and g_{OO} of full solvated (50 H_2O) simulations on Phe, Tyr and Trp.*

6.2 Free energies

6.2.1 Al binding energies

The methodology used for estimating the free energies from MD simulations was introduced in section 2.4.3.

Free energies in this section were estimated from the full solvated systems measuring the distances between C_1 (or C_α) carbon and the Al^{+3}

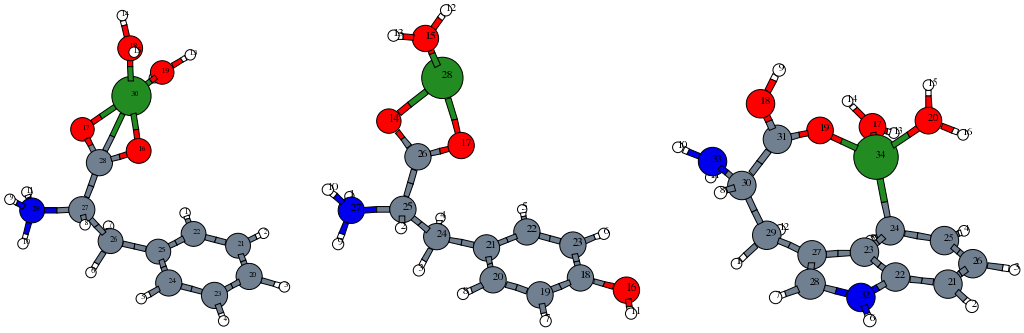

a) phe C_1=25 b) tyr C_1=21 c) trp C_1=27

Figure 6.6: *Figure showing the C_1 carbons.*

The process of ripping the distances from the whole trajectory was made with a modified version of an analysing code initially developed by the group of Prof. Kari

From	To	ΔE	Error	
Al-Phe	(cation-π)	∞	4.05	$\pm$ 0.55
	(Open)	∞	3.05	$\pm$ 0.37
	(cation-π)	Irekia	2.05	$\pm$ 0.25
Al-Tyr	(Open)	∞	9.44	$\pm$ 0.99
Al-Trp	(Open)	∞	22.7	$\pm$ 1.99

Table 6.1: *Different binding energies in kcal/mol of AAA-Al^{+3} complexes in full solvation environment.*

Laasonen, and the pictures at Fig. 6.7, 6.8 and 6.9 were generated by a self made code.

Fig. 6.7 **a)** shows an Al-C_1 distance population histogram and the corresponding Helmholtz free energy profile. Two different zones can be appreciated, first one belongs to the structure where Al^{+3} is having cation-π interactions with the ring, and the second one belongs to the structure with the open aromatic side chain. This way, the binging energies for both open close conformations can be calculated and also the transition energy from open to closed conformation.

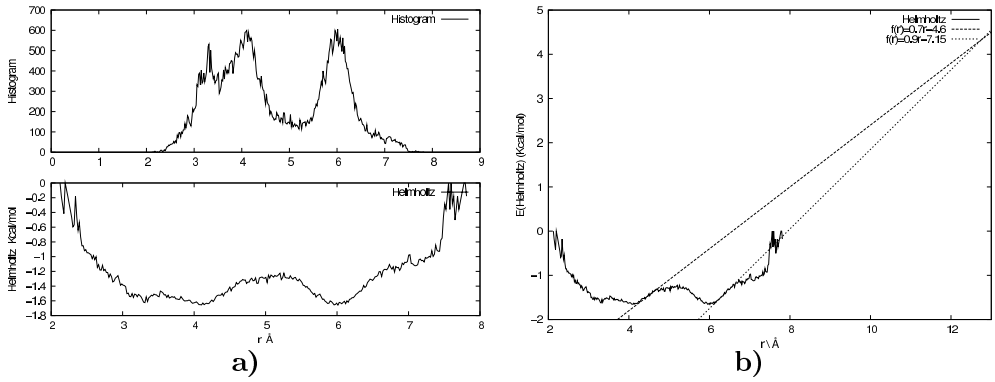

Figure 6.7: **a)** *Population histograms and Helmholtz's free energy profile for Al^{+3} binding on Phe, and* **b)** *Extrapolation of the free energy curve from open and close equilibrium points to infinite (half lattice further).*

According to the data in table 6.1 the energy needed to eject the Al^{+3} from the tetra-/tricoordinated Phe is substantially lower than in the cases of Tyr and Trp. The energy needed for Phe to overcome cation-π interactions is almost the half of the binding energy.

The AAA-Al^{+3} binding energies in the cases of Tyr and Trp have been calculated just for the open structures (the ones without cation-π interactions), and according

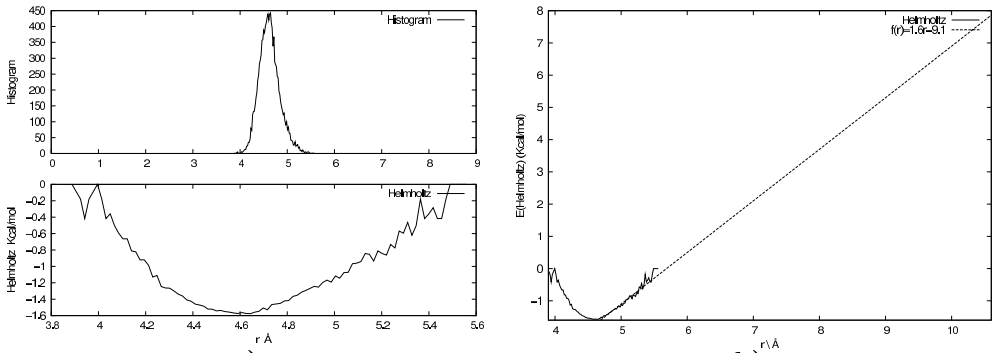

Figure 6.8: **a)** *Population histograms and Helmholtz's free energy profile for* Al^{+3} *binding on Tyr, and* **b)** *Extrapolation of the free energy curve from equilibrium point to infinite (half lattice further).*

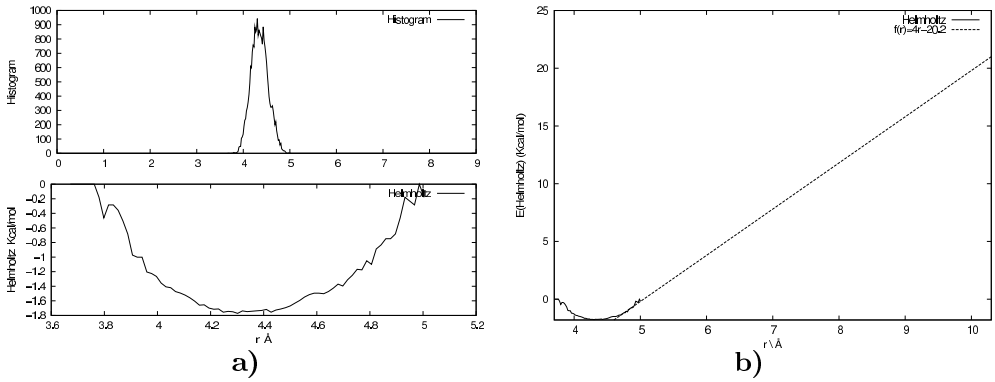

Figure 6.9: **a)** *Population histograms and Helmholtz's free energy profile for* Al^{+3} *binding on Trp, and* **b)** *Extrapolation of the free energy curve from equilibrium point to infinite (half lattice further).*

to the results, binding energy compared to Phe is two times higher for the case of Tyr and five times higher for the case of Trp. The interaction of the Al^{+3} is weaker when binding to Phe compared to the one Tyr, because Tyr's -OH produces more negative charge on the ring, therefore attracting the Al^{+3} more strongly. Trp has a double ring and on one of the rings it has a nitrogen, which seems to make cation-π interactions stronger.

From	To	ΔE
Tyr-Al^{+3}-$(H_2O)_4$	Tyr-Al^{+3}-$(H_2O)_3$ + H_2O	47.5
Trp-Al^{+3}-$(H_2O)_4$	Trp-Al^{+3}-$(H_2O)_3$ + H_2O	56.1
Al^{+3}-$(H_2O)_5$	Tyr-Al^{+3}-$(H_2O)_4$ + H_2O	19.0

Table 6.2: *Estimation of the dehydration energy (in kcal/mol) for pentacoordinated Al^{+3} in different environments. Calculations have an error of 10 %.*

6.2.2 Dehydration free energies

Dehydration energy for these complexes can be estimated in the same way as in the simulations on Al^{+3} on water solution.

Taking as a reference the longest Al-O distance on the first solvation layer of the Tyr and Trp simulations, partition function and Helmholtz free energy curve were calculated (Fig. 6.10) and the measured results are shown in the table 6.2.

If we compare the data with the one obtained in Al^{+3} solution, a much higher dehydration energy can be observed. Actually, being carboxylate one of the ligands around Al^{+3} instead of a water molecule, produces a two or three times higher energy values.

On other hand, as can be seen in Fig. 6.4, Al-O distance is shorter for the case of Al^{+3} solution, but according to the graphics in Fig. 6.10, the waters with longest Al-O distances for first solvation layer form an stronger bond and appear to an slightly shorter distances.

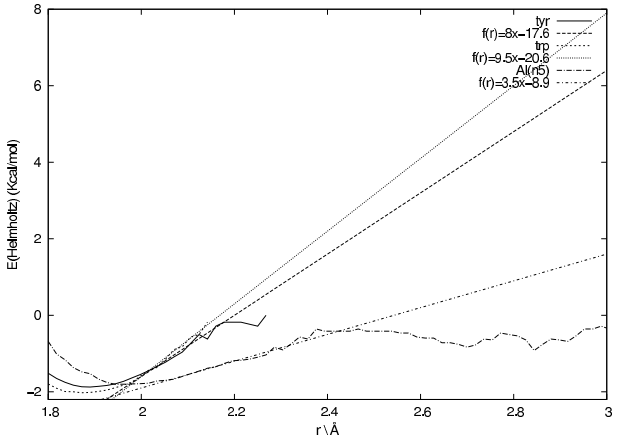

Figure 6.10: *Extrapolation of the dehydration Helmholtz free energy curve of Al^{+3}-water from Tyr, Trp and Al^{+3} solution.*

6.3 Conclusions

- Cation-π interactions are unfavored in solution.
- Pentacoordinated structures keep stable over 100 ps.
- It is possible to keep a tricoordinated structure stabilized by -OH anions for at least some tens of picoseconds.
- The dehydration energy for Al^{+3} on the Al^{+3}-AAA complex solution is two or three times higher than in Al^{+3} solution.
- The binding energy of Al^{+3} in Trp is about two times higher than in the case of Tyr and for times higher than in Phe.

Chapter 7

Discussion

The first three chapters of this thesis, introduced the Al and AAA topic, reviewed the theoretical tools and described the background research on the field.

After studying the behavior of the Al^{+3} in water solution in chapter 4, the stability of tetra-, penta- and hexacoordination was confirmed, but also the low energy barrier from pentacoordinated towards hexacoordinated. Later on, dehydration energy calculations show that pentacoordinated structure is not as stable as tetra- and hexacoordinated ones.

Therefore, 4-6 ligands could be expected around the Al^{+3} on AAA-Al^{+3} solution.

From the study on the microsolvated structures of AAA-Al^{+3} clusters in chapter 5, the coordination number of Al^{+3} is expected to be between 4 and 6. For the cases of mono- and dihydration, Al^{+3} tries to increase it's coordination number, but for tri- and tetrahydration theres some kind of equilibrium, where due to the steric repulsion of the ligands, cation-π interactions are neglected.

Although the coordination in general is expected to be between 4 and 6, in the case of full solvation shown in chapter 6, the possibility of some kind of stability was found also for tricoordination.

Making an interpretation of the effect of the aluminum on AAA, naked amino acids and amino acids in solution show CS charge distribution, and most meaningful effect on the presence of the Al^{+3} cation would be to produce a ZW charge redistribution.

Performed calculations show clearly CS charge distribution on naked amino acids while AAA-Al^{+3} clusters show ZW, and surprisingly, for monohydrated AAA-Al^{+3} clusters have CS. For the rest of microhydration states and in water solution ZW charge distribution was found.

This way, charge distribution of the amino acids on a protein where Al^{+3} has approached would depend on the number surrounding waters. It would not be probable to have just one surrounding water molecule in water solution, but in protein environment the amount of free water molecules is limited, and therefore the possibility of monohydration is not so improbable.

So, the effect of the aluminum in the charge distribution of the amino acids depends on the amount of water ligands around Al^{+3}, and due to the limited amount of water molecules in the protein environment. It would be possible to keep the original CS structure, but on other hand, it is more probable to have some other microhydration state which would produce ZW structures, and consequently a change in the properties of the amino acid and it's effect on the whole protein.

Next challenge would be to find out the effect of the charge redistribution on protein level, or said in another words, the effect of the charge redistribution produced by the aluminum at protein level, and it's biological consequences. As an example, it would be specially interesting to be able to simulate the β-Amyloid protein which suspected to be behind the Alzheimer disease, but due to the huge number of atoms involved, it would be necessary to choose some other simulation method, such as classical dynamics or semiempiric, which would neglect the electronic structure, or otherwise QM/MM methods.

Without loosing accuracy, a bigger system could be chosen, so instead of amino acids, a peptide or protein fragment could be simulated. The computational cost for a simulation of around 500 atoms would be some thousands of hours with CPMD code. Fortunately, nowadays, in a proper supercomputing infrastructure, with some thousand CPUs this could be simulated in a few days.

Bibliography

[1] Txurruka, J. M. *Eboluzioaren Inguruan.* EHU-ko argitarapen zerbitzua, 1986.

[2] Rengel, Z. Aluminum cycling in the soil-plant-human continuum. *BioMetals* **17** (2004), 669–689.

[3] Holm, R. H., Kennepohi, P., and Solomon, E. I. Structural and Functional Aspects of Metal Sites in Biology. *Chem. Rev.* **96** (1996), 2239–2314.

[4] Williams, R. What is wrong with aluminium? The J.D. Birchall memorial lecture. *J. Inorg. Biochem.* **76** (1999), 81–88.

[5] Rezabal, E., Mercero, J. M., Lopez, X., and Ugalde, J. M. A study of the coordination shell of aluminium(III) and magnesium(II) in model protein environments: Thermodynamics of the complex formation and metal exchange reactions. *Inorg. Biochem.* **100** (2006), 374–384.

[6] Elixabete Rezabal, X. L., Jose M. Mercero and Ugalde, J. M. Protein Side Chains Facilitate Mg/Al Exchange in Model Protein Binding Sites. *Chem. Phys. Chem.* **8** (2007), 2119–1200.

[7] Alfredo Sanz-Medel, R. M., Ana B. Soldado Cabezuelo and Polak, T. B. The chemical speciation of aluminium in human serum. *Coord. Chem. Rev.* **228** (2002), 373–383.

[8] Nagaoka, M. H. and Maitani, T. Binding affinity of aluminium to human serum transferrin and effects of carbohydrate chain modification as studied by HPLC/high-resolution ICP-MS. *J Inorg Biochem* **99** (2005), 1887–1894.

[9] Harris, W. R. and Messori, L. A comparative study of aluminum(III), gallium(III), indium(III), and thallium(III) binding to human serum trasferrin. *Coord. Chem. Rev.* **228** (2002), 237–262.

[10] Harris, W. R. and Sheldon, J. Equilibrium Constants for the Binding of Aluminum to Human Serum Transferrin. *J Inorg Chem* **29** (1990), 119–122.

[11] Paik, S. R., Lee, J.-H., Kim, D.-H., Chang, C.-S., and Kim, J. Aluminum-Induced Structural Alterations of the Precursor of the Non-Aβ Component of Alzheimer's Disease Amyloid. *Archives of Biochemistry and Biophysics* **344** (1997), 325–334.

[12] Kawahara, M. Effects of aluminum on the nervous system and its possible link with neurodegenerative diseases. *Journal of Alzheimer's Disease* **8** (2005), 171–181.

[13] Klatzo, I., Wisniewski, H., and Streicher, E. Experimental production of neurofibrillary degeneration I. Light microscopic observation. *J. Neuropathol. Exp. Neurol.* **24** (1965), 187–199.

[14] Miura, T., Suzuki, K., Kohata, N., and Takeuchi, H. Metal Binding Modes of Alzheimer's Amyloid β-Peptide in Insoluble Aggregates and Soluble Complexes. *Biochemistry* **39** (2000), 7024–7031.

[15] Ricchelli, F., Drago, D., Filippi, B., Tognon, G., and Zatta, P. Aluminum-triggered structural modifications and aggregation of β-amyloids. *Cell. Mol. Life. Sci.* **62** (2005), 1724–1733.

[16] Banks, W. A., Niehoff, M. L., Drago, D., and Zatta, P. Aluminum complexing enhances amyloid β protein penetration of blood-brain barrier. *Brain Research* **1116** (2006), 215–221.

[17] Exley, C. *Aluminium and Alzheimers's dissease: The science that describes the link.* Elsevier, 2001.

[18] Jansson, E. T. Aluminum exposure and Alzheimer's dissease. *Journal of Alzheimer's Disease* **3** (2001), 541–549.

[19] Rowatt, E., Sorensen, E. S., Triffit, J., Viess, A., and Williams, R. J. P. An Examination of the Binding of Aluminum to Protein and Mineral Components of Bone and Teeth. *J. Inorg. Biochem.* **68** (1997), 235–238.

[20] Haug, A. and Vitorello, V. Aluminium coordination to calmodulin: thermodynamic and kinetic aspects. *Coord. Chem. Rev.* **149** (1996), 113–124.

[21] Aquino, A. J. A., Tunega, D., Haberhauer, G., Gerzabek, M. H., and Lischka, H. A density-functional investigation of aluminium(III)-citrate complexes. *PCCP* **3** (2001), 1979–1985.

[22] de Noronha, A. L. O., aes, L. G., and Duarte, H. A. Structure and Thermodynamics Analysis of the First Mononuclear Aqueous Aluminum Citrate Complex Using DFT Calculations. *J. Chem. Theor. Comp.* **3** (2007), 930–937.

[23] Rubini, P., Lakatos, A., Champmartin, D., and Kiss, T. Speciation and structural aspects of interactions of Al(III) with small biomolecules. *Coord. Chem. Rev.* **228** (2002), 137–152.

[24] Ma, J. C. and Dougherty, D. A. The Cation-π Interaction. *Chem. Rev.* **97** (1997), 1303–1324.

[25] Dougherty, D. A. Cation-π Interactions in Chemistry and Biology: A New View of Benzene, Phe, Tyr, and Trp. *Science* **271** (1996), 163–168.

[26] Allen, M. P. *Introduction to Molecular Dynamics Simulation*, vol. 23 of *NIC*. John von Neumann Institute for Computing, Jü, 2004.

[27] Hohenberg, P. and Kohn, W. Inhomogeneous Electron Gas. *Physical Review* **136** (1964), B864–B871.

[28] W.Kohn and Sham, J. Self-Consistent Equations Including Exchange and Correlation Effects. *Physical Review* **140** (1965), A1133–A1138.

[29] Perdew, J. P., Burke, K., and Ernzerhof, M. Generalized Gradient Approximation Made Simple. *Phys. Rev. Lett.* **77** (1996), 3865–3868.

[30] Trygve Helgaker, P. J. and Olsen, J. *Molecular Electronic-Structure Theory*. Wiley, 2000.

[31] v3.11.1, C. (Revision A11). Copyright IBM Corp 1990-2006, Copyright MPI fr Festkrperforschung Stuttgart 1997-2001. www.cpmd.org.

[32] Vanderbilt, D. Soft self-consistent pseudopotentials in a generalized eigenvalue formalism. *Physical Review B* **41** (1990), 7892–7895.

[33] Laasonen, K., Car, R., Lee, C., and Vanderbilt, D. Implementation of ultrasoft pseudopotentials in ab initio molecular dynamics. *Phys. Rev. B* **43** (1991), 6796–6799.

[34] Thomas Williams, C. K. e. a. GnuPlot.

[35] Leach, A. R. *Molecular Modelling: Principles and Applications*. Pearson Education EMA-Prentice Hall, 2001, 2 edn.

[36] Woodcock, L. V. Isothermal molecular dynamics calculations for liquid salts. *Chem. Rev. Lett.* **10** (1971), 257–261.

[37] Nos, S. A unified formulation of the constant temperature molecular dynamics methods. *J. Chem. Phys.* **81** (1984), 511–.

[38] Hoover, W. G. Canonical dynamics: Equilibrium phase-space distributions. *Phys. Rev. A* **31** (1985), 1695.

[39] Evans, D. J. and Holian, B. L. The NoseHoover thermostat. *J. Chem. Phys.* **83** (1985), 4069.

[40] Schrödinger, E. An Undulatory theory of the mechanics of atoms and molecules. *Physical Review* **28** (1926), 1049–1079.

[41] Marx, D. and Hutter, J. *Ab initio molecular dynamics:Theory and Implementation*, John von Neumann Institute for Computing, Jülich, 2000, vol. 1 of *NIC*, pp. 3001–449.

[42] Barbara Kirchner, A. P. S. and Hutter, J. CPMD manual, Copyright IBM Corp 1990-2001, Copyright MPI für Festkörpeforschung Stuttgart 1997-2005.

[43] Car, R. and Parrinello, M. Unified Approach for Molecular Dynamics and Density-Functional Theory. *Physical Review Letters* **55** (1985), 2471–2474.

[44] Marzari, N. and Vanderbilt, D. Maximally localized generalized Wannier functions for composite energy bands. *Phys. Rev. B* **56** (1997), 12847–12865.

[45] Sprik, M. and Ciccotti, G. Free energy from constrained molecular dynamics. *J. Chem. Phys.* **109** (1998), 7737–7744.

[46] P., E. Die Berechnung optischer und elektrostatischer Gitterpotentiale. *Ann. Phys.* **369** (1921), 253–287.

[47] Swaddle, T. W., Rosenqvist, J., Yu, P., Bylaska, E., Philips, B. L., and Casey, W. H. Kinetic Evicence for Five-Coordinatin in $AlOH(aq)^{-2}$ Ion. *Science* **308** (2005), 1450–1453.

[48] Takashi Ikeda, M. H. and Kimura, T. Hydrolysis of $AlOH(aq)^{-2}$ from constrained molecular dynamics. *J. Chem. Phys.* **124** (2006), 074503–1.

[49] Ruiz, J. M., McAdon, M. H., and Garcés, J. M. Aluminum Complexes as Moldels for Broensted Acid Sites in Zeolites: Structure and Energetics of $[Al(OH)_4]^-$, $[Al(H_2O)_6]^{3+}$, and Intermediate Monomeric Species $[Al(OH)_x(H_2O)_{n-x}\cdot mH_2O]^{3+}$ Obtained by Hydrolysis. *J. Phys. Chem. B* **101** (1997), 1733–1744.

[50] Kowall, T., Caravan, P., Hourgeois, H., Helm, L., Rotzinger, F., and Merbach, A. Interpretation of Activation Volumes for Water Exchange Reactions Revised: Ab Initio Calculations for Al^{+3},Ga^{+3} and In^{+3}, and New Experimental Data. *JACS* **120** (1998), 6569–6577.

[51] Yang, W., Qian, Z., Miao, Q., Wang, Y., and Bi, S. Density functional theory study of the aluminium (III) hydrolysis in aqueous solution. *PCCP* **11** (2009), 2396–2401.

[52] Kluge, S. and Weston, J. Can a Hydroxide Ligand Trigger a Change in the Coordination Number of Magnesium Ions in Biological Systems? *Biochemistry* **44** (2005), 4877–4885.

[53] Sillanpää, A., Päivärinta, J. T., Hotokka, M. J., Rosenholm, J. B., and Laasonen, K. A Computational Study of Aluminium Hydroxide Solvation. *J. Phys. Chem* **105** (2001), 10111–10122.

[54] Charles W. Bock, A. K. K., George D. Markham and Glusker, J. P. The arrangement of first- and second-shell water molecules around metal ions: effects of charge and size. *Theor. Chem. Acc.* **115** (2006), 100–112.

[55] Frisch, M. J., Trucks, G. W., Schlegel, H. B., Scuseria, G. E., Robb, M. A., Cheeseman, J. R., Montgomery, J. A., Jr., Vreven, T., Kudin, K. N., Burant, J. C., Millam, J. M., Iyengar, S. S., Tomasi, J., Barone, V., Mennucci, B., Cossi, M., Scalmani, G., Rega, N., Petersson, G. A., Nakatsuji, H., Hada, M., Ehara, M., Toyota, K., Fukuda, R., Hasegawa, J., Ishida, M., Nakajima, T., Honda, Y., Kitao, O., Nakai, H., Klene, M., Li, X., Knox, J. E., Hratchian, H. P., Cross, J. B., Bakken, V., Adamo, C., Jaramillo, J., Gomperts, R., Stratmann, R. E., Yazyev, O., Austin, A. J., Cammi, R., Pomelli, C., Ochterski, J. W., Ayala, P. Y., Morokuma, K., Voth, G. A., Salvador, P., Dannenberg, J. J., Zakrzewski, V. G., Dapprich, S., Daniels, A. D., Strain,

M. C., Farkas, O., Malick, D. K., Rabuck, A. D., Raghavachari, K., Foresman, J. B., Ortiz, J. V., Cui, Q., Baboul, A. G., Clifford, S., Cioslowski, J., Stefanov, B. B., Liu, G., Liashenko, A., Piskorz, P., Komaromi, I., Martin, R. L., Fox, D. J., Keith, T., Al-Laham, M. A., Peng, C. Y., Nanayakkara, A., Challacombe, M., Gill, P. M. W., Johnson, B., Chen, W., Wong, M. W., Gonzalez, C., and Pople, J. A. Gaussian 03, Revision C.02. Gaussian, Inc., Wallingford, CT, 2004.

[56] G.Schaftenaar and Noordik, J. Molden: a pre- and post-processing program for molecular and electronic structures. *J. Comput.-Aided Mol. Design* **14** (2000), 123–134.

[57] Rodziewicz, P. and Doltsinis, N. L. Ab Initio Molecular Dynamics Free-Energy Study of Microhydration Effects on the Neutral-Zwitterion Equilivrium of Phenylalanine. *ChemPhysChem* **8** (2007), 1959–1968.

[58] Lavina C. Snoek, R. T. K. and Simons, J. P. A spectroscopic and computational exploration of tryptophan-water cluster structures in the gas phase. *PCCP* **4** (2002), 2130–2139.

[59] Ding, Y. and Krogh-Jespersen, K. The glycine zwitterion does not exist in the gas phase: results from a detailed ab initio electronic structure study. *Chem. Phys. Let.* **199** (1992), 261 – 266.

[60] Hodges, M. P. xmakemol, http://www.nongnu.org/xmakemol/.

[61] Dunbar, R. C. Complexation of Na and K to Aromatic Amino Acids: A density Functional Computational Study of Cation- Interactions. *J. Phys. Chem. A* **104** (2000), 8067–8074.

[62] Costanzo, F. and Valle, R. G. D. CarParrinello MD Simulations for the Na^+Phenylalanine Complex in Aqueous Solution. *J. Phys. Chem.* **112** (2008), 12783–12789.

[63] Emmanuel A. Meyer, R. K. C. and cois Diederich, F. Interactions with Aromatic Rings in Chemical and Biological Recognition. *Angewandte Chemie Int. Ed.* **42** (2003), 1210–1250.

[64] Jan P. Nordin, B. L. P., David J. Sullivan and Casey, W. H. An ^{17}O-NMR Study of the Exchange of Water on $AlOH(H_2O)_5^{2+}$ (aq). *J. Inorg. Chem.* **37** (1998), 4760–4763.

[65] Rezabal, E., Marino, T., Mercero, J., Russo, N., and Ugalde, J. Complexation of Al(III) by the aromatic aminoacids in the gas phase. *Inorg. Chem.* **46** (2007), 6413–6419.

[66] Mercero, J. M., Fowler, J. E., and Ugalde, J. M. Aluminum(III) interactions with the acidic amino acid chains. *J. Phys. Chem. A* **102** (1998), 7006–7012.

[67] Mercero, J., Fowler, J. E., and Ugalde, J. M. Aluminum(III) interactions with the acid derivative amino acid chains. *J. Phys. Chem. A* **104** (2000), 7053–7060.

[68] Laasonen, K., Pasquarello, A., Car, R., Lee, C., and Vanderbilt, D. Car-Parrinello molecular dynamics with Vanderbilt ultrasoft pseudopotentials. *Phys. Rev. B* **47** (1993), 10142–10153.

[69] Silvestrelli, P. L. and Parrinello, M. Structural, electronic, and bonding properties of liquid water from first principles. *J. Chem. Phys.* **111** (1999), 3572.

[70] Knight, W. D., Clemenger, K., de Heer, W. A., Saunders, W. A., Chou, M. Y., and Cohen, M. L. Electronic Shel Structure and Abundances of Sodium Clusters. *Phys. Rev. Let.* **52** (1984), 2141–2144.

[71] Lang, N. D. and Kohn, W. Theory of Metal Surfaces: Work Function. *Phys. Rev. B* **3** (1971), 1215–1223.

[72] Eric J. Bylaska, J. R. R., Marat Valiev and Weare, J. H. Structure and dynamics of the hydration shlls of Al^{+3} ion. *J. Chem. Phys.* **126** (2007), 104505.

[73] Hay, M. B. and Myneni, S. C. B. Geometric and Electronic Structure of the Aqueous $Al(H_2O)_6^{+3}$. *J. Phys. Chem. B* **112** (2008), 10595–10603.

[74] Bol, W. and Welzen, T. The interpretation of X-ray diffraction by aqueous solutions of aluminum(III) nitrate and chromium(III) nitrate. *Chem. Phys. Lett.* **49** (1977), 189.

[75] Caminiti, R., Licheri, G., Piccaluga, G., Pinna, G., and Radnai, T. Order phenomena in aqueous $AlCl_3$ solutions. *J. Chem. Phys.* **71** (1979), 2473–2476.

[76] Carminiti, R. and Radnai, T. *Z. Naturforsch. A* **35** (1980), 1368.

[77] Laasonen, K., Larrucea, J., and SillapÄÄ, A. Ab Initio Molecular Dynamics Study of a Mixture of HF(aq) and HCl(aq). *J. Phys. Chem. B* **110** (2006), 12699.

[78] Mercero, J. *Aluminum (III) interactions with aminoacid chains.* Ph.D. thesis, UPV/EHU (2001).

[79] Rezabal, E. *Binding and specificity of Aluminium in proteins.* Ph.D. thesis, UPV/EHU (2007).

[80] Stepanian, S. G., I. D. Reva, E. D. R., and Adamowicz, L. Conformational Behavior of α-Alanine. Matrix-Isolation Infrared and Theoretical DFT and ab Initio Study. *J. Phys. Chem.* **102** (1998), 4623.

[81] Siu, F. M., Ma, N. L., and Tsang, W. Cation-π interactions in Soldiated Phenylalanine Complexes: Is Phenylalanine in the Charge-Solvated or Zwitterionic Form? *JACS* **123** (2001), 3397.

[82] Dudev, T. and Lim, C. Monodentate versus Bidentate Carboxylate Binding in Magnesium and Calcium Proteins: What Are the Basic Principles? *J. Phys. Chem. B* **108** (2003), 4546–4557.

[83] SGI/IZO-SGIker, T. UPV/EHU (supported by the Development and Innovation - Fondo Social Europeo, MCyT and Basque Government) is gratefully acknowledged for generous allocation of computational resources.

[84] The autor thankfully acknowledges the computer resources, technical expertise and assistance provided by i2Basque.

[85] The author thankfully acknowledges the computer resources, technical expertise and assistance provided by the Barcelona Supercomputing Center - Centro Nacional de Supercomputación.

eman ta zabal zazu

Universidad del País Vasco
Euskal Herriko Unibertsitatea

Kimika Fakultatea
Polimeroen Zientzia eta Teknologia Departamentua

Aluminio katioiaren amino azido aromatikoen gaineko eraginaren azterketa konputazionala

DOKTORETZA TESIA

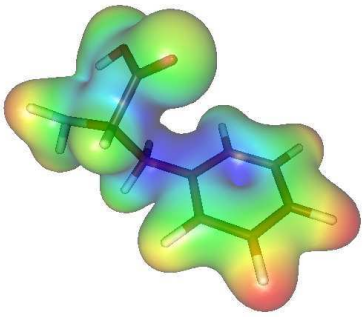

Julen Larrucea Corchero
Donostia, 2009-ko Iraila

Aluminio katioiaren amino azido aromatikoen gaineko eraginaren azterketa konputazionala

Doktorego tesia

Julen Larrucea Corchero
Zuzendaria: Jesus M. Ugalde profesorea

2009.eko ekainaren 15

"Shut up and calculate"

David Mermin

" - *calcular y*
\+ *artículos con los cálculos ya hechos"*

Mario Piris

"I think I can safely say that nobody understands quantum mechanics"

Richard P. Feynmann

Eskerrak

Eskerrak emateko orduan zaila egiten da lau urte hauetan zehar nigan eta nire lanaren gainean eragina izan duen pertsona guztiak aipatzea.

Hasteko, nola ez, tesi hau posible egin duen nire tesi zuzendari izan den Jesus M. Ugalde profesoreari eskerrak eman nahi dizkiot, bera baita Finlandian nengoela etxera bueltatzeko eta nire ikerkuntza ildo nagusia garatzeko behar izan dudan aukera eman didana.

Ez da erraza izan tesi hau aurrera ateratzea, baina Jesusi esker beti behar izan dudan guztia eskuratzeko aukera izan dut, eta guztia diodanean, nire ekimen guztiekiko izan daitekeen konfiantza guztia bezalako gauzak esan nahi dut. Gainera, bere taldean lan egiteak, nire konputazio kluster propioa izatea edo munduko hirugarren superkonputagailurik indartsuena erabiltzea bezalako aukera ikaragarriak ekarri dizkit.

Zaila egiten zait beste tokiren batean hemen sentitzen den askatasuna eta konfiantza senti daitekeenik imaginatzea.

Jesusez gain, azken lau urte hauetan nire lankideak izan diren "konstanteak" ere badaude, bulegoa alaitzen duen Xabi, nire krisi momentuetan aguantatzen nauen Txema, "the great" Txoni, kuantika eta bizitzari buruz izugarri erakutsi nauen "Profesor" Mario eta edozertarako izugarri balio duen Elena aipatu behar ditut nahitaez; denbora pasa ahala, nolabait nire bizitzaren parte txikitxo bat izatera pasa direlako.

"Konstante" mantendu diren lankideez aparte, badaude momenturen batean doktoradutzako "habitik" atera ziren Joni, Iñaki, Eli eta Eider zeintzuekin momentu politak izan ditudan, edo nire ondoren habira sartu diren Oier, Elisa eta Jon Mikel.

...eta doktoradutzako habian egon edo egon izan direnez aparte, Andreas eta Ivan lankideak ere aipatu behar ditut, edo noizean behin gurekin izan den Eduardo Ludeña profesorea.

Eta kostanteez hitz eginda, azken urteotan benetan konstante mantendu izan

den zerbait, bazkaltzeko ordua izan da, ordu batetan alegia, eta ia ordua bezain konstante mantendu dinenak bazkariaren inguruan nirekin aktualitate eta zientzia eztabaidak konpartitzen ari izan diren lagunak daude, hala nola, Iñaki (berriz ere), Eneko, Aizpea, Fernando, Ana, DIPC-ko guztiak Andres, Daniel, Elton, Thomas eta Vito barne eta nola ez, eremu atomikotik kanpo zientziaren ikuspuntu berri bat zabaldu digun Mikel "Kinti".

Garai batetik hona, bazkal ondoren Berioko parketxoan "Larru & Kinti" albokari panderujole bikoteren entsaiorik ez dagoenetik auzokoak lasai egin dezakete biaoa.

Gertu daudenez gain, tesi honen eraikuntzan eragina izan duten beste pertsona aipagarri batzuk daude. Hasteko Ouluko Kari Laasonen profesorea aipatu beharra dago, bera baita CPMD munduan sartu ninduena eta azken lau urteotan ere edozein momentutan laguntzeko prest egon dena. Ondoren Oulun ezagutu nituen Giorgio Lanzani eta Jaime Zaratiegui lagun/lankideak, kimika teoriko eta ordenagailuei buruzko trikimailu guztiak erakutsi zizkidatenak, eta Maurizio, Anne, Yrjö eta Johannarekin gertatu den bezala azken urte hauetan nigandik urruti baina gertu egon direnak.

Zaila litzateke tesi honekin laguntzen saiatu zaizkidan pertsonen zerrenda bat egitea, baina aipatu behar ditut halaber, Ari Seitsonen, Axel Kohlmeyer eta Pradip Biswas emandako laguntza kuantiko/konputazionalarengatik, Hannele Ylilehtö eta Markku Pulkkinen (eta beraien alabak Marika, Riikka eta Johanna) euren eskuzabaltasunarengatik eta neure ikerkuntza konputazionala medikuntzaren munduarekin lotzen laguntzeagatik edo Nico, fisikoki Tarragonako doktoradutzako kurtsoetan eta Perugiako Euro Masterrean baino ikusi ez garen arren, sarearen bidez etengabe elkarri adiskidetasun eta kode fragmentuak bidaltzen aritu garelako.

Lan honetan influentzia zuzenik izan ez duten arren, arazo konputazionaletatik pixka bat deskonektatzen lagundu izan didaten musika taldeetako lagunak ere badaude: *Xau*-ko Joseba, Gontxas, Aizpea eta Unai eta *Sabur*-eko Arantza, Amaia eta Ruth. Baita *Suomitar* Euskal Herria-Finladia elkarte kulturaleko kideak, momentu on asko eskeini dizkidatelako. Bestalde, nire tesiarengatik arduratzen aritu den Itsaso ere eskertu behar dut, ta Itxaso eta Björn Suediako kontaktuak ere.

Azkenik, nire familiari eskerrak eman nahi dizkiot, eta bereziki beti nire ondoan egon diren Encarni eta Gabi nire gurasoei, ...eta nola ez, Teresa amumari eta zoritxarrez tesi honen bukaera ikusiko ez duen, baina nire bihotzean beti egongo den Agustina amumari, nire alde egindako otoitz guztiengatik eta nire helburuak lor ditzadan jarri izan dizkidaten argizari guztiengatik. Tesi hau zuei dedikatua dago.

Laburdurak eta Konbertsioak

Laburdurak

MD	Dinamika Molekularra (Molecular Dynamics)
CPMD	Car-Parrinello Dinamika Molekularra (Car-Parrinello Molecular Dynamics)
AIMD	Ab-Initio Dinamika Molekularra (Ab-Initio Molecular Dynamics)
DFT	Dentsitate Funtzionalaren Teoria (Density Functional Theory)
RDF	Erradial Distribuzio funtzioa)
PBC	Muga Periodikozko Baldintzak (Periodic Boundary Conditions)
Al	Aluminioa
COO^-	Karboxilato anioia
AAA	Amino Azido Aromatikoa
Phe	Fenilalanina
Tyr	Tirosina
Trp	Triptophanoa
C_α / C_1	Alfa Karbonoa. Eraztun aromatikoan albo kateari lotuta dagoena.
u.a.	Unitate Atomikoak
a.m.u.	Masa Atomikoaren Unitatea
Ry	Rydberg
ps	piko-segundo
OM	Orbital Molekularra

Konbertsio Faktoreak

urrats denbora	1 u.a.= 0.0241888428 10^{-15}s
distantzia	1 Bohr = 1 a_0 = 0.529177249 Å
energia	1 Ha = 27.21161 eV = 627.5095 kcal/mol = 2625.5 kJ/mol
uhin lauen mozketa (cutoff)	1 Ry = 1/2 Ha = 13.6058 eV

Gaien Aurkibidea

1. Kapitulua

Sarrera: Aluminioaren biokimikaren garrantzia

Aluminioa (Al) hirugarren metalik ugariena eta lur gainazaleko hirugarren elementurik ugariena da. Aluminioa, lurzoruan, aluminosilikato mineral bezala agertzen da, baina horren parte txiki bat baino ez dago izaki bizidunongan eragin dezaketen konposatu disolbagarri eran.

Hala ere, hain ugaria izan arren, aluminoa ez da funtsezko bioelementua [1], eta gaur egunerarte ez da aluminiorik behar duen inongo erreakzio biologikorik aurkitu. Bestalde, gizarte modernoak aluminioaren presentzia sustatzen du, bai uretan, zein janarietan edo airean [2], zeinetan aluminioz pozoindutako euritik landareetara, elikadura katera, etab. pasatzen den.

Gizarte modernoaren ondorioz, aluminioa bide ezberdinak erabiliz barneratzen da gure organismoetan, esate baterako janari edo edarien latetatik, aluminiozko paper edo antitranspiranteetatik etab .

Aluminioa toxikoa dela aurkitua da, baina gaur egun bere toxikotasunaren kimika ez dago oraindik guztiz ulertua. Hainbat metalek funtzio biologiko erabakigarriak dauzkate eta normalean biomolekulei *binding sites* edo lotura guneetatik itsasten zaizkie [3]. Aluminioaren kasuan, orokorrean, esan genezake aluminioak antzekotasunak dituela beste bi elementu talderekin: kaltzioa edo magnesioa bezalako dibalenteekin eta kromo edo burdina bezalako tribalenteekin[4]. Beraien kimikaren antzekotasunak direla eta Aluminioa eta magnesioaren arteko lehia interes berezikotzat hartu izan da [5][6].

Gizakien kasuan, aluminioaren toxikotasun prosezua transferrinei itsasteko momentuan hasten da. Trasnferrinak, ornodun eta intsektuentan Fe (III)-aren bahiketa eta garraio prosezua burutzen duten proteinen familia da. Nahiz eta aluminioa Fe(III) desplazatzeko gai ez dela frogatua egon, trasnferrinan lotura gune asko gelditzen dira libre non aluminioa itsas daitekeen, izatez, onartua dago serumean disolbatuta dagoen aluminioaren %90 edo gehiago trasnferrinei lotuta dagoela [7][8], Fe(III) egon beharko litzatekeeneko lotura guneetan [9].

Bestalde, aluminio-trasferrina konplexuaren egonkortasuna dela eta [10], behin aluminioa trasferrinaren lotura gunera lotzean, bertan gelditzen da era iraunkorrean,

beste katioi metalikoren bat egon zitekeen tokian, honen ondorioz proteina osoan eragina sortuz [11].

Aluminioa beste zenbait gaixotasun neurodegeneratiborekin erlazionatua izan da [12]. Izatez, Albo Patogenesi Amiotrofikoa (ALS) eta Parkinson Dementia (PD) bezalako gaixotasunen jatorria aluminio mailen igoera eta kaltzio eta magnesio mailen jaitsierari lotuta dagoela aurkitua da. Partikularki, aluminioaren eta Alzheimerraren arteko lotura lehen aldiz Klatzo-ren taldeak proposatua zuen 1965ean [13], animalien burmuinean sartutako aluminioak Alzheimera duten gaixoetan agertzen den neurozuntzen degenerazioa eragiten zuela konturatu zirenean [14][15].

Aluminioa odolean garraiatzen denez, odol-burmuin langa dela eta, burmuinean aluminio kontzentrazioa erlatiboki baxuagoa da, baina bestalde, aurkitua da aluminioak amyloid-β proteinarekin konplexua sortzen duenean, honen burmuinera barneratzeko gaitasuna areagotzen duela [16].

Aluminioa eta Alzheimer gaixotasunaren arteko lotura aztertzen duten beste ikerketa asko egin izan dira, eta gaur egun, dagoeneko zeharo onartuta dago bien arteko lotura [17] [18].

Bestalde, aluminioa beste zeinbait biomolekuletara itsasteko joera ere aurkitu da, hala nola, osteopontina, osteoklazina eta fospoforina (hortz eta hezurretan) [19], Ca^{+2} ioien garraiatzalea den kalmodulina proteina [20], besteak beste erroen exudaziotik edo deskonposoturiko materiatik datorren azido zitrikoa [21] [22], eta beste hainbat [23].

Aluminioa eta proteinen arteko interakzio hauek guztiak ulertzearen koxka beraien kimikan dago, hau da, aluminioa nola, non, noiz eta zergatik itsasten zaien biomolekula ezberdinei, eta prozesu hauetan benetan gertatzen denaren irudi molekular bat osatzean.

Kasu honetan, ikuspuntu molekular hau hartu ahal izateko beharrezko tresnak kimika kuantikoak emanak izango dira. Bestalde, metodo kuantiko hauen kostu konputazionala, aztertzen den sistemaren atomo kopuruaren laugarren berreduraren proportzionala denez, sistemaren tamaina ahalik eta gehien murriztu behar da, eta beraz erronka, ikertu beharreko fenomenoa deskribatuko duen sistemarik txikiena aukeratzea izango da.

Beraz..., aluminioa proteinetan itsasten da, eta proteinak amino azidoez eginak daudenez, lehenengo hurbilketa aluminioa eta amino azidoez osaturiko sistemak ikertzea izango litzateke. Bestalde, beste zenbait ikerkuntza lanek frogatu dutenez, katioi-π interakzioak garrantzi berezia dutela dakigu [24][25], eta π elektroiak aromatizitatea erakusten duten amino azidoetan baino ez ditugu aurkituko, hots, amino azido aromatikoetan, zeinak hiru baino ez diren: Fenilalanina (Phe), Tirosina (Tyr) eta Triptofanoa (Trp). Beraz, hasierako hurbilketa, aluminioak proteinetan duen eragina, aluminio eta amino azido aromatikoez osaturiko sistema txikietara murriz

genezake.

Lan honetan erabili den ikerketa metodoa, eredu teorikoen bidez deskribaturiko kalkulu estatiko eta dinamikoen arteko nahaste batez osatuta dago. Kalkulu estatikoak, egitura jakin batzuen datu zehatzak lortzeko erabili dira eta dinamikoak egituren denboraren menpeko eraldaketa aztertzeko eta datu estatistikoak eskuratzeko. Erabili diren eredu teorikoak lehen printzipioen edo *ab-initio* izenez ezagutzen diren parametro enpirikorik gabeko zehaztasun ahalik eta handieneko ekuazioetan oinarrituta daude. Ab-initio tekniken erabilpena beharrezkoa da, atomoen egitura elektronikoa modelatu ahal izateko eta lotura kimikoak deskribatu ahal izateko.

Egindako lanaren emaitzak, hiru ataletan aurkeztuko dira. Lehenengoan aluminioak disoluzioan duen jokaera orokorra aztertuko da, bigarrenean aluminioak isolaturiko amino azidoetan eta mikrosolbatazio egoeran sortzen duen eragina aztertuko da eta hirugarrenean disoluzio inguruneko aluminioaren amino azidoenganako eragina deskribatuko da.

2. Kapitulua

Tresneria Konputazionala

2.1 Sarrera

Arlo honetako gainontzeko ikerketetan ez bezala, projektu honetan erabiliko den tresneria, metodo teoriko eta konputazional hutsetan oinarriturik egongo da.

Ondorengo kapituluan kimika teorikoari buruzko oinarrizko kontzeptu batzuei gainbegirada bat ematego zaizkie, emaitzak textuinguruan jartzeko helburuarekin.

Ikerkuntza honetan erabili den oinarrizko metodoetako bat Dinamika Molekularra (Molecular Dynamics edo MD) deitzen da, eta bereziki lagungarria da sistema molekularren jokaera ulertzeko orduan.

Sir Isaac Newtonek 1687-an bere "PhilosophiæNaturalis Principia Mathematica" argitaratu zuenetik, gizakiok gertaera naturalak hobeto ulertzeko eta aurresateko gai izan gara, bertan aurkeztu zen mekanika klasikoaren eredua eta berari dagozkion ekuazioak erabiliz.

Izatez, mekanika klasikoaren eredua jarraituz, erraz uler daiteke billar mahai baten gainean, bata bestearekin talka egiten dabiltzan pelota batzuen jokaera, eta are gehiago... euren jokaera aurresan genezake, etorkizun hurbil batean non egongo diren edo zeinekin talka egingo duten jakin genezakeela.

Hau posible izanda, hots, fisikaren legeak erabiliz pelota batzuen jokaera eta propietateak aurresateko gai baldin bagara, zergatik ez aplikatu antzerako metodo bat maila molekularrean?

Kimikari gehienek, momenturen batean, beraien ontzi koloretsuetan gertatzen ari dena ez ulertzearen inpotentzia sentitzen dute, baina izatez, ontzi koloretsu hauek eta berauen edukia atomoz osaturik dago, eta hurbilketa izugarri kaxkar bat eginez billar mahai horren gainean dauden bolen deskribapena egin daitekeen bezala, atomoz osaturiko sistema bat azter genezake. Beraz, zergatik ez aplikatu mekanikaren lege hauek atomoetan? Zergatik ez atomoen higidura aurresaten saiatu? ...eta atomoak ekuazioen bidez ulertuak izan badaitezke, eta munduan dagoen guztia atomoz eginda dagoela kontutan izanda ...mundua guztia simula eta uler genezakeela suposa al daiteke?!

Erantzuna **EZ**ezkoa da. Naturaren konplexutasunak eta sistemen tamainak kalkuluak konputazionalki garestiegi bihurtzen dituztelako.

Hala ere, sistemak sinplifikatuz eta teorietan hurbilketak aplikatuz, fenomenoen gako-guneetan dauden atomoak simula ditzakegularik, informazio oso baliogarria eskura daiteke.

2.1.1 MD kontzeptua ulertzeko eredu sinple bat

Dinamika Molekularra (MD) kimika teorikoaren tresna bat da, fisikaren lege ezberdinak erabiliz sistema bateko partikulak espazioan hedatzen dituena, sistema horren denborarekiko azterketa posible eginez.

Sistema bateko partikulak bata bestearekiko duten interakzioak banan banan hartuta ikertuak izan daitezke. Partikulen arteko indarrak jakinak badira, abiadurak jakin daitezke, beraz sistema denboran eta espazioan hedatzea posiblea da.

Hau egingo lukeen kode baterako algoritmo baten zirriborroa erraz idatz daiteke:

1. Kargatu simulazioa egiteko beharrezko parametroak (pausu kopurua, urrats denbora, tenperatura, simulazio kutxaren tamaina...)
2. Kargatu hasierako koordenatu eta abiadurak ($\mathbf{r}_1, \mathbf{v}_1, \mathbf{r}_2, \mathbf{v}_2, \mathbf{r}_3, \mathbf{v}_3, ...$)
3. Kalkulatu sistemaren tenperatura partikulen abiaduran oinarrituta

$$\overline{E_K} = \overline{\left[\frac{1}{2} m \dot{\mathbf{r}}^2\right]} = \frac{3}{2} NkT,$$

   non $\overline{E_K}$ batazbesteko energia zinetikoa, m partikularen masa, $\dot{\mathbf{r}}$ partikularen abiadura, k Boltzmann-en konstantea ($1.38 \times 10^{-23} JK^{-1}$) eta T sistemaren tenperatura diren

4. Eskalatu partikulen abiadurak termostatoak edo bereskalaketa faktoreak emandako tartean sar daitezen
5. Partikulen posizioak bereskalatu, Muga Periodikozko Baldintzen (PBC) bidez posizio bektoreak simulazio gelaxkaren tamainaz zaituz, partikula guztiak simulazio kutxaren barruan sar daitezen
6. Partikulen arteko indarrak kalkulatu. Hau era erraz (baina ez oso zehatz) batean egin daiteke, gehiago barik Lennard-Jones 12-6 bezalako bikote potentzial bat erabiliz [26]

$$V_{LJ} = 4\epsilon \left[\left(\frac{\sigma}{\mathbf{r}}\right)^{12} - \left(\frac{\sigma}{\mathbf{r}}\right)^{6} \right],$$

eta partikula bakoitzerako indarrak eta azelerazioak kalkulatuz banan banan

$$\mathbf{F}_i = -\nabla V_i = m\ddot{\mathbf{r}}_i.$$

7. Partikulak euren posizio berrietara hedatu

$$\mathbf{r}_i(t+\delta t) = \mathbf{r}_i(t) + \dot{\mathbf{r}}_i\delta t + \frac{1}{2}\ddot{\mathbf{r}}_i\delta t^2 + \ldots$$

8. Denbora $t = t + \delta t$-ra mugitu

9. Prosezu hau, eskatutako pausuak bezain beste aldiz egin izan bada, simulazioa gelditu, bestela bigarren urratsera bueltatu, koordenatu berriak kargatu eta begizta jarraitu

Beraz, pausu bakoitzeko trajektoriak eta sistemaren gainontzeko parametro interesgarriak jazo ditzazkegu.

Simulazioaren "kalitatea", partikulen interakzioak deskribatzen dituzten ekuazioen atzean dagoen teoriaren araberakoa da.

Metodoaren hautaketa faktore ezberdinak kontutan harturik egin behar da, hots, eskuragarri dauden baliabide konputazionalak, gure sistemaren tamaina edo ikertu nahi ditugun interakzioen natura.

Interakzioen deskribapen fisikoaren zehaztasuna normalean kostu konputazionalaren proportzionala izango da. Adibide bezala, ab-initio teknikak erabiltzekotan, eskalaketa edo kalkulua burutzeko denbora kopurua, atomo kopuruaren laugarren berreduraren proportzionala izango da, eta egitura elektronikoa arbuiatzen duen indar eremuetan oinarritutako dinamika molekular klasiko baten kasuan atomo kopuruaren karratuaren proportzionala baino ez da.

Dinamika molekular klasikozko metodoak bereziki interesgarriak dira sistema handiak aztertzeko, baina orokorrean ez dute balio egitura elektronikoa deskribatzeko, beraz, orokorrean ez dute balio lotura kimikoa era inplizitu batean aztertzeko. Ab-initio teknikak ordea, egitura elektronikoa deskribatzen dute, baina sistema txikiagoekin lan egin behar izatearen muga ezartzen dute.

Gure ikerkuntza aluminio atomoek, urarekin eta aminoazido aromatikoekin dituzten interakzioetan zentratuta dago (adib. lotura kobalentea, H-zubiak, katioi-π interakzioak, ...), eta interakzio hauek izaera ia gustiz elektronikoa dutenez, ab-initio tekniken erabilpena beharrezkoa egingo zaigu.

2.2 Sistemaren ab-initio deskribapena

Aurreko atalean dinamika molekularrerako adibide sinple bat aurkeztu da. Proposaturiko algoritmoak Lennard-Jones potentzialean oinarrituta dago, baina sistema molekular baten jokaera hobeto azaltzea nahi izanez gero eredu hobeagoetara jo behar da, hots, mekanika kuantikoak emandako kontzeptuetan oinarritutakoak.

Aurkez ditzagun beraz mekanika kuantikoaren oinarrizko kontzeptuetako batzu.

2.2.1 Dentsitate Funzionalaren Teoria (DFT)

Mekanika klasikoa Newtonen legeetan oinarritzen den bezala, mekanika kuantikoak Schrödinger-en ekuazioa erabiltzen du sistemen ebazpenerako. Zoritxarrez, ekuazio honen konplexutasun maila exponentzialki areagotzen da partikula kopuruarekin, izatez gaur egun ezinezkoa da Schrödingerren ekuazioa hainbat elektroidun sistemetarako ebaztea. Ondorioz, hurbilketetara jo behar da.

Hartree-Fock bezalako hurbilketa ezagunek, oinarri bezala elektroi anitz dituzten uhin funtzio korapilotsuak hartzen dituzte.

Funtzio korapilotsu hauek ebaztearen alternatiba bat Dentsitate Funtzionalaren Teoria (DFT) erabiltzea da. DFT-ren arabera, sistema oso bat, oinarrizko egoera barne, sistema horren elektroi dentsitatearen bidez deskriba daiteke. Ondorioz, N elektroi dituen sistema batean, uhin funtzio elektronikoa 3N koordenatuen menpekoa baldin bada, sistema osorako izugarrizko aldagai kopurua lortzen dugu, baina beste aldean ordea, DFT-k zein soilik hiru koordenatu espazialen menpekoa den, elektroi dentsitatea erabiltzeko aukera eskeintzen du.

Sistema baten propietateak dentsitate elektronikoan oinarritutako metodoetan deskribatzearen ideia, hasiera batean, Thomas-Fermi ereduan aurkeztua izan zen. Gaur egun DFT bezala ezagutzen duguna, Hohenberg eta Kohn-ek [27] 1964-an beraien bi teoremen bidez aurkeztu zutenaren ondorioa da.

Teorema hauetako lehenengoak, partikula anitz dituen sistema bateko oinarrizko egoerako ρ elektroi dentsitatea eta Ψ oinarrizko egoera horretako uhin funtzioaren artean erlazio biuniboko bat dagoela dio.

$$\rho(r) = \sum_{i=1}^{N} |\Psi_i(\mathbf{r}|^2. \tag{2.1}$$

Era honetan, sistemaren $E[\rho]$ energia eta kanpoko $\nu_{ext}(\mathbf{r})$ potentziala soilik ρ_0 oinarrizko egoerako dentsitatearen bidez zehaztuak daude, hots

$$E_0 = E_0[\rho_0] \tag{2.2}$$

$$E_0 = T_0[\rho] + \int \rho(\mathbf{r})\nu_{ext}(\mathbf{r})d\mathbf{r} + \mathbf{V}_{ee}[\rho_0] \tag{2.3}$$

non $T[\rho_0]$ energia zinetikoa eta $\mathbf{V}_{ee}[\rho_0]$ elektroi-elektroi interakzio energia diren.

Bigarren teoremak energia bariazionalaren printzipioa aurkezten du. Hau da, $(\tilde{\rho})$ funtzional unibertsal baten existentzia proposatzen du, zeinetan energia minimoa lortzeko era bakarra, benetako ρ_0 oinarrizko egoerako energiaren funtzionala sartzea baino ez den,

$$E[\tilde{\rho}] \geq E[\rho_0]. \tag{2.4}$$

Dena den, Hohenberg eta Kohnen teoremak ez dira eraikitzaileak, ez baitigute benetako dentsitatearen funtzional totala ematen, bakar bakarrik bere existentzia frogatzen dute.

Hurrengo urtean, Kohn eta Sham-ek energia zinetikoa, erreferentziazko sitema irudikari baten, s izanda sistema, energia zinetikoaren bitartez adieraztea proposatu zuten, N elektroi ez elkarrekintzaileren kasurako [28]

$$T_s[\rho_s] = \sum_i^N \langle \phi_i^{KS} | -\frac{1}{2}\nabla^2 | \phi_i^{KS} \rangle. \tag{2.5}$$

Sistema artifizial honen, eta guk benetan interesatuta gaudenaren arteko lotura $\nu_{ext,s}$ potentzial efektiboaren bidez emana dator. Potentzial honen balioa auker-atzerako orduan, kontutan izan behar da orbital karratuen modulu guztien baturak erabiliz lortutako dentsitatea, juxtu gure sistema errealeko elektroi elkarrekintzaile-dun oinarrizko egoeraren dentsitatearen bera izatea,

$$\rho(\mathbf{r}) = \rho_0(\mathbf{r}) = \sum_i^n |\phi_i^{KS}(\mathbf{r})|^2, \tag{2.6}$$

non $\phi_i^{KS}(\mathbf{r})$ Kohn-Sham orbital ortonormalak diren. Dentsitate elektronikoa eta ener-gia zinetikoaren adierazpenak, elektroi ez elkarrekintzailedun determinante bakarreko uhin funtzioetarako zehatzak dira. Energia zinetiko eta elektroien arteko interakzio energiaren desberdintasuna sistema erreal eta erreferentziazkoan

$$\Delta T[\rho] \equiv T[\rho] - T_s[\rho] \tag{2.7}$$

$$\Delta V_{ee}[\rho] \equiv V_{ee}[\rho] - \frac{1}{2}\int\int \frac{\rho(\mathbf{r}_1)\rho(\mathbf{r}_2)}{|\mathbf{r}_1 - \mathbf{r}_2|} d\mathbf{r}_1 d\mathbf{r}_2. \tag{2.8}$$

da.

Hohenberg-Kohn ekuazioan 2.3 ordezkatuz gero

$$E^{KS}[\rho] = \int \rho(\mathbf{r})\nu_{ext}(\mathbf{r})d\mathbf{r} + T_s[\rho] + \frac{1}{2}\int\int \frac{\rho(\mathbf{r}_1)\rho(\mathbf{r}_2)}{|\mathbf{r}_1 - \mathbf{r}_2|}d\mathbf{r}_1 d\mathbf{r}_2 + E_{xc}[\rho] \tag{2.9}$$

lortzen dugu, zeinetan

$$E_{xc}[\rho] \equiv \Delta T[\rho] + \Delta V_{ee}[\rho]. \tag{2.10}$$

$E_{xc}[\rho]$ korrelazio-elkartukatze funtzionalak elektroien interakzio ez klasioen partea adierazten duen eta erreferentzizko sistema eta errealaren arteko energia zinetikoen diferentzia. Kohn-Sham orbitalak 2.9 ekuazioa minimizazioaren bidez aurkitzen dira, $\langle\phi_i|\phi_j\rangle = \delta_{ij}$ konstante mantenduz. Honek Kohn-Sham ekuazioa eramaten du

$$\left\{-\frac{1}{2}\nabla^2 + \nu_{xc} + \int \frac{\rho(\mathbf{r}')}{|\mathbf{r} - \mathbf{r}'|}d\mathbf{r}' + \nu_{xc}\right\}\psi_i(\mathbf{r}) = \epsilon_i\psi_i(\mathbf{r}), \tag{2.11}$$

zeina era autokonsistentean ebatzia izan behar den.

Trukaketa-korrelazio pontentzialaren adierazpen zuzen bakarra,

$$\nu_{xc}(\mathbf{r}) \equiv \frac{\delta E_{xc}[\rho(\mathbf{r})]}{\delta\rho(\mathbf{r})}, \tag{2.12}$$

ezagutzekotan, 2.11 ekuazioa askatzea Schrödinger ekuazio elektroniko zehatza ebaztearen baliokidea litzateke. Zoritxarrez, nahiz eta ν_{xc} horren inguruan lan handia egin izan (eta egiten ari) den arren, trukaketa-korrelazio potentzial zehatza ez da ezaguna. Hala ere, zenbait hurbilketa on eskuragarri ditugu.

Hortaz, egitura elektronikoaren kalkuluaren kalitatea, E_{xc}-aren hurbilketaren kalitateaz dependatzen du.

Potentzial honentzako hurbilketarik errazena Dentsitate Lokalaren Hurbilketa (Local Density Approximation, LDA) izenekoa da, non lokalki uniformea den ρ dentsitate elektronikoa asumitzen den. LDA funtzionalaren energia hurrengo adierazpenaren bidez emana dator

$$E_{xc}^{LDA}[\rho] = \int \rho(\mathbf{r})\epsilon_{xc}^{LDA}(\rho)d\mathbf{r} \tag{2.13}$$

non $\epsilon_{xc}(\rho)$ elektroi gasaren korrelazio eta trukaketa energien batura den.

Ondorengo hurbilketa, dentsitate elektronikoaz gain, $\nabla\rho(\mathbf{r})$ dentsitatearen gradiente bat gehitzea ere izan zitekeen. Kasu hau GGA (Generalized Gradient Approximation) [29] bezala ezagutzen da. Hain bat funzional ezberdin garatu izan dira GGA-ren ezparruaren barruan.

Lan honetan aukeratutako trukaketa-korrelazio funtzionala, PBE bezala ezagutzen dena da, Perdew, Burke eta Ernzerhof-en lanaren ondorio izan zena [29].

PBE funtzionalaren kasuan, trukatze-korrelazio energia 2.13 ekuazioaren kasuan egindako era berean egin daiteke

$$E_{xc}^{PBE}[\rho] = \int \rho(\mathbf{r})\epsilon_{xc}^{PBE}(r_s(\mathbf{r}, s(\mathbf{r}, \xi(\mathbf{r}))))(\rho)d\mathbf{r}, \tag{2.14}$$

non s dentsitate gradiente murriztua den

$$s = \frac{|\nabla\rho|}{2k_F\rho}, \tag{2.15}$$

ξ espin polarizazioa den

$$\xi = \frac{\rho_\uparrow - \rho_\downarrow}{\rho}, \tag{2.16}$$

k_F Fermi erradioa

$$k_F = (3\pi^2\rho)^{\frac{1}{3}}, \tag{2.17}$$

eta r_s the Wigner-Seitz erradioa den

$$r_s = \left(\frac{4\pi\rho}{3}\right)^{-\frac{1}{3}}. \tag{2.18}$$

2.2.2 Oinarri funtzioak

MO edo orbiltal molekularrak eraikitzeko bi era ezberdin daude: numerikoki edo algebraikoki, oinarri funtzioen multzoen hedapen lineal bidez. Zenbakizko hurbilketak zehaztasun eta malgutasun handia eskeintzen dute baina euren sare puntu kopuru handia dela eta, nahiko traketsak dira konputazionalki kudeatzeko. Arrazoi hori dela medio, sistema poliatomikoetarako hurbilpen algebraikoen erabilpena beharrezkoa egiten da, non ψ_{MO} orbital molekularrak χ_i orbital atomikoen konbinazio linean bezala hedatzen diren, elektroi bakarreko funtzio analitiko sinpleen multzo bat bezala [30],

$$\psi_{MO}(\mathbf{r}) = \sum_i^n c_i\chi_i(\mathbf{r}), \tag{2.19}$$

eta χ_i-ren formaren arabera oinarri funtzioak mota ezberdinetakoak izan daitezke.

Funtzio hauek orbital atomikoak dira eta normalean atomoetan zentratuta daude, baina baita loturetan, ez-loturazko elektroi bikoteetan etab.-etan.

Sinpleenak Slater Motako Orbitalak (STO-ak) dira, zeinak ondoko forma duten

$$\chi_i^{STO}(\mathbf{r}) = Nr^{n-1}e^{\zeta\mathbf{r}}Y_{lm}(\theta, \varphi) \tag{2.20}$$

non n zenbaki kuantiko nagusia den (n= 1, 2, 3, ...), N normalizazio konstantea, $r = |\mathbf{r}|$ nukleo atomikotik elektroirainoko distantzia, ζ gainontzeko elektroiengatik apantaiatuta izan ondoren, elektroiak pairatzen duen karga efektiboarekin erlazionaturiko konstante bat eta $Y_{lm}(\theta, \phi)$ harmoniko esferikoak.

Beste orbital atomiko mota bat Gaussiar Motako Orbitalak dira (GTO) zeinak honelako itxura bat duten

$$\chi_i^{GTO}(\mathbf{x}) = Nx^l e^{\alpha \mathbf{r}^2} \chi_i^{GTO}(\mathbf{y}) = Ny^m e^{\alpha \mathbf{r}^2} \chi_i^{GTO}(\mathbf{z}) = Nz^n e^{\alpha \mathbf{r}^2} \tag{2.21}$$

non l zenbaki kuantiko orbitala den.

Atomoan zentraturiko oinarri funtzioak konputazionalki efektiboakgoak dira gas faseko eta orbital lokalizatuen kalkuluetarako. Hala ere, hauen erabilpena sistema konplexuetan edo hidrogeno loturak dituzten kasuetan errore bat eragiten du: Oinarri Funtzioen Gainezarpen Errorea (BSSE). BSSE-a uhin funtzioa adierazteko oinarri funtzio ez-osoak erabiltzearen ondorioa da.

Era ezberdinak daude BSSE-a saiezteko, baina gas fasean, hoberena beste oinarri funtzio mota batera aldatzea da.

Projektu honetan erabiltzen den CPMD[31] kodeak erabiltzen dituen oinarri funtzioak Uhin Lauak (PW) izenekoak dira. Uhin lauak bereziki komenigarriak dira uhin funtzioa sistema periodikoetan adierazteko, esate baterako PBC edo gelaxka periodikozko baldintzak erabiltzerakoan.

PW oinarri funtzioak honelako itxura bat dute

$$\chi_i^{PW}(\mathbf{r}) = \Omega^{-\frac{1}{2}} e^{i\bar{\mathbf{G}}_\nu \cdot \bar{\mathbf{r}}} \tag{2.22}$$

non Ω simulazio gelaxkaren bolumena den eta $\mathbf{G}_\nu$ simulazio gelaxkaren elkarrekiko sarearen bektoreak diren.

Praktikan, sarritan uhin lauak oinarri funtzioak "guneko potentzial efektibo" edo pseudo potentzialekin batera erabiltzen dira, honela uhin lauak balentziazko elektroien karga dentsitatea deskribatzeko baino ez dira erabili behar.

2.2.3 Pseudo Potentzialak

Pseudo potentzial kontzeptua 1930. hamarkadan argitaratu zen lehen aldiz Hans Hellmann-en eskutik. Ideia, gune atomikoaren elektroi guztiak kontutan hartzen dituen egoera potentzialak, guneko potentzial efektiboen bidez ordezkatzea da, barneko elektroiak "izoztuta" mantenduz balentziazko elektroiak aske utzi eta explizituki kalkulatuz.

Gunetiko distantzia jakin batera, pseudo potentzialak adostasun onargarri bat erakusten dute elektroi guztiak kontutan hartzen dituen potentzialekin. Distantzia

hau mozketa erradioa (*cuttof radius*, $\mathbf{r}_c$) edo mozketa puntua bezala ezagutzen da eta handiagoa edo txikiagoa izan daiteke pseudo potentzialaren zurruntasunaren edo biguntasunaren arabera.

Pseudopotentzial arruntenak Norma-Kontserbatzaileak (Norm-Conserving) eta ultra-leunak (ultra-soft) dira. Pseudo potentzial norma-kontserbatzaileak erreferentzi egoera atomikoetatik eratorriak dira, ondorioz pseudo eta elektroi guztidun balentzia egoera propio elektronikoak energia eta anplitude (ondorioz dentsitatea ere) beretxua izan behar dute r_c erradio batetik kanporuntz.

Norma-kontserbatzaile pseudo potentzial batek ondoko forma du

$$V^{PP}(\mathbf{r},\mathbf{r\prime}) = \left[V_{gune}(\mathbf{r}) + \Delta V_{lokala}(\mathbf{r})\delta_{\mathbf{r},\mathbf{r\prime}} + \sum_{k,l} P_k^{\star}(\mathbf{r}) h_{kl} P_l(\mathbf{r\prime}) \right], \tag{2.23}$$

non ΔV_{lokala} eta P_k projektoreak atomoan zentraturiko funtzioak diren, ondoko itxurarekin

$$\varphi(\mathbf{r}) = \varphi(|r - \mathbf{R}_I|) Y_{lm}(\theta,\phi), \tag{2.24}$$

$Y_{lm}(\theta,\phi)$ harmoniko esferikoak eta $\mathbf{R}_I$ posizio atomikoak izanik.
2.24 ekuazioa uhin lauetan hedatuz,

$$\varphi(\mathbf{r}) = \sum_{\mathbf{G}} \varphi(G) e^{i\bar{\mathbf{G}}\cdot\bar{\mathbf{r}}} S_I(\mathbf{G}) Y_{lm}(\tilde{\theta},\tilde{\phi}) \tag{2.25}$$

eran berridatz daiteke, non S_I egitura faktoreak diren, ondoko eran hedatuak

$$S_I(\mathbf{G}) = e^{-i\mathbf{G}\cdot\mathbf{R}_I}. \tag{2.26}$$

Norma-kontserbatzaile pseudo pontentzialetaz gain badaude mozketa puntu txikiagoa duten beste pseudo potentzial mota ezberdin batzu, zeinei leunagoak direla esaten zaien, hau da azkarrago konbergitzen dutenak, baina aldi berean ez horren trasferibleak. Trasferibilitatea ingurune ezberdinetan emaitz errealista berdinak eskuratzean datza, hau da, pseudo pontentzial norma-kontserbatzaileak ingurune ezberdinetan fidagarritasun beretxuko emaitzak emango dituzte, baina pseudo pontentzial leunak ez dute zertan.

Projektu honetan, ez pseudo potentzial leunak, baizik eta ultra leunak erabili izan dira, Vanderbilt-en psuedo potentzial ultra leunak alegia [32] [33]. Pseudo potentzial hauek erabiltzeko korapilotsuak izateagatik ezagunak dira, baina beraien zehaztasuna aztertu nahi den sistemarako frogatu ondoren uhin lauen mozketa puntu baxuagoen erabilpena ahalbidetzen dute eta ondorioz etekin konputazional hobeagoa.

Uhin lauen mozketa puntu hau Rydberg-etan (Ry) neurtzen da arrazoi historikoak direla medio, eta balio tipikoen artean 70 Ry Norma-kontserbatzaileetarako eta 35

ultra leunetarako da.

Mozketa puntu hau, pseudo potentzialez deskribaturiko sistema baten uhin funtzioak (edo potentzialak) bere elektroi guztidun sistema analogiarekin konparatuz determina daiteke. Hau 2.2.3 irudian ikus daiteke, non $\mathbf{r}$ jakin batetara ($\mathbf{r}_c$), sistema bien uhin funtzioak edo potentzialak gainezartzen diren.

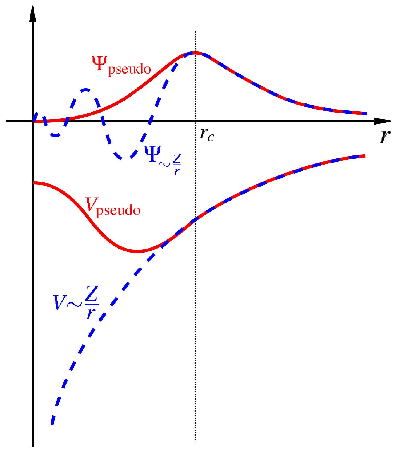

Figure 2.1: *Coulomb potentzialdun uhin funtzioa nuklearra (urdinez) eta pseudo pontentzialez deskribaturiko beste baten (gorriz) arteko konparaketa. Uhin funtzio erreala eta pseudo potentzialen bidez deskribaturikoa $\mathbf{r}_c$ erradio batetik gora baliokide bihurtzen dira.*

Mozketa puntuak bilatzeko beste erizpide edo trikimailu bat, projektu honetan erabilitakoa da, energiaren mozketa erizpidearekiko konbergentzia aztertuz hain zuzen. Pseudo potenzialak zehatzak nahikoak direla onartzen badugu, erabateko gainezarpena izan beharko lukete mozketa puntu jakin batetik aurrera. Bestalde, zenbat eta mozketa puntua handiagoa izan, orduan eta kostu konputazional handiagoa suposatzen dute (integral gehiago askatu behar baitira), beraz interesgarria da mozketa puntu hori ahalik eta txikien aukeratzea, hau da $\mathbf{r}_c$ bilatzea.

Honen arabera, nahikoa handia den mozketa puntu batetara, posible da atomo baten energia zehatza kalkulatzea. Beraz, mozketa puntua progresiboki birkalkulatuz, puntu batera heltzean lehenengo puntuarekiko energia diferentzia esanguratsua bihurtzen da (ikus 2.2 irudia), ondorioz, hori izango da hain zuzen $\mathbf{r}_c$ mozketa puntu erizpidetzat har dezakegun puntua.

2.2 irudiak[1] Vanderbilt pseudo pontentzial ezberdinen konbertsio energiaren mozketa puntuarekiko dependentia erakusten du. Ikus daitekeen bezala, 30 Ry.-tik gora energia nahiko konbergiturik agertzen da kasu guztietan.

[1]Bai grafika hauek zein tesi honetan agertzen diren gainontzeko grafikak, gnuplot [34] programaren bidez sortuak izan dira.

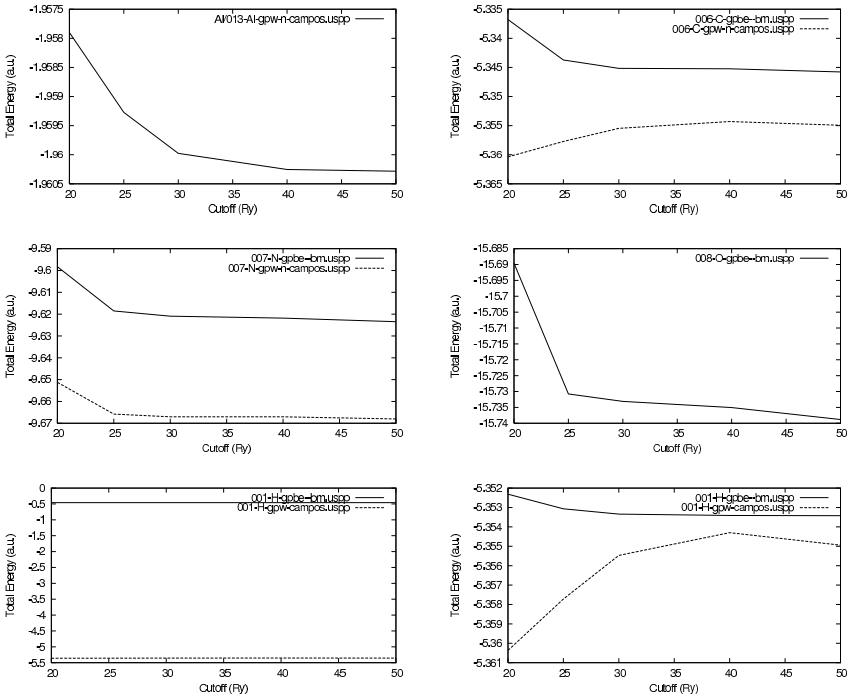

Figure 2.2: *Energia totala vs Uhin lauen mozketa puntuaren arteko adierazpen grafikoa zenbait Vanderbilt pseudo pontentzialentzako. Azken irudia handituta dago konbergentzia kurba hobeto bereizteko.*

2.2.4 Hedapen algoritmoak

Sistema baten indarrak ezagunak badira, Newtonen bigarren legearen bidez $\ddot{\mathbf{r}}$ azelerazioak kalkulatuak izan daitezke ere, eta ondorioz $\dot{\mathbf{r}}$ abiadurak eta $\mathbf{r}$ posizioak.

$$\mathbf{r} = \int \left[\frac{d\mathbf{r}}{dt}\right] dt = \iint \left[\frac{d^2\mathbf{r}}{dt^2}\right] d^2t. \tag{2.27}$$

Hala ere, dinamika molekularraren helburua atomoen posizioak hedatzea da eta lan horretarako "hedapen algoritmo", "diferentzia finituzko metodo" edo "integratzaile" bezala ezagutzen direnak erabiltzen dira. Algoritmo hauek guztiak urrats denboraren iraupenaren unean indarrak konstante mantentzen direla suposatzen dute, eta posizioak eta propietateak Taylor serieen garapen bidez garatuak izan daitezke [35]:

$$\mathbf{r}(t+\delta t) = \mathbf{r}(t) + \delta t\dot{\mathbf{r}}(t) + \frac{1}{2}\delta t^2\ddot{\mathbf{r}}(t) + \dots$$
$$\dot{\mathbf{r}}(t+\delta t) = \dot{\mathbf{r}}(t) + \delta t\ddot{\mathbf{r}}(t) + \dots$$
$$\ddot{\mathbf{r}}(t+\delta t) = \ddot{\mathbf{r}}(t) + \dots$$

Sistema bat hedatzeko erarik sinpleena Euler-en integratzailea erabiliz da, zeinetan zuzenean aipatu berri den ekuazioa aplikatzen den. Verlet-en algoritmoa ordea, t aldiuneko posizio eta azelerazioak erabiltzen ditu, eta aurreko pausuko, hots $\mathbf{r}(t-\delta t)$-ko posizioak

$$\mathbf{r}(t+\delta t) = \mathbf{r}(t) + \delta t\dot{\mathbf{r}}(t) + \frac{1}{2}\delta t^2\ddot{\mathbf{r}}(t) + \dots$$
$$\mathbf{r}(t-\delta t) = \mathbf{r}(t) - \delta t\dot{\mathbf{r}}(t) + \frac{1}{2}\delta t^2\ddot{\mathbf{r}}(t) - \dots$$

Verlet algoritmoak ez ditu abiadurak era explizituan erabiltzen eta honek arazo bat suposa dezake zenbait kasutan. Verlet algoritmoaren zenbait moldapen algoritmo egin izan dira, esate baterako "leap-frog" (igel jauzilaria) algoritmoa:

$$\mathbf{r}(t+\delta t) = \mathbf{r}(t) + \delta t\dot{\mathbf{r}}(t+\frac{1}{2}\delta t)$$
$$\dot{\mathbf{r}}(t+\frac{1}{2}\delta t) = \dot{\mathbf{r}}(t-\frac{1}{2}\delta t) + \delta t\ddot{\mathbf{r}}(t) \qquad (2.28)$$

"Abiadura Verlet" (Velocity Verlet) algoritmoak posizio, abiadura eta azelerazioak ematen ditu aldiune bererako

$$\mathbf{r}(t+\delta t) = \mathbf{r}(t) + \delta t\dot{\mathbf{r}}(t) + \frac{1}{2}\delta t^2\ddot{\mathbf{r}}(t)\dot{\mathbf{r}}(t+\delta t) = \dot{\mathbf{r}}(t+\delta t) + \frac{1}{2}\delta t[\ddot{\mathbf{r}}(t) + \ddot{\mathbf{r}}(t+\delta t).] \quad (2.29)$$

CPMD kodeak Abiadura Verlet algoritmoa erabiltzen du.

2.2.5 Tenperaturaren kontrola

Dinamika molekularrezko simulazio batetan, energia zinetiko totalak fluktuatzeko joera dauka, eta fluktuazio hauek batzutan partikulak nahi ez ditugun egoera batzutara eraman ditzazkete. Sistema jakin batzuen dinamika molekularrezko simulazioak egitean desiragarria da molekulek egoera errealean tenperatura jakin batetan izango luketen jokaeraren baliokidea izatea. Esate baterako, sistema biologikoak simulatzean, molekulek ingurunearen araberako energia zinetikoa izan beharko lukete, eta arrazoi bereziren batengatik kontrakoan interesatuta ez egotekotan, molekulek 300

K-i legokiokeen energia zinetikoaren banaketa izan beharko lukete. Hortaz, orokorrean ez luke sentzurik izango sistema biologiko bat 1000 K-etan simulatzea, ez baita posible naturan tenperatura horretan dauden biomolekularik aurkitzea.

Sistemaren tenperatura $\overline{E_k}$ batazbesteko energia zinetikoaren adierazpenetik zuzenean kalkula daiteke

$$\overline{E_k} = \frac{1}{2}\frac{1}{N}\sum_{i=1}^{N} m_i \dot{\mathbf{r}}_i{}^2 = \frac{3}{2}k_B T \rightarrow T = \frac{1}{3Nk_B}\sum_{i=1}^{N} m_i \dot{\mathbf{r}}_i{}^2 \tag{2.30}$$

$k_B = \frac{R}{N_A}$ den R gas idealaren konstantea izanik ($8.3144\frac{J}{K.mol}$) eta N_A Avogadro zenbakia ($6.022.10^{23}\frac{partikula}{mol}$).

Zorionez, badago "termostato" izenaz ezagutzen den, sistemaren tenperatura fluktuazioak kontrolatzeko trikimailu matematiko/konputazional bat.

Simulazio baten tenperatura kontrolatzeko erarik sinpleena, tenperatura finkatzea da (adibidez 300 K) eta horren inguruan $\pm\Delta$T goi eta behe mugak jartzea, adibidez $\pm$ 20K. Era honetan, simulazio pausu bakoitzeko, nukleoen energia zinetikoa birkalkulatua da eta ondoren operazio logiko sinple bat egiten da:

```
if (T > (300+20)) (T<(300-20))
 then
   {
     RESFACTOR = T(t) / 300
     do i=N
        v(i)= v(i) * sqrt(RESFACTOR) / N
     enddo
   }
endif
```

Era honetan, energia zinetiko totalak sistemaren tenperatura tarte batetik kanpo jartzen duenean, partikula bakoitzaren energia berreskalatua izango da diferentziaren erro karratuarekin. Metodo hau "berreskalaketa bidezko tenperatura kontrola" ("temperature control by rescaling" [36]) deitzen da.

Hala ere, badaude beste termostato mota ezberdin batzu, zeinak tenperaturaren fluktuazioak berreskalaketa prozezu leundu baten bidez egiten dutenak, adibidez Nose[37]-Hoover[38] termostatua [39], zeina projektu honetako sistema gustiz solbatatuen simulazioetan erabilia izan den.

2.3 Ab-Initio Dinamika Molekularra

2.1.1. atalean mekanika Newtondarrak gobernaturiko dinamika molekularrerako lehen sarrera bat aurkeztu da, baina hemendik aurrera ikusiko ditugun partikulen arteko in-

terakzioak mekanika kuantikoaren ekuazioen bidez deskribatuak izango dira. Bestalde, formulazio matematiko ezberdin bat erabiliko da, formulazio Lagrangiarra.

Mekanika Lagrangiarrean aurkeztu beharreko lehenengo kontzeptua "lagrangiarra" da. Sistema baten lagrangiarra, energia zinetikoa eta energia potentzialaren arteko kenketaren bidez emana dator

$$\mathcal{L} = \mathcal{T} - \mathcal{V}. \tag{2.31}$$

Mekanika Lagrangiarraren arabera, sistema baten Lagrangiarra ezaguna bada, higidura ekuazioak zuzenean lortu daitezke, adierazpen Lagrangiarra Euler-Lagrange ekuazioan ordezkatuz,

$$\frac{d}{dt}\left(\frac{\partial \mathcal{L}}{\partial \dot{\mathbf{r}}_i}\right) - \frac{\partial \mathcal{L}}{\partial \mathbf{r}_i} = 0 \quad , \quad i = 1, \ldots, N. \tag{2.32}$$

zeinetan $\ddot{\mathbf{r}}$ azelerazioaren menpeko adierazpen bat lortzen den eta hortik atomoen higidura deskribatuko duten hedapen algoritmoak erator daitezkeen (ikusi 2.2.4 atala).

Mekanika klasikoaz gobernaturiko dinamika molekularraren kasuan ez bezala, abinitio dinamika molekularrean partikulek denboraren menpeko Schrödingeren ekuazioa [40] erabiltzen du

$$i\hbar\frac{\partial}{\partial t}\Phi(\{\mathbf{r}_i\},\{\mathbf{R}_i\};t) = \mathcal{H}\Phi(\{\mathbf{r}_i\},\{\mathbf{R}_i\};t). \tag{2.33}$$

$\{\mathbf{R}_i\}$ nukleoen eta $\{\mathbf{r}_i\}$ elektroien posizio bektoreak izanik.

Ekuazio honetan partikulen Φ uhin funtzioen gainean eragiten duen $\mathcal{H}$ eragile Hamiltondarra definitua behar da.

Sistema molekular batentzako eragile Hamiltondar standard bat, nukleo eta elektroien energia zinetiko eta potentzial eta nukleo eta elektroien arteko korrelazio terminoen arteko batura bezala eraiki daiteke [41]

$$\begin{aligned}
\mathcal{H} &= -\sum_I \frac{\hbar^2}{2M_i}\nabla^2{}_I - \sum_i \frac{\hbar^2}{2m_e}\nabla^2{}_i + \sum_{i<j}\frac{e^2}{|\mathbf{r_i}-\mathbf{r_j}|} + -\sum_{I,i}\frac{e^2 Z_I}{|\mathbf{R_I}-\mathbf{r_i}|} + \sum_{I<J}\frac{e^2 Z_I Z_I}{|\mathbf{R_I}-\mathbf{R_J}|} \\
&= -\sum_I \frac{\hbar^2}{2M_i}\nabla^2{}_I - \sum_i \frac{\hbar^2}{2m_i}\nabla^2{}_i + V_{n-e}(\{\mathbf{r_i}\},\{\mathbf{R_I}\}) \\
&= -\sum_I \frac{\hbar^2}{2M_i}\nabla^2{}_I + \mathcal{H}_e(\{\mathbf{r_i}\},\{\mathbf{R_I}\}).
\end{aligned} \tag{2.34}$$

non $\{\mathbf{r_i}\}$ elektroien eta $\{\mathbf{R_I}\}$ nukleoen askatasun mailak diren hurrenez hurren.

Φ uhin funtzio molekularrak, nukleoen eta elektroien koordenatuak banandurik izan behar ditu, eta hau era sinple batean hurbildua izan daiteke, biak bananduta idatzita eta fase faktore bat gehituta gehiago barik,

$$\Phi(\{\mathbf{r_i}\},\{\mathbf{R_I}\};t) \approx \Psi(\{\mathbf{r_i}\};t)\chi(\{\mathbf{R_I}\};t)exp\left[\frac{i}{\hbar}\int_{t_0}^{t} dt' \tilde{E}_e(t')\right], \tag{2.35}$$

non uhin funtzio elektroniko eta nuklearra bananduta normalizatzen diren denbora aldiune bakoitzeko, esate baterako, $\langle\chi;t|\chi;t\rangle = 1$ eta $\langle\Psi;t|\Psi;t\rangle = 1$, hurrenez hurren. Horrez gain, fase faktore egoki bat gehitzen da ere, bukaerako ekuazioak itxura trinkoago bat izan dezan, hots

$$\tilde{E}_e = \int d\mathbf{r}d\mathbf{R}\Psi^*(\{\mathbf{r_i}\};t)\chi^*(\{\mathbf{R_I}\};t)\mathcal{H}_e\Psi(\{\mathbf{r_i}\};t)\chi(\{\mathbf{R_I}\};t),$$

zeina uhin funtzio totalerako determinante bakarreko ansatz konfigurazio bezala ezagutzen den.

Ansatz hau, Born-Oppenheimerenarekin alderatuta, fase faktorea alde batera utzita, aldagai azkar eta motelak banatzean bereizten da. Born-Oppenheimer-en ansatz-a ondoko eran idazten da

$$\Phi_{BO}(\{\mathbf{r_i}\},\{\mathbf{R_I}\};t) = \sum_{k=0}^{\infty} \tilde{\Psi}_k(\{\mathbf{r_i}\},\{\mathbf{R_I}\};t)\tilde{\chi}_k(\{\mathbf{R_I}\};\mathbf{t}). \tag{2.36}$$

Adierazpen hau 2.34 adierazpenean eta 2.35 ansatz-a 2.33 ekuazioan ordezkatu ondoren, ezkerreko partea $\langle\Psi|$ eta $\langle\chi|$ adierazpenekin biderkatuz hurrenez hurren eta energiaren kontserbazioa $d\langle\mathcal{H}\rangle/dt \equiv 0$ baldintzaren bidez inposatuz, emaitza

$$i\hbar\frac{\partial\Psi}{\partial t} = -\sum_i \frac{\hbar^2}{2m_e}\nabla^2{}_i\Psi + \left\{\int d\mathbf{R}\chi^*(\{\mathbf{R_I}\};t)V_{n-e}(\{\mathbf{r_i}\},\{\mathbf{R_I}\})\chi(\{i\mathbf{R_I}\,t)\right\}\Psi$$

$$i\hbar\frac{\partial\chi}{\partial t} = -\sum_i \frac{\hbar^2}{2M_I}\nabla^2{}_i\chi\left\{\int d\mathbf{r}\Psi^*(\{\mathbf{r_i}\};t)\mathcal{H}_e(\{\mathbf{r_i}\},\{\mathbf{R_I}\})\Psi(\{\mathbf{r_i}\};t)\right\}\chi$$

da, zeina denboraren menpeko eremu autokontsistentearen (TDSCF) oinarria definitzen duen, elektroi eta nukleoak kuantikoki mugitzen baitira denboraren menpeko potentzial efektibo batean (edo autokontsistenteki lortutako bataz besteko eremuetan).

Puntu honetara helduta, nukleoak partikula klasikotzat tratatu ahal izateako hur-

bilketa baten beharrean gaude. Hurbilketa hau uhin funtzio nuklearrak berridatziz lor daiteke

$$\chi(\{\mathbf{R_i}\};t) = A(\{\mathbf{R_I}\};t)e^{\left[\frac{iS(\{\mathbf{R_I}\};t)}{\hbar}\right]} \tag{2.37}$$

A anplitude S fase faktore terminoen menpean.

Beraz, uhin funtzio nuklearrerako ansatz berri hau TDSCF ekuazioan 2.37 ordezkatuz

$$\frac{\partial S}{\partial t} + \sum_I \frac{1}{2M_I}(\nabla_I S)^2 + \int d\mathbf{r}\Psi^*\mathcal{H}_e\Psi = \hbar^2 \sum_I \frac{1}{2M_I}\frac{\nabla_I^2 A}{A} \tag{2.38}$$

$$\frac{\partial A}{\partial t} + \sum_I \frac{1}{M_I}(\nabla_I S) + \sum_I \frac{1}{2M_I} A(\nabla_I^2 S) = 0 \tag{2.39}$$

"fluido kuantikoaren adierazpen dinamikoa" bezala ezagutzen dena lortzen dugu, zeinetatik denboraren menpeko Schrödinger ekuazioa ebatz daitekeen. $\hbar \to 0$ muga klasikoa hartuz gero, 2.38 ekuazioko eskuin aldeko terminoa desagertzen da, beraz,

$$\frac{\partial S}{\partial t} + \sum_I \frac{1}{2M_I}(\nabla_I S)^2 + \int d\mathbf{r}\Psi^*\mathcal{H}_e\Psi = 0$$

zeinak Hamilton-Jacobi formulazioaren antza duen

$$\Psi = \frac{\partial S}{\partial t} + \mathcal{H}(\{\mathbf{R}\}_\mathbf{I}, \{\nabla_\mathbf{I}\mathbf{S}\}) = \mathbf{0}$$

dinamika klasikorako, ondoko hamiltondar klasikoarekin

$$\mathcal{H}(\{\mathbf{R}\}_I, \{\mathbf{P}\}_I) = T(\{\mathbf{P}\}_I) + V(\{\mathbf{P}\}_I)$$

non $\mathbf{P} \equiv \nabla_I S$ eta 2.38 ekuazioari dagozkion higidura ekuazio Newtondarrak

$$\frac{d\mathbf{P_I}}{dt} = -\nabla_I \int dt\Psi^*\mathcal{H}_e\Psi$$

adierazpenaren bidez lor daitezkeen, edo beste era batera idatzita

$$\begin{aligned} M_I\ddot{\mathbf{R}}_\mathbf{I}(t) &= -\nabla_I \int d\mathbf{r}\Psi^*\mathcal{H}_e\Psi \\ &\quad -\nabla_I V_e^E(\{\mathbf{R_I}\}(t)), \end{aligned} \tag{2.40}$$

non nukleoak klasikoki mugitzen diren, elektroiek sorturiko V_e^E potentzial efekti-

boaren arabera. Potentzial efektibo hau, 2.37 ekuaziotik abiatuta garatu daiteke

$$V_e^E = \int d\mathbf{r}\Psi_0^*\mathcal{H}_e\Psi_0 \equiv E_0(\{\mathbf{R_I}\}) \tag{2.41}$$

eta nukleoak beraren arabera mugituko dira.

2.41 ekuazioko potentziala Schrödinger denboraren independientea den ekuzioren bidez kalkulatua izan daiteke, zeina normalean gurputz anitzeko kontribuzioen bidez moztua izaten den

$$V_e^E \approx V_e^{hurbildua}(\{\mathbf{R_i}\}) = \sum_{I=1}^{N} v_1(\mathbf{R_I}) + \sum_{I<J}^{N} v_2(\mathbf{R_I},\mathbf{R_J}) + \sum_{I<J<K}^{N} v_3(\mathbf{R_I},\mathbf{R_J},\mathbf{R_K}) + \dots$$

2.3.1 Born-Oppenheimer Dinamika Molekularra

Born-Oppenheimer hurbilketan nukleoak ekuazio klasikoen bidez deskribatzen dira eta egitura elektronikoa pausu bakoitzeko Schrödingerren ekuazioa estatikoki (denboraren independienteki) askatuz gehitzen da [42]. Honen ondorioz adieraz daitekeen dinamika molekularrezko metodoa hurrengo adierazpenaren bidez definitzen da

$$M_I\ddot{\mathbf{R}}_I(t) = -\nabla_I min_{\{\Psi_0\}}\{\langle\Psi_0|\mathcal{H}_e|\Psi_0\rangle\} \tag{2.42}$$

$$E_0\Psi_0 = \mathcal{H}_e\Psi_0. \tag{2.43}$$

Pausu bakoitzero oinarrizko egoera elektronikoa eskuratu behar delarik. Hartree-Fock-en hurbilketa aplikatu ondoren,

$$\begin{array}{c} M_I\ddot{\mathbf{R}}_I(t) = -\nabla_I min_{\{\psi_i\}}\left\langle\Psi_0|\mathcal{H}_e^{HF}|\Psi_0\right\rangle \\ 0 = -\mathcal{H}_e^{HF}\psi_i + \sum_i \Lambda_{i,j}\psi_j. \end{array} \tag{2.44}$$

Hau era Langrangiarrean ere idatzia izan daiteke

$$\mathcal{L} = -\langle\Psi_0|\mathcal{H}_e|\Psi_0\rangle + \sum_{i,j}\Lambda_{i,j}(\langle\psi_i|\psi_j\rangle - \delta_{i,j}), \tag{2.45}$$

non $\Lambda_i j$ Lagrangeren biderkatzaileak diren.

Lagrangiar hau orbitalekiko deribatuz

$$\frac{\delta\mathcal{L}}{\delta\psi_i^*} = 0,$$

Hartree-Fock-en ekuazioetara garamatza

$$\mathcal{H}_e^{HF}\psi_i = \sum_j \Lambda_{ij}\psi_j.$$

2.3.2 Car-Parrinello Dinamika Molekularra

Car-Parrinello metodoak Lagrangiar berezi bat proposatzen du, zeinetan nukleoen kasuan, 2.45 ekuazioko energia potentzial eta mugaketa terminoetaz aparte, beste bi termino gehitzen dituen nukleoen eta elektroien energia zinetikoarentzat [43]. Elektroien energia zinetiko hau era pseudo-klasiko batean deskribatzen da "masa fiktizio" deritzon μ termino baten bidez. Bestalde, uhin funtzio elektronikoa denborarekiko deribatuz, nolabaiteko "abiadura" bat lortzen da

$$\mathcal{L}_{CP} = \sum_i \frac{1}{2}\mu_i \left\langle \dot{\psi}_i | \dot{\psi}_i \right\rangle + \sum_i \frac{1}{2} M_i \dot{\mathbf{R}}_\mathbf{i}^2 - \langle \Psi_0 | \mathcal{H}_e | \Psi_0 \rangle + \sum_{i,j} \Lambda_{i,j} \left(\langle \psi_i | \psi_i \rangle - \delta_{i,j} \right). \quad (2.46)$$

Eredu klasikoaren era berean, higidura ekuazioak Euler-Lagrange ekuazioen (2.32) bidez lor daitezke

$$\begin{array}{c} \frac{d}{dt}\left(\frac{\partial \mathcal{L}_{CP}}{\partial \dot{\mathbf{R}}_i}\right) - \frac{\partial \mathcal{L}_{CP}}{\partial \mathbf{R}_i} = 0 \\ \frac{d}{dt}\left(\frac{\partial \mathcal{L}_{CP}}{\partial \dot{\psi}_i^*}\right) - \frac{\partial \mathcal{L}_{CP}}{\partial \psi_i^*} = 0 \end{array} \quad (2.47)$$

eta askatu eta Hartree-Fock hurbilketa aplikatu ondoren, Car-Parrinelloren higidura ekuazioak hauek izango dira:

$$\begin{array}{c} M_I \ddot{\mathbf{R}}_I(t) = -\frac{\delta E}{\delta \mathbf{R_I}} \\ \mu_i \ddot{\psi}_i(t) = -\frac{\delta E}{\delta \psi_i^*} + \sum_i \Lambda_{i,j}\psi_j \end{array} \quad (2.48)$$

zeinak 2.45 ekuazioarekin konparatuta, ez duten pauso bakoitzero oinarrizko egoera elektronikoa lortzea eskatzen.

2.46 ekuazioko 2 eta 3. terminoak askatzetzeko, beharrezkoa da Schrödingerren ekuazio elektronikoa [40] askatzea, baina horren ordez DFT-a erabiltzen da.

2.4 Analisi tresnak

Hurrengo atalean emaitzen aurkezpena egiterakoan erabiliko diren analisi tresna batzuk aurkeztuko dira.

2.4.1 Wannier funtzioak

Kalkulu periodikoetan, Wannier funtzioak uhin lauen alternatiba bat dira, zenbait baldintzetan exponentzialki lokalizatuak izan daitezkeeneko abantailarekin [44] [42]. Funtzio hauek normalean Bloch-en orbitalen eraldaketa unitarioaren bidez lortzen dira

$$\Psi(\mathbf{r}) = \Psi_i(\mathbf{r}, \mathbf{k}) = e^{i\mathbf{k}\cdot\mathbf{r}} u_i(\mathbf{r}, \mathbf{k}) \tag{2.49}$$

non $\mathbf{k}$ Brillouin zonako lehen bektorea den

$$u_i(\mathbf{r}, \mathbf{k}) = u_i(\mathbf{r} + \mathbf{L}, \mathbf{k}) \tag{2.50}$$

non L gelaxka bektore zuzenak diren.

Maximoki lokalizaturiko Wannier Futzioak, sistema isolatuetako Boys-en lokalizaturiko orbitalen analogo periodikoak dira.

Praktikan, gure kasurako, Wannier funtzioak edo Wannier Funtzioen Zentruak (WFC) loturen zentruak non kokatzen diren esango dizkiguten puntu batzu baino ez dira izango.

WFC-ak CPMD kodearen bidez zuzenean kalkula daitezke.

2.4.2 Energiak eta tenperaturak

CPMD-n energia totala, energia zinetikoa, energia externoa (pseudopotentzial lokal eta ez lokalena), E_{XC} korrelazio-trukaketa energia eta energia E_{ES} elektrostatikoen baturaren bidez kalkulatzen da.

$$E_{osoa} = E_{zin} + E^{PP}_{lokala} + E^{PP}_{ez-lokala} + E_{XC} + E_{ES}, \tag{2.51}$$

non

$$E_{zin} = \sum_{\mathbf{k}} w_{\mathbf{k}} \sum_i \sum_{\mathbf{G}} \frac{1}{2} f_i(\mathbf{k}|\mathbf{G}+\mathbf{k}|^2 |c_i(\mathbf{G}, \mathbf{k})|^2 \tag{2.52}$$

$$E^{PP}_{lokala} = \sum_I \sum_{\mathbf{G}} \Delta V^I_{local}(\mathbf{G}) S_I(\mathbf{G}) \rho^\star(\mathbf{G}) \tag{2.53}$$

$$E^{PP}_{ez-lokala} = \sum_{\mathbf{k}} w_{\mathbf{k}} \sum_i f_i(\mathbf{k}) \sum_I \sum_{\alpha,\beta \in I} (F^\alpha_{I,i}(\mathbf{k}))^\star h^I_{\alpha\beta} F^\beta_{I,i}(\mathbf{k}) \tag{2.54}$$

$$E_{XC} = \omega \sum_{\mathbf{G}} \varphi_{XC}(\mathbf{G}) \rho^\star(\mathbf{G}) \tag{2.55}$$

$$E_{ES} = 2\pi\omega \sum_{\mathbf{G}\neq 0} \frac{|n_{tot}(\mathbf{G})|^2}{G^2} + E_{ovrl} + E_{self}. \tag{2.56}$$

Sistemaren tenperatura, zuzenean kalkula daiteke hurrengo adierazpenetik

$$\overline{E_k} = \frac{1}{2}\frac{1}{N}\sum_{i=1}^{N} m_i \dot{\mathbf{R}}_i{}^2 = \frac{3}{2}kT \rightarrow T = \frac{1}{3Nk}\sum_{i=1}^{N} m_i \dot{\mathbf{R}}_i{}^2 \tag{2.57}$$

non $k = \frac{R}{N_A}$, R gas idealen konstantea izanda ($8.3144\frac{J}{K.mol}$) eta N_A Avogadro zenbakia ($6.022.10^{23}\frac{partikula}{mol}$).

2.4.3 Energia askeak

Ab-initio dinamika molekularren munduan, normalean energia askeen kalkulaketa meta-dinamikak bezalako eragiketa konplexuen bidez egiten dira, baina projektu honetan, energia askeak mekanika estadistikoan egindako hurbilketa baten bidez kalkulatuko dira [45].

Gure sistemek multzo kanonikoa (NVT) erabiltzen dutenez, era errazenean kalkula genezakeen energia aske "mota" Helmhotz energia askea (A) da, zeina ondoko eran defini daitekeen

$$A = \langle E \rangle - TS = -k_B T \ln Z, \tag{2.58}$$

non $\langle E \rangle = U$ energia totala den, S entropia, k_B Boltzmann konstaltea eta Z partizio funzioa, zeina gure kasuan honela definitzen den

$$Z = \sum_j e^{-\beta E_j}, \tag{2.59}$$

eta "alderantzizko tenperatura" bezala ezagutzen den $\beta = \frac{1}{k_B T}$.

Hemendik aurrera, Helmholtz energia askea kalkulatzeko erabiliko dugun hurbilketa.

Z-ren balioa "j"-n dauden egoera kopurua bezala hurbil genezake.

Hortik abiatuta, har dezagun atomo biren arteko R distantzia erreakzio koordenatu monodimentsional bezala, eta zatikatu dezagun Δr tartero. Har dezagun "j"-ren balioa Δr tartean dauden egoera kopurutzat (R distantzia aurkitzen deneko egoera kopuru osoa).

Ondoren, x ardatzean Δr-naka zatikaturiko r aldagaia eta y ardatzean trajektoria osoan zehar zenbatu ahal izan den Δr tartean dauden R distantzia kopurua dituen histograma bat eraiki behar da (ikus 2.4.3 irudia)

Era honetan partizio funtzioaren parekoa den funtzio bat sortu dugu, zeinak Helmholtz energia askearen ekuazioan (2.58) ordezkatuz aukeraturiko erreakzio koordenatuaren energia profila emango digun.

A energia honen irudikapen grafiko bat egiterakoan 2.4.3 irudiko grafika bezalako bat lortuko genuke.

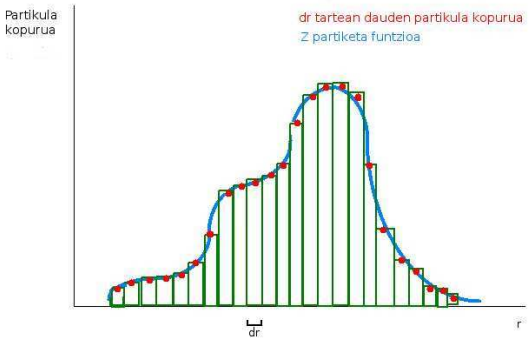

Figure 2.3: *Trajektoria batetan Δr tarte bakoitzeko R distantzia zenbat aldiz aurkitzen deneko histograma.*

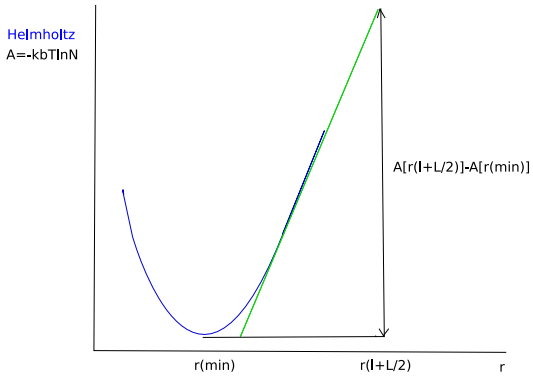

Figure 2.4: *r inguruko Helmholtz energia askearen profila. Grafikoak minimo bat erakusten du r_{min} puntuan eta lerro berdeak kurbaren tangentea infinituari dagokion distantziararte extrapolatzen du.*

2.4.3 grafikaren bidez posible da hainbat energia ezberdin estimatzea. Atomo bi horien arteko distantzia bi aukera ditzazkegu, adibidez lotura luzeera eta infinitua, eta hortik lotura distantziaren energia, edo era berean, uretan dagoen katio bat solbatatzen ari diren urek lehenengo eta bigarren geruzen arteko trukaketak egiteko beharrezko energiaren estimazioa egin daiteke.

PBC erabiltzen ari garelez, infinituko distantzia simulazio gelaxkaren (L) distantziaren erdia bezala estimatu daiteke, hau da, lotura energia bat kalkulatzeko, hasierako puntua l lotura luzeera izango da eta bukaerakoa $r = l + \frac{L}{2}$. Horrela ez izatekotan, atomek euren errepikapen periodikoak ikusiko lituzkete. Beste era batera esanda, "infinitura" heltzeko, partikula kutxaren ertzeraino eraman behar da.

Infinitu distantziara kokatuta dagoen distantzia ez da loturari dagokion Helmholtz energia diagraman adierazita egongo, beraz kurbaren extrapolazioaren bidez lortutako funtzio bat lor dezakegu, eta $r = l + \frac{L}{2}$ balio hori funtzio horretan ordezkatuta infinituzko distantziari legokiokeen energia eskuratuko genuke.

Beste alde batetik, naturan, aminoazido aromatikoen eta aluminioaren arteko interakzioak ingurune ez isolatuan gertatzen dira, beraz lotura energiak ez dute bakarrik hurbilen dauden atomoetan dependituko, baizik eta inguruneko (disolbatzaileko) atomo guztiek sortutako eragin globalaren menpe egongo da ere. Hau kristaletan Madelung konstantearen bidez neurtzen den faktorearekin aldera zitekeen. CPMD-k [31] efektu hau integralen trasformazio metodoaren bidez egiten du, zehazki Ewald metodoaren bidez [46].

Hori dela eta, gure sistemak ingurune biologikoak simulatu nahi dituztelez, Helmholtzen energia askeak solbaatzio osozko egoeran baino ez dira kalkulatuko.

Projektu honetan, Helmholtzen energia askeen kalkulua idazleak egindako kode txiki baten bidez egin da, idazlearen web horrian era askean eskuragarri dagoena.

2.4.4 Erradial Distribuzio Funtzioak

Erradial Distribuzio Funtzioak (RDF edo "g") material batean dagoen atomoen arteko distantzien dentsitatea neurtzen duen funtzio bat da.

Distribuzio hau experimentalki kalkula daiteke argi dispertsioz edo x-izpien hauts difrakzio bidez egindako neurketen bidez.

Konputazionalki, RDFak mekanika estadistikoa erabiliz kalkula daitezke,

$$g_{AB} = \frac{V}{N_B}\frac{1}{N_A}\left\langle \sum_{i}^{N_A}\sum_{ij}^{N_B}\frac{\delta(\mathbf{r}-\mathbf{r}_{ij})}{4\pi\mathbf{r}^2}\right\rangle, \tag{2.60}$$

non N zenbakia A eta B atomo moten kopurua den eta δ Dirac-en delta funtzioa.

Praktikan, RDFak grafikoki adieraziak izan daitezke (RDF vs $|\mathbf{r}|$), lotura distantzia edo distantzia aipagarriei dagozkien tokietan tontor batzuk erakutsiko dituztelarik. Tontorren altuera distantzia horretara dauden atomo (edo atomo mota) bikoteen arteko distantzia kopuruaren proportzionala izango da eta tontor edo bandaren zabalerak loturaren trinkotasunaren ideia bat emango digu.

2.60 ekuazioaren arabera, "g vs r" kurbaren azpiko azalerak A eta B partikulen kopuru osoa emango liguke, eta kurba hau zatika hartuz posiblea da distantzia jakin batetara dauden partikula kopurua lortzea, hau da, koordinazio zenbakia.

Koordinazio zenbakia ΔV bolumen jakin batetara, $G_{ij}(\mathbf{r})$ erradial distribuzio funtzioaren hiru koordenatu espazialekiko (r, φ eta θ) integrazioz emana dago

$$n_{ij}(\Delta V) = \rho_j \int_{r_i}^{r_f} \int_{\varphi_i}^{\varphi_f} \int_{\theta_i}^{\theta_f} G_{ij}(\mathbf{r}) r^2 \sin\theta d\theta d\varphi dr. \tag{2.61}$$

non, ρ_j aldagaia j-ren dentsitatea den.

2.4.4 irudiak RDF bat eta bere integralaren adibide bat erakusten du.

3 Å ingurutara dagoen lehenengo tontorra aluminiotik gertuen dagoen oxigenoari dagokio, kobalenteki lotuta dagoena, edo lehenengo solbatazio geruza alegia. Bigarren tontorra, 3.4 Å inguru, karboxilatoan kokatuta dagoen bigarren oxigenoari dagokio, eta 4 Å-tara kokatuta dagoena bigarren solbatazio geruzari dagokio.

2.4.4 irudiko puntudun lerroak ur disoluzioan dagoen Al^{+3} katioi baten RDFaren integrala adierezaten du. Lehengo solbatazio geruzari dagokion distantzian maila bat bereiz daiteke eta bigarren tontorraren gainean integralak beste maila bat erakusten du, normalizatu ezkero atomo kopurua adierazten duena

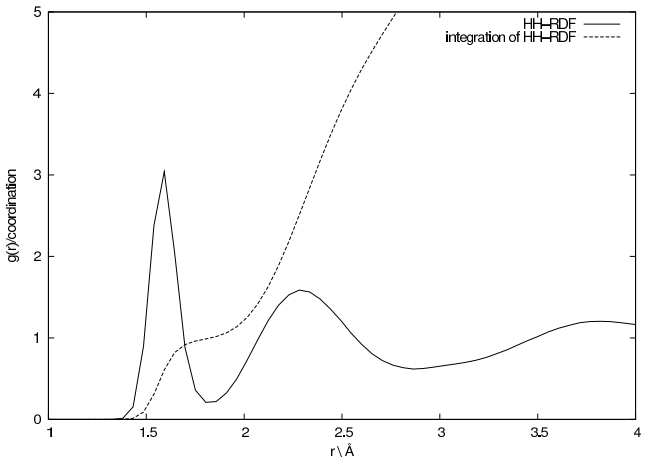

Figure 2.5: *Tyr, Al atomo bat eta 50 ur molekuladun sistema baten simulazio batetik kalkulatutako g_{HH} (edo HH-RDF)-a. Lerro jarraiak RDF-a deskribatzen du eta ez jarraiak honen integrala. RDFak H-H distantziarik laburrena (uraren hidrogenoen arteko ditantzia alegia) 1.6 Å-koa dela eta 2.3 Å-tara kokaturik dagoen tontorrak, pixka bat urrutirago dauden H-ak ere daudela (H-loturatik zeharkatuz). Integralak lehengo tontorraren erantzule diren atomo kopurua bat dela, oxigenoak hidrogeno bi lotuta dauzkala alegia, eta bigarren tontorraren atzean bi eta hiru atomore arteko kopuru bat.*

Lan honetako RDF-ak hasiera batean Ouluko unibertsitateko Kari Laasonen profesorearen taldeak idatziriko kode baten oinarritutako, norberak eraldatutako kode batez kalkulatuak izan dira.

2.4.5 Difusioa

Dinamika molekularrezko simulazio batean atomoak mugitzen dira, hortaz atomoen hasiera eta bukaerako kokapenak ez dira berdinak. Fenomeno hau difusio bezala ezagutzen da. Difusioa Desplazamenduaren Bataz Besteko Erroaren (MSD) edo difusio koefizientearen bidez kalkula daiteke.

MSD-a bere definiziotik zuzenean kalkulatua izan daiteke

$$MSD = \left\langle |\mathbf{R}(t) + \mathbf{R}(0)|^2 \right\rangle , \tag{2.62}$$

eta difusio konstantea

$$D = \lim_{t\to\infty} \frac{\left\langle |\mathbf{R}(t) + \mathbf{R}(0)|^2 \right\rangle}{6t}. \tag{2.63}$$

Gure simulazioek hutsean eginda daude, beraz sistema osoaren traslazioak ez du inongo eraginik eta horrez gain, energiak barne koordenatuetan kalkulatuak dira, errotazio eta bibrazio askatasun graduak barne parametroez baino dependitzen ez dutelarik.

Tesi honetako simulazioetan difusioa sistemaren masa zentrua simulazioan zehar zenbateraino mugitu den zehazteko erabil daiteke.

3. Kapitulua

Aurretik AAA eta Al^{+3}-aren inguruan egindako ikerketa

Katioi-π interakzio ez kobalenteak izanik, natura bereziki indartsua dute. Bestalde, beraien egitura proteinikoak egonkortzeko eragina [25] dela eta, kimika eta biologia arloetan interes berezikotzat hartuak izan dira.

Projektu hau, aluminioak amino azido aromatikoengan duen eragina aztertzera zuzenduta dago, baina emaitzak aurkeztu baino lehen, gai honen inguruan aurretik egin izan diren beste ikerketa batzuen emaitzak aurkeztuko dira.

3.1 Al^{+3} Solbatazioa uretan

Projektu honetan katioi-π interakzioak aluminio eta aminoazido aromatikoen artean ikertuko dire lez, eta ingurune biologikoa ingurune aquosoa izan ohi denez, interesgarria da lehenengo eta behin Al^{+3} katioiak uretan duen jokabidea aztertzea. Beraz, hasierako pausua, Al^{+3} ur puruan duen jokabidea ulertzea da, baina lan hau dagoeneko aski ikertua izan da dagoeneko, ikus adibidez: Thomas W. Swaddle [47] edo Takashi Ikeda [48] lanak, zeinetan CPMD-ren bidez lorturiko konformazio posibleak era zehaztu batean azaltzen diren.

Ikerketa hauen arabera, Al^{+3}-ren koordinazioa ur disoluzioan pH-aren menpekoa da. Era honetan, pH = 3.0 disoluzio azidoetan Al^{+3}-a sei-koordinatuta (hexakoordinatua) dago, beraz, lehenengo solbatazio geruza oktahedrikoa da. Kontrara, pH > 7 duten disoluzio basikoetan koordinazioa argi eta garbi laukoa da (tetrakoordinatua), eta ondorioz lehenengo solbatazio geruza egitura tetrahedrikoa du. Bestalde, pH = 5.0-ko disoluzioan Al^{+3}-aren koordiazioa bost (pentakoordinatua) dela aurkitu izan da [47] [49] zeina lan honetan ongi deskribatua izango den. Heptakoorinazioa ez da posiblea, mugapen geometrikoak direla medio [50].

Eskala mikroskopikoan, sistema txikietan koordinazioa eta pH-aren arteko lotura lehen geruzako -OH taldeen presentziaren arabera egin daiteke [51], honela $[Al(H_2O)_6]^{+3}$ hexakoordinatua litzateke, eta $[Al(OH)_4]^{-}$ tetrakoordinatua.

Bestalde, -OH ligandoen bidezko Al^{+3}-aren karga neutralizazioa eta koordinazio zenbakiaren arteko erlazio biuniboko bat dago ere. Izan ere, Mg^{+2} katioaren ka-

su beretsurako, aurkitua izan da -OH_2 bat -OH batez ordezkatzeak Mg^{+2} katioaren koordinazioa seitik bostera jeitsi dezakeela, eta bostetik laura bi -OH lingando ordezkatzekotan [52].

Al^{+3}-ur konplexuen egiturari buruz, eredu sinpleenetik ere distantzia eta angelu asko neur zitezkeen, eta hori azidotasun egoera, tenperatura, teoria maila,...ezberdinetarako [53]. Lan honetan, datu horietako gutxi batzuk baino ez ditugu kontutan hartuko, aztertu diren fenomenoak hobeto ulertzen laguntzen gaituztenak, alegia. Distantzia horietako garrantzitsuenetariko bat Al-O lehenengo eta bigarren solbatazio geruzetarainoko distantzia da, eta beste ikerkuntza batzuek lortu dituzten balioak bataz beste 1.9 eta 3.9 Å-ekoak [54] izan dira hurrenez hurren. Datu hauek lan honetan lortutakoekin bat datoz.

3.1 irudiak geometria optimizazio[1] baten ondoren jazotako solbatazio geruzen parametroen estimazio bat erakusten du. Lehenengo solbatazio geruzak koordinazio oktahedrikoa erakusten du, koordinazio maximoarekin (6) eta bigarren koordinazio geruza ur posible guztietatik batzu baino ez ditu erakusten (gogoratu egoera likidoa dela, ez kristala).

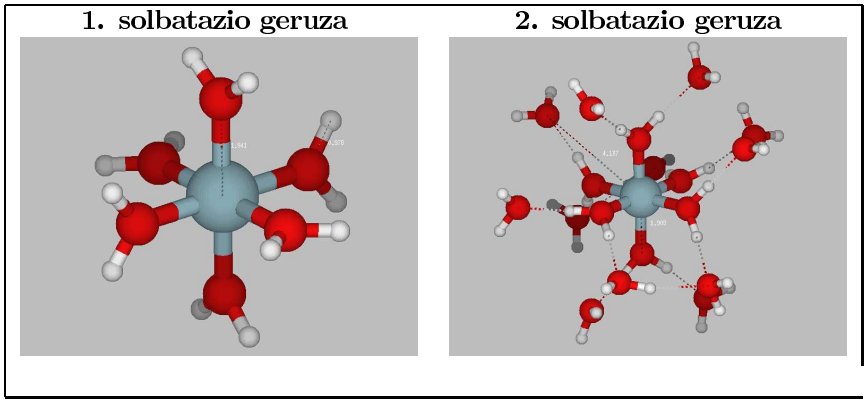

Figure 3.1: *Gaussian 03 [55] bidez egindako B3LYP/6-31++G(d,p) mailako geometri optimizazio batetatik jazotako Al^{+3}-aren inguruko lehenengo eta lehenengo bi solbatazio geruzak.*

3.2 AAA eta Al^{+3}

Projektu honetan aztertuak izango diren sistemak amino azido aromatikoez eta aluminioz osatatuta daude, beraz, gutxienez aluminioaren lehenego koordinazio geruza-

[1] "Gaussian 03" [55] bidezko geometria optimizazioa, B3LYP/6-31++G(d,p) mailan. Irudiak Molden-ekin [56] sortuak.

ko ligandoetako bat amino azidoren bateko zatiren bat izan behar du.

Simulazioak egiteko orduan, egonkortasun egoki bat erakusten duen egituretatik abiatu behar gara, eta kasu hauetan, bereziki interesgarria litzateke Al^{+3}-a hoberen egonkortzen den gunean kokatzea, hori baita errealitatean sarrien ekupatuko duen tokia. Al^{+3}-a erosoen lotuko litzatekeen tokiaren hasierako ideia bat egiteko, egokia da isolaturiko amino azidoen karga banaketaren ideia bat hartzea.

Badago kontutan hartu beharreko gauza bat: gas egoerako amino azido hutsak eta ur disoluzioan (katioirik gabe) disolbaturikoak karga solbatatuzko egitura dute [57] [58] [59], baina gure kalkuluek hiru karga ordenamendu ezberdin erakusten dituzte:

- Karga Solbatatua (**CS**): forma nominala edo ez-ionizatua, karga banaketa uniformea. Normalean honek -NH_2 eta -COOH taldeak daudela esan nahi du.
- Zwitterionikoa (**ZW**): nahiz ta karga totala neutroa izaten jarraitu, atomo ezberdinetan karga formal positibo eta negatiboak daude. Amino azido Zwitterionikoak, normalean -COO^- eta -NH_3^+ taldeak dauzkate.
- Zwitterioniko Inbertitua (**IZW**): kasu hau karga banaketa Zwitterionikoaren kasu partikular bat izan zitekeen, baina hidrogeno batzuk mugituz eta O eta N-ren seinuak aldatuz. Era honetan, N-ak karga negatiboa jazotzen du, eta -COO taldeak positiboa (ikus 3.2 irudia). Kasu hau, Al^{+3} katioiak nitrogenoaren gainean sortzen duen polarizazio handia dela eta gertatzen da.

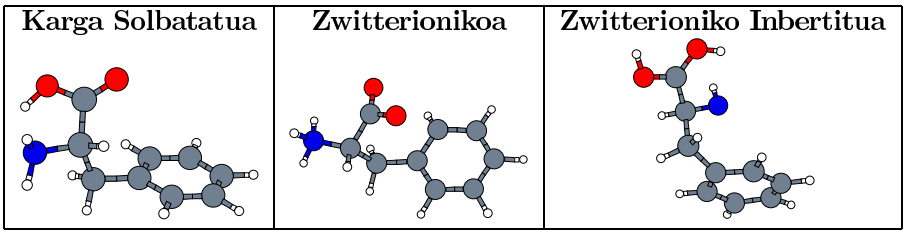

Figure 3.2: *Amino azidoetako karga banaketa ezberdinak (Irudiak xmakemol [60]-en bidez).*

Al^{+3}-aren kokalekuarentzako hasierako proposamen bat, karga elektrostatikoaren banaketan oinarrituz egin zitekeen. Era honetan, Al^{+3}-a potentzial elektrostatiko negatiboenena duten guneetan lotuko litzateke. 3.3 irudiak potentzial elektrostatikoaren ideia bat ematen digu.

Mapa hauen arabera, lotura gune probableena amino (-NH_2) eta karbonilo (-COOH) taldeetan legoke.

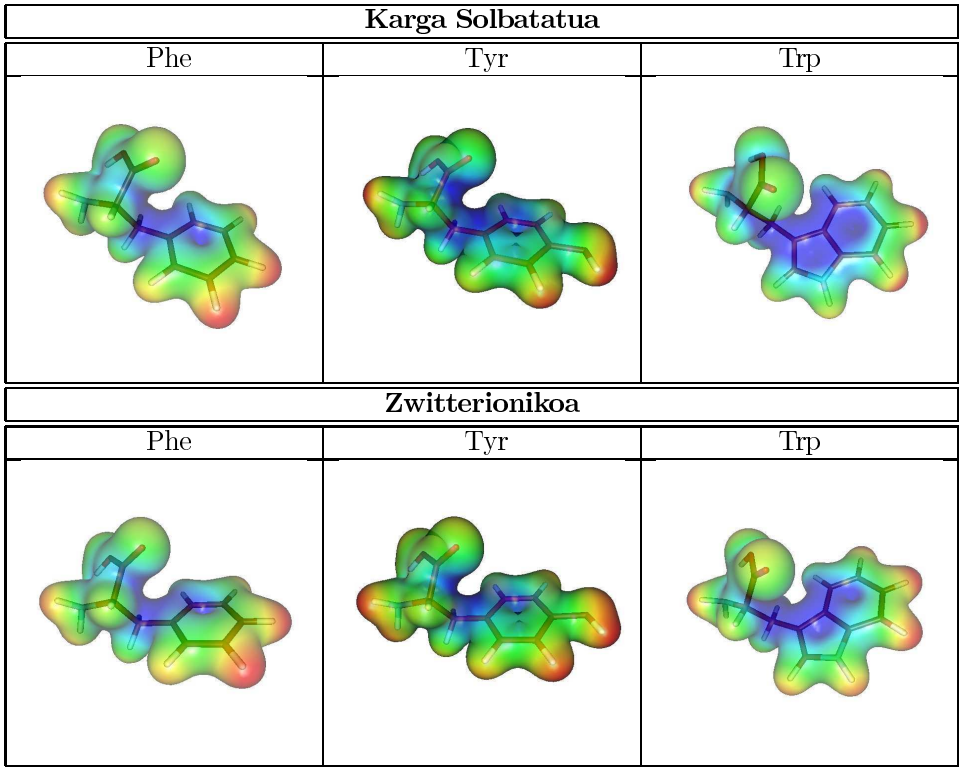

Figure 3.3: *Karga Solbatatu eta karga banaketa Zwitterionikodun amino azido hutsen kolorez kodeturiko isodentsitatezko gainazalaren bidez lorturiko potentzial elektrostatikoa. Urdina negatiboa da, orlegia neutroa eta gorria positiboa.*

Betalde, beraien natura gogorra dela eta katioi-π elkarrekintzen garrantzia kontutan hartu behar da [25] eta ondorioz Al^{+3}-ak amino eta karbonilo taldeekin duen elkarrekintzetaz gain, eraztun aromatikoarekin duen interakzioan ere kontu berezia jarriko da.

Ideia hauek, bibliografia konputazional [61] [62] eta experimentaleko [63] ikerkuntzetan aurkitutakoekin bat eginak izan dira, hasierako geometria optimoak aurkitzeko asmoarekin.

Horretaz gain, MD simulazio gehienetan, Al^{+3}-aren inguruko -OH_2 ligando kopurua konstante dihardu [64] eta ez dago ur elkartrukaketarik lehenengo eta bigarren solbatazio geruzen artean.

Al-O loturaren erdibizitza, momentuan eskuragarri dugun azpiegitura konputazionalean CPMD simulazioek iraun dezaketen denbora baino askoz luzeagoa da, beraz printzi-

pioz ez da inongo lehenego eta bigarren soatazio geruzen arteko ur elkartrukaketarik espero.

4. Kapitulua

Al^{+3} ur disoluzioan: deskribapen zehaztua

Aluminioa lur azaleko hirugarren elementu ugariena da. 1825-ean lehen aldiz isolatua izan zenetik, aluminioa hainbat erabilpen teknologikotan erabilia izan da eta ondorioz beronen presentzia gure inguruneetan arrunta bihurtu da.

Ioien inguruko solbatazio geruzetako ur molekulen egitura eta dinamika ulertzea, funtsezko zeregin bat da ur disoluzioko hainbat prozesuen interpretaziorako.

Kapitulo honek Al^{+3}-aren solbatazio geruza ezberdinen egitura eta portaera aztertzera bideratuta dago, honen bidez amino azidoekin duen erlazioa hobeto ulertzeko helburuarekin.

Al^{+3}-aren inguruko ingurunea hain bat kalkulu estatiko zein dinamiko eginez ikertua izan da.

Lehenengo eta behin, erreferentzizko datuak izatearren solbatazio geruzaren irudi bat eraiki izan da kalkulu estatikoak erabiliaz. Ondoren CPMD [31] bidezko dinamika molekularrezko simulazioak egin izan dira, Al^{+3}-aren ur disoluziozko koordinazio ezberdinak simulatuz.

Aluminioaren solbatazio geruzen inguruan egin izan diren ikerketa gehienak estatikoki burutuak izan dira edota gas faseko ideia erabiliaz eta aluminioak $Al(H_2O)_m(OH)_n^{3-n}$ itxurako egiturak sortuko dituela suposatuz, ikuspuntu kimiko batetatik sentzuzkoa izango litzatekeena [65][66][67]. Kapitulu honetako kalkuluetan, Al^{+3}-aren inguruko urak H_2O bezala mantendu dira eta dinamika molekularrezko simulazioek gas faseko hurbilketa hau nahi eta nahiez bete behar ez dela erakutsi dute.

4.1 Al^{+3}-aren inguruko 1. eta 2. solbatazio geruzuak

4.1.1 Kalkulu Estatikoak

Al^{+3} katioiaren inguruko ligandoekiko erakarpen indarra finkatua dagoelez, lehenengo eta bigarren solbatazio geruzetarainoko distantzia geruza bakoitzeko koordinazioaren araberakoa izango da.

Zenbait kalkulu estatiko egin izan ditugu RDFetako emaitzekin konparazioak egin ahal izateko. 4.1 taulako irudi eta datuak Gaussian 03[55]-rekin B3LYP/6-311++G(d,p) funtzionala/oinarria teori mailan egindako geometria optimizazioen

emaitza da. Hasierako egiturak Al^{+3} atomo bat eta batetik zazpirainoko ur molekula kopuruak erabiliz sortuak izan dira. Zazpi ur molekula dituen kasua ez da hemen kontutan hartuko, espero genezakeen bezala [50], geometria optimizaziozko prozesuan ur molekuletako bat bigarren solbatazio geruzara jauzi egiten duela ikusten bait da, sistema hexahidratatuaren baliokide bat sortzen delarik (ur batekin gehiago).

Emaitzei lehen begirada bat emanez, suposa genezakeen bezala, Al eta O-ren arteko distantzia handitu egiten da solbatazio geruzari ur molekulak gehitu ahala, baina bestalde, Al^{+3}-k zenbat eta bere karga gehiago konpartitu, O bakoitzak parte txikiagoa jasoko du, eta ondorioz indar gehiagorekin erakarriko ditu bere H-ak (fenomeno hau 4.1 irudian ikus daiteke).

Gainontzeko datuek ez daukate joera argirik, O-Al-O angelua kenduta, zeina arrazoi geometriko argiengatik koordinazoarekin txikitzen den.

	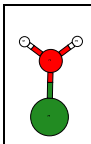	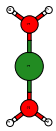	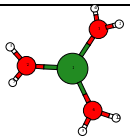	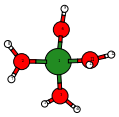	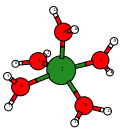	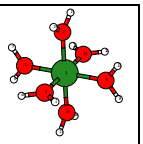
n	1	2	3	4	5	6
r_{AlO}	1.76	1.76	1.79	1.83	1.87-1.93	1.91-1.96
r_{OH}	1.02	1.00	0.99	0.98	0.79-0.81	0.97
r_{AlH}	2.50	2.50	2.52	2.54-2.55	2.58-2.65	2.63-2.64
α_{HOH}	107.5	106.3	106.3	106.3-106.4	106-107	106-107
α_{OAlO}		179.9	119.8	107.8-110.0	94,110,139,170	89-90

Table 4.1: *Al^{+3} + nH_2O konplexuentzako parametro ezberdinak: koordinazioa handitu heinean r_{AlO}-a handitu eta r_{OH} txikitu egiten da.*

4.1.2 Erradial Distribuzio Funtzioak

Kalkulu estatikoen bidezko hasierako ikuspegiaren ondoren, dinamika molekularraren bidezko espazio konfigurazionalaren laginketa hobeago bat egin da.

Dinamika molekularrezko simulazioak Car-Parrinello Dinamika Molekularrezko metodoa [43] erabiliz egin dira, CPMD [31] kodearen bidez.

Sistemaren tenperatura totala, 300 K inguru mantendu da Nose[37]-Hoover[38] termostatoa [39] erabiliz.

Elektroiak DFT bidez deskribatuak izan dira, zehazki PBD [29] dentsitatearen funtzionala erabiliz, CPMD-rako bereziki garaturiko[33][68] Vanderbilt pseudopotentzial ultraleunenkin [32] batera. 30 Ry-tako uhin lauen mozketa erradioa, 900 a.m.u.-zko masa elektroniko fiktizioa (μ) eta 7 u.a.-kozko urrats denborarekin.

Hidrogenoak (protioak) deuterioez ordezkatuak izan dira, urrats denbora erabilgarriaren luzeera luzatzearen helburuarekin, experimentalki ur astunaz egin diren

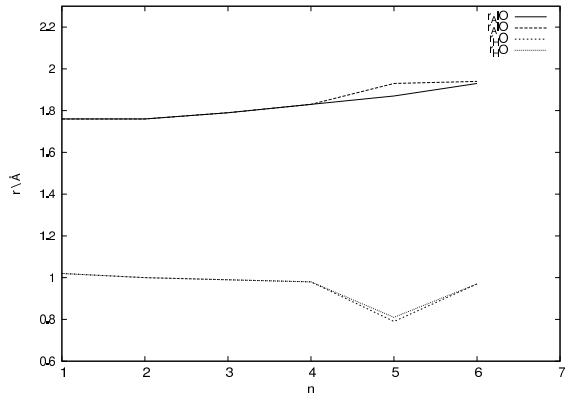

Figure 4.1: *Koordinazio zenbaki ezberdinetarako (1etik 6rako)* $r_{Al^{+3}O}$ *eta* r_{OH}*-ak irudikatzen dituen grafika. Zenbat eta koordinazio altuagoa, orduan eta* $r_{Al^{+3}O}$ *altuagoa eta* r_{OH} *baxuagoa.*

propietate eta kimikaren neurketak emaitz beretsuak ematen baitituzte. Deuterioen jokabidea hidrogenoenarekin konparatua izan da RDFen konparaketaren bidez emaitz parekoak emanez [69].

Sistemaren karga totala (+3 Al^{+3}-ren karga dela eta) jellium-a [70][71] erabiliz neutralizatua izan da. Simulazioak 100 ps-tik gorako denboraz kalkulatuak izan dira, estatistiken zehaztasuna handitzearen helburuarekin. Bataz besteko ioi desplazamenduak 22.62 (n=4), 28.84 (n=5) eta 35.61 (n=6) suertatu dira, simulazioan zeharreko sistemen egonkortazuna adieraziz.

Simulazio gelaxkaren tamaina, sistemaren dentsitatea uraren dentsitatearen berdina izan zedin kalkulatua izan zen, hau da 1 gr zentrimetro kubikoko. Unitate atomikoekin lan egin ahal izateko ekuazio bat garatu daiteke:

$$dentsitatea = 1\,\frac{\cancel{gr}}{\cancel{cm^3}} \times \frac{6.022.10^{23}\ a.m.u.}{1\,\cancel{gr}} \times \frac{1\,\cancel{zm^3}}{10^{-24}\,\mathring{A}^3} = 6.022.10^{-1}\,\frac{a.m.u.}{\mathring{A}^3} \quad (4.1)$$

$$L = \sqrt[3]{\frac{masa\ osoa}{dentsitate}} = \sqrt[3]{\frac{\sum n_{atomo} \times M_{masa\ molarra}}{0.06022}}$$

Gure kasuan, simulazio kutxa kubiko batentzako gelaxkaren sare parametroa 12.62 Å-tan zehaztua izan da.

Simulaturiko sistemek tamaina eta atomo kopuru berdina dute, baina hasierako egitura ezberdinak. Hiru hasierako egitura ezberdin sortu izan ziren Al^{+3} katioiak tetra, penta eta hexa-koordinazio izanez, alegia. Erradial Distribuzio Funtzioak 100 ps-tako trajektorietatik kalkulatuak izan ziren eta pentakoordinatuaren kasuan,

Al^{+3}-ak hexakoordinaziora jauzi egiten dueneko azkeneko tartea arbuiatua izan da. Tri- eta hepta-koordinaturiko Al^{+3}-a simulatzeko saiakerak egin izan ziren ere, baina geometria optimizazioan bertan egiturak berehala tetra edo hexakoordinatura jauzi egin izan dute.

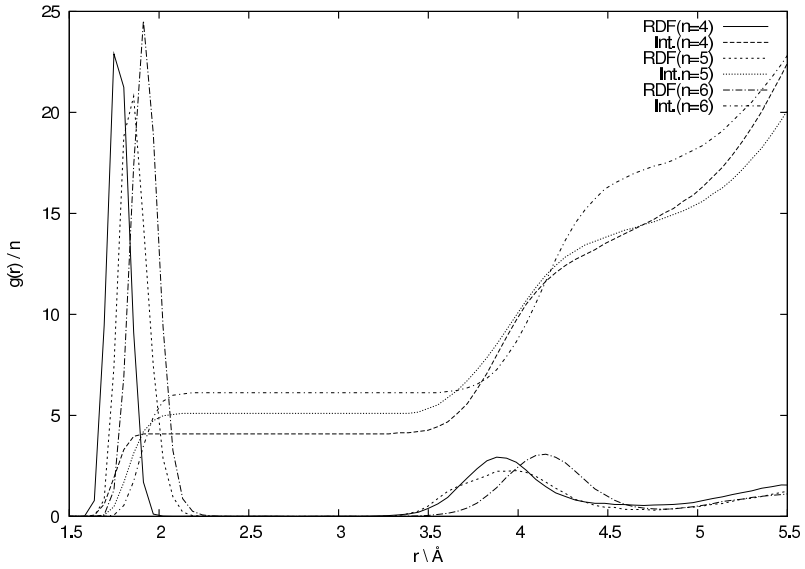

Figure 4.2: *50 H_2O + Tyr + Al^{+3} dituzten tetra-, penta- eta hexakoordinaturiko sistemen g_{AlO} eta beroni dagokien integralak.*

4.3 irudiko RDFen itxurari erreparatuz gero, koodinazioaren lotura distantziren gaineko eragina aski argi gelditzen da tontorren desplazamenduaren bidez.

Lehen tontorraren azterketa zehatzago bat eginda (ikus 4.3 **a)** irudia) lehenengo solbatazio geruzaren Al-O distantzia aztertu daiteke. Tetrakoordinazioaren kasuan, lehen tontorrak nolabaiteko alaka aurkezten du zeina mota ezberdinetako O-en presentzia adierazten duen. Era honetan -**O**H-a ezker muturraren bidez deskribatzen da eta lotura luzeera pixka bat luzeagoarekin, eskuin muturrean, -**O**H_2-a bidez. Efektu hau gehien bat tetra- eta pentakoordinazioaren kasuan ikusia izan da, eta ondorioz -OH-en presentzia tetra- eta penta-koordinazioaren kasuan baino ez da ikusia izan.

RDFan nabari daitekeen bezala, tetrakoodinaturiko egiturak -**O**H-a 1.74 Å-tara erakusten du eta -**O**H_2-rena 1.80 Å-etara eta pentakoordinatuan 1.80 eta 1.86 Å hurrenez hurren. Bestalde, tontorren altuerek tetrakoordinatuean -OH-ren lehenengo geruzako presentzia -OH_2-rena baino nabarmenagoa dela adierazten du eta pentakoordinatuan ordea -OH_2 nagusitzen da -OH-ren aldean.

Tetra- eta penta-koordinaturiko sistemetan ikusten den -OH ligandoen presentziaren

zergatia Al^{+3}-ren kargan aurkitu daiteke, Al^{+3}-ren karga inguruko ur molekula neutroen polarizaturiko karga negatiboen kontribuzia baino askoz haundiagoa bait da, eta ondorioz O-etatik tiratu eta zenbaiten H-ak askatzen direlarik.

Hexakoordinazioaren kasuan, Al^{+3}-ren inguruko uren banakako kontribuzioek Al^{+3}-aren karga neutralizatzeko gai ei dira, eta ondorioz ez dago -OH ligandoen presentzia egonkor nabarmenik eta $-OH_2$-ko O-a 1.93 Å-etako distantziara ageri da.

Emaitz hauek 4.1 taulan agertzen direnekin konparatuta (1.83, 1.87-1.93, 1.91-1.97 Å) distantzia pixka bat laburragoak erakusten dituzte, simulazioan zehar gertatutako uren deprotonazioa dela eta.

Aurretik Mg^{+2}-aren inguruan egindako ikerketen arabera, $-OH_2$ bat -OH batekin ordezkatuz gero seitik bosterako koordinazio murrizketa bat eragin dezake eta bostetik laura bi -OH ligando ordezkatzekotan [52].

Gaussian 03 [55] eta B3LYP/6-31+G**-tan egindako egitura hexakoordinatuaren beste ikerketa estrukturalen datuekin konparatuta, lehenengo solbatazio geruza 1.92 Å-tara kokaturik legoke [54], gure emaitzetan baino pixka bat gertuago.

Solbatazio geruza	1.	2.
G03	1.93-1.94	3.96
RDF	1.91-1-96	4.14
Ref.[54]	1.92	3.97-3.99
Ref.[72]	1.94	4.08-4.12
Ref.[73]	1.85-2.0	4.01
Ref.[74] (Exp)	1.87-1.90	
Ref.[74][75][76](Exp)		4.01-4.15

Table 4.2: *Metodo ezberdinekin lorturiko Al-O distantziak eta konparaketa beste ikerkuntza batzuetan lortutakoenekin.*

	r_{AlO} (Å)	
Geruza	**1.**	**2.**
n=4	1.75-1.80	3.87
n=5	1.85	3.99
n=6	1.91	4.15

Table 4.3: *RDFetatik lorturiko Al-O distantzien bidezko Al^{+3}-ren inguruko lehenengo eta bigarren solbatazio geruzen deskripzioa.*

4.4 **a)** irudian koordinazioaren Al-H distantziaren gaineko influentzia argi bat ikusten da, influentzia hau Al-O-ren kasuan lortutakoaren antzekoa izanik. Tontorrak 2.51 (n=4), 2.57 (n=5) eta 2.62 (n=6) Å-etako distantzietara kokaturik daude lehenengo solbatazio geruzako H-entzat. 4.1 taulako datuekin konparatuta (2.54-2.55, 2.58-2.65 and 2.63-2.64 Å) balioak zertxobait txikiagoak dira, hydrogenoen ordez deuterioak erabiltzearen ondorioz seguruenik.

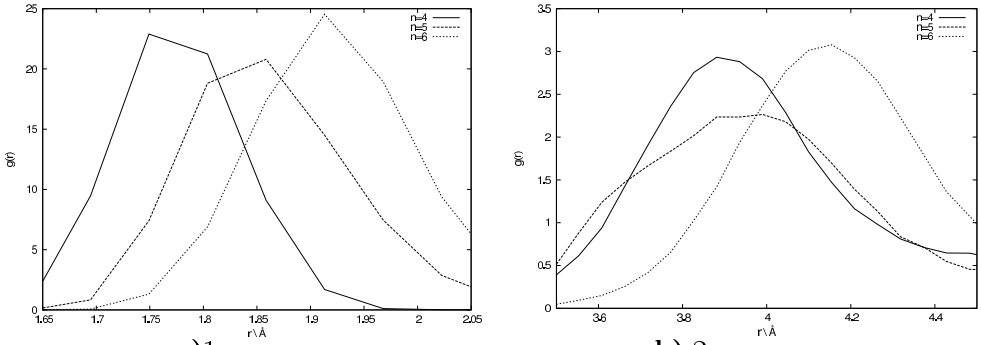

a)1. geruza **b)** 2. geruza

Figure 4.3: *Gustiz disolbaturiko Al^{+3} katioi batean, koordinazio zenbaki ezberdinetarako lorturiko g_{OAl}-ren lehenengo eta bigarren solbatazio geruzen tontorren ikuspegi zehaztua.*

Penta- eta hexa-koordinazioko kasuetan ez bezala, tetrakoordinaziozko kasuan lehen tontorraren eskuinetara 3 Å-eko distantziara albo-tontor bat ageri da, zeinak ezberdintasun aipagarri bat suposatzen duen. Albo-tontor honen jatorria aluminioaren kargaren uren gaineko eraginean dago, non zenbat eta ligando gehiagoz inguratuta egon are gehiago sakabanatzen den karga, eta ondorioz egitura tetrakoordinatuaren karga kontzentrazio altuak -OH-en presentzia bultzatzen du $-OH_2$-enaren ordez, eta -**OH** hauek dira hain zuzen 3 Å-n kokatuta dagoen tontorraren sortzaileak.

Bigarren solbatazio geruzako hidrogenoek bereziki kanporuntz desplazaturik daude hexakoordinatuaren kasuan. RDF-ek banda garbiago bat erakusten dute tetra- eta hexa-koordinatutako simulazioekin konparatuta. Honen arrazoia egitura oktahedrikoaren egonkortasun bereziki handian dago, hau da, geometria horretan ligandoen posizioak ez duela hain beste fluktuatzen eta ez die bigarren geruzako urei gehiago hurbiltzen uzten.

g_{OH}-ren kasuan (ikus 4.4 **b)** irudia), estadistikak sistema osoari dagozkio eta 4.1 taulako datuekin konparatuta, bataz besteko balioak zehazki berdinak dira, 0.98 Å-etara kokatuak, beste ikerketa batzuenganako adostazun onargarri bat erakutsiz [53]. Azidotasun handiko azidoen soluzioekin konparatuta [77], Al^{+3}-ren azidotasuna ez da behar bezain handia ur disoluzioan hidronio ioien presentzia sortarazteko, eta ondorioz ez da albo-tontorrik ageriko g_{OH}-ko lehenengo tontorraren alboan(ostera 1.5 Å aldera egon beharko litzateke).

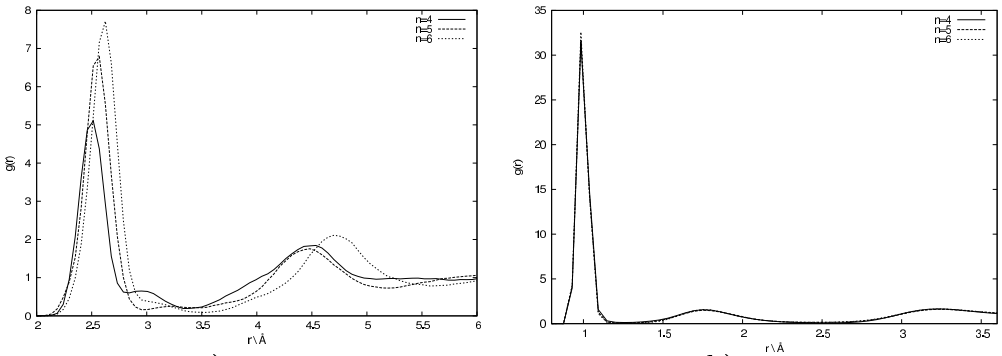

a) g_{AlH} **b)** g_{OH}

Figure 4.4: a)*g_{AlH}-ak Al-H distantziak koordinazioarekin batera handitzen dela erakusten du. Lehenengo tontorrak n=4-koaren kasuan -OH-ari dagokion albo-tontor bat erakusten du eta bigarren geruza n=6-aren kasuan bereziki desplazatuta dago kanporantz egitura oktahedrikoaren egonkortasuna dela eta.* **b)***g_{OH}-ak jokaera baliokide bat erakusten du koordinazio ezberdinetarako. Ez dago hidronioaren presentziaren aztarnarik.*

4.2 Deshidrataziozko Helmhotz Energia Askeak

Deshidrataziozko Helmholtz energiak 2.4.3 atalean azalduriko metodoaren bidez kalkula daitezke.

r_{AlO} distantzietatik eraikitako histograma eta bere F(r)=-K_BTln P(r) ekuazioaren bidezko Helmholtz energiarako eraldaketa 4.5 **a)** irudian ikus daitezke.

4.2 irudiko RDFen kasuan gertatzen den bezala, lehenengo solbatazio geruza 1.8 Å inguruan kokaturiko tontor estuago batengatik deskribatuta dago eta bigarren solbatazio geruza 3.9 Å inguruan kokaturiko bandaren bidez. Histograma/Helmholtz eta RDFen arteko desberdintasuna, histograma distantzia bakar bat neurtuz eraikita dagoela da, eta RDFan ordea distantzia kopuru handi baten arteko bataz besteko bat da.

4.5 **b)** irudiak Al^{+3}-aren inguruko lau oxigenoentzako Helmholtz energia askeko profila erakusten du, eta deshidrataziozko energia baliorik txikiena lortzearren kanporuntz desplazatuen dagoen oxigenoari dagokiona aukeratu da. Hau da, zenbat eta oxigenoa kanporago egon, orduan eta energia gutxiago behar da gustiz kanpora ateratzeko. Azkenik 4.5 **c)** irudian energia kurbaren lehenengo solbatazio geruzatik bigarren geruzarainoko extrapolazioa ikus daiteke, honen bitartez egoera bien arteko energia diferentzia kalkula daiteke.

Al^{+3} pentakoodinatuaren simulazioa bereziki interesgarria da, bigarren solbatazio geruzako uretako batek lehenengo solbatazio geruzara jauzi egiten baitu. 4.6 irudiak

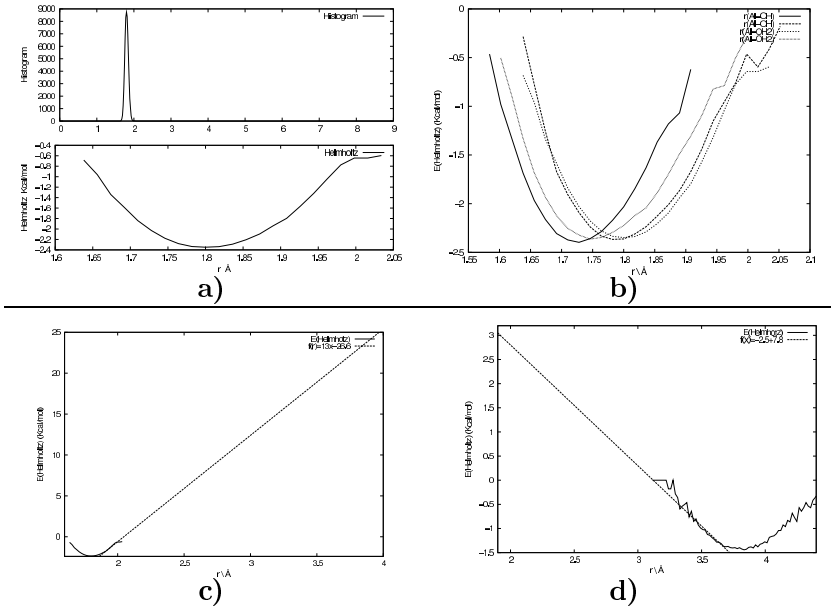

Figure 4.5: *n=4:* **a)** *Lotura distantzia (r_{AlO}) vs pausuko kasu kopurua adierazten dituen histograma eta beraren Helmholtz energia aske profilezko eraldaketa lehen solbatazio geruzako lau urentzako sistema tetrakoordinatuan. H bakarra duten O-ek Al-tik gertuago daude.* **c)** *lehenengo solbatazio geruzari dagokion kurbaren tangentearen bigarren geruzarainoko (3.9 Å) extrapolazioa.* **d)** *c) irudiaren berdina baina bigarren geruzatik lehenengora atzerantzko extrapolazioa eginez.*

lehen geruzako Al-O distantziak erakusten ditu, eta argi ikus daiteke O6-ko (lerro marroia) 5 Å ingurutik 2 Å-rainoko jauzia.

Fenomeno honek, aurretik erabili izan dugun interpolazio-extrapolazio teknika bera erabiliz, energia askeko profila era bikoitzean kalkulatzeko aukera ematen digu. Kasu honetan lehenengo eta bigarren solbatazio geruzak atomo bikote bakar bat erabiliz deskribatzeko aukera izan dugu (Ikus 4.7 **a)** irudia).

Egitura pentakoordinatuaren kasurako, solbatazio geruzak ongi deskribatuak ikus daitezke 4.7 **a)** irudian.

4.7 **b)** iruditik, lotura energia eta lehen geruzatik bigarrenera ur bat ateratzeko energia estima daitezke. Egitura pentakoordinatuaren (4.2 taulatik) 1.85 Å-tara kokaturiko lehenengo solbatazio geruzatik ur bat egoztekotan, egitura tetrakoordinatua bihurtuko litzateke, beraz ura egitura tetrakoordinatuari legokiokeen bigarren solbatazio geruzaraino, hots 3.87 Å-etaraino, bultzatu beharko litzateke.

Egitura pentakoordinatuaren energia interpolatuz lorutako kurbaren tangentearen

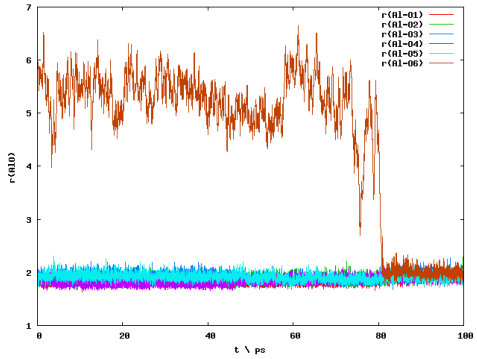

Figure 4.6: *n=5: Gustiz disolbaturiko (50 H_2O) Al^{+3} pentakoordinatuaren simulaziotik kalkulaturiko lehen geruzako r_{AlO} distantziak. O6-ak bigarren geruzatik lehenegora jauzi egiten du.*

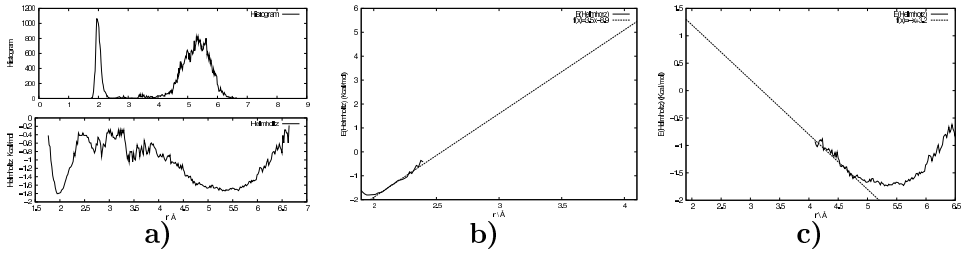

Figure 4.7: *n=5:* **a)** *Populazio histograma eta Helmholtz energia askerako konbertsiorako grafika egitura pentakoordinaturako* **b)** *Lehen solbatazio geruzako kurbaren tangentearen bigarren solbatazio geruzarainoko extrapolazioa erakusten du.* **c)** *n6-tik n5-erako alderantzizko extrapolazioa (n6-ren deshidratazioa edo n5-en hidratazioaren baliokidea).*

bigarren solbatazio geruzarainoko extrapolazioak ematen duen energiaren balioa eta lehen soltatazio geruzaren oreka puntuari dagokionaren arteko aldea, ΔE= 5.6 kcal/mol-koa da, hau da, lehen geruzatik bigarrenera ur bat ateratzeko beharko litzatekeen energiaren estimazioa.

Tetrakoordinaturiko egituran, kurbaren interpolazioaren tangentea $f(x) = 13x - 26.6$ funtzioaren bidez adierazi daiteke, eta trikoordinatuaren bigarren solbatazio geruzarainoko (≈ 3.85 Å) extrapolaturiko puntuarekiko energia diferentzia, ΔE= 25.8 kcal/mol-tzat estima daiteke. Ur molekula bera infinituraino ateratzeko 81 kcal/mol estimatu dira, zeinak sentzua duen, aluminioak ez baitu gustoko ingurune urtsuetan koordinazio hain txikirik izatea.

4.4 taulan hidratazio egoera posible guztientzako lehenengo solbatazio geruzatik

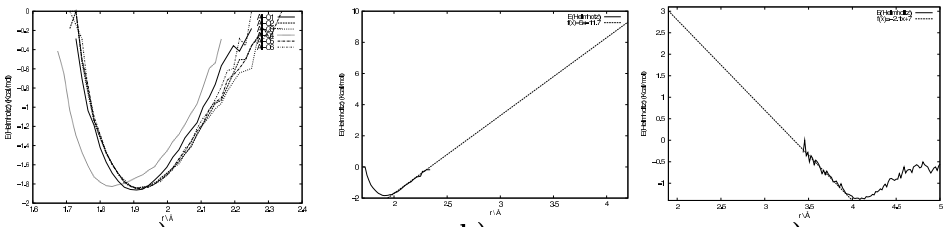

Figure 4.8: *n=6:* **a)** *Helmholtz energia askearen profila egitura hexakoordinatuaren lehen solbatazio geruzako sei urentzat. Hidrogeno bakarra duen oxigenoa Al-tik gertuago dago.* **b)** *Lehen solbatazio geruzako kurbaren tangentearen bigarren solbatazio geruzarainoko extrapolazioa.* **c)** *b)-ren berdina baina atzerantzko extrapolazia eginez.*

bigarrenera ur molekula bat ateratzeko eta lehenengotik infinitura (deshidratazioa, alegia) ateratzeko energiak ikus daitezke.

Erreakzioa			$\Delta E_{1\to2}$	$\Delta E_{1\to\infty}$
$Al(H_2O)_4$ - H_2O	$\rightarrow$	$Al(H_2O)_3$	25.9	81.0
$Al(H_2O)_5$ - H_2O	$\rightarrow$	$Al(H_2O)_4$	5.6	19.0
$Al(H_2O)_6$ - H_2O	$\rightarrow$	$Al(H_2O)_5$	10.0	31.1

Table 4.4: *Al-ur klusterrentzako 1. solbatazio geruzatik bigarren geruzara eta infinitura (deshidratazioa) ur molekula bat ateratzeko energia (kcal/mol).*

4.3 Ondorioak

- Aurretik egindako ikerketek [47][48] zioten bezala, egindako simulazioetatik, bai tetra- zein penta- edo hexa-koordinaturiko egituren egonkortasuna berresten da, egitura pentakoordinatuak tetra- edo hexakoordinaziora jauzi egiteko joera duelarik.
- Al^{+3}-ren lehen solbatazio geruzako uretan, Al-O distantzia koordinazio zenbakia igo ahala handitzen da da O-H distantzia txikitzen delarik.
- Tetra- eta pentakoordinazioaren kasuetan Al^{+3}-ak lehen solbatazio geruzako urak deprotonatzen ditu, ondorioz -OH_2 eta -OH ligandoez inguratuta gelditzen delarik.
- Hexakoordinaturiko egituran, Al^{+3}-aren karga inguruko sei uren kontribuzioarekin konpentsatzen da eta ondorioz simulazioetan ez da ur ligandoen deprotonaziorik ematen.

- Egitura tetrakoordinatuaren kasuan energia gehien behar da bai ur bat bigarren solbatazio geruzara jauzi egin dezan, zein ura gustiz kentzeko. Honek Al^{+3}-aren ligandoen beharra adierazten du.
- Egitura pentakoordinatuak energia gutxiago behar du ur molekula bat kanporatzeko, egonkorra izan arren egitura tetra- eta hexakoordinatuak are egonkorragoak direlako.

5. Kapitulua

AAAk Mikrohidrataturiko Al^{+3}-arekin

5.1 Sarrera

Katioi-π izenez ezagutzen den katioi eta eraztun aromatikoaren arteko interakzioa [25], gas faseko lotura indar ez-kobalente indartsuenetakotzat hartzen da [24]. Katioi-π interakzioak, likido egoeran ematen dira [24], non katioiak ongi solbataturik dauden eta desolbatazio energia gainditu behar den, eraztuna eta katioaren interakzioa lortzeko.

Katioi-π interakzioak proteinetan ematen dira. Izatez proteinak osatzen dituzten 20 aminoazido naturaletatik hiruk (Phe, Tyr eta Trp) ezaugarri guztiz aromatikoak dituzte, eta ondorioz katioi-π interakzioak sor ditzazkete.

Disoluzioan dauden katioiak ongi solbataturik daudenez, lotura gune posibleek desolbatazio energia gainditu behar dute katioa uretatik erauzteko, baina zoritxarrez, ingurure urtsuko lotura energia hauek ez daude oraindik gustiz ulertuak, egindako neurketa kuantitatiboak gehien bat amino azidoen arteko interakzioetan zentratuak baitaude.

Kapitulo honetan Al^{+3} katioia eta amino azido aromatikoen arteko interakzioen deskribapen zehatza egingo da talde honetan aurretik egin diren beste ikerkuntza batzuen jarraipen modura [78][79].

5.2 Energia Minimodun Konplexuak

Sistema baten energia bere erdibizitzaren alderantziz proportzionala denez, eta egitura baten erdibizitza berau aurkitzeko probabilitatearen proportzionala denez, argi dago egituren energia kontutan hartu beharreko zerbait dela.

Projektu honetan, hiru amino azido aromatikoen konfigurazio espazioa aztertuko da, konformazio ezberdin posibleen energia minimoak bilatuz eta aztertuz.

Guztira, 60 egituratik gora aztertu dira, gutxienez 4 amino azido bakoitzarentzat (2 CS (karga solbatatu) + 2 ZW (Zwitterioniko)), 12 Al^{+3}-ren lotura gune posible ezberdinentzako, eta 36 mikrohidrataziozko egoera ezberdinetarako (batetik lau ur molekuletara).

Egituren analisia, egitura bakoitzarentzako geometria optimizaziozko kalkuluen bidez egin da, eta emaitzen sinesgarritasuna bermatzeko kalkuluak bi kode ezberdin erabiliz egin dira.

Lehen geometria optimizazioa eta frekuentzia kalkulua Gaussian 03 [55] kodea erabiliz egin izan da. Teoria maila, elektroi guztiak kontutan hartzen dituen 6-31+G (d,p) oinarri estandarraren bidez egin da B3LYP (Becke3 Lee-Yang-Parr) dentsitatearen funtzionala erabiliz. Ondoren frekuentzia kalkuluak burutu izan dira, egitura desegonkortu dezaketen modu normalik ez daudela ziurtatzeko.

Bigarren geometria optimizazioa CPMD [31] kodearen bidez egin izan da, PBE [29] dentsitatearen funtzionala, CPMD-rentzat bereziki garaturiko Vanderbilt-en pseudo potentzial ultra-leunak [32][33][68] erabiliz, uhin lauen mozketa erizpidea 30 Rykoa izanik.

Hurrengo atalean hainbat taula aurkeztuko dira, egitura egonkortuak eta berauen energia minimoeneko egiturarekiko energia diferentzia (ΔE kcal/mol-eko unitateetan) erakutsiz. Honez gain erreferentziazko beste zenbait neurketa erakusten dira ere, guzti hau kode biekin lortutako emaitzetarako.

5.2.1 Katioi-π interakzioak bentzeno eta fenolaren eraztunetan

Katioi-π interakzioa amino azido aromatiko-Al^{+3} klusterretan aurki daitezkeen interakzio ez-kobalente indartsunetariko bat da. Atal labur honek katioi-π interakzioen eraztunaren gaineko eragina deskribatuko da.

Katioia eta eraztunaren arteko loturaren indarraren idea bat hartzearren Al^{+3} katioiak bentzeno eta fenolarekin dituen elkarrekintak azter ditzazkegu. Konparaketa honek erreferentzi bezala balioko digu ere aurrerago aurkeztuko diren sistemen interpretazioa egiteko, azken finean Phe eta Tyr-en eraztun aromatikoak (albo kate aromatikoa kenduta) bentzeno eta fenola baitira.

Al^{+3}-en bentzeno eta fenolarekiko lotura energia 5.2.1 eta 5.2.1 irudietan agertzen diren erreakzioen bidez kalkula daiteke. Kalkuluak Gaussian 03 [55]-ren bidez egin izan dira, B3LYP/6-311++G(d,p) funtzional/oinarria erabiliz.

5.2.1 irudiko egituretatik konproba daitekeen bezala, Al^{+3}-eraztun lotura energia 20 kcal/mol inguru handiagoa da fenolaren kasuan, fenolaren -OH-aren presentziak elektroi dentsitate handiagoa sortarazten duelako eraztunean, eta beraz Al^{+3} erakarriago sentitzen da.

Bentzenoaren erreferentzizko datuak bentzeno-Al^{+3} konplexuarenarekin konparatuz gero, eraztunaren tamainaren areagopen bat nabaritu daiteke, eta gauza bera fenolaren kasuan, zeinetan Al^{+3}-a eraztunaren zentrutik desplazatua agertzen den, -OH-rantzko norantzan.

Al^{+3}	+	bentzeno	→	bentzeno-Al^{+3} konplexua
		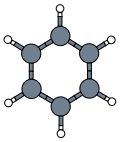		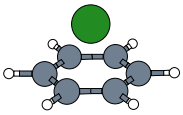
		d_{CC}=1.39 d_{CH}=1.08		d_{CC}=1.44 d_{CH}=1.09 d_{CAl}=2.19
-240.4048	-	-232.3113	→	-473.2970
ΔE = -0.5809 u.a. x 627.51 $\frac{kcal}{u.a.}$ = -364.52 kcal/mol				

Figure 5.1: *Al^{+3}-en bentzenoren eraztunarekiko lotura energia kalkulatzeko erreakzioa eta zenbait distantzia Å-etan.*

Al^{+3}	+	fenol	→	fenol-Al^{+3} konplexua
		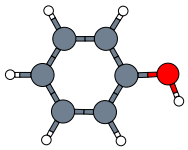		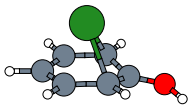
		d_{CC}=1.39 d_{CH}=1.08		d_{CC}=1.42-1.47 d_{CH}=1.09 d_{CAl}=2.17-2.39
-240.4048	-	-307.5587	→	-548.5794
ΔE = 0.6159 u.a. x 627.51 $\frac{kcal}{u.a.}$ = -386.48 kcal/mol				

Figure 5.2: *Al^{+3}-ren fenolaren eraztunarekiko lotura energia kalkulatzeko erreakzioa eta zenbait distantzia Å-etan.*

5.2.2 Amino Azido Hutsak

Geometri optimizaziozko kalkuluek argi erakusten dutenaren arabera, amino azido hutsek CS karga distribuzioak nahiago dituzte, zeinak bat egiten duen beste hainbat ikerketa ezberdinekin [61] [58]. Bestalde, Phe eta Tyr-entzako **a-b** eta **c-d** irudien arteko konparaketak erakusten digunaren arabera, alaninaren kasuan gertatzen den bezala [80], albo kate aromatikoaren orientazioak eragin oso txikia dauka energia osoarengan.

ZW egiturak, mugaturiko geometria optimizazioaren bidez kalkulatuak izan dira, zeren bestela zuzenean CS-ra eroriko bailirakete. Hiru kasuetan hirugarren egiturak **c** frekuentzia negatiboren bat aurkezten du (hori dela eta "∗" batekin adieraziak daude), zeinak amino azido hutsak ZW egituran izateko zailtasuna erakusten duen. Egitura hauek taulan gehituak izanaren zergaitia, ZW egituren albo kate aro-

matikoaren orientazioaren eragin energetikoa konparatu ahal izatean dago.

Hurrengo tauletan agertuko diren datuetan, "Eg. Zbk." Egitura Zenbakia adierazten du, honen bidez zenbaki bereko amino azido ezberdinen egiturak konpara daitezkeelarik, hau da, hasierako egiturak sortu zireneko erizpidearen araberako zenbakia. "G03" Gaussian 03 eta "CPMD" CPMD kodeen bidez lorturiko kalkuluen emaitzak direla adierazten du.

ΔE (kcal mol^{-1})	**a** (CS)	**b** (CS)	**c** (ZW)	**d** (ZW)
		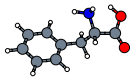	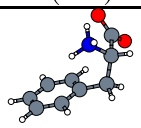	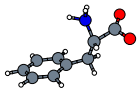
Eg. Zbk.	2	1	4	3 $*$
G03	0.00	0.01	15.76	16.47
CPMD	0.01	0.00	133.1	12.83

Figure 5.3: *Phe-rentzako energia minimodun egiturak. Energiek CS egiturenganako zaletasun argi bat erakusten dute.*

ΔE (kcal mol^{-1})	**a** (CS)	**b** (CS)	**c** (ZW)	**d** (ZW)
	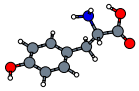	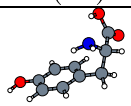	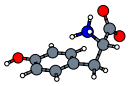	
Eg. Zbk.	1	2	3 $*$	4
G03	0.00	0.06	15.81	16.48
CPMD	0.00	0.04	12.90	13.55

Figure 5.4: *Tyr-rentzako energia minimodun egiturak. Energiek CS egiturenganako zaletasun argi bat erakusten dute.*

ΔE (kcal mol^{-1})	**a** (CS)	**b** (CS)	**c** (ZW)	**d** (ZW)
				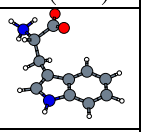
Eg. Zbk.	1	2	3 $*$	4
G03	0.00	6.41	14.88	23.79
CPMD	0.00	7.62	12.00	20.69

Figure 5.5: *Trp-rentzako energia minimodun egiturak. Energiek CS egiturenganako zaletasun argi bat erakusten dute.*

Dist. (Å)	Phe	Tyr	Trp
r_{CC}	1.40	1.40	1.40
r_{CH}	1.08	1.08	1.08
r_{CN}	1.47	1.47	1.47
r_{NH}	1.01	1.01	1.01
r_{CO}	1.21	1.21	1.21
$r_{CO(H)}$	1.33	1.34	1.34

Table 5.1: *Energia minimodun amino azido hutsen (5.2.2, 5.2.2 eta 5.2.2 irudietako* **a**)*) egituren erreferentzizko distantziak Å-etan.* r_{CC} *eta* r_{CH} *eraztun aromatikoko CC eta CH distantziei dagozkien luzeerak dira.*

5.2.2 taulak Al^{+3}-k sortarazten dituen egitura aldaketak aztertzeko erabiliko diren erreferentzi datu batzu adierazten ditu.

Lan hau Al^{+3}-ren amino azidoen gaineko eragina aztertzera bideraturik dagoelez, amino azido huts hauek erreferentzitzat erabiliko dira soilik.

5.2.3 Amino Azidoen Konplexaketa Al^{+3}-rekin

Al^{+3} katioiaren presentziak, bere karga positiboa dela eta, karga berantolaketa bat sortarazten du amino azidoengan.

Al^{+3}-rentzako lotura gune ezberdin guztiak karboxilatoa (-COOH edo $-COO^-$ eran), nitrogenoa ($-NH_2$ eran) eta eraztun aromatikoarem gaineko π elektroietara mugatuta daude. Ikus 3.3 irudia karga elektrostatikoaren banaketaren isodentsitatezko maparentzako.

Emaitzak adierazten duten arabera, Al^{+3}-arentzako lotura gunerik egokiena, eraztun aromatikoa da, $-COO^-$-z jarraiturik eta azkenik $-NH_2$.

Karga banaketa Al^{+3}-ren kokapenaren menpean dago, hots, konplexuak ZW egitura izango du baldin eta Al^{+3}-a $-NH_2$ loturik ez badago, eta egonez gero, konformazioa CS izango da, kasu honetan -COOH-ra lotuta egongo delarik ere. Al^{+3}-a $-NH_2$-ari loturik dagoenean baina ez -COOH-ari karga banaketazko eredu berri bat agertzen da Zwitterioniko Inbertitua (IZW) bezala izendatu duguna.

IZW egituraren kasua 5.2.3 taulako **e** egituran ikus daiteke.

5.2.3 taulako COO^--ren **d** (ZW), **e** (IZW) eta **f** (CS) egituren Mulliken kargak aztertuz, **f** egituraren karga nabarmenki altuagoa ikusten da (0.39) **e** (0.11) eta **d**-renekin (-0.16) konparatuta.

Energia minimodun egiturak ez dira baliokideak hiru amino azidoentzat. Hiru kasuetan minimoek ZW karga banaketa daukate eta Tyr eta Trp-n Al^{+3}-ak karboxilatoarekiko lotura bihortzekoaren (kelatoaren) bidez koordinazio geruza betetzea bilatzen du baina harrigarriki Phe-k, hortz bakarreko egituran erakusten du energia minimoena, koordinazio elementu bi baino ez dituelarik.

Al^{+3}-ari koordinatuta		Karga Banaketa
$-COO^-$	$-NH_2$	
$\surd$	$\surd$	CS
$\otimes$	$\otimes$	CS
$\surd$	$\otimes$	ZW
$\otimes$	$\surd$	IZW

Table 5.2: *Al^{+3}-aren lehen solbatazio geruzaren ligandoen menpeko karga banaketa. $\surd$-k lehen geruzan honelako elementu bat dagoela esan nahi du eta $\otimes$ ezentz.*

ΔE	**a** (ZW)	**b** (CS)	**c** (ZW)	**d** (ZW)	**e** (IZW)	**f** (CS)
	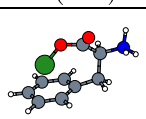	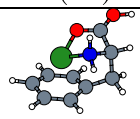	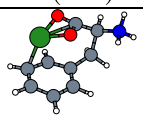	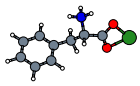		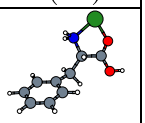
	4.2	2.1	4.1	3.1	1.2	1.1
G03	0.00	0.28	1.16	16.36	18.70	22.91
CPMD	1.58	0.00	2.54	17.70	20.51	25.80

Figure 5.6: *Phe-Al^{+3} konplexua: **e**-k IZW egitura dauka. Energia diferentzietatik katioi-π interakzio sendotasuna nabari daiteke.*

ΔE	**a** (ZW)	**b** (CS)	**c** (ZW)	**d** (ZW)	**e** (ZW)	**f** (CS)	**g** (CS)
	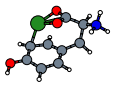	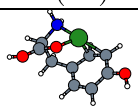	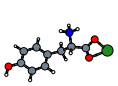	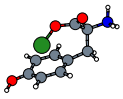	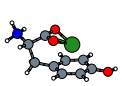	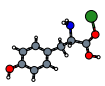	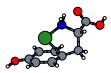
	4.1	2.1	3.1	4.3	4.2	1.1	1.2
G03	0.00	0.60	2.69	2.84	5.00	7.51	36.44
CPMD	0.03	0.00	2.15	2.53	1.25	8.87	21.09

Figure 5.7: *Tyr-Al^{+3} konplexua: Energia diferentzietatik katioi-π interakzio sendotasuna nabari daiteke.*

Fenomeno honentzako erantzun posible bat 5.2.1 ataleko datuen interpretazioaren bidez bila daiteke. Izatez, oxigenoaren karga negatiboa dela eta, eraztun fenolikoak gogorrago heltzen dio Al^{+3}-ari, honen ez-neutralizaturiko karga gehiago hutsiz, eta ondorioz karboxilatoaren oxigenoak erakartzeko beharrezko indar elektrostatiko gutxiago hutsiz. Berdin gertatzen da Trp-arekin, baina oxigenoaren ordez nitrogenoarekin.

Emaitz hauek aurretik Na^+-ekin egindako ikerketen [81] emaitzekin alderatuz Al^{+3}-arenganako jokaera ezberdin bat adierazten dute, Na^+-ekin egindako ikerketa hauetan katioiak CS egitura egonkortzen zuela aurkitu bait zen. Nahiz eta 5.2.3, 5.2.3

ΔE	**a** (ZW)	**b** (CS)	**c** (ZW)	**d** (ZW)	**e** (CS)
	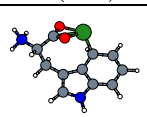	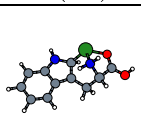	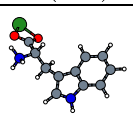	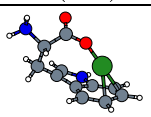	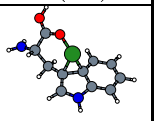
	4.1	1.1	3.1	4.2	2.1
G03	0.00	8.42	11.40	14.84	50.31
CPMD	0.00	9.91	17.81	11.21	45.05

Figure 5.8: *Trp-Al^{+3} konplexua: Energia diferentzietatik katioi-π interakzio sendotasuna nabari daiteke.*

eta 5.2.3 egituretako **b)** egiturek katioiaren nitrogeno eta oxigenoaren gaineko "itsasketa" efektuarengatik egonkortuak izan, **a)** egiturek energia baxuagoa daukate, eta ZW dira.

5.2.4 AAA-Al^{+3} Konplexuen Mikrohidratazioa

Monohidratazioa

Al^{+3}-ari loturiko ur molekula batek beronen karga sakabanatzera laguntzen du, gainontzeko ligandoenganako erakarpen indarra ahulagoa izango delarik.

Al^{+3}-ren koordinazio zenbakia gutxienez 4 izan behar dela suposa daiteke, hortaz, koordinazio elementuetako bat ura baldin bada beste hiru elementu gehiago behar dira lehen solbatazio geruza egonkortzeko.

5.2.4 taulan eta ondoren aurkeztuko direnetan, "Ir." koordenatu atomikoen adierazpen grafikoa da, hots egituraren irudia. "Let." egitura horri deitzeko erabiliko den letra adierazten du, "n" Al^{+3}-aren koordinazio zenbakia adierazten du, "KB" Karga Banaketa adierazten du (CS, ZW edo IZW), "ΔE" energia minimoen duen egiturarekiko energia diferentzia adierazten du kcal mol^{-1} unitateetan, eta azkenik r_{AlO}, r_{AlN} eta r_{AlC_α} Al^{+3}-tik (karboxilatoko) oxigeno, (aminoko) nitrogeno eta alfa karbonorako distantzia minimoak adierazten dituzte hurrenez hurren.

Amino azido ezberdinentzako egindako kalkuluek jokaera baliokide bat erakusten dute energia minimoeneko egiturentzat. Hiru kasuetan minimo globalak CS eta $-COO^-$, $-NH_2$, ura eta eraztun aromatikoarekiko tetrakoordinatuak agertzen dira. Trp-aren kasuan, G03 bidez kalkulaturiko "a" egitura "b" egiturarekin lehian agertzen da, zeina CPMD bidezko kalkuluetan minimo global bezala agertzen den.

Monohidrataziozko kasu honek ezberdintasun handi bat suposatzen du, Al^{+3}-AAA konplexu bakarra baita zeinetan CS karga banaketa minimo globaltzat neurtua izan den. Gainontzeko kasuetan, bai Al^{+3}-AAA, zein di-, tri- eta tetrahidrataturiko egituretan, energia minimoko egituraren karga banaketa ZW izan da.

Phe + Al^{+3} + 1 H_2O								
Ir.	Let.	n	KB	Kodea	ΔE	r_{AlO}	r_{AlN}	r_{AlC_α}
	a	4	CS	G03	0.00	1.82	1.99	2.03
				CPMD	0.00	1.81	1.98	2.03
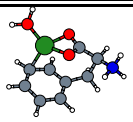	b	4	ZW	G03	4.85	1.88	4.52	2.99
				CPMD	2.35	1.87	4.49	2.91
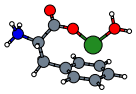	c	3	ZW	G03	6.94	1.70	5.01	2.50
				CPMD	5.53	1.69	4.97	2.46
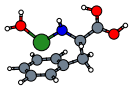	d	3	IZW	G03	33.37	4.43	1.81	2.26
				CPMD	29.93	4.43	1.80	2.24
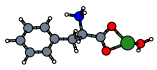	e	3	ZW	G03	38.99	1.89	4.55	6.08
				CPMD	33.53	1.88	4.53	6.06
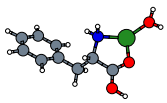	f	3	CS	G03	48.61	1.80	2.02	4.69
				CPMD	44.82	1.79	2.01	4.69

Table 5.3: *Monohidrataturiko Phe-Al^{+3} konplexua.*

Al^{+3}-ak koordinaziozko elementuen beharrean dagoelez, koordinazio zenbaki altuagoko egiturak egonkorragoak izango dira. Bestalde, karboxilatoko oxigenoek Al^{+3}-rekin bihortzeko (kelato) lotura erraz sor dezaketen arren, orokorrean esterikoki faboratuagoa dago nitrogenoari lotzea, errezagoa baita 4 atomotako kate bat tolestea 3 atomotako bat baino.

Aurretik suposa genezakeenez [82], hortz bakarreko eta bihortzekoaren arteko energia langa nahiko txikia dela aurkitu izan dugu.

Katioi-π interakziorik gabeko egiturak argi eta garbi gaitzetsita daude eta 5.2.4 **d** irudiko IZW egitura aurretik antzerako ikerketetan ikusia izan ez den zerbait da.

Kode ezberdinekin lortutako emaitzen azterketa eginez, energia aldetik orokorrean

Tyr + Al^{+3} + 1 H_2O								
Ir.	Let.	n	KB	Kodea	ΔE	r_{AlO}	r_{AlN}	r_{AlC_α}
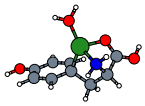	a	4	CS	G03	0.00	1.85	1.98	2.03
				CPMD	0.00	1.84	1.97	2.03
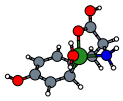	b	4	ZW	G03	5.35	1.82	1.99	2.04
				CPMD	3.07	1.81	1.98	2.03
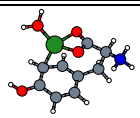	c	4	ZW	G03	7.48	1.89	4.52	3.00
				CPMD	4.76	1.88	4.49	2.91
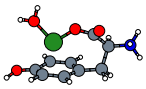	d	3	ZW	G03	8.99	1.71	4.49	2.42
				CPMD	5.55	1.70	4.91	2.36
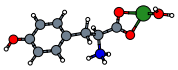	e	3	ZW	G03	30.85	1.93	4.57	6.11
				CPMD	33.96	1.92	4.54	6.08
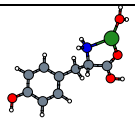	f	3	CS	G03	37.09	1.87	2.11	5.45
				CPMD	31.47	1.84	2.08	5.41

Table 5.4: *Monohidrataturiko Tyr-Al^{+3} konplexua:*

CPMDk Gaussianek baino energia diferentzia baxuagoak ematen dituela ikusten da, Trp-aren **a** eta **c** egiturak salbuespen izanik.

Egiturazko datuak oso beretxuak dira. r_{AlO} distantzien balioak berdinak edo 0.01 Å txikiagoak dira CPMDaren kalkuluetan Gaussinen kalkuluein konparatuta. r_{AlN} distantziaren kasua korapilotsuagoa da konparatzeko, zuzenean loturik ez dauden kasuetan distantzia handiak izan ditzazketelako tartean, eta horrek emaitz oso ezberdinak jazotzea eragin dezakeelako. Zuzenean loturik daudeneko kasuak CS eta IZW karga banaketak dituztela dakigu, eta hauei dagozkien distantziak konparatuta, berriz ere Al-N distantziak 0.01 Å laburragoak dira CPMDaren kalkuluetan Gaussianekoekin konparaturik. Azkenik r_{AlC_α} distantzien kasurako ere Al-N kasuko

Trp + Al^{+3} + 1 H_2O								
Ir.	Let.	n	KB	Kodea	ΔE	r_{AlO}	r_{AlN}	r_{AlC_α}
	a	4	CS	G03	0.00	1.84	1.99	3.27
				CPMD	1.33	1.83	1.98	3.24
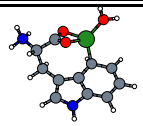	b	4	ZW	G03	0.43	1.88	4.55	3.48
				CPMD	0.00	1.86	4.54	3.46
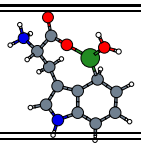	c	4	ZW	G03	11.95	1.68	5.12	3.34
				CPMD	13.43	1.67	5.08	3.26
	d	3	ZW	G03	44.52	1.95	4.53	5.01
				CPMD	43.36	1.95	4.52	5.15
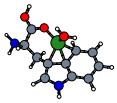	f	3	CS	G03	44.69	1.76	4.62	2.14
				CPMD	42.04	1.75	4.60	2.14

Table 5.5: *Monohidrataturiko Trp-Al^{+3} konplexua:*

antzeko arazo bat dugu, katioi-π interakziorik ez dauden kasuetarako distantzia diferentziak nahiko handiak izan daitezkeelako. Monohidrataziozko kasu honetan, katioi-π interakzioak nagusitzen dira zeinetan r_{AlC_α}-ren balioa aurreko kasuetan bezala 0.01 Å inguru baxuagoa da CPMDarentzako, baina hala ere egitura irekiak ere kalkulatuak izan dira, zeinetan distantzia ezberdintasuna 0.14 Å-etako ezberdintasuna izatera heldu diren.

Dihidratazioa

Al^{+3}-aren inguruko bigarren ur molekula sartzeak kasu guztietako koordinazio zenbakia 4tik gora izatea eragiten du.

Bi mikrosoltabaziozko uren kasuan, Al^{+3}-AAA egituren kasuan ikusi den bezala, energia minimoko egiturek ZW karga banaketa erakusten dute. CS egiturekiko energia diferentzia hainbat kcal mol^{-1}-ekoa da kasu guztietan, zeinak ZW egituraren nagusitasuna adierazten duen. Phe-aren kasuan IZW egituraren energia handiak,

karga banaketa hau ia arbuiagarritzat hartzeko iradokitzen digu.

Kasu honetan, 5.2.3 atalean bezala, energia minimodun konplexuak hortz bakarrekoak dira Phe eta Tyr-entzat bihortzerantzako langa txiki batekin ($\sim$ 5-7 kcal/mol), baina jokaera hau kontrakoa suertatzen da Trp-arentzat, zeinak bihortzeko egitura egonkorragotzat erakusten duen eta horrez gain energia langa esanguratsu bat duen hortz bakarreko egiturarekiko.

Koordinazio zenbakia 4 da Phe eta Tyr-en energia minimodun egiturentzako eta 5 Trp-arentzat, zeina harrigarria iruditu daiteke Phe eta Tyr-ek bihortzeko egituraruntz duten energia langa txikia ikusita. Barrera hau erraz gaindi zitekeen eta pentakoordinazioa lortu.

Katioi-π interakzioen garrantzia, egitura irekiek orokorrean daukaten energia diferentzia handiagoaren bidez ikus daiteke.

Kode ezberdinen bidez lorturiko energiaren konparaketa bat eginez gero, monohidratazioaren kasuan gertatu den bezala, egituren energia minimoeneko egiturarekiko energia diferentzia orokorrean pixka bat baxuagoa da CPMDrekin egindako kalkuluetan Gaussianekoekin alderatuta. Salbuespenak Tyr-aren **b** eta **c** eta Trp-aren **b**, **c**, **d** eta **f** izanik zeinetan energia balioak CPMDaren kasuan Gaussianen kasuan baino pixka bat altuagoak diren.

Tyr-aren **e** egituraren kasuan energia diferentzia nabarmenki handi bat neurtu izan da, G03-eko kalkuluak CPMD-koak baino 5.89 kcal mol^{-1} gehiago erakutsi ditu.

r_{AlO} distantziari buruz, balio berdintxuak jazo dira edo 0.01 Å inguru baxuagoak CPMDaren kasurako. Berdin r_{AlN} distantziaren kasurako, nahiz ta egiturak ZW izan. r_{AlC_α} distanziak 0.02 Å inguru baxuagoak izatera hel daitezke CPMDaren kasuan eta salbuespen bezala, Phe-aren **a** egituran 0.05 Å baxuago agertzen da. Lehen haipatutako tarteko atomoen kopuak sortzen dituen askatasun graduen ondorioz, eta salbuespen bezala, Phe-aren **b** egituran distantzia pixka bat luzeagoa agertzen da CPMDaren kasurako.

Trihidratazioa

Al^{+3}-aren inguruko hirugarren urak mono- eta dihidratazioarekiko aldaketa esanguratsu bat suposatzen du. Al^{+3}-ak gutxienez tetrakoordinazioa bilatzen du, eta hirugarren mikrosolbataziozko urak amino azidoarekiko esterikoki errazagoa den lotura bat sortzen laguntzen dio. Bestalde, amino azidoarekiko lotura bikoitzak (bihortzekoak edo N+O) pentakoordinazioa lortzeko aukera sortzen du.

Edozein kasutan, Tyr-aren "b" egitura salbu, hexakoordinazioa eta katioi-π interakzioak ez dute esterikoki bateragarriak ematen. Hori dela eta, trihidratazio eta tetrahidratazioarako katioi-π interakzioak desfaboratuak daude, eta interakzio hauek izateko aukera bakarra ur molekularen bat bigarren solbatazio geruzara egoztea da.

Phe + Al^{+3} + 2 H_2O								
Ir.	Let.	n	KB	Kodea	ΔE	r_{AlO}	r_{AlN}	r_{AlC_α}
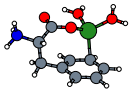	a	4	ZW	G03	0.00	1.76	5.10	3.13
				CPMD	0.00	1.76	5.09	3.08
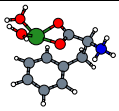	b	5	ZW	G03	5.40	1.91	4.59	3.08
				CPMD	4.36	1.90	4.57	3.11
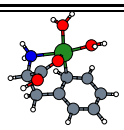	c	5	CS	G03	6.25	1.86	2.08	2.10
				CPMD	7.38	1.85	2.07	2.11
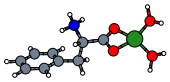	d	4	ZW	G03	15.30	1.82	4.52	5.88
				CPMD	12.65	1.81	4.49	5.85
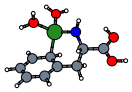	e	4	IZW	G03	27.19	4.45	1.81	2.60
				CPMD	26.82	4.44	1.80	2.57
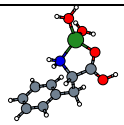	f	4	CS	G03	28.14	1.78	1.92	4.45
				CPMD	27.49	1.76	1.91	4.42

Table 5.6: *Dihidrataturiko Phe-Al^{+3} konplexua.*

Energia minimodun egituren karga banaketa, berriz ere, ZW bezala agertzen da eta CS-ekiko energia diferentziak sistema dihidratatuan baino esanguratsuagoak bihurtzen dira. Honek esan nahi du, aztertutako egitura guztietan, ZW egiturek CS dutenak baino energia diferentzia baxuagoa izango dutela. Bestalde, CS egiturak Al-N loturarekin erlazio biuniboko bat dutelez, Al^{+3}-ren koordinazioa N-rekin desfaboratua egongo da. Phe-aren IZW egituraren energia nabarmenki handia da besteekin konparatuta.

Trihidratazioaren kasuan, CPMD eta Gaussianen arteko energia diferentziaren joerak aldatzen du. Kasu honetan, Phe eta Trp-aren kasu baterako kenduta, energia berdinak edo pixka bat handiagoak agertzen diran CPMDaren kasurako.

Tyr + Al^{+3} + 2 H_2O								
Ir.	Let.	n	KB	Kodea	ΔE	r_{AlO}	r_{AlN}	r_{AlC_α}
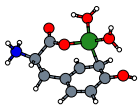	a	4	ZW	G03	0.00	1.76	5.11	3.19
				CPMD	0.00	1.75	5.10	3.13
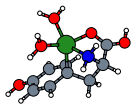	b	5	CS	G03	6.49	1.93	2.02	2.10
				CPMD	7.18	1.92	2.02	2.10
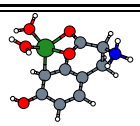	c	5	ZW	G03	7.10	1.91	4.61	3.19
				CPMD	5.53	1.91	4.59	3.12
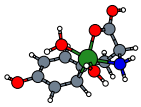	d	5	CS	G03	9.02	1.86	2.08	2.61
				CPMD	7.75	1.85	2.07	2.55
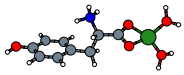	e	4	ZW	G03	15.80	1.82	4.50	5.86
				CPMD	9.91	1.79	4.48	5.83
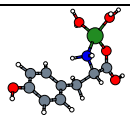	f	4	CS	G03	29.86	1.77	1.93	4.44
				CPMD	25.59	1.75	1.92	4.42

Table 5.7: *Dihidraturiko Tyr-Al^{+3} konplexua.*

r_{AlO} eta r_{AlN} distantzien balioak berriz ere beretxuak dira edo gehien jota 0.02 Åbaxuagoak CPMDaren kasuan. Phe-aren **f** egiturak distantzia nahiko luzeak erakusten ditu kode biekin Al-COO-ren artean dagoen tarte zabala dela eta (ez dago zuzenean Al-ari lotuta). r_{AlC_α} distantzien balioak orokorrean nahiko beretxuak dira ere, CPMDarentzako balioak 0.02 Å inguru baxuagoak izanik. Salbuespen bezala, Tyr-aren **e** egituran 0.05 Å-etako balio ezberdintasun izatera heltzen da, eta Trp-aren **a**, **c** eta **d** egituretan CPMDaren emaitzek 0.01 Å luzeagotzeat agertzen dira.

Tetrahidratazioa

Laugarren ur baten presentziak Al^{+3}-aren penta eta hexakoordinazioa eragiten du.

Trp + Al^{+3} + 2 H_2O								
Ir	Let.	n	KB	Kodea	ΔE	r_{AlO}	r_{AlN}	r_{AlC_α}
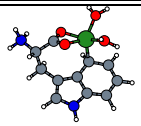	a	5	ZW	G03	0.00	1.88	4.66	3.57
				CPMD	0.00	1.88	4.65	3.56
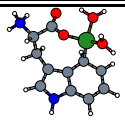	b	4	ZW	G03	0.09	1.76	5.06	3.55
				CPMD	0.36	1.76	5.05	3.55
	c	5	CS	G03	13.12	1.94	2.02	2.07
				CPMD	13.83	1.93	2.01	2.08
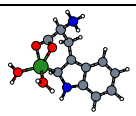	d	5	ZW	G03	15.08	1.93	4.41	2.97
				CPMD	15.95	1.92	4.40	2.96
	f	4	CS	G03	39.15	1.79	4.56	2.01
				CPMD	39.66	1.77	4.54	2.01

Table 5.8: *Dihidrataturiko Trp-Al^{+3} konplexua.*

Energia minimodun egiturak ZW dira era argi batean eta ZW eta CS-ren arteko energia diferentziak trihidratazioaren kasuan baino handiagoak bihurtzen dira. Kasu honetan Phe-aren IZW egiturak, energia nahiko handiena izateaz gain, G03-ren bidez egindako frekuentzia kalkuluetan frekuentzia irudikariak aurkeztu ditu, beraz, egitura honen egonkortasuna ez da kontutan hartzeko bezalakoa.

Zaila litzateke ZW eta CS egituren arteko energiaren diferentziaren estimazio bat egitea, egitura zeharo ezberdinak baitira, Al^{+3}-ak CS egitura posible egiten duen N-ra lotzen delarik, H-en posizioa ere aldatuz.

Trihidrataziozko kasuan bezala, katioi-π interakzioak posible dira baldin eta soilik baldin ur molekuletako bat bigarren solbatazio geruzara egozten bada.

Phe eta Tyr-en kasuan, energia minimodun konplexuak bihortzekoak dira eta Trp-aren kasuan hortz bakarrekoa, baina hortz bakar eta bihortzeko egituren arteko diferentzia ez da esanguratsuki handia.

Kode ezberdinekin lortutako datuen konparaketa eginez, trihidratazioaren ka-

Phe + Al^{+3} + 3 H_2O								
Ir.	Let.	n	KB	Kodea	ΔE	r_{AlO}	r_{AlN}	r_{AlC_α}
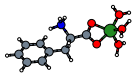	a	5	ZW	G03	0.00	1.87	4.56	5.98
				CPMD	0.00	1.86	4.55	5.95
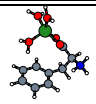	b	5	ZW	G03	0.19	1.87	4.56	4.17
				CPMD	0.42	1.86	4.55	4.12
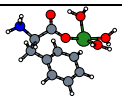	c	4	ZW	G03	4.04	1.83	5.27	3.39
				CPMD	4.97	1.84	5.27	3.38
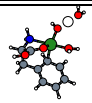	d	5	CS	G03	10.77	1.88	2.11	2.73
				CPMD	10.10	1.87	2.10	2.72
	e	5	CS	G03	12.77	1.86	2.01	3.79
				CPMD	13.54	1.86	2.00	3.75
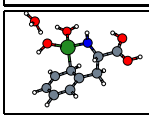	f	4	IZW	G03	31.88	4.43	1.83	2.62
				CPMD	30.38	4.41	1.82	2.60

Table 5.9: *Trihidrataturiko Phe-Al^{+3} konplexua.*

suan gertatu den bezala, hainbat kasutan CPMDaren energiak Gaussianen bidez lortutakoak baino altuagoak agertu dira eta diferentzietako batzu hainbat kcal/moletakoak izatera heltzen dira, zeinak aurreko mikrohidratazio ezberdindun kalkuluekin ezberdintasun esanguratsu bat suposatzen duen.

r_{AlO}, r_{AlN} eta r_{AlC_α} distantzien kasuan ere, ezberdintasun bat dago aurreko kasuekin konparatuta. Izan ere, kasu hauetan Phe-aren CPMDaren kalkuluetatik lorturiko distantziek gehien jota 0.02 Å laburragoak izatearen joera mantentzen dute, baina Tyr eta Trp-aren kasuetan joera horretaz gain, Tyr eta Trp-arentzako hiruna kasu aurkitu dira zeinetan distantziak luzeagoak diren CPMD bidezko kalkuluetan.

5.2.5 Energia Minimodun Konplexuen Egonkortasuna

Energia minimoa erakusten zuten egituretatik abiatuta CPMD dinamika molekularrezko simulazioak burutu dira egituren giro tenperaturako egonkortasuna berrezteko helburuarekin.

Tyr + Al^{+3} + 3 H_2O								
Ir.	Let.	n	KB	Kodea	ΔE	r_{AlO}	r_{AlN}	r_{AlC_α}
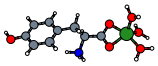	a	5	ZW	G03	0.00	1.87	4.55	5.95
				CPMD	0.00	1.85	4.53	5.93
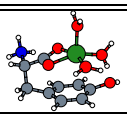	b	6	ZW	G03	1.69	1.92	4.57	3.94
				CPMD	4.97	1.92	4.57	3.91
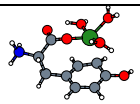	c	5	ZW	G03	7.15	1.80	5.22	3.29
				CPMD	10.69	1.80	5.20	3.26
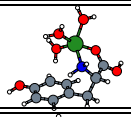	d	5	CS	G03	12.68	1.86	2.01	3.77
				CPMD	14.77	1.86	2.00	3.73
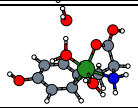	e	5	CS	G03	14.62	1.87	2.11	2.64
				CPMD	14.76	1.87	2.10	2.59
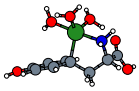	f	5	CS	G03	25.99	3.38	2.06	2.14
				CPMD	27.85	3.42	2.07	2.17

Table 5.10: *Trihidrataturiko Tyr-Al^{+3} konplexua.*

Guztira 12 egitura ezberdin simulatu dira, bakoitza 20 ps-ko denbora tartez, eta horietatik 11k beraien hasierako konformazioa mantendu izan dute, beraien egonkortasuna berretsiz.

Tetrahidrataturiko Trp-aren kasuan, hasierako **a** egiturak **c** egiturara jauzi egiten du, karboxilatoarekiko duen lotura bihortzekoko Al-O lotura bat apurtuz. Gertaera hau egitura bien arteko energia langa txikiaren ondorioz gertatu da, giro tenperaturako simulazio batean gertatzen diren energia totalaren fluktuazio txikiak eraginda.

5.3 Egitura Azterketa

5.3.1 Lotura Distantziak

5.2.5 atalerako egindako energia minimoeneko konplexuen simulazioetatik RDF-ak kalkulatuz hauen egituraren bates besteko parametroak kalkulatu dira.

Trp + Al^{+3} + 3 H_2O								
Ir.	Let.	n	KB	Kodea	ΔE	r_{AlO}	r_{AlN}	r_{AlC_α}
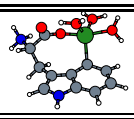	a	5	ZW	G03	0.00	1.85	4.95	3.69
				CPMD	0.00	1.86	4.97	3.70
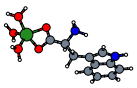	b	5	ZW	G03	7.37	1.86	4.53	5.94
				CPMD	3.39	1.84	4.52	5.92
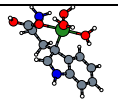	c	5	ZW	G03	8.93	2.00	3.55	2.09
				CPMD	9.73	1.98	3.53	2.10
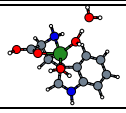	d	5	CS	G03	9.63	1.90	2.07	2.08
				CPMD	9.74	1.90	2.06	2.09

Table 5.11: *Trihidrataturiko Trp-Al^{+3} konplexua.*

5.3.1, 5.3.1 eta 5.3.1 tauletan aurkezten diren balioetan, d_{OAl} Al^{+3}-tik gertuen dagoen karboxilatoaren O-rainoko distantzia da, zeina orokorrean Al-O distantziarik laburrena den.

d_{AlC} Al^{+3}-tik hiru C mota ezberdinetarainoko distantziak. Laburtuz, Al^{+3}-tik eraztuneko C-etarainoko distantziak, orokorrean, 2 Å ingurura egongo da katioi-π interakzioak dituzten egituretan, eta 5.9-8.7 Å tartean egitura irekietan. Karboniloaren C-arainoko distantzia, 2.6 Å inguruan dago hortz bakarreko egituretan, eta 2.3 Å bi hortzeko egituretan. Albo kate aromatikoko gainontzeko C-etarainoko distantziak nahiko arbitrarioak dira, katearen tolesdura txiki batekin asko aldatzen batira.

Al^{+3}-tik C_1 edo C_α-rainoko distantzia, katioi-π interakzioen presentziaren adierazgarri da. Orokorrean hitz eginda, d_{AlC_1} distantzia 3.5 Å-etik behera dutenak katio-*pi* interakzioak erakutsiko dituzte eta egitura irekietan ordea, distantzia hau 4-8 Å tartean kokatua egongo da.

d_{CC}-k karbonoen arteko distantziarik laburrena adierazten du, eta egindako simulazioetako kalkulu guztietan balio berdin berdina lortu izan da, 1.4 Å hain zuzen. Berdin d_{CH} eta d_{NH} distantziarako, zeinetan kalkulu guztietan zehazki 1.09 eta 1.01 Å-etako balioak lortu diren hurrenez hurren.

C-N distantziak balio ezberdinak aurkezten ditu, zeinetan Phe eta Tyr-en kasuetan, lehenengoa albo katearekin lotzen duen C-arekiko distantzia izango den (1.47 Å inguru), eta gainontzeko balioak, kateko edota eraztunaren gainonzteko C-etarainoko

Phe + Al^{+3} + 4 H_2O								
Ir.	Let.	n	KB	Kodea	ΔE	r_{AlO}	r_{AlN}	r_{AlC_α}
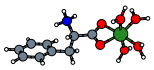	a	6	ZW	G03	0.00	1.90	4.61	6.03
				CPMD	0.00	1.89	4.60	6.00
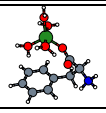	b	5	ZW	G03	3.19	1.79	5.28	4.13
				CPMD	2.55	1.79	5.28	4.11
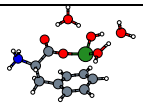	c	4	ZW	G03	8.99	1.78	5.35	3.40
				CPMD	4.43	1.77	5.33	3.38
	d	6	CS	G03	16.67	1.89	2.07	2.99
				CPMD	17.79	1.89	2.07	2.99
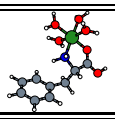	e	6	CS	G03	19.96	1.87	2.02	4.64
				CPMD	20.78	1.86	2.02	4.62
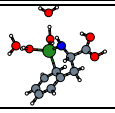	f $*$	4	IZW	G03	37.21	4.32	1.83	2.66
				CPMD	32.45	4.28	1.83	2.65

Table 5.12: *Tetrahidratataturiko Phe-Al^{+3} konplexua.*

distantziak adieraziko dituzten. Trp-aren kasuan ordea, baliorik txikienek eraztunean kokatuta dagoen N-tik eraztuneko C-etarainoko distantziak neurtuko ditu (1.48-1.56 Å tartean).

C-O distantzia mota ezberdinak neurtu izan dira. 1.25 Å-etara dagoen distatzia, hortz bakarreko loturaren kasuan, gertuen dagoen oxigenoarekiko distantziari dagokio. 1.33 Å-tara dagoena, Al^{+3}-a karboxilatoaren oxigeno biei lotuta dagoen kasuko Al-O distantzia bien batez besteko distantzia da.

Bestalde, 2.40 Å aldera, monodentatuan, Al^{+3}-ari loturik ez dagoen bigarren oxigenorako distantzia da.

5.3.2 Wannier Funtzioak

Beste ikerketa batzuen erizpideak jarraituz [62], 2.4.1 atalean aurkeztu diren Wannier Funtzioen kontzeptua erabiliko da.

Tyr + Al^{+3} + 4 H_2O								
Ir.	Let.	n	KB	Kodea	ΔE	r_{AlO}	r_{AlN}	r_{AlC_α}
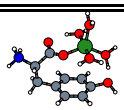	a	5	ZW	G03	0.00	1.81	5.32	4.20
				CPMD	0.00	1.82	5.32	4.20
	b	6	ZW	G03	3.57	1.89	4.60	6.00
				CPMD	0.97	1.88	4.59	5.98
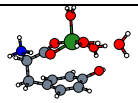	c	5	ZW	G03	8.22	1.90	4.56	4.18
				CPMD	6.08	1.90	4.55	4.16
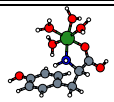	d	6	CS	G03	15.46	1.88	2.03	4.09
				CPMD	14.01	1.88	2.03	4.06
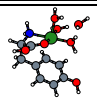	e	5	CS	G03	22.75	1.90	2.07	2.97
				CPMD	19.93	1.90	2.06	2.96
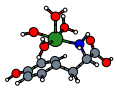	f	6	CS	G03	38.53	3.50	2.05	2.27
				CPMD	36.35	3.52	2.05	2.31

Table 5.13: *Tetrahidrataturiko Tyr-Al^{+3} konplexua.*

Maximoki lokalizaturiko Wannier Funtzioen Zentroen (WFC) azterketa eginez sistemaren egitura elektronikoaren eta lotura kimikoen izaeraren ideia bat har daiteke.

CPMD kodea egitura elektonikoan oinarritzen delez, CPMD bidezko kalkuluetatik zuzenean karga elektronikoaren banaketaren informazio zehaztua eskura dezakegu, esate baterako WFC-ak.

5.9 irudian maximoki lokalizaturiko WFC-ak irudikatu dira. Irudian ikus daitekeenez, lotura kimiko (kobalente) bakoitza kokatzen den puntuan WFC bat dago, eta bestalde ez loturazko elektroi bikoteak dituzten atomoen gainean ere WFC-a adierazten duen puntu beltza ikus daiteke.

Irudi hauen bidez katioi-π interakzioen natura aztertu nahi da, hots, Al^{+3} eta eraztun aromatikoaren arteko interakzioak izaera kobalentea ote duen edo ez, eta irudian ikus daitekeen bezala eraztuna eta aluminioaren artean badago puntu beltz bat, zeinak interakzioaren nolabaiteko izaera kobalentea azpimarratzen duen.

Interakzio honek printzipioz izaera elektrostatiko hutsa izan beharko luke, baina

Trp + Al^{+3} + 4 H_2O								
Ir.	Let.	n	KB	Kodea	ΔE	r_{AlO}	r_{AlN}	r_{AlC_α}
	a	6	ZW	G03	0.00	1.92	4.53	4.48
				CPMD	0.00	1.92	4.53	4.42
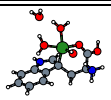	b	5	ZW	G03	0.85	2.02	3.53	2.12
				CPMD	2.09	1.99	3.52	2.13
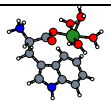	c	5	ZW	G03	1.33	1.86	4.89	3.90
				CPMD	2.41	1.87	4.91	3.93
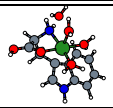	d	6	CS	G03	12.54	1.94	2.04	2.22
				CPMD	14.02	1.93	2.03	2.26

Table 5.14: *Tetrahidrataturiko Trp-Al^{+3} konplexua.*

ur 1	2 ur	3 ur	4 ur
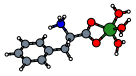	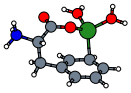	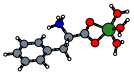	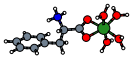

Hidr.	d_{OAl}	d_{AlC}	d_{AlC_1}	d_{CC}	d_{CN}	d_{CH}	d_{CO}	d_{NH}
1× H_2O	1.79-1.87	2.03 2.57-2.65 3.05	2.60	1.40	1.47-1.57 2.40-2.50 3.04-3.12	1.09	1.25-1.32	1.01
2× H_2O	1,87	2.10-2.17 2.73 3.50-3.80	2.97	1.40	1.48 3.66 5.30-6.50	1.09	1.25-1.32	1.01
3× H_2O	1.87	2.26 3.74 4.52	5.93	1.40	1.48-1.56 2.49-2.57 2.80	1.09	1.32	1.01
4× H_2O	1.95	2.26-2.35 3.74-3.82 4.60-4.70	6.01	1.40	1.48-1.56 2.49-2.57 2.80	1.09	1.32	1.01

Table 5.15: *Phe-aren energia minimodun egituren simulazioetatik RDF-en bidez kalkulaturiko erreferentzizko distantziak Å-etan.*

Al^{+3}-aren kargak eraztun aromatikoan sortzen duen kargaren birbanaketak eraztun aromatikoaren gainean dentsitate altuko hodei elektroniko bat kokatzen du zeinak

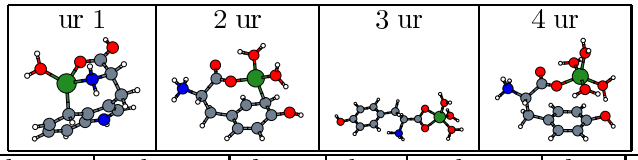

Hidr.	d_{OAl}	d_{AlC}	d_{AlC_1}	d_{CC}	d_{CN}	d_{CH}	d_{CO}	d_{NH}
1× H_2O	1.79-1.87	2.03 2.47-2.57 3.74	2.05	1.40	1.48-1.57 2.40-2.50 2.87-2.96	1.09	1.25-1.32	1.01
2× H_2O	1,87-1.87	2.10-2.17 2.73 3.83	3.06	1.40	1.48-1.57 2.49-2.57 3.83-3.89	1.09	1.25-1.32	1.01
3× H_2O	1.87	2.26 3.74	5.94	1.40	1.48-1.56 2.49-2.57 2.80.2.90	1.09	1.32	1.01
4× H_2O	1.95	2.26-2.34 3.74-3.82	5.97	1.40	1.48-1.56 2.49-2.57 2.80-2.90	1.09	1.32	1.01

Table 5.16: *Tyr-aren energia minimodun egituren simulazioetatik RDF-en bidez kalkulaturiko erreferentzizko distantziak Å-etan.*

Al^{+3}-rekin kobalentetzat har zitekeen interakzio bat sortzen duen.

Jokaera orokor bat nabaritu daiteke simulazio guztietan. Esan bezala, Al^{+3} eta eraztun aromatikoaren artean kokatuta dagoen WFC-ak beraien arteko interakzioaren natura kobalentea adierazten digu. Aluminioaz aparte, ur molekulen kasuan O-H loturentzako WFC bana dago eta beste bi oxigeno bakoitzean gainezarrita, berauen bikote bakartiengatik. Bestalde C-C, C-H, C-N eta C-O loturen artean ere WFC-ak ikus daitezke.

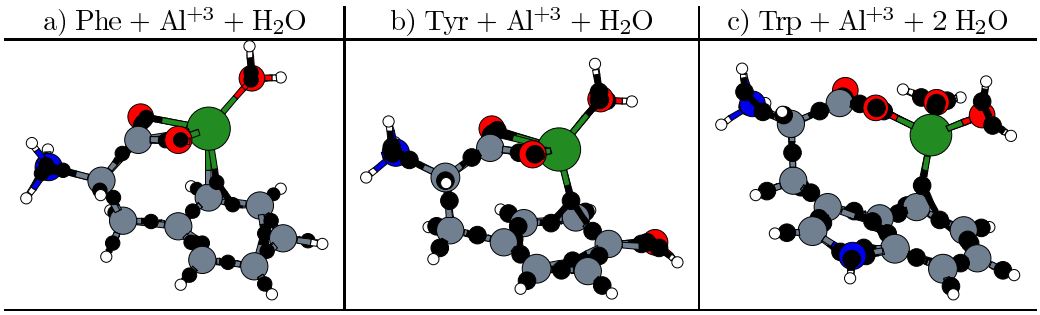

Figure 5.9: *Lagin ezberdinentzako maximoki lokalizaturiko WFC-ak esfera beltzez adieraziak.*

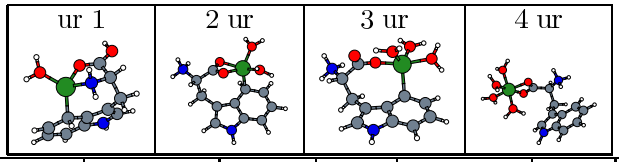

Hidr.	d_{OAl}	d_{AlC}	d_{AlC_1}	d_{CC}	d_{CN}	d_{CH}	d_{CO}	d_{NH}
1× H_2O	1.86	2.03 2.47-2.57 3.74	5.97	1.40	1.32-1.41 2.26-2.50 3.23 3.66-3.75	1.09	1.25-1.33	1.01
2× H_2O	1.86-1.95	2.10-2.17 2.73 3.83	3.59	1.40	1.32-1.41 2.49-2.50 3.66-3.75	1.09	1.25-1.33	1.01
3× H_2O	1.86-195	2.26 3.74	3.71	1.40	1.32-1.41 2.49-2.50 3.66.2.75	1.09	1.25-1.33	1.01
4× H_2O	1.72-1.95	2.26-2.34 3.74-3.82	5.47	1.40	1.32-1.48 2.35-2.50 3.66-2.75	1.09	1.25-1.33	1.01

Table 5.17: *trp-aren energia minimodun egituren simulazioetatik RDF-en bidez kalkulaturiko erreferentzizko distantziak Å-etan.*

5.4 Ondorioak

- Amino azido aromatiko hutsek CS karga banaketa dute argi eta garbi, eta albo kate aromatikoaren orientazioak ez du eragin nabarmenik energia osoarengan.
- Ez mikrosolbataturiko klusterretan, karga banaketa ZW da era argi batean eta Al^{+3}-a eraztun aromatikoa, eta karboxilatoko oxigeno bat edo biekin koordinatuta dago (bat Phe-aren eta bi Tyr eta Trp-en kasuetan).
- Monohidrataturiko klusterren energia minimoeneko egiturek CS karga banaketa daukate eta Al^{+3}-a eraztun aromatikoa, (karboxilatoko) O-a eta N-arekin koordinatuta daude.
- Dihidrataturiko klusterren energia minimoeneko egiturak ZW karga banaketa daukate, eta Al^{+3}-a eraztuna eta karboxilatoko bat (trp) edo bi (Phe/Tyr) oxigenorekin koordinaturik dago.
- Katioi-π interakzioak hiru ur molekula mikrosolbatatzaile baino gutxiago dituzten kasutan baino ez dira garrantzitsuak. Mikrohidrataziozko ur molekula kopuru handiagoetarako, katioi-π interakzioak eta interakzio elektrostatikoen

arteko lehiak Al^{+3}-ak eraztun aromatikoaren ordez ligandotzat urak aukeratzea eragiten du.

- IZW-zko karga banaketa Phe-an baino ez da aurkitu. Energia aldetik, orokorrean minimoa baino energia nahiko altuagoa daukate ($\approx$ 20-30 kcal/mol).
- Ez mikrosolbataturiko egoeran egindako AAA-Al^{+3} egituren kalkuluetan, Al^{+3}-aren partetik koordinazio zenbakia ahalik eta altuena, hots, 3 izan zitekeela espero zitekeen, baina energia minimodun egituren kasuan, Phe-aren **a** egitura biko kooordinazio baino ez izanik, bere antzekoak den **b** egiturak baino energia pixka bat baxuagoak erakusten du G03-zko kasuan. CPMD-rekin ordea, koordinazioa 3 duen egitura bat agertzen da egonkorrenatzat.
- Mikrosolbataturiko AAA-Al^{+3} klusterretan, koordinazio zenbaki altuagoa faboratzen da mikrosolbataziozko ur baten kasuan, hots, tetrakoordinatuak nagusitzen dira. Dihidrataturiko egituretan, Trp-aren kasuan bezala pentakoordinazioa lortzeko aukera izan arren, Phe eta Tyr-aren kasuetan karboniloaren oxigenoetako bat askatzeko joera du. Trihidratatuetan, eraztun aromatikoa ligandotzat izateak suposatzen duen eragozpen esterikoa dela eta, pentakoordinazioa nagusitzen da. Tetrahidratazioan, 5 eta 6 koordinazioaren arteko lehia bat agertzen da, karboniloaren oxigeno bat edo biak lotzen direneko kasuen artean.
- Lotura distantziak 0.01 Å inguru laburrago agertzen dira CPMD bidez egindako kalkuluetan Gaussian 03-ren bidez egindakoetan baino.

6. Kapitulua

AAA-Al^{+3} konplexuak disoluzio ingurunean

Aurreko kapituluan egitura mikrosolbatatuekin egindako kalkuluak, isomeroen arteko propietateak konparatzeko helburuarekin egin dira.

Hurrengo kapituluan, AAA-Al^{+3} konplexuen disoluzioko jokaera simulatuko da, eta disoluzioa nolabait kuantizatzearren 50 ur (disolbatzaile) molekulez inguratutako konplexuak sortu dira, beste antzerako ikerketa batzuen adibidea jarraituz [62].

Dinamika molekularrezko simulazioak, Car-Parrinello metodoan [43] oinarritutako CPMD kodearen [31] bidez egin dira, guztira 100 ps-tik gorako trajektoria bana lortu arte.

Sistemaren tenperatura osoa, 300 K-etan finkatu da, Nose[37]-Hoover[38] termostatoa [39] erabiliaz.

Atomoak DFT-ren bidez deskribatuak izan dira, PBE funtzionalaren [29] bidez. Guneko elektroiak, CPMD-rako bereziki [68] garaturiko [33] Vanderbilt pseudopotentzial ultraleunen [32] bidez ordezkatuak izan direlarik. Uhin lauen mozketa erizpidea 30 Ry.-tan zehaztu da, μ masa elektroniko irudikaria 900 a.m.u. eta urrats denbora 7 u.a.-koa izanik.

Simulazio gelaxkaren tamaina, dentsitate osoa ur likidoarena (hots 1 gr/zm^3) izateko kalkulatua izan da, eta gure kasuetan, gelaxka kubikoa izanik, sare parametroa 12.18 Å ingurukoa da, amino azidoek atomo ezberdinak dituztela kontutan izanik.

Disoluziozko simulazio hauen atomo kopuru erlatiboki handia dela (≈ 175) kontutan izanda, eta bestalde simulazioak 100 ps-tik gora simulatu izanak, simulazio benetan garestiak bihurtzen ditu, eta zientzilari konputazionalon CPU kopuru txikiegia izatearen betiko arazoa dela eta, ezin izan dira amino azido bakoitzarentzako egitura eta koordinazio ezberdinak aztertu, ur disoluziozko Al^{+3}-aren kasuan egin zen bezala.

Ideia bat egitearren, simulazio hauetako bakoitzak 800 CPU ordu baino gehiago kontsumitu ditu, EHU-ren "Arina" [83] konputaziozko azpiegituran, lan bakoitzaren batez besteko kontsumoa 60-100 CPU ordu tartean egonik. Prezio hain garesti honek, egitura optimoenak eta hauen kopuru minimoa aukeratzeko erantzunkizuna ekartzen du.

Kalkuluak gehien bat Arinan egin diren arren, tesi honetan aurkezten diren

emaitzetako batzu i2Basque [84] eta BSC-ko Mare Nostrum-eko [85] baliabideetan kalkulatuak izan dira ere.

6.1 RDF-ak eta lotura distantziak

Simulazio hauetarako, Al^{+3}-aren inguruko koordinazio geruzetan agertuko diren elementuak karboxilaren oxigenoa(k) eta disolbatzailearen urak izango dira, Al-N elkarrekintzarik ez daudelarik.

Phe-aren simulazioa tetrakoordinaturik hasi zen, dihidrataturik, hortz bakarreko konformazioa (bi ur, eraztun aromatiko eta karboxilatoko oxigenoa), eta simulazioak trikoordinaziorantz jotzen du, eraztun aromatikoarekiko elkarrekintzak galtzen direlarik. Phe-ak hain koordinazio baxua izatearen erantzuna, disolbatzailearen eraginean egon daiteke, izan ere, disolbatzaileko ur molekulek Al^{+3}-aren karga sakabanatzen laguntzen dute, eta trikoordinazio hori, nahiz ta printzipioz desfaboratua egon, nolabait egonkortua agertzen da. Honek ez du esan nahi Phe-aren konplexuaren disoluzio egoerako egiturarik egonkorrena trikoodinatua denik, bakarrik existitzen dela eta denbora tarte nahiko luze batez ($\approx$ 100 ps) egonkor mantendu dela, baina aurretik ikusitakoaren arabera [47][48], koordinazioaren ikuspuntutik aztertuta, bigarren geruzako ur molekuletako batek bigarren geruzatik lehenengorako langa zeharkatuz gero egitura egonkorrago baten aurrean geundeke.

Dena den, nahiz eta Al^{+3}-ak Phe-aren kasuan hiru ligando baino ez izan, karga aldetik asetuta dago, -OH bien eta carboxilatoaren karga negatiboek Al^{+3}-arena konpentsatzen baitute.

Ondorioz, Phe-aren kasuan ikusi den bezala, disoluzio ingurunean, katioiaren karga errazago sakabanatzen (disipatzen) da disolbatzailearen molekulei esker, eta ondorioz katioi-π interakzioek garrantzia galtzen dute Al-ur interakzioen aldean.

Tyr eta Trp-aren kasuan, simulazioak pentakoordinaturiko eta hortz bakarreko egitura tetrahidratatuetatik abiatu ziren, eta 100 ps baino gehiagoz egonkor mantendu dira.

6.2 irudiko grafikak hiru sistemen g_{OAl}-a irudikatzen du. Tetrakoordinaturiko Phe-arentzako lehenengo tontorra 1.79-1.90 Å aldera agertzen den bitartean, Tyr eta Trp-en sistemei dagozkienak 1.9-2.0 Å-etara agertzen dira. Bigarren solbatazio geruzari dagokion banda, 4.0-4.1 Å-etara agertzen da Phe-aren kasuan, eta 4.0 Å-etara Tyr eta Trp-arentzat.

RDF-en integralek, Phe-arentzako 3-ko balioa hartzen dute lehen geruzaren gainean, hau da, Al^{+3}-ak batez beste 3 ligando dituela, hots, ur biak eta karboxilatoaren oxigenoa. Phe-aren bigarren solbatazio geruzaren oxigeno kopurua 8-10 bitartean dago. Tyr eta Trp-arentzat lehenengo koordinazio geruzako oxigeno (edo ligando) kopurua berbera da, hau da, pentakoordinatua. Bigarren solbatazio geruzan ordea, Tyr-aren

kasuan 12 ur molekula zenba daitezkeen bitartean, Trp-an 8 ur baino ez daude batez beste.

g_{HAl}en irudikapenak erakusten duen itxura, g_{OAl}-renaren antzekoa da. Kasu honetan, integralek 8 hidrogeno erakusten dituzte lehen solbatazio geruzan Tyr eta Trp-arentzako eta 4-6 Phe-arentzako. Berriz ere, Phe-aren lehenengo tontorra distantzia laburragoetara agertzen da 2.50-2.55 Å-etara, koordinazio txikiagoa dela eta. Tyr eta Trp-ari dagozkien tontorrak distantzia pixka bat luzeagotara kokatura daude, 2.61-2.70 Å-etara hain zuzen. Trp-aren tontorrak orain alaka bat erakusten du, zeinak -**O**H-en presentzia adierazten du.

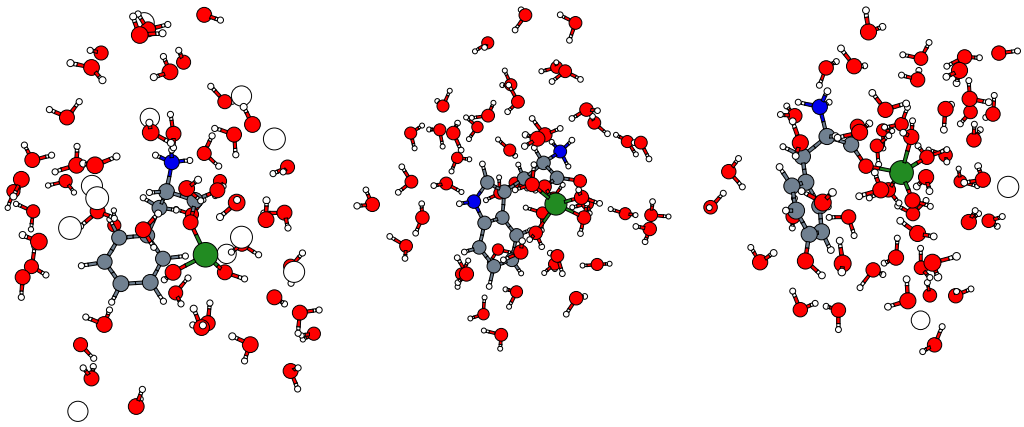

Figure 6.1: *phe, Tyr eta Trp-aren Al^{+3}-rekin sortzen duten konplexuen disoluzioaren (50 H_2O) zenbait irudi.*

RDF datu hauek 4 kapituluko Al^{+3} disoluzioetakoekin konparatuz, Al^{+3}-aren solbatazio geruzen jokaera ezberdina nabaritu daiteke.

6.4 **a)** irudiak erakusten duelez, koordinazio zenbaki berdinetan, O-Al distantzia laburragoa agertzen da amino azidoen disoluzioarekin egindako RDF-etan aluminiozko disoluzioarekin egindakoetan baino ($\approx$ -0.1 Å Al^{+3} disoluzioan). Antzeko jokaera bat ikus daiteke H-Al distantziaren kasuan (ikus 6.4 **b)** irudia).

Al^{+3}-ak amino azidoen presentzian koordinazio geruzak distantzia handiagoetara erakustearen arrazoietako bat, amino azidoak berak sortzen duen aldarapen esterikoa da.

g_{HO} eta g_{OO}-ak disoluziorako espero genezakeen jokaera daukate. g_{HO}-ak guztiz gainezarriak daude hiru kasuetarako, 1.02 Å-etara H-O lotura distatziari dagokion tontor bat adierazten dutelarik. Tontor bakar eta argi bat dago, albo tontorrik gabe, beraz amino azido hauen disoluzietan ez da hidronioen presentziarik somatuko, edo beste era batera esanda, ez dago uraren disoziaziorik.

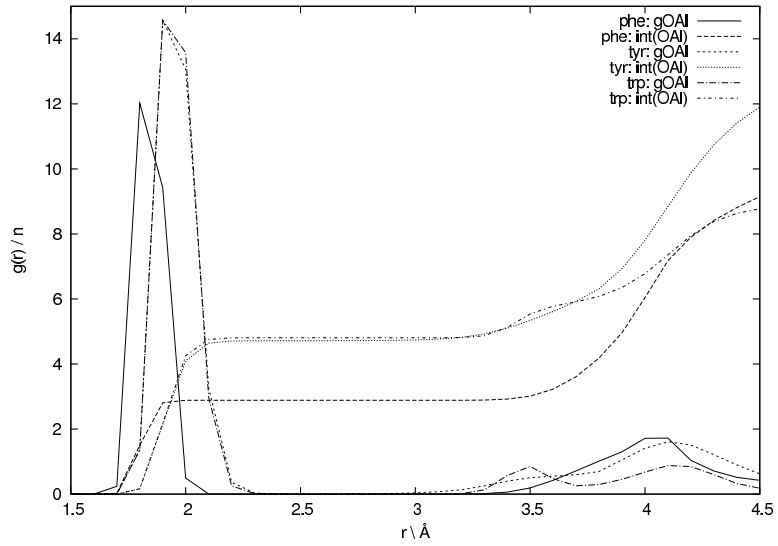

Figure 6.2: *phe, Tyr eta Trp-aren disoluzioen* g_{OAl}.

g_{OO}-en kasuan ere hiru funtzioak nolabait gainezarriak daude. Lehen tontorra 2.8 Å-tara agertzen da, zeina disoluzioko ur molekulen oxigenoei dagokien.

Bestalde, hiru sistemen g_{OO}-ak albo tontor txiki bat erakusten du 2.3 (phe) eta 2.4 (tyr eta Trp) Å-etara, karboxilatoaren oxigeno biei dagokiena.

6.2 Energia Askeak

6.2.1 Al^{+3}-ren lotura energia

MD simulazioetatik energia askeak estimatzeko metodoa 2.4.3 atalean aurkeztua izan da.

Atal honetako energia askeak, guztiz disolbaturiko sistemetan Al^{+3} katioitik C_1 (edo C_α) karbonora neurtuz estimatu dira.

Distantzia horiek trajektoria osotik erauztearen lana, hasiera batean Kari Laasonen profesorearen taldeak garatutako koden baten bertsio bermoldatu baten bidez egin izan da, eta 6.7, 6.8 and 6.9 irudiak idazleak eginiko kodeen bidez egin izan dira.

6.7 **a)** irudiak Al-C_1 distantziaren populazio histograma eta beroni dagokion Helmholtzen energia askearen profila erakusten ditu. Bi zonalde ezberdin nabarmendu daitezke. Ezkerrerago dagoenak, Al^{+3}-ak eraztun aromatikoarekin katioi-π

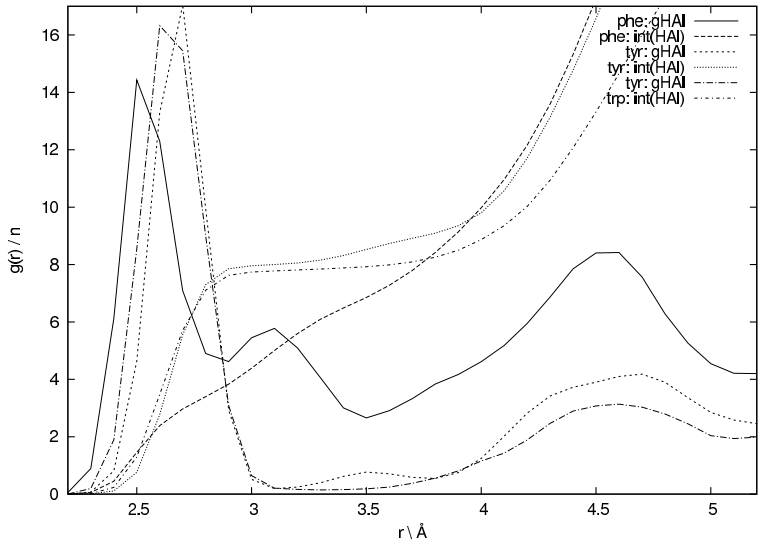

Figure 6.3: *phe, Tyr eta Trp-aren disoluzioen g_{HAl}.*

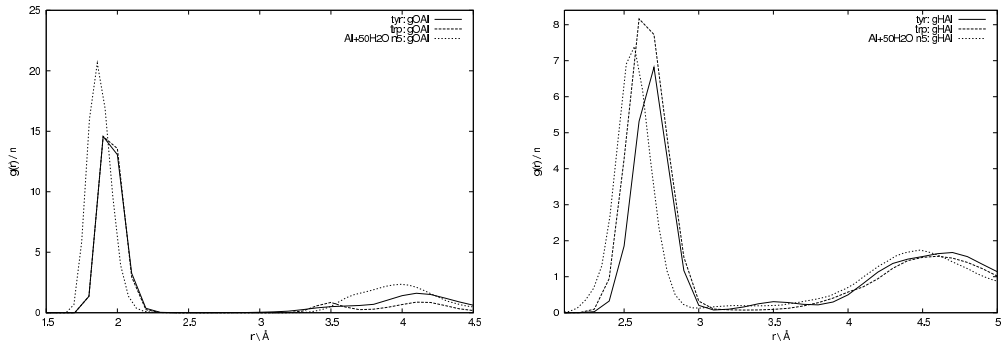

a)g_{OAl} **b)** g_{HAl}

Figure 6.4: *Pentakoordinaturiko Tyr-Al^{+3}, Trp-Al^{+3} eta Al^{+3} hutsaren disoluziotik ateratako g_{OAl} eta g_{HAl}-en konparaketa.*

interakzioak izaten ari dituen hasierako zatiari dagokio, eta eskuinerago dagoenak ordea, egitura (albo kate aromatikoa) irekita dagoen denborari dagokio. Era honetan bai egitura ireki zein itxiarentzatko lotura energiak zein itxitik irekirako (edo alderantziz) trantsizio energiak kalkula daitezke.

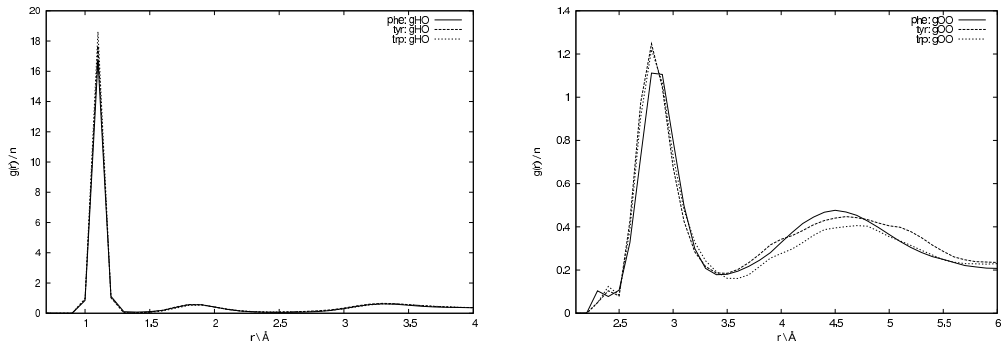

a)g_{HG} b) g_{OO}

Figure 6.5: *phe, Tyr eta Trp konplexuen disoluzioaren g_{HO} eta g_{OO}.*

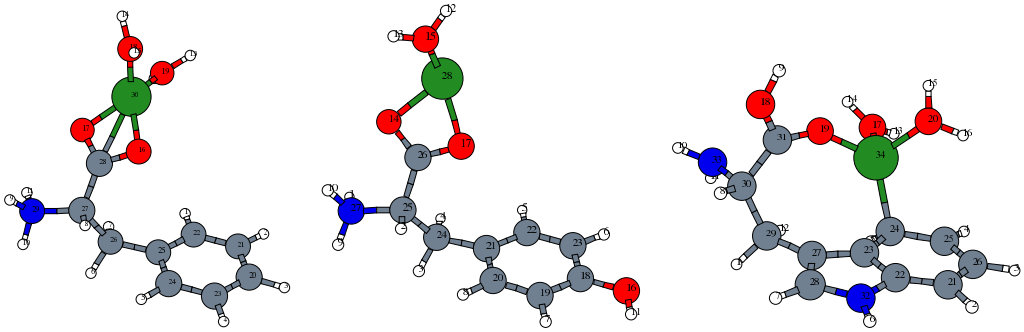

a) Phe C_1=25 b) Tyr C_1=21 c) Trp C_1=27

Figure 6.6: *C_1 karbonoak erakusten dituen irudia.*

6.1 taulan adierazten diren datuen arabera, tetra-/trikoordinaturiko Phe-aren egituratik Al^{+3}-a erauzteko energia Tyr eta Trp-ren kasuetan baino nabarmenki baxu-

	Nondik	Nora	ΔE	Errorea
Al-Phe	(katioi-π)	∞	4.05	$\pm$ 0.55
	(Irekita)	∞	3.05	$\pm$ 0.37
	(katioi-π)	Irekia	2.05	$\pm$ 0.25
Al-Tyr	(Irekia)	∞	9.44	$\pm$ 0.99
Al-Trp	(Irekia)	∞	22.7	$\pm$ 1.99

Table 6.1: *Disoluzio inguruneko AAA-Al^{+3} konplexuen lotura energia ezberdinak Kcal/-mol unitateetan.*

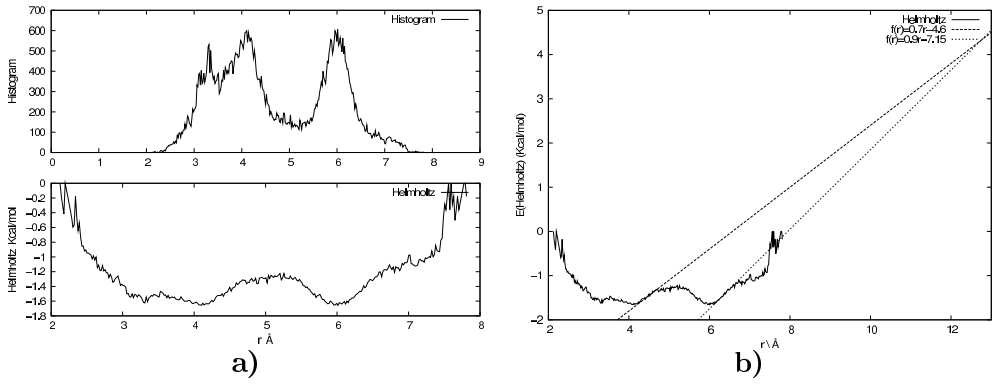

Figure 6.7: **a)** *Populazio histograma eta beroni dagokion Helmholtz energia askearen profila Phe-Al^{+3} kasurako, eta* **b)** *Energia askeko kurbaren tangentearen oreka distantzia eta infiniturainoko extrapolazioa.*

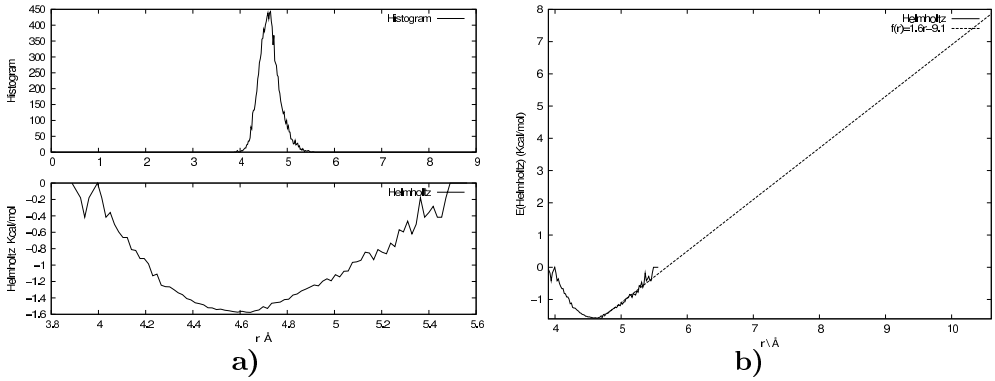

Figure 6.8: **a)** *Populazio histograma eta beroni dagokion Helmholtz energia askearen profila Tyr-Al^{+3} kasurako, eta* **b)** *Energia askeko kurbaren tangentearen oreka distantzia eta infiniturainoko extrapolazioa.*

agoa da. Phe-ak katioi-π lotura gainditzeko behar duen energia, ia Al-eraztun lotura energiaren erdia da.

Tyr eta Trp-en kasuetako AAA-Al^{+3} lotura energiak, irekitako egiturarentzako (katioi-π interakzio gabearentzako) kalkulatu dira soilik, eta emaitzen arabera, lotura energia Phe-arekiko bikoiztu egiten da Tyr-aren kasurako, eta bost aldiz handiagoa Trp-aren kasurako. Al^{+3}-ak Phe-arekin duen lotura Tyr-arekin duena baino ahulagoa da, Tyr-ak -OH taldearen bidez eraztunean karga negatibo gehiago sortzen

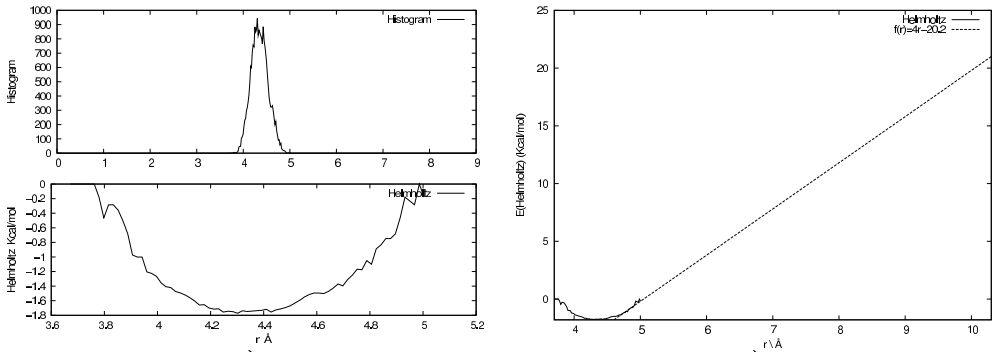

Figure 6.9: **a)** *Populazio histograma eta beroni dagokion Helmholtz energia askearen profila Trp-Al^{+3} kasurako, eta* **b)** *Energia askeko kurbaren tangentearen oreka distantzia eta infiniturainoko extrapolazioa.*

duelako eta honela Al^{+3}-a gehiago erakartzen duelako. Trp-ak eraztun bikoitza du eta eraztunetako batean nitrogeno bat, eta horren eraginez katioi-π interakzioak era esanguratsu batean indartzen direla ikusten da.

6.2.2 Deshidrataziozko energia askeak

Ur disoluziozko Al^{+3} simulazioetatik deshidratazio energia estimatu izan zen era berean, konplexu hauetan ere deshidratazio energia kalkula daiteke.

Pentakoordinaturiko Tyr eta Trp-ren egituretatik Al^{+3}-tik hurrutien dagoen lehenengo solbatazio geruzako ur molekularaino distantzia erizpidetzat hartuz, partiketa funtzioa eta Helmholtzen energia askeko kurbak kalkulatu dira (ikus 6.10 irudia) eta emaitz bezala 6.2 taulan ikus daitezkeen balioak kalkulatuak izan dira.

Datuak aztertzeko orduan, Al^{+3}-aren disoluzioarekin konparatuz gero, deshidrataziozko energia askoz altuagoen aurrean aurkitzen garela ikus daiteke. Hain zuzen, Al^{+3}-aren ligandoetako bat amino azidoetako karboxilato taldea izanik, horren ordez ur bat egongo litzatekeeneko kasuan baino energia bikoitza eta hirukoitzaren arteko balioen aurrean aurkitzen gara.

Bestalde, 6.4 irudian ikus zitekeen bezala, Al-O distantziak laburragoak dira Al^{+3} disoluzioaren kasurako, baina 6.10 irudietako kurbek erakusten dutenaren arabera, lehenengo solbatazio geruzako Al-O distantziarik handieneko urek, itxura trinkoagoa dute eta distantzia pixka bat txikiagoaetara daude.

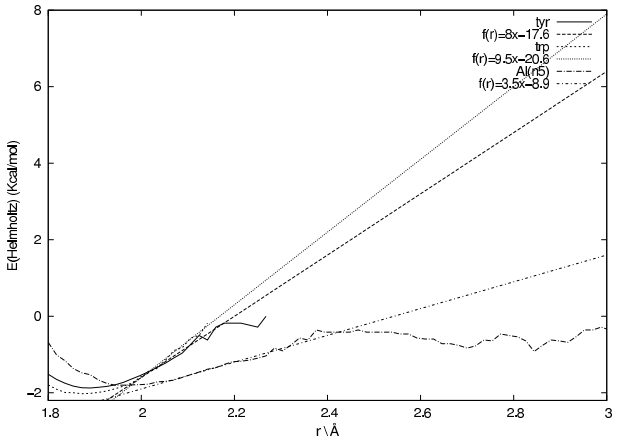

Figure 6.10: *Tyr eta Trp aminoazidoekin lotutrik eta ur disoluzioan dauden Al^{+3} katioientzako deshidratazio energiak estimatzeko Helmholtz energia askearen kurbaren extrapolazioa.*

Nondik	Nora	ΔE
Tyr-Al^{+3}-$(H_2O)_4$	Tyr-Al^{+3}-$(H_2O)_3$ + H_2O	47.5
Trp-Al^{+3}-$(H_2O)_4$	Trp-Al^{+3}-$(H_2O)_3$ + H_2O	56.1
Al^{+3}-$(H_2O)_5$	Tyr-Al^{+3}-$(H_2O)_4$ + H_2O	19.0

Table 6.2: *Pentakoordinaturiko Al^{+3} katioia ligando ezberdinak duelarik, deshidratatzeko beharrezko energiaren estimazioa kcal/mol-etan. Kalkuluak % 10 inguruko errorea du.*

6.3 Ondorioak

- Katioi-π interakzioak desfaboratuta daude disoluzio ingurunean.
- Egitura pentakoordinatuak gutxienez 100 ps-z mantentzen dira.
- Posiblea da trikoordinaturiko Al^{+3}-zko egitura bat -OH anioien presentziaren bidez gutxienez hain bat hamarka ps-z egonkor mantentzea.
- Al^{+3}-AAA konplexuen disoluzioetako Al^{+3}-arekiko deshidratazio energia, Al^{+3}-zko disoluzioaren kasuan baino bi edo hiru aldiz handiagoa izan daiteke.
- Al^{+3}-aren Trp-arekiko lotura energia, Tyr-arekiko duenaren bikoitza inguru da, eta Phe-arekiko duenaren laukoitza.

7. Kapitulua

Eztabaida

Tesi honen lehenengo hiru kapituluetan, Al eta AAA-en gairi sarrera bat eman zaio, erabilia izan den tresneria teorikoari gainbegirada bat eman eta gaiaren inguruko ikerkuntzaren textuingurua azaldu da.

4. kapituluan Al^{+3}-aren disoluziozko jokaera aztertu ondoren, tetra-, penta- edo hexakoordinazioa izan dezakeela berrestu da, baina hala ere, egitura pentakoordinatuak hexakoordinatura jauzi egiteak eta ondoren egindako ur deshidrataziozko energien kalkuluak adierazten duten bezala, egitura pentakoordinatua ez da tetra- eta hexakoordinatua bezain egonkorra.

Hau kontutan izanik, AAA-Al^{+3}-zko disoluzioan, Al^{+3}-aren inguruan 4-6 ligando egongo direla aurresan genezake.

5. kapituluan aurkeztu den egituren azterketatik mikrosolbatauriko AAA-Al^{+3} egituretan Al^{+3}-aren koordinazio zenbakia 4 eta 6 tartean kokoatuta dago. Mono- eta dihidratauriko egituretan orokorrean Al^{+3}-ak bere koordinazioa igotzen saiatzen du, baina tri- eta tetrahidratauriko egituretan nolabaiteko oreka lortzen dela nabaritu daiteke, zeinetan ligandoen aldarapen esterikoak direla eta, katioi-π interakzioak eragozten diren.

Hala ere, 6. kapituluan ikusi den bezala, nahiz eta koordinazioa orokorrean 4 eta 6 bitartean egongo den, posiblea da ur kopuru handia eskuragarri izatea eta ala ere Al^{+3}-ak trikoordinazioan nolabaiteko egonkorketa bat aurkitzea.

Aluminioaren AAA-enganako eragina aztertzerako orduan, amino azidoen hutseango eta ur disoluzioko egiturak beti CS karga banaketa dutela kontutan izanda, Al^{+3}-ak sortaraziko lukeen aldaketa nabarmenena ZW karga banaketa sortaraztea litzateke.

Egindako kalkuluetan, amino azido hutsek CS karga banaketa erakutsi dute argi eta garbi, AAA-Al^{+3} klusterrak ordea ZW, eta harrigarria izan arren monohidratauriko AAA-Al^{+3} klusterretan, berriz ere CS karga banaketa ikusi da. Gainontzeko mikrohidratazio egoeretan eta disoluzioan karga banaketa ZW izan da era argi batean.

Honen arabera, ur disoluzioan legoken proteina batetara Al^{+3} katioi bat gerturatuz gero, aldiunero izango lituzkeen ur molekula kopuruaren arabera karga banaketa bat edo bestea izan lezake. Alde batetik, ur disoluzioan ez litzateke bat ere arrunta

Al^{+3}-a ur molekula bakar bati lotuta egotea, baina bestelde, proteinak dauden zenbait guneetan dagoen ur molekula kopuru eskasa dela eta ez litzateke horren zaila mikrosolbataziozko ur molekula bakarra izatea.

Aluminioaren amino azidoen karga banaketaren gaineko eragina beraz, Al^{+3}-ari loturiko ur molekula kopuruarekiko menpekotasuna du eta amino azido horiek kokaturik leudekeen ingurune proteinikoaren ur molekulen urritasunak monohidratazioa posible egingo lukeelez, printzipioz jatorrizko CS egitura mantentzea posible izango litzateke. Baina bestalde, askoz probableagoa litzateke amino azidoa beste hidratazio egoera batetan aurkitzea, zeinarekin ZW karga banaketa egongo litzateke, horrek suposatuko lukeen propietate aldaketarekin eta proteina osoaren gainean sortuko lukeen eraginarekin.

Hurrengo erronka, CS egituren ordez ZW-ak jartzeak sortuko lukeen proteina mailako eragina izango litzateke, hau da, aluminioak amino azidoetan eragindako karga banaketak proteina osoan sortaraziko lukeen aldaketa, eta honek izango lituzkeen ondorio biologikoak. Adibide bezala, bereziki interesgarria litzateke, Alzheimerraren gaixotasunaren atzean dagoen Amiloid-β proteina simulatu ahal izatea, baina proteinaren atomo kopuru handia dela eta, beharrezkoa litzateke simulazio klasiko edo semienpirikoetara jotzea, zeinak Al^{+3}-aren interakzioak deskribatzen dituen egitura elektronikoa arbuiatzen duten, edo bestela QM/MM metodoak.

Zehaztasuna galdu gabe, sistema handiago bat har zitekeen ere, amino azidoen ordez proteina zati edo peptido oso bat simulatuz. Sistema honen simulazio labur baten kostu konputazionala, 500 atomo inguruko peptidoa harturik milaka ordutakoa izango litzateke CPMD bezalako kode bat erabiliz. Zorionez, honelako simulazio bat, gaur egungo azpiegitura superkonputazional batean, milla bat prosezagailu erabilita, egun gutxitan burutu zitekeen.

Bibliografia

[1] Txurruka, J. M. *Eboluzioaren Inguruan.* EHU-ko argitarapen zerbitzua, 1986.

[2] Rengel, Z. Aluminum cycling in the soil-plant-human continuum. *BioMetals* **17** (2004), 669–689.

[3] Holm, R. H., Kennepohi, P., and Solomon, E. I. Structural and Functional Aspects of Metal Sites in Biology. *Chem. Rev.* **96** (1996), 2239–2314.

[4] Williams, R. What is wrong with aluminium? The J.D. Birchall memorial lecture. *J. Inorg. Biochem.* **76** (1999), 81–88.

[5] Rezabal, E., Mercero, J. M., Lopez, X., and Ugalde, J. M. A study of the coordination shell of aluminium(III) and magnesium(II) in model protein environments: Thermodynamics of the complex formation and metal exchange reactions. *Inorg. Biochem.* **100** (2006), 374–384.

[6] Elixabete Rezabal, X. L., Jose M. Mercero and Ugalde, J. M. Protein Side Chains Facilitate Mg/Al Exchange in Model Protein Binding Sites. *Chem. Phys. Chem.* **8** (2007), 2119–1200.

[7] Alfredo Sanz-Medel, R. M., Ana B. Soldado Cabezuelo and Polak, T. B. The chemical speciation of aluminium in human serum. *Coord. Chem. Rev.* **228** (2002), 373–383.

[8] Nagaoka, M. H. and Maitani, T. Binding affinity of aluminium to human serum transferrin and effects of carbohydrate chain modification as studied by HPLC/high-resolution ICP-MS. *J Inorg Biochem* **99** (2005), 1887–1894.

[9] Harris, W. R. and Messori, L. A comparative study of aluminum(III), gallium(III), indium(III), and thallium(III) binding to human serum trasferrin. *Coord. Chem. Rev.* **228** (2002), 237–262.

[10] Harris, W. R. and Sheldon, J. Equilibrium Constants for the Binding of Aluminum to Human Serum Transferrin. *J Inorg Chem* **29** (1990), 119–122.

[11] Paik, S. R., Lee, J.-H., Kim, D.-H., Chang, C.-S., and Kim, J. Aluminum-Induced Structural Alterations of the Precursor of the Non-Aβ Component of Alzheimer's Disease Amyloid. *Archives of Biochemistry and Biophysics* **344** (1997), 325–334.

[12] Kawahara, M. Effects of aluminum on the nervous system and its possible link with neurodegenerative diseases. *Journal of Alzheimer's Disease* **8** (2005), 171–181.

[13] Klatzo, I., Wisniewski, H., and Streicher, E. Experimental production of neurofibrillary degeneration I. Light microscopic observation. *J. Neuropathol. Exp. Neurol.* **24** (1965), 187–199.

[14] Miura, T., Suzuki, K., Kohata, N., and Takeuchi, H. Metal Binding Modes of Alzheimer's Amyloid β-Peptide in Insoluble Aggregates and Soluble Complexes. *Biochemistry* **39** (2000), 7024–7031.

[15] Ricchelli, F., Drago, D., Filippi, B., Tognon, G., and Zatta, P. Aluminum-triggered structural modifications and aggregation of β-amyloids. *Cell. Mol. Life. Sci.* **62** (2005), 1724–1733.

[16] Banks, W. A., Niehoff, M. L., Drago, D., and Zatta, P. Aluminum complexing enhances amyloid β protein penetration of blood-brain barrier. *Brain Research* **1116** (2006), 215–221.

[17] Exley, C. *Aluminium and Alzheimers's dissease: The science that describes the link.* Elsevier, 2001.

[18] Jansson, E. T. Aluminum exposure and Alzheimer's dissease. *Journal of Alzheimer's Disease* **3** (2001), 541–549.

[19] Rowatt, E., Sorensen, E. S., Triffit, J., Viess, A., and Williams, R. J. P. An Examination of the Binding of Aluminum to Protein and Mineral Components of Bone and Teeth. *J. Inorg. Biochem.* **68** (1997), 235–238.

[20] Haug, A. and Vitorello, V. Aluminium coordination to calmodulin: thermodynamic and kinetic aspects. *Coord. Chem. Rev.* **149** (1996), 113–124.

[21] Aquino, A. J. A., Tunega, D., Haberhauer, G., Gerzabek, M. H., and Lischka, H. A density-functional investigation of aluminium(III)-citrate complexes. *PCCP* **3** (2001), 1979–1985.

[22] deÑoronha, A. L. O., aes, L. G., and Duarte, H. A. Structure and Thermodynamics Analysis of the First Mononuclear Aqueous Aluminum Citrate Complex Using DFT Calculations. *J. Chem. Theor. Comp.* **3** (2007), 930–937.

[23] Rubini, P., Lakatos, A., Champmartin, D., and Kiss, T. Speciation and structural aspects of interactions of Al(III) with small biomolecules. *Coord. Chem. Rev.* **228** (2002), 137–152.

[24] Ma, J. C. and Dougherty, D. A. The Cation-π Interaction. *Chem. Rev.* **97** (1997), 1303–1324.

[25] Dougherty, D. A. Cation-π Interactions in Chemistry and Biology: A New View of Benzene, Phe, Tyr, and Trp. *Science* **271** (1996), 163–168.

[26] Allen, M. P. *Introduction to Molecular Dynamics Simulation*, vol. 23 of *NIC*. John von Neumann Institute for Computing, Jü, 2004.

[27] Hohenberg, P. and Kohn, W. Inhomogeneous Electron Gas. *Physical Review* **136** (1964), B864–B871.

[28] W.Kohn and Sham, J. Self-Consistent Equations Including Exchange and Correlation Effects. *Physical Review* **140** (1965), A1133–A1138.

[29] Perdew, J. P., Burke, K., and Ernzerhof, M. Generalized Gradient Approximation Made Simple. *Phys. Rev. Lett.* **77** (1996), 3865–3868.

[30] Trygve Helgaker, P. J. and Olsen, J. *Molecular Electronic-Structure Theory*. Wiley, 2000.

[31] v3.11.1, C. (Revision A11). Copyright IBM Corp 1990-2006, Copyright MPI fr Festkrperforschung Stuttgart 1997-2001. www.cpmd.org.

[32] Vanderbilt, D. Soft self-consistent pseudopotentials in a generalized eigenvalue formalism. *Physical Review B* **41** (1990), 7892–7895.

[33] Laasonen, K., Car, R., Lee, C., and Vanderbilt, D. Implementation of ultrasoft pseudopotentials in ab initio molecular dynamics. *Phys. Rev. B* **43** (1991), 6796–6799.

[34] Thomas Williams, C. K. e. a. GnuPlot.

[35] Leach, A. R. *Molecular Modelling: Principles and Applications*. Pearson Education EMA-Prentice Hall, 2001, 2 edn.

[36] Woodcock, L. V. Isothermal molecular dynamics calculations for liquid salts. *Chem. Rev. Lett.* **10** (1971), 257–261.

[37] Nos, S. A unified formulation of the constant temperature molecular dynamics methods. *J. Chem. Phys.* **81** (1984), 511–.

[38] Hoover, W. G. Canonical dynamics: Equilibrium phase-space distributions. *Phys. Rev. A* **31** (1985), 1695.

[39] Evans, D. J. and Holian, B. L. The NoseHoover thermostat. *J. Chem. Phys.* **83** (1985), 4069.

[40] Schrödinger, E. An Undulatory theory of the mechanics of atoms and molecules. *Physical Review* **28** (1926), 1049–1079.

[41] Marx, D. and Hutter, J. *Ab initio molecular dynamics:Theory and Implementation*, John von Neumann Institute for Computing, Jülich, 2000, vol. 1 of *NIC*, pp. 3001–449.

[42] Barbara Kirchner, A. P. S. and Hutter, J. CPMD manual, Copyright IBM Corp 1990-2001, Copyright MPI für Festkörpeforschung Stuttgart 1997-2005.

[43] Car, R. and Parrinello, M. Unified Approach for Molecular Dynamics and Density-Functional Theory. *Physical Review Letters* **55** (1985), 2471–2474.

[44] Marzari, N. and Vanderbilt, D. Maximally localized generalized Wannier functions for composite energy bands. *Phys. Rev. B* **56** (1997), 12847–12865.

[45] Sprik, M. and Ciccotti, G. Free energy from constrained molecular dynamics. *J. Chem. Phys.* **109** (1998), 7737–7744.

[46] P., E. Die Berechnung optischer und elektrostatischer Gitterpotentiale. *Ann. Phys.* **369** (1921), 253–287.

[47] Swaddle, T. W., Rosenqvist, J., Yu, P., Bylaska, E., Philips, B. L., and Casey, W. H. Kinetic Evicence for Five-Coordinatin in $AlOH(aq)^{-2}$ Ion. *Science* **308** (2005), 1450–1453.

[48] Takashi Ikeda, M. H. and Kimura, T. Hydrolysis of $AlOH(aq)^{-2}$ from constrained molecular dynamics. *J. Chem. Phys.* **124** (2006), 074503–1.

[49] Ruiz, J. M., McAdon, M. H., and Garcés, J. M. Aluminum Complexes as Moldels for Broensted Acid Sites in Zeolites: Structure and Energetics of $[Al(OH)_4]^-$, $[Al(H_2O)_6]^{3+}$, and Intermediate Monomeric Species $[Al(OH)_x(H_2O)_{n-x}{\cdot}mH_2O]^{3+}$ Obtained by Hydrolysis. *J. Phys. Chem. B* **101** (1997), 1733–1744.

[50] Kowall, T., Caravan, P., Hourgeois, H., Helm, L., Rotzinger, F., and Merbach, A. Interpretation of Activation Volumes for Water Exchange Reactions Revised: Ab Initio Calculations for Al^{+3},Ga^{+3} and In^{+3}, and New Experimental Data. *JACS* **120** (1998), 6569–6577.

[51] Yang, W., Qian, Z., Miao, Q., Wang, Y., and Bi, S. Density functional theory study of the aluminium (III) hydrolysis in aqueous solution. *PCCP* **11** (2009), 2396–2401.

[52] Kluge, S. and Weston, J. Can a Hydroxide Ligand Trigger a Change in the Coordination Number of Magnesium Ions in Biological Systems? *Biochemistry* **44** (2005), 4877–4885.

[53] Sillanpää, A., Päivärinta, J. T., Hotokka, M. J., Rosenholm, J. B., and Laasonen, K. A Computational Study of Aluminium Hydroxide Solvation. *J. Phys. Chem* **105** (2001), 10111–10122.

[54] Charles W. Bock, A. K. K., George D. Markham and Glusker, J. P. The arrangement of first- and second-shell water molecules around metal ions: effects of charge and size. *Theor. Chem. Acc.* **115** (2006), 100–112.

[55] Frisch, M. J., Trucks, G. W., Schlegel, H. B., Scuseria, G. E., Robb, M. A., Cheeseman, J. R., Montgomery, J. A., Jr., Vreven, T., Kudin, K.Ñ., Burant, J. C., Millam, J. M., Iyengar, S. S., Tomasi, J., Barone, V., Mennucci, B., Cossi, M., Scalmani, G., Rega, N., Petersson, G. A., Nakatsuji, H., Hada, M., Ehara, M., Toyota, K., Fukuda, R., Hasegawa, J., Ishida, M., Nakajima, T., Honda, Y., Kitao, O., Nakai, H., Klene, M., Li, X., Knox, J. E., Hratchian, H. P., Cross, J. B., Bakken, V., Adamo, C., Jaramillo, J., Gomperts, R., Stratmann, R. E., Yazyev, O., Austin, A. J., Cammi, R., Pomelli, C., Ochterski, J. W., Ayala, P. Y., Morokuma, K., Voth, G. A., Salvador, P., Dannenberg, J. J., Zakrzewski, V. G., Dapprich, S., Daniels, A. D., Strain,

M. C., Farkas, O., Malick, D. K., Rabuck, A. D., Raghavachari, K., Foresman, J. B., Ortiz, J. V., Cui, Q., Baboul, A. G., Clifford, S., Cioslowski, J., Stefanov, B. B., Liu, G., Liashenko, A., Piskorz, P., Komaromi, I., Martin, R. L., Fox, D. J., Keith, T., Al-Laham, M. A., Peng, C. Y., Nanayakkara, A., Challacombe, M., Gill, P. M. W., Johnson, B., Chen, W., Wong, M. W., Gonzalez, C., and Pople, J. A. Gaussian 03, Revision C.02. Gaussian, Inc., Wallingford, CT, 2004.

[56] G.Schaftenaar and Noordik, J. Molden: a pre- and post-processing program for molecular and electronic structures. *J. Comput.-Aided Mol. Design* **14** (2000), 123–134.

[57] Rodziewicz, P. and Doltsinis, N. L. Ab Initio Molecular Dynamics Free-Energy Study of Microhydration Effects on the Neutral-Zwitterion Equilivrium of Phenylalanine. *ChemPhysChem* **8** (2007), 1959–1968.

[58] Lavina C. Snoek, R. T. K. and Simons, J. P. A spectroscopic and computational exploration of tryptophan-water cluster structures in the gas phase. *PCCP* **4** (2002), 2130–2139.

[59] Ding, Y. and Krogh-Jespersen, K. The glycine zwitterion does not exist in the gas phase: results from a detailed ab initio electronic structure study. *Chem. Phys. Let.* **199** (1992), 261 – 266.

[60] Hodges, M. P. xmakemol, http://www.nongnu.org/xmakemol/.

[61] Dunbar, R. C. Complexation of Na and K to Aromatic Amino Acids: A density Functional Computational Study of Cation- Interactions. *J. Phys. Chem. A* **104** (2000), 8067–8074.

[62] Costanzo, F. and Valle, R. G. D. CarParrinello MD Simulations for the Na^+Phenylalanine Complex in Aqueous Solution. *J. Phys. Chem.* **112** (2008), 12783–12789.

[63] Emmanuel A. Meyer, R. K. C. and cois Diederich, F. Interactions with Aromatic Rings in Chemical and Biological Recognition. *Angewandte Chemie Int. Ed.* **42** (2003), 1210–1250.

[64] Jan P.Ñordin, B. L. P., David J. Sullivan and Casey, W. H. An ^{17}O-NMR Study of the Exchange of Water on $AlOH(H_2O)_5^{2+}$ (aq). *J. Inorg. Chem.* **37** (1998), 4760–4763.

[65] Rezabal, E., Marino, T., Mercero, J., Russo, N., and Ugalde, J. Complexation of Al(III) by the aromatic aminoacids in the gas phase. *Inorg. Chem.* **46** (2007), 6413–6419.

[66] Mercero, J. M., Fowler, J. E., and Ugalde, J. M. Aluminum(III) interactions with the acidic amino acid chains. *J. Phys. Chem. A* **102** (1998), 7006–7012.

[67] Mercero, J., Fowler, J. E., and Ugalde, J. M. Aluminum(III) interactions with the acid derivative amino acid chains. *J. Phys. Chem. A* **104** (2000), 7053–7060.

[68] Laasonen, K., Pasquarello, A., Car, R., Lee, C., and Vanderbilt, D. Car-Parrinello molecular dynamics with Vanderbilt ultrasoft pseudopotentials. *Phys. Rev. B* **47** (1993), 10142–10153.

[69] Silvestrelli, P. L. and Parrinello, M. Structural, electronic, and bonding properties of liquid water from first principles. *J. Chem. Phys.* **111** (1999), 3572.

[70] Knight, W. D., Clemenger, K., de Heer, W. A., Saunders, W. A., Chou, M. Y., and Cohen, M. L. Electronic Shel Structure and Abundances of Sodium Clusters. *Phys. Rev. Let.* **52** (1984), 2141–2144.

[71] Lang, N. D. and Kohn, W. Theory of Metal Surfaces: Work Function. *Phys. Rev. B* **3** (1971), 1215–1223.

[72] Eric J. Bylaska, J. R. R., Marat Valiev and Weare, J. H. Structure and dynamics of the hydration shlls of Al^{+3} ion. *J. Chem. Phys.* **126** (2007), 104505.

[73] Hay, M. B. and Myneni, S. C. B. Geometric and Electronic Structure of the Aqueous $Al(H_2O)_6^{+3}$. *J. Phys. Chem. B* **112** (2008), 10595–10603.

[74] Bol, W. and Welzen, T. The interpretation of X-ray diffraction by aqueous solutions of aluminum(III) nitrate and chromium(III) nitrate. *Chem. Phys. Lett.* **49** (1977), 189.

[75] Caminiti, R., Licheri, G., Piccaluga, G., Pinna, G., and Radnai, T. Order phenomena in aqueous $AlCl_3$ solutions. *J. Chem. Phys.* **71** (1979), 2473–2476.

[76] Carminiti, R. and Radnai, T. *Z. Naturforsch. A* **35** (1980), 1368.

[77] Laasonen, K., Larrucea, J., and SillapÄÄ, A. Ab Initio Molecular Dynamics Study of a Mixture of HF(aq) and HCl(aq). *J. Phys. Chem. B* **110** (2006), 12699.

[78] Mercero, J. *Aluminum (III) interactions with aminoacid chains.* Ph.D. thesis, UPV/EHU (2001).

[79] Rezabal, E. *Binding and specificity of Aluminium in proteins.* Ph.D. thesis, UPV/EHU (2007).

[80] Stepanian, S. G., I. D. Reva, E. D. R., and Adamowicz, L. Conformational Behavior of α-Alanine. Matrix-Isolation Infrared and Theoretical DFT and ab Initio Study. *J. Phys. Chem.* **102** (1998), 4623.

[81] Siu, F. M., Ma, N. L., and Tsang, W. Cation-π interactions in Soldiated Phenylalanine Complexes: Is Phenylalanine in the Charge-Solvated or Zwitterionic Form? *JACS* **123** (2001), 3397.

[82] Dudev, T. and Lim, C. Monodentate versus Bidentate Carboxylate Binding in Magnesium and Calcium Proteins: What Are the Basic Principles? *J. Phys. Chem. B* **108** (2003), 4546–4557.

[83] EHU-ko. (Garapen eta berrikuntza - Europarrerako fondo soziala, MCyT eta Eusko Jaurlaritzak finantziaturiko) SGI/IZO-SGIker haipatu beharra dago azpiegitura konputazionalaren eskeintza eskuzabalarengatik.

[84] Egileak i2Basque-ri haipamen bat egin nahi dio konputaziozko baliabide eta laguntza serbitzuengatik.

[85] Egileak haipamen bat egin nahi dio Barcelona Supercomputing Center - Centro Nacional de Supercomputación entitateak eskeinitako konputaziozko baliabide eta laguntza serbitzuarengatik.